DEVELOPMENT OF NEW CHEMISTRY FOR A DUAL USE HYDRAZINE THRUSTER

SWITCHABLE ROOM TEMPERATURE IONIC LIQUIDS

A STUDY OF SILANE GRAFTING TO MODEL POLYETHYLENE COMPOUNDS

SYNTHESIS OF THE NOVEL HYDRAZINE REPLACEMENT FUEL MOLECULES 1,1-DIMETHYL-2-[2-AZIDOETHYL]HYDRAZINE AND 1,1-DIMETHYL-2-[2-AZIDOETHYL]HYDRAZONE

A Dissertation
Presented to
The Academic Faculty

By

Hillary Anne Huttenhower

In Partial Fulfillment
Of the Requirements for the Degree
Doctor of Philosophy in Chemistry

Georgia Institute of Technology

August, 2010

DEVELOPMENT OF NEW CHEMISTRY FOR A DUAL USE HYDRAZINE THRUSTER

SWITCHABLE ROOM TEMPERATURE IONIC LIQUIDS

A STUDY OF SILANE GRAFTING TO MODEL POLYETHYLENE COMPOUNDS

SYNTHESIS OF THE NOVEL HYDRAZINE REPLACEMENT FUEL MOLECULES 1,1-DIMETHYL-2-[2-AZIDOETHYL]HYDRAZINE AND 1,1-DIMETHYL-2-[2-AZIDOETHYL]HYDRAZONE

Dr. Charles L. Liotta, Advisor
School of Chemistry and Biochemistry
Georgia Institute of Technology

Dr. Charles A. Eckert
School of Chemical and Biomolecular Engineering
Georgia Institute of Technology

Dr. David M. Collard
School of Chemistry and Biochemistry
Georgia Institute of Technology

Dr. Rigoberto Hernandez
School of Chemistry and Biochemistry
Georgia Institute of Technology

Dr. Amyn Teja
School of Chemical and Biomolecular Engineering
Georgia Institute of Technology

Date Approved: April 6, 2010

For Mom, Dad, and John-
Who all believed in me even when I didn't believe in myself

ACKNOWLEDGEMENTS

First and foremost, I would like to thank my advisor, Dr. Charles Liotta. I came to Georgia Tech specifically to work in his research group, and I have never once been disappointed. I would also like to thank my co-advisor, Dr. Charles Eckert. I have learned so much from both of these two researchers. Before I began graduate school, I never could have imagined the opportunities and experiences that awaited me here, and so many of them were thanks to the fact that I had these two gentlemen on my side. I would also like to thank the researchers at American Pacific that I have been fortunate enough to work with over the years. Some of the most interesting experiences that I have had have come out of collaboration with this company.

Next, I would like to thank my committee. Everyone in academia is busy all the time, so I appreciate you finding time in your schedules to read my work and advise me during my time here. I would also like to thank every single member of the Eckert-Liotta group, past and present that I have worked with over the years. Ours truly is a collaborative group, and I couldn't have done this without any of you. There are a few members in particular over the years that I couldn't have gotten by without. Ejae John, my first mentor in lab, Stuart Terrett, the best undergrad anyone could ask for, Kristen Kitagawa, my office mate and fellow traveler on this crazy journey for so many years, Pamela Pollet, who keeps us all on track, thank you to all of you.

A lot of the analysis necessary for this thesis could not be performed in house, so I would like to acknowledge all who helped with that. Thank you to Jung-il Hong for performing all the XRD analysis, Jeannette Taylor and Art McCanna at the Robert P. Apkarian Integrated Electron Microscopy Core facility at Emory University for

performing TEM and SEM imaging, Oguz Karvan and the other members of the Koros group for the BET analysis, and the workers at Columbia Analytical Services for running all metals analysis and expediting them for free when I asked.

I also need to thank my friends and especially my family. I hope my parents know how truly grateful I am, from the bottom of my heart, for all that they have done for me over the past five years of graduate school. I never ever would have made it through or even stayed sane without their love and support. It means so much to know that I can always count on them. Also, to my friend, Sara Campbell, though we were at different universities, we went through this crazy chemistry graduate school journey together, and it so helped to have someone to commiserate with. Though some may find this unusual, I also need to thank my cat, Winston, for all the moral support he's given me over these years. At this point, I think he knows as much about this research as I do, since his favorite place while I was writing this dissertation was curled up around my computer. Finally, to my long-time boyfriend John, you have been a best friend, a source of comfort, a reminder that there is far more to life than work. We both know it's been a bumpy road, but I'm glad we went through it together.

When I actually take the time to step back and realize it, I know that I am truly blessed in so many ways, and I just want to thank God and everyone else who makes that possible.

TABLE OF CONTENTS

LIST OF TABLES

LIST OF FIGURES

LIST OF SYMBOLS AND ABBREVIATIONS

$\lambda_{max:}$	Wavelength of maximum absorption
μS:	microSiemens
AgTFA:	Silver trifluoroacetate
AMPAC:	American Pacific Corporation
BAA:	Bromoacetaldehyde
BADA:	Bromoacetaldehyde diethyl acetal
BET:	Brunauer, Emmett and Teller surface area
[bmim][Cl]:	n-Butylimidazolium chloride
CI-MS:	Chemical ionization – mass spectrometry
$[C_6mim][BF_4]$:	Hexylmethylimidazole tetrafluoroborate
^{13}C NMR:	Carbon – 13 Nuclear magnetic resonance spectroscopy
COSY NMR:	Correlation spectroscopy nuclear magnetic resonance spectroscopy
DABCO:	1,4-Diazabicyclo-[2-2-2]-octane
DBU :	1,8-Diazabicyclo[5-4-0]undec-7-ene
De-DMAEH:	1,1-Dimethyl-2-[2-azidoethyl]hydrazone
DEPT NMR:	Distortionless enhancement by polarization transfer nuclear magnetic resonance spectroscopy
DMAEH:	1,1-Dimethyl-2-[2-azidoethyl]hydrazine
DMAP:	Dimethylaminopyridine
DMAZ:	2-Dimethylaminoethylazide
DMF:	*N,N*-dimethyl formamide
DMSO:	Dimethylsulfoxide
DSC:	Differential scanning calorimeter
EHS:	Environmental health and safety
EI-MS:	Electron impact – mass spectrometry
ESI-MS:	Electrospray ionization – mass spectrometry
EtOAc:	Ethylacetate
FAB-MS:	Fast atom bombardment – mass spectrometry
GC-MS:	Gas chromatography - mass spectrometry
GC-TCD:	Gas chromatography - thermal conductivity detector
GPC:	Gel permeation chromatography
^{1}H NMR:	Proton nuclear magnetic resonance spectroscopy
HPLC:	High performance liquid chromatography
HSQC:	Heteronuclear single quantum coherence
IL:	Ionic liquid
^{i}PrOH:	Isopropanol
IR:	Infrared spectroscopy
LC-MS:	Liquid chromatography - mass spectrometry
LC-UV-MS:	Liquid chromatography - Ultraviolet-visible spectroscopy and mass spectrometry
LDPE :	Low density polyethylene
MALDI-MS:	Matrix assisted laser desportion/ionization – mass spectrometry

MeLi:	Methyllithium
MeOH:	Methanol
MMH:	Monomethylhydrazine
NASA:	National Aeronautics and Space Administration
NIOSH:	National Institute for Occupational Safety and Health
NMR:	Nuclear magnetic resonance spectroscopy
OSHA:	Occupational Safety and Health Administration
PhLi:	Phenyllithium
PVP:	Polyvinylpyrrolidone
RF:	Radio frequency
RTIL:	Room temperature ionic liquid
SEM:	Scanning electron microscopy
SOMO:	Singly occupied molecular orbital
TBACl:	Tetrabutylammonium chloride
TEM:	Transmission electron microscopy
TESA:	(3-Aminopropyl)triethoxysilane
TESAC:	3-(Triethoxysilyl)-propylammonium 3-(triethoxysilyl)-propyl carbamate
TGA:	Thermogravimetric analysis
THF:	Tetrahydrofuran
TLC:	Thin layer chromatography
TMBG:	2-Butyl-1,1,3,3-tetramethylguanidine
TMBG MC:	2-Butyl-1,1,3,3-tetramethylguanidiniummethylcarbonate
TMBG MC IL:	2-Butyl-1,1,3,3-tetramethylguanidinium methylcarbonate ionic liquid
TMG:	Tetramethylguanidine
TMSA:	(3-Aminopropyl)trimethoxysilane
TMSAC:	3-(Trimethoxysilyl)-propylammonium 3-(trimethoxysilyl)-propyl carbamate
TMSCN:	Trimethylsilyl cyanide
UV:	Ultraviolet
UV-Vis:	Ultraviolet-Visible spectroscopy
VTMS:	Vinyl trimethoxysilane
VTPS:	Vinyl triphenylsilane
XRD:	X-ray diffraction

SUMMARY

This thesis focuses on the development of new compounds or new processes that are more environmentally friendly and economical than those currently in use. The decomposition of hydrazine, a well established liquid rocket fuel for both the aerospace and defense industries, to the product ammonia is studied. Control of this reaction will allow hydrazine to be used as a propellant for both chemical and electric propulsion. From this a dual stage thruster will be developed that will be more efficient than current systems decreasing the amount of propellant needed and allowing for either a larger mission payload or a longer duration of individual missions. Hydrazine, while beneficial and well established, is also highly toxic, so other work in this thesis focuses on the synthesis of the novel molecule 1,1-dimethyl-2-[2-azidoethyl]hydrazine or DMAEH and its hydrazone intermediate 1,1-dimethyl-2-[2-azidoethyl]hydrazone or De-DMAEH as less toxic hydrazine replacements.

Novel "switchable" solvents have been investigated in this research. These are solvents that can change from molecular liquids to ionic liquids and back, simply with the addition or removal of CO_2 from the system. They can be used for a variety of applications, including as solvents for a reaction and separation system. Due to the recyclable nature of these solvents, waste is decreased making their development and implementation both environmentally and economically beneficial. Finally, the grafting reaction of vinyl silanes onto a hydrocarbon backbone is investigated. Fundamental work is being performed to study the graft distribution, selectivity and mechanism by which this reaction occurs. A more thorough understanding of how this reaction proceeds will allow for the development of a more efficient industrial process.

CHAPTER ONE
INTRODUCTION

Hydrazine is the liquid propellant of choice for most military orbital and deep space rockets, as well as many commercial satellites. Due to this, engines are currently manufactured, and certified for use with this propellant. While this type of chemical propulsion engine provides high thrust for rapid maneuvering, it is less attractive in situations where long term life is required.[1] On the other end of the spectrum, electric propulsion using an inert gas such as xenon as the propellant provides very low thrust, but has a very high specific impulse (impulse obtained per mass unit of propellant), meaning the propellant is used efficiently.[2] Combining these two types of propulsion systems into a single thruster would provide a flexible system in which a single engine could efficiently fulfill both short term and long term needs of a space mission. For example, the chemical propulsion would fuel rapid high thrust maneuvers to put a satellite into orbit and electrical propulsion would control the minor course corrections required to keep that satellite in orbit over a several year life span. Ideally both types of propulsion would be fueled by the same propellant.

As chemical propulsion engines are already certified for use with hydrazine, this chemical seems the ideal choice as a propellant feed source for electric propulsion as well. Hydrazine itself is not an efficient fuel for electric propulsion,[3] however, ammonia, a hydrazine decomposition product, can be.[4] To be effective for electric propulsion, the amount of ammonia must be the dominant product in the decomposition stream (at least 75 mol%). In Chapter Two, the synthesis and analysis of supported metal catalysts for hydrazine decomposition are discussed. The ability of these catalysts to

selectively decompose hydrazine into ammonia is investigated using a reactor and detector system that has been designed and constructed in our lab. The ultimate goal of this project is to combine the most affective of these catalysts with an electric propulsion thruster being developed by the research group of Dr. Mitchell Walker to build a working dual-propulsion thruster fueled by the single propellant hydrazine.

In Chapter Three, novel "switchable" ionic liquids are investigated. Common organic solvents have fixed properties such as viscosity and polarity. This can be a disadvantage in some applications, such as large multi-step syntheses as solvent may have to be removed and changed between each step. On an industrial scale, this creates a lot of waste, which has a major economic and environmental impact. Having a solvent whose properties could be "switched" or changed between steps by an inert mechanism such as irradiating light or bubbling a gas could help alleviate this problem.

We have developed two types of switchable ionic liquids: a two component system based on a pentasubstituted guanidine and alcohol and a one component system derived from silylated amines. For both systems, the switch occurs by the addition of or removal of carbon dioxide from the system. In Chapter Three we explore the synthesis and complete characterization of these switchable liquids in both their neutral and ionic form. The use of these ionic liquids as a recyclable medium for two applications, as a reaction solvent with a built in separation mechanism, as well as for the extraction of alkanes from bitumen are examined.

In the wire and cable industry, low density polyethylene (LDPE) is frequently used as a means of insulating the cables.[5-6] However, LDPE has low thermal and chemical stability.[7] To overcome these obstacles, the polymer is cross-linked, which

increases its thermal and chemical resistance as well as its long-term durability.[8] The most common method of inducing cross-linking is by first grafting a cross-linker precursor such as vinyl trimethoxysilane (VTMS) to the polymer chain, and then exposing the grafted material to moisture which induces cross linking via the reactive VTMS sites.[9] The mechanism of the grafting reaction is currently not well understood, however, and no means currently exists of controlling the grafting distribution. In Chapter Four, the peroxide initiated grafting of vinyl silanes onto a hydrocarbon backbone is investigated. The polyethylene model compounds dodecane and heptane are used to study graft distribution and the radical reaction mechanism. By chromatographic separation, individual grafted fractions are isolated so that a regio-selective analysis can be performed. The affect of carbon dioxide on the grafting mechanism is also examined. Ultimately, the fundamental information learned about this reaction mechanism will be used to develop a more efficient industrial process.

Finally in Chapter Five, we return to liquid rocket fuels. As discussed previously, hydrazine is a common and well used liquid rocket fuel due to its high thrust, high specific impulse compared to other liquid rocket fuels (though not compared to other propulsion methods), and the large quantity of hot expanding gases produced from a very small amount of liquid hydrazine. However, it is also toxic and a known carcinogen with high vapor pressure.[10] Finding a suitable replacement for hydrazine is an area of much interest both to the private and government aerospace industries. If a new, cost competitive liquid rocket fuel were developed that could maintain the same favorable propellant characteristics as hydrazine but that has fewer hazards to humans and the environment, there would potentially be a large commercial market. To meet his goal,

our group proposed the novel molecule 1,1-dimethyl-2-[2-azidoethyl]hydrazine or DMAEH as well as its hydrazone intermediate 1,1-dimethyl-2-[2-azidoethyl]hydrazone or De-DMAEH as possible replacements. Chapter Five discusses the synthesis and purification of these molecules starting from commercially available small organic starting materials.

1.1 References

1. Zheng, M.; Chen, X.; Cheng, R.; Li, N.; Sun, J.; Wang, X.; Zhang, T.; *Catalytic Decomposition of Hydrazine on Iron Nitride Catalysts,* Catal. Commun., 2006, **7,** p: 187-191.

2. Goebel, D. M.; Katz, I.; *Fundamentals of Electric Propulsion: Ion and Hall Thrusters,* JPL Space Science and Technology Series, John Wiley and Sons, March 2008.

3. Willis, C.; Lossing, F. P.; Back, R. A.; *The Heat of Formation of N_2H_2 and the Proton Affinity of N_2*, Can. J. Chem., 1976, **54(1),** p: 1-3.

4. Esker, D. W.; Kroutil, J. C.; Checkley, R. J. *Radiation Cooled MPD Arc Thruster,* NASA CR 72557, Report MDC H296, 1969.

5. Barzin, J.; Azizi, H.; Morshedian, J.; *Preparation of Silane-Grafted and Moisture Crosslinked Low Density Polyethylene. Part II: Electrical, Thermal and Mechanical Properties*, Polym,-Plast. Tech. Eng., 2007, **46**: p. 305-310.

6. Dufton, P. W.; *Recent Development in Polymer for Wire and Cable: An Insulation Report,* Raptra Technology Ltd.: UK, 1995.

7. Jiao, C.; Wang, Z.; Gui, Z.; Hu, Y.; *Silane Grafting and Crosslinking of Ethylene-Octene Copolymer,* Eur. Polym. J., 2005, **41:** p. 1204-1211.

8. Barzin, J.; Aziz, H.; Morshedian, J.; *Preparation of Silane-Grafted and Moisture Cross-lInked Low Density Polyethylene: Part I: Factors Affecting Performance of Grafting and Cross-Linking,* Poly.-Plast. Tech. Eng., 2006, **45:** p. 979-983.

9. Venkatraman, S.; Kleiner, L.; *Properties of Three Types of Crosslinked Polyethylene,* Adv. Polym. Tech., 1989, **9:** p. 265-270.

10. Richman, D. W.; Griffith, K. N.; Liotta, C. L.; Pollet, P.; *Investigation of Ignition Delay: Novel Beta-Substituted Ethylazide Derivatives as Potential New Liquid Propellant Fuels* Report, SBIR FA9300-05-M-3013, 2006.

CHAPTER TWO
DEVELOPMENT OF NEW CHEMISTRY FOR A DUAL USE HYDRAZINE THRUSTER

2.1 Introduction

Although hydrazine can be used as bipropellant, it is more traditionally used as monopropellant for chemical propulsion. Hydrazine decomposition is catalyzed by metals such as iridium into a mixture of ammonia, hydrogen, and nitrogen, the composition of which is of no interest to traditional chemical propulsion. The important characteristic is that the reaction produces a large volume of very hot gas (up to 800°C)[1] from a small amount of liquid hydrazine. This hot gas is focused through a nozzle providing the thrust, the amount of which varies, depending on the engine and desired use.

For the present work, the interest lies in focusing and controlling this reaction by designing, synthesizing, and testing a catalyst or a pre-catalyst that decomposes hydrazine at temperatures between 25-75ºC in a controlled manner. The aim is to selectively produce the highest amount of ammonia possible, to be subsequently used as a propellant for electric propulsion. Although electric propulsion does not yield as high of a thrust as chemical propulsion, it provides higher thrust control. Therefore electric propulsion is advantageous for applications like satellite relocation or trajectory adjustment. Combining both electric and chemical propulsion from a sole propellant is an attractive avenue for satellite technology as it will couple high trust (for take-off) with precise thrust (for trajectory adjustment). This directly translates to significant cost gain by increasing a satellite's lifetime while causing little to no change in its overall weight.

Controlling the decomposition of hydrazine is a key challenge in developing a dual propulsion system that uses hydrazine as the sole propellant for electric and

chemical propulsion. There are two major pathways in which hydrazine can decompose; (1) into nitrogen and hydrogen (Equation 2.1) and (2) into nitrogen and ammonia (Equation 2.2). Both of these decomposition pathways are exothermic and as heat builds up decomposition towards hydrogen and nitrogen (Equation 2.2) becomes the dominant pathway. In addition at even higher temperatures the decomposition of ammonia to hydrogen and nitrogen (Equation 2.3) also becomes significant. The catalysts being developed in this work are designed to provide the right balance between efficiency and chemoselectivity in that the decomposition should primarily yield ammonia (Equation 2.2) and that the exothermicity of the reaction should be limited to minimize the occurrence of the undesired pathways (Equation 2.1 and 2.3).[2]

$$N_2H_4 \rightarrow N_2 + 2H_2 \qquad \text{(Equation 2.1)}$$

$$3N_2H_4 \rightarrow N_2 + 4NH_3 \qquad \text{(Equation 2.2)}$$

$$4\,NH_3 + N_2H_4 \rightarrow 3N_2 + 8H_2 \qquad \text{(Equation 2.3)}$$

For this work, the metals nickel, copper, rhodium, ruthenium, cobalt and iridum have been chosen for examination based on their known activity towards hydrazine decomposition and selectivity for the formation of ammonia.[3] We have developed methods to synthesize and support these catalysts both as nanoparticles and as layers of metal on a solid surface and each is being tested for their catalytic activity and selectivity for the formation of ammonia for ultimate use in an electric propulsion system (Equation 2.2).

2.2. Background

2.2.1 Hydrazine Decomposition

As discussed above, hydrazine decomposition can form either hydrogen and nitrogen, or nitrogen and ammonia as products (Equation 2.1 and Equation 2.2). Ultimately, which decomposition products are favored is determined by the metal catalyst, and the temperature range of the reaction.[4] As a decomposition mechanism, literature suggests no scrambling of nitrogen atoms, based on ^{15}N labeled hydrazine studies (Figure 2.1).[4] By this mechanism, hydrazine adsorbs to the catalyst surface by hydrogen abstraction to form an adsorbed N_2H_2 molecule (Step 1, Figure 2.1). This reacts by a concerted mechanism with a second hydrazine molecule in the vapor phase to form ammonia and nitrogen (Step 2, Figure 2.1).

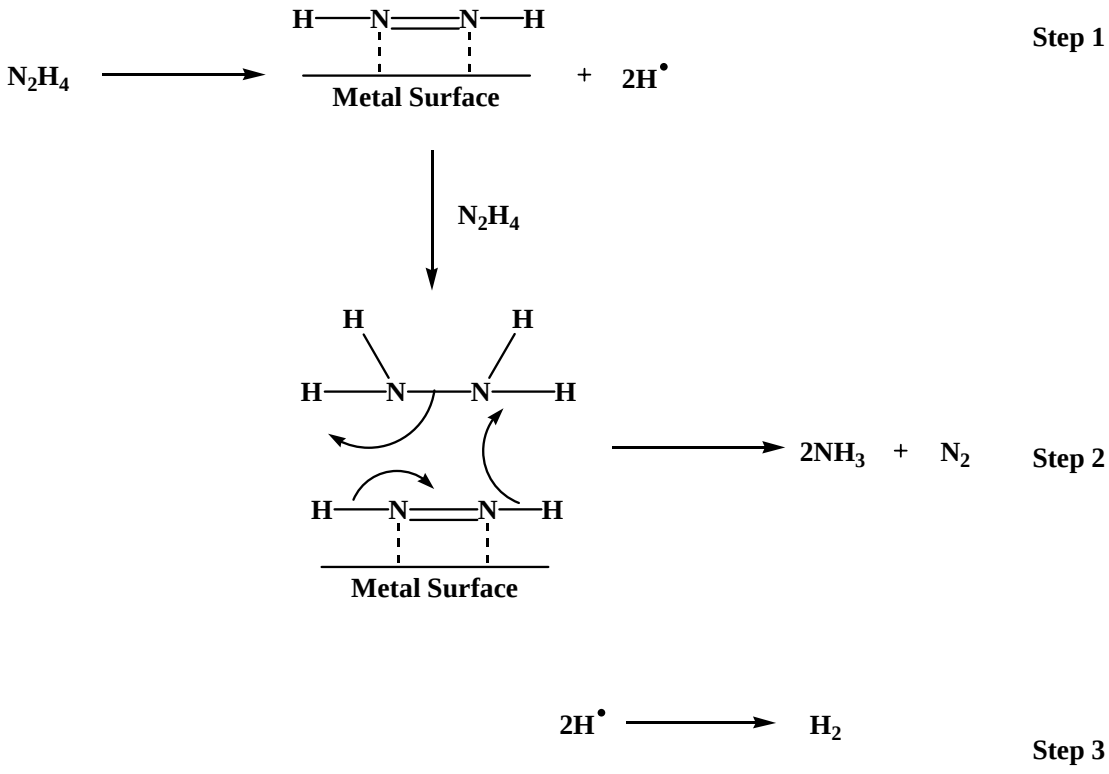

Figure 2.1 Proposed hydrazine decomposition mechanism

Hydrazine decomposition has been studied over metal thin films[5-6], hot wires[7-8], metal foils[9-11], on a single metal crystal[12-14], and over metal powders and supported catalysts[3,15-18]. For our work we are most interested in the results over metal powders and supported catalysts as they are most directly comparable to the supported catalysts that we are developing.

The behavior of these metal catalysts is defined in terms of their activity which is the ability to convert hydrazine to products, and selectivity which is their preference for the formation of nitrogen and hydrogen (Equation 2.1) versus the formation of ammonia (Equation 2.2) during decomposition. For the current research, a catalyst with high activity and low selectivity is desired. Work performed by Maurel *et al*[3] on metal catalysts supported on alumina granules studied selectivity and activity of iridium, rhodium, nickel, platinum, cobalt, ruthenium, palladium, silver and copper at temperatures <180°C. In his work, it was found that these metals decrease in activity in the following order:

Ir > Rh > Ni ~ Pt ~ Co ~ Ru > Pd ~ Ag ~ Cu

However, in terms of selectivity, a very different order is followed. In order of decreasing selectivity:

Pd > P t> Rh > Ni > Ir ~ Ru > Cu > Co > Ag

From this information, it was decided to focus on Cu, Ni, Co, Ir, Rh, and Ru for this research, as they appear to have the best potential in terms of activity and selectivity.

2.2.2 Catalyst Synthesis

In the thin film studies by Al-Haydari and coworkers in 1985, catalysts of iron, nickel and copper were prepared by evaporation of metal filaments onto a glass surface to form a thin film.[19] Hydrazine decomposition over these thin films was tested in the temperature range of 0°C-120°C. While all three, showed high activity with complete decomposition of hydrazine, nickel showed the lowest selectivity, corresponding to highest ammonia formation, with 81.86% of the product stream at 120°C. Thin film type catalysts are one method that can be used. However, an alternate preparation is to adsorb a nanoparticle catalyst onto a solid support such as silica or alumina.

Most literature methods involve a procedure for mixing the catalyst precursor with or impregnating it on the solid support first, then forming the catalyst on the solid surface.[20-25] This is generally done by impregnating solid support particles with a metal salt complex which is then reduced by hydrogen gas at high temperatures. Maurel *et al* used this method in their catalyst activity studies.[3] In their work, 0.2-0.4mm alumina granules were used as support. Metal salts were deposited by soaking these granules in aqueous solutions of the salts. These were then dried, placed in a hydrogen gas stream and heated to 500°C. The catalysts were held at 500°C in hydrogen for ten hours to carry out complete reduction. The iridium catalyst Shell 405 that is currently used for chemical propulsion is also made by a variation of this method.[24] Solid alumina support is impregnated with aqueous iridium chloride salt solution. The solid is dried, decomposed in a 350°C air stream and re-impregnated with another layer of metal salt. This layering and decomposition can occur up to 20 times to achieve the desired catalyst loading. Final reduction is done in a hydrogen gas stream at 500°C-550°C.[24]

Metal nanoparticles possess unique properties (such as enhanced catalytic activity and chemoselectivity) often different from the bulk metals because of their nanoscale dimensions and resulting high surface to mass ratio.[26] A plethora of methods for the preparation of metal nanoparticles are reported in the literature detailing ways to achieve precise control of their size.[26-38] While some methods require the use of specific capping agents in the nanoparticle synthesis[26] other methods use ethylene glycol as both the solvent and the capping agent.[27-28] For example, Couto and coworkers carried out the synthesis of nickel nanoparticles (Equation 2.4) using nickel chloride hexahydrate reduced by sodium borohydride in ethylene glycol in the presence of the capping agent polyvinylpyrrolidone (PVP, Figure 2.2).[26] In contrast, Wu and coworkers reported the preparation of nickel nanoparticles via the reduction of nickel chloride with hydrazine hydrate in the presence of sodium hydroxide in ethylene glycol, which was both the solvent and capping agent (Equation 2.5) .[27]

$$NiCl_2 \cdot 6H_2O + 3NaBH_4 + n\text{PVP} \rightarrow Ni(PVP)_n + 11H_2 + 2HCl + 3NaBO_2 \quad \text{(Equation 2.4)}$$

$$2NiCl_2 + N_2H_4 + 4NaOH \rightarrow 2Ni + N_2 + 4H_2O + 4NaCl \quad \text{(Equation 2.5)}$$

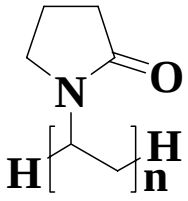

Figure 2.2 Polyvinylpyrrolidone (PVP) capping agent

Both Couto's capping method, as well as Wu's ethylene glycol method, and modifications of it have been tried for the synthesis of nickel nanoparticles, as well as copper, iridium, ruthenium, rhodium, and cobalt nanoparticles for use in this research.

2.2.3 Liquid Chemical Propulsion

Chemical rocket propulsion as it is known today began with the work of Dr. Robert Goddard in 1928. In modern liquid propulsion, either fuel and oxidant are pumped into a combustion chamber, or fuel is passed over a heterogeneous catalyst bed within a combustion chamber. The fuel is ignited to produce a large quantity of high pressure, high velocity gases. These gases are then focused through a nozzle which provides the thrust and lift for the rocket. In the space shuttle main engines, liquid oxygen and liquid hydrogen are used as the liquid propellant. However, for most military orbital and deep space rockets, as well as many commercial satellites, hydrazine is the liquid propellant of choice, and engines are currently designed, manufactured, and certified for use with this propellant. This type of propulsion is ideal in situations that call for high thrust such as the rapid maneuvers needed to control the adjustment of orbits and attitudes of space vehicles.[39] However, along with the high thrust comes a generally low specific impulse of 230-250 seconds (change in momentum per unit of propellant used by weight) making traditional chemical propulsion less attractive in situations where long term use or life is needed.

2.2.4 Electric Propulsion

Electric propulsion is defined as any propellant technology in which electricity is used to increase exhaust velocity.[40] In this type of propulsion, there is low thrust, but high specific impulse, so the amount of propellant necessary is greatly decreased compared to standard chemical propulsion. It is ideal for long term space missions where small course corrections and changes are needed over time. In electric propulsion systems, a plasma source is used to ionize a propellant gas stream, generally a heavy inert gas such as xenon (Figure 2.3). These ions are then accelerated by either an electrothermal, electrostatic, or electromagnetic method.[40] It is the acceleration of these ions along a fixed path that provides the thrust for propulsion.

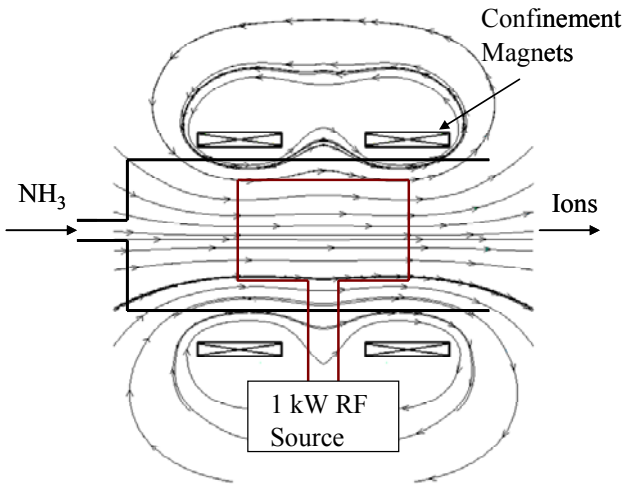

Figure 2.3 Ionization of ammonia gas stream by RF Source. Arrows show the path of ions traveling through the thruster.

For the electric propulsion thruster being designed for this work, ionization of the ammonia gas stream will be done by a helicon plasma generator. A helicon is an efficient plasma generator that uses radio frequency (RF) waves to deposit energy into a gas, resulting in ionization. In this work, an RF signal is transmitted into the ammonia

and the energy is absorbed by the electrons. This energizes the electrons to the point that they can break free from the atoms, forming ions. Additional ions are also formed as collisions between electrons and other neutral molecules take place within the gas stream.

The acceleration will then be done by an electrostatic method meaning that ions will be accelerated along electric field lines created by a drop in electrostatic potential between two regions. This is a commonly used method for electric propulsion thrusters[41-44] as the specific impulse of the thruster can then be set by the potential drop across the grids, and is solely dependent on the power available to the thruster as opposed to the internal energy of the propellant itself.

While inert gases such as xenon are the most common propellants for electric propulsion, some prior work has been done on the use of ammonia as propellant. Esker, *et al* at McDonnell Research laboratories tested ammonia as thruster propellant, both in short term tests and in lifetime tests of 508 hours. Over the course of this lifetime test, specific impulse was found to be 1900 seconds, indicating that ammonia has high specific impulse, and therefore long lifetime and efficiency that we are interested in for our research.[45] However, this thruster was never actually flown, and to our knowledge, no ammonia based electric propulsion thruster has ever actually been flight tested.

A small amount of work has also been done on the ionization potential of hydrazine itself as a propellant for electric propulsion, without any prior decomposition. However, it has been found that it is not a very efficient fuel molecule to ionize. This is due to the fact that when hydrazine is ionized, it fragments into nitrogen and hydrogen ions.[46] Only the N_2+ ion is useful for acceleration for electric propulsion, so the energy that goes into the fragmentation and formation of hydrogen ions is wasted. By

decomposing the hydrazine by a chemical process first into a product stream that is mostly ammonia, fragmentation during ionization does not occur, allowing a much higher percentage of the electric power input in the system to translate directly into thrust.

2.2.5 Benefits of a Dual Propulsion System

The ultimate goal of this project is the development of a dual use hydrazine thruster. This thruster will use decomposition of a single propellant, hydrazine, to fuel both a liquid chemical propulsion thruster, as well as an electric propulsion thruster. By using hydrazine as the propellant for both, liquid hydrazine thrusters, which have been used in flight for years can continue to be used as is. No new liquid propulsion system will have to be developed and re-certified, and having a single propellant to fuel both systems makes the entire thruster more efficient.

A dual propulsion mode thruster of this type will combine the high thrust, low specific impulse operation of a chemical system with the low thrust, high specific impulse operation of an electric propulsion system. This gives flexibility not currently seen in space craft as a single engine will now be able to efficiently fulfill both short term needs of a system such as rapid high thrust maneuvers to put a satellite into orbit and long term needs such as the minor course corrections required to keep that satellite in orbit over a several year life span. Current systems use one engine type or the other, based on what is most beneficial for the mission, which leads to sacrifices being made either in power, speed, propellant weight or cost. The flexibility of our system should lead to a decrease in the amount of propellant needed, allowing for either a larger mission payload or a longer duration of individual missions.

To our knowledge, the only other dual stage rocket engines currently in development do not involve a single propellant source, nor do they incorporate multiple propulsion modes. Instead, they involve the use of multiple fuel mixtures to carry out two types of chemical propulsion.[47-48] For example, one proposed design involves standard catalytic decomposition of hydrazine in one stage, while in the second stage, nitrogen tetroxide is added to act as an oxidizer to yield higher energy and higher thrust chemical propulsion.[48] These designs are very different from what we are proposing, and do not have the high specific impulse, long lifetime and efficiency benefits that our system will have due to the incorporation of electric propulsion.

In this research, metal catalysts are being designed analyzed and tested for their activity and selectivity in the decomposition of hydrazine. The decomposition must be at low temperatures (between 25-75ºC) and take place in a controlled manner, leading to a large amount of ammonia. Ammonia is desired as it will lead to the most efficient electric propulsion. Whichever catalyst shows the most promise, will be used to develop this two stage engine.

2.3. Results and Discussion

2.3.1 Catalyst Synthesis

2.3.1.1 Nanoparticle Synthesis

Due to the high ammonia yields seen with thin film studies,[19] nickel was chosen as the initial metal for catalyst development and testing. A standard nanoparticle synthesis method that could then be applied to multiple metals was developed using the nickel procedure. Initially, the method developed by Couto and coworkers was

employed.[26] Following this method, nickel chloride hexahydrate (0.01mmol) and 40,000Mw PVP (0.0003mmol) were dissolved in ethylene glycol (25mL). This was heated to 140°C with vigorous stirring. At temperature, sodium borohydride was added (4.76mmol) with continued stirring. After reacting for 2 hours, the solution was cooled and acetone was added to the solution (50mL) to precipitate nanoparticles. Particles were collected by centrifugation and dried.

For these initial syntheses, only qualitative analysis was performed. Only nickel nanoparticles, not nickel oxide or unreacted starting material will exhibit magnetic properties. Magnetic nanoparticles were consistently formed by this method using 40,000Mw PVP. When imaged by transmission electron microscopy (TEM, Figure 2.4 A) and analyzed using the Image J software, the size histogram (Figure 2.4 B) showed an average particle size of 6nm with a standard deviation of ±2nm. However this may not be completely representative as the sample examined contained only about a hundred particles. While this is a reasonable size and standard deviation, ultimately this method was not pursued further due to difficulties in preparing a sizeable amount of materials for further analysis and use. When the reaction was run on a larger scale, a correspondingly larger amount of product was not successfully isolated.

The method published by Wu and co-workers was then employed.[27] This method involves the reduction of nickel chloride in ethylene glycol by hydrazine monohydrate in the presence of sodium hydroxide. After modifications and optimization to suit our needs, this reaction was consistently run by dissolving nickel chloride (0.5mmol) and solid sodium hydroxide (1.8mmol) in ethylene glycol (25mL) at 60°C with vigorous stirring. After complete dissolution of solid reactants, hydrazine

A.

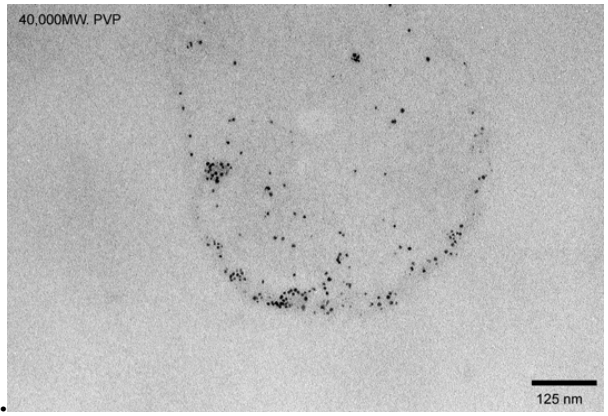

B.

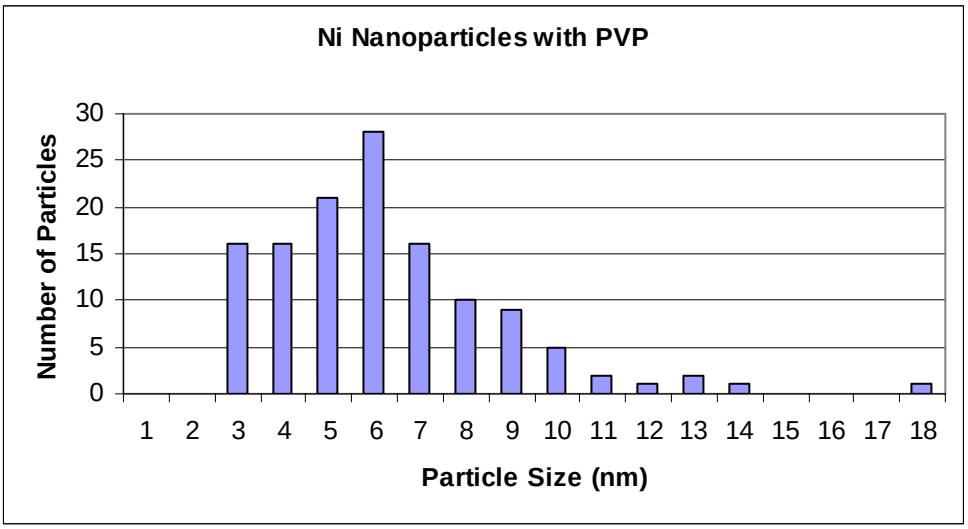

Figure 2.4 A. TEM image of particles made using 40,000 MwPVP and **B**.the corresponding particle size histogram.

monohydrate (0.3mL, 6.2mmol) was added. Reaction continued for 1 hour at 60°C, after which time it was cooled to room temperature. UV-vis analysis was used to track the disappearance of $NiCl_2$ starting material. The $NiCl_2$ starting salt solution showed a sharp peak with a wavelength of maximum absorption at 287nm. This was no longer present in the product particle solution. Complete reduction was confirmed by chlorine elemental analysis, which consistently showed 0% chlorine remaining in the isolated nanoparticle samples. Particles were isolated by centrifugation, washed with ethanol, and dried

overnight in a vacuum oven heated at 80°C. The particles were found to be magnetic, and could be isolated in 95% yield.

To confirm nickel(0) formation, x-ray diffraction (XRD) analysis was used. The XRD obtained contains 5 peaks which correspond to those expected for face centered cubic nickel metal (Figure 2.5). This confirms that no nickel oxide is present, as nickel oxide would show a sharp peak at ~63° that is not visible in this spectrum.[49]

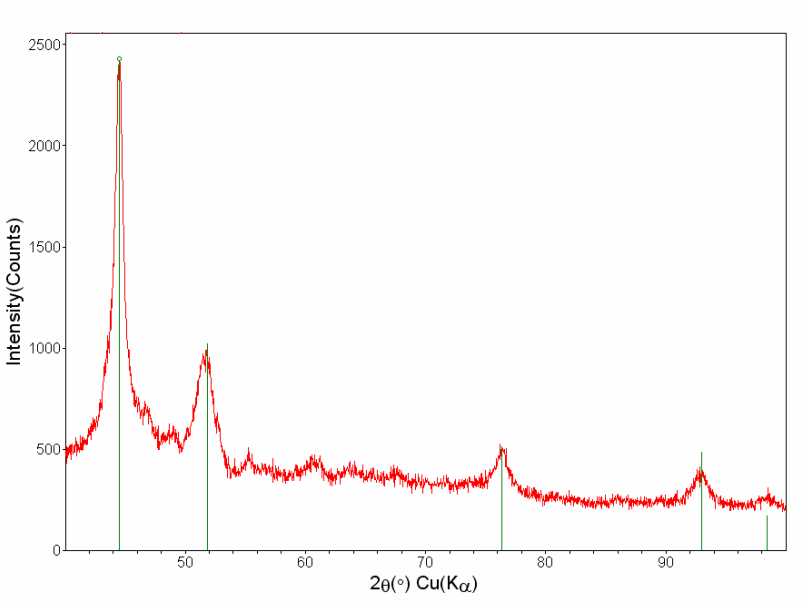

Figure 2.5 XRD spectra of Ni nanoparticles

Also from the XRD, the peak shape and size were used to calculate an average particle size. This was done by the JADE software using a method based on the Debye-Scherrer equation, and gave an average particle size of 8nm.

To confirm this particle size, this sample was also imaged by TEM (Figure 2.6 A). From this TEM, a size histogram was made using the ImageJ software (Figure 2.6 B). This showed the particles to have an average size of 6nm with a standard deviation of ±4nm. While this standard deviation is larger than desired in most cases, and likely

A.

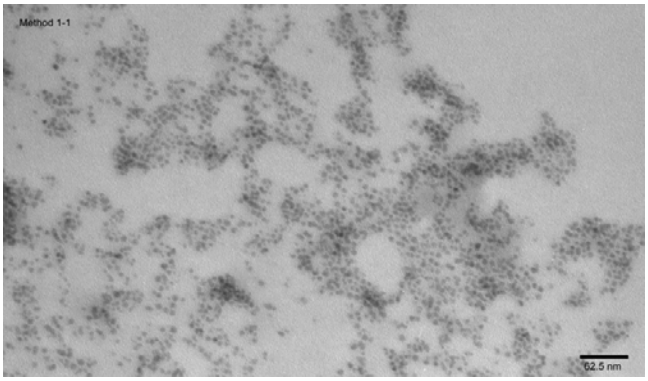

B.

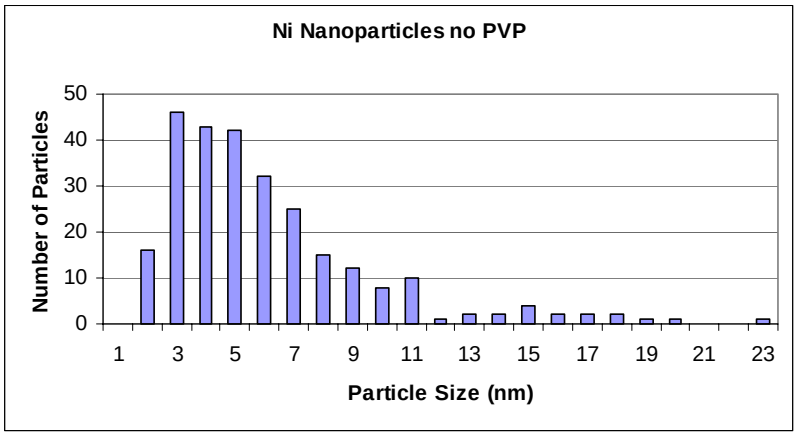

Figure 2.6 A.TEM of nickel nanoparticles and **B.** the resulting particle size distribution histogram

caused by a lack of addition capping agent such as PVP in the reaction, it was not considered a detriment to our purposes at this time.

By making minor changes to reaction time and temperature, the same nanoparticle synthesis method used successfully for nickel nanoparticle formation was also used for the formation of nanoparticles of copper, cobalt, ruthenium, rhodium and iridium. With copper, both CuCl and $CuCl_2$ were examined as nanoparticle precursors (Equation 2.6 and 2.7).

$$4CuCl + N_2H_4 + 4NaOH \rightarrow 4Cu + 4NaCl + 4H_2O + N_2 \qquad \text{(Equation 2.6)}$$

$$2CuCl_2 + N_2H_4 + 4NaOH \rightarrow 2Cu + 4NaCl + 4H_2O + N_2 \qquad \text{(Equation 2.7)}$$

With both, copper salt (0.5mmol) and solid sodium hydroxide (1.8mmol) were dissolved in ethylene glycol (25mL) at 60°C with vigorous stirring. After complete dissolution of solid reactants, hydrazine monohydrate (0.3mL, 6.2mmol) was added, and the mixture continued to react for 1 hour at 60°C. Nanoparticles made from each salt were analyzed both by UV-vis and by TEM imaging. Copper nanoparticles exhibit a Plasmon band traditionally at 570nm in the UV-vis.[50] The broader the band is, the broader the size distribution of the nanoparticles. $CuCl_2$ appears to produce a very broad size distribution of particles (Figure 2.7) while the particles from CuCl are of a much narrower size range (Figure 2.8).

This was confirmed when TEM imaging was used to look at the particles made from both $CuCl_2$ (Figure 2.9) and CuCl (Figure 2.10). The actual particle size distribution determined from these images is consistent with the general distribution obtained from the UV-vis, as the particles formed from $CuCl_2$ were found to have an

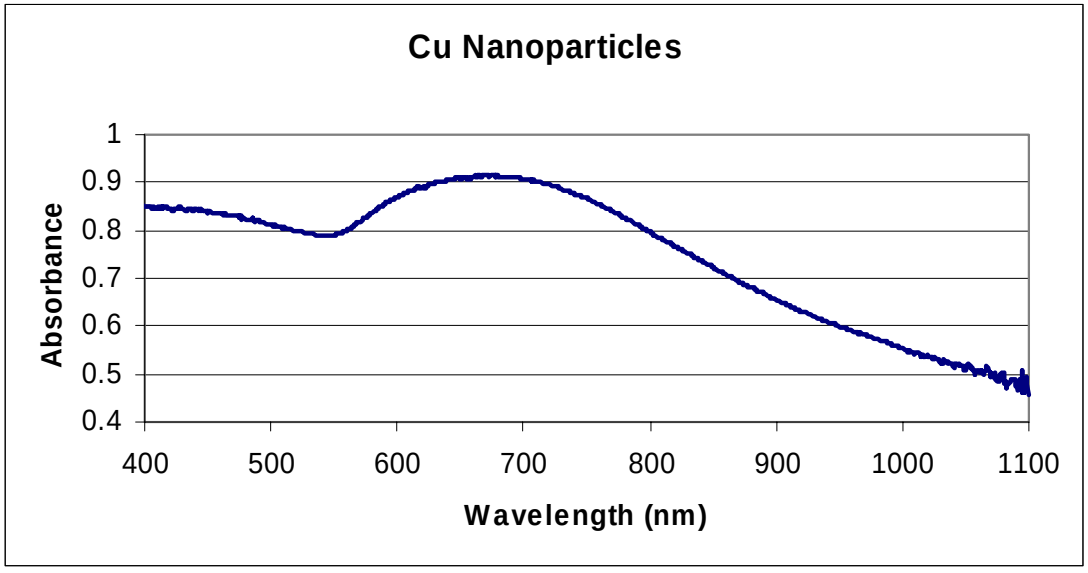

Figure 2.7 UV-vis of Cu nanoparticle solution formed from $CuCl_2$ precursor

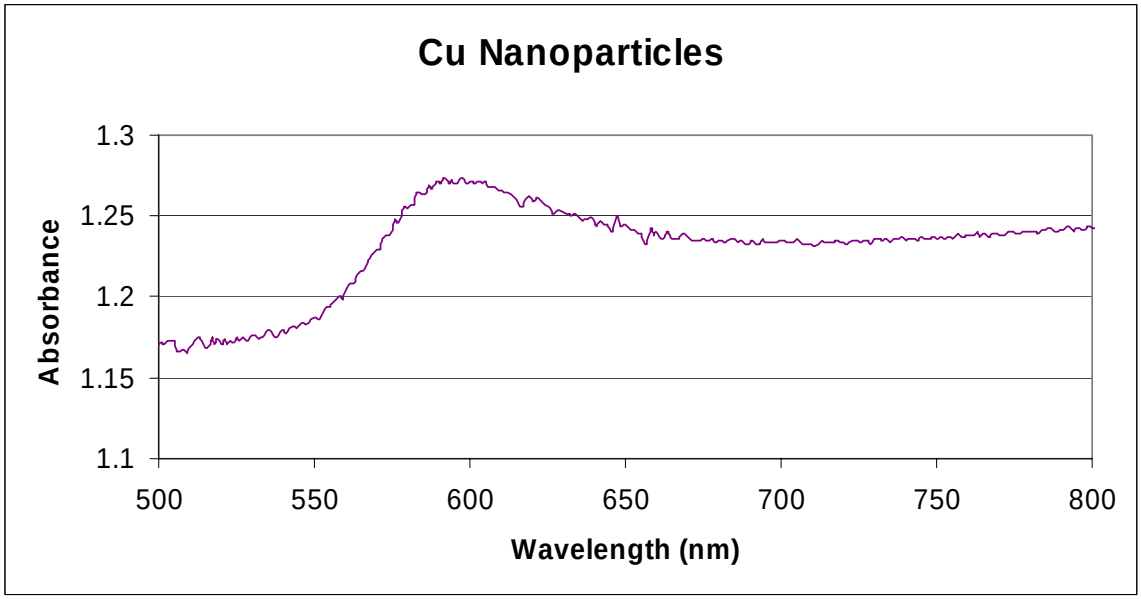

Figure 2.8 UV-vis of Cu nanoparticles formed from CuCl precursors

A. 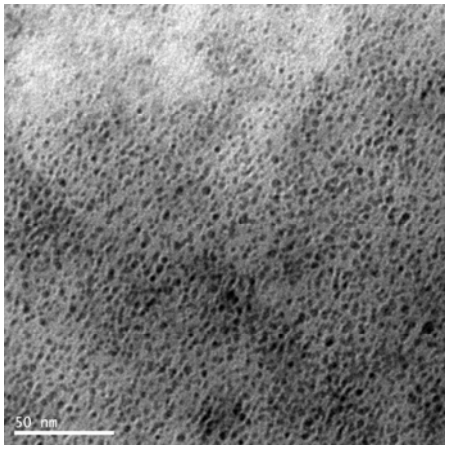

B. 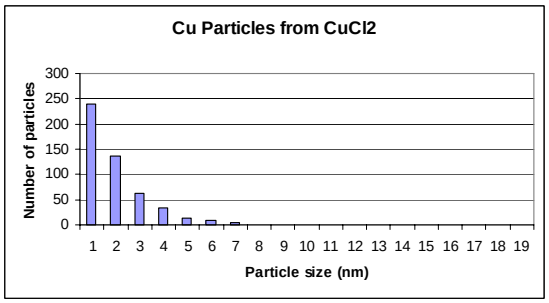

Figure 2.9 A. TEM image and **B**. size histogram of Cu particles from $CuCl_2$

A. 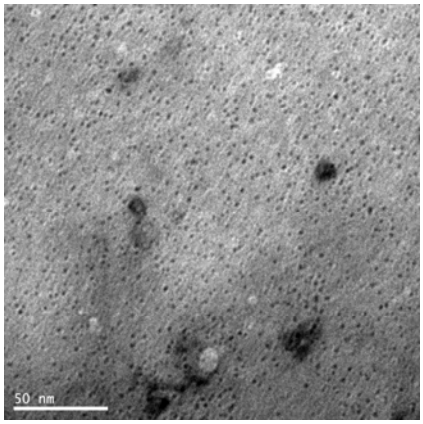

B. 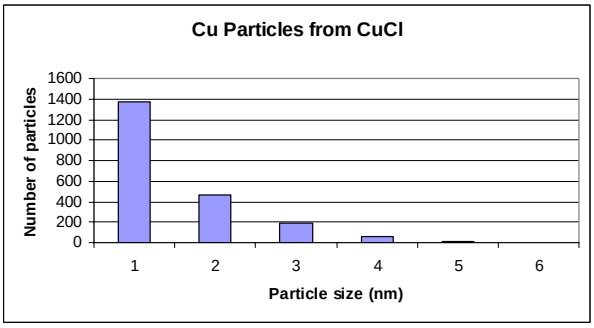

Figure 2.10 A. TEM image and **B**. size histogram of Cu particles from CuCl

average size of 2.0nm ±1.7nm (Figure 2.9) while the particles from CuCl were only 1.4nm ± 0.90nm (Figure 2.10). Isolated yield and conversion, as determined by chlorine analysis, were also examined for the two different precursors. Particles with CuCl as precursor were isolated in 92% yield, and showed complete conversion (0% Cl remaining). The particles from $CuCl_2$ appeared to have higher 99% yield, but chlorine analysis indicated only 99.48% conversion (0.58% Cl remaining).

XRD analysis confirmed the formation of only copper(0), not copper oxide in the particles made from CuCl (Figure 2.11), while the particles from $CuCl_2$ showed a mix of copper(0) and Cu_2O formation (Figure 2.12)[51]. Based on these results, all further copper work was carried out using CuCl as the precursor molecule.

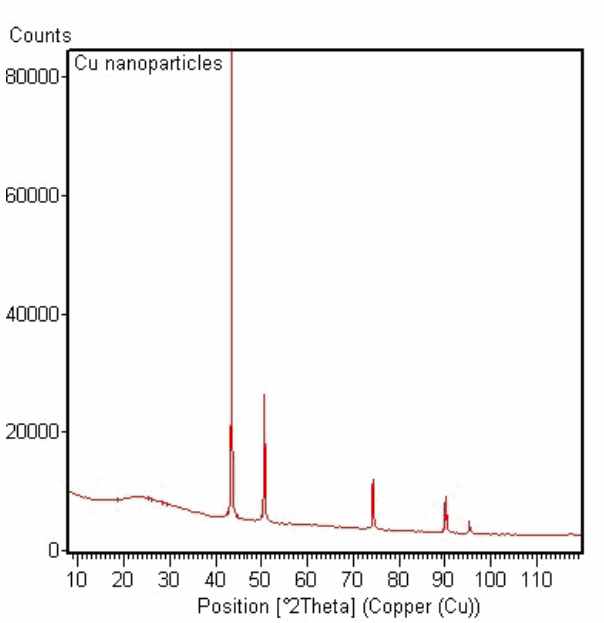

Figure 2.11 XRD of particles made from CuCl showing only Cu(0) formation

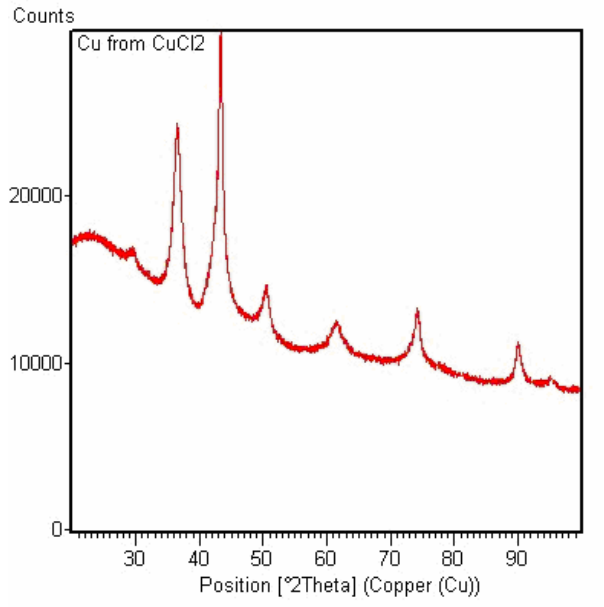

Figure 2.12 XRD of particles made from $CuCl_2$ showing a mix of Cu(0) and Cu_2O

The cobalt salt $CoCl_2$ follows a similar reduction reaction to the nickel salt (Equation 2.8)

$$2CoCl_2 + N_2H_4 + 4NaOH \rightarrow 2Co + 4NaCl + 4H_2O + N_2 \qquad \text{(Equation 2.8)}$$

However, unlike nickel, before reduction occurs, cobalt forms a complex with hydrazine, $Co(N_2H_4)_6^{2+}$.[52] This complex gives the solution a characteristic pink color and is known to be very stable.[34,52] The actual reduction took place at elevated temperature (190°C) for twelve hours. All other reaction conditions and concentrations remained the same.

Before particles were isolated, UV-vis was used to check for complete disappearance of starting material, by comparing the signal obtained from the $CoCl_2$ starting solution and the post-reaction solution (Figure 2.13). From this, it appeared that the reaction had gone to completion as $CoCl_2$ showed a peak with a wavelength of maximum absorption at 529nm, which was not present in the post-reaction solution.

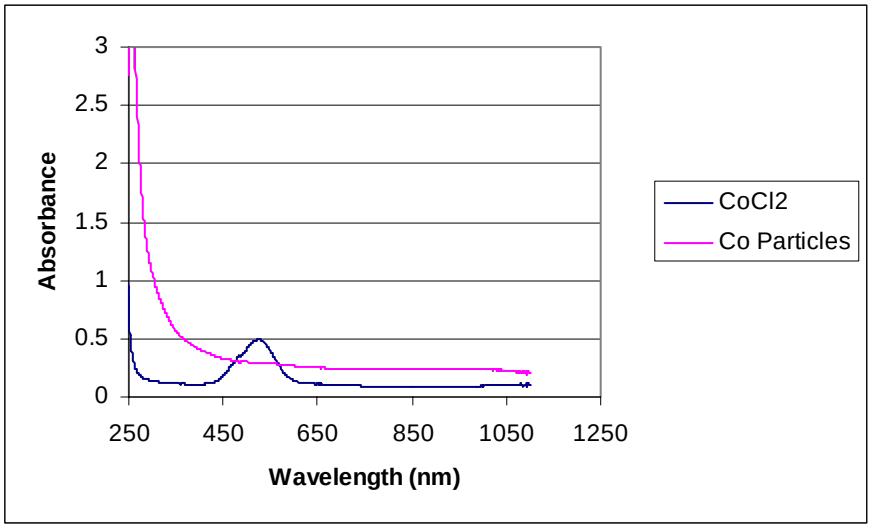

Figure 2.13 UV-vis spectrum of $CoCl_2$ starting solution and Co nanoparticle solution

Particles were collected by centrifuge, washed with ethanol, and dried overnight in a vacuum oven set at 80°C. The dried particles were magnetic, as expected for cobalt, and isolated in 67% yield. Cl elemental analysis showed no Cl remaining either in the isolated particles or in the collected supernatant layer.

TEM imaging showed a sample of Co particles evenly dispersed on the solid support, appearing in the image as black spots (Figure 2.14 A). From this image, a particle size histogram was developed (Figure 2.14 B). The Co particles formed were found to be 1.2nm ±0.9nm in diameter.

A.

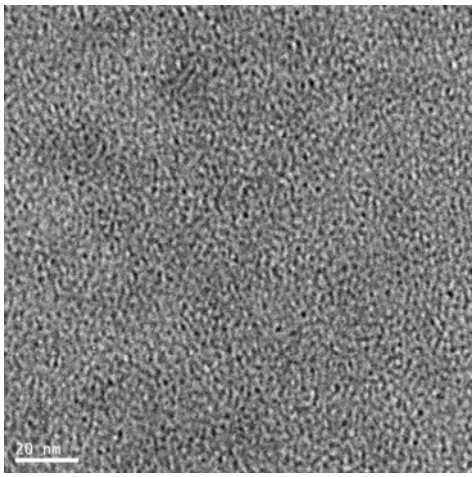

B.

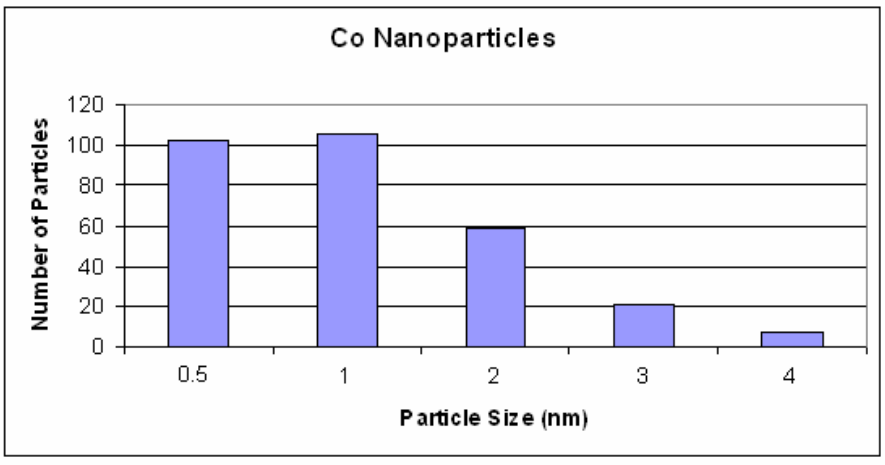

Figure 2.14 A. TEM image of Co nanoparticles and **B.** the resulting size histogram

XRD analysis of these particles showed only two small peaks. This is typical, as it is difficult to obtain clear sharp peaks for Co metal in such a small nanoparticle size range. However, these peaks were consistent with two of the peaks for face centered cubic cobalt(0).

To form ruthenium nanoparticles, reduction of the $RuCl_3$ salt was carried out (Equation 2.9).

$$4\ RuCl_3 + 12NaOH + 3N_2H_4 \rightarrow 4Ru + 12NaCl + 12H_2O + 3N_2 \qquad \text{(Equation 2.9)}$$

The same concentrations and procedure were followed as with previous metals, however both reaction temperature and time were increased. It was not unexpected that ruthenium required a higher temperature to reduce, as in the literature methods studied, reduction was carried out at temperatures ranging from 120°C to 198°C.[30-32,55] $RuCl_3$ (0.5mmol) and solid sodium hydroxide (1.8mmol) were dissolved in ethylene glycol (25mL) at 60°C with vigorous stirring. After complete dissolution of solid reactants, hydrazine monohydrate (0.3mL, 6.2mmol) was added. Reaction temperature was increased to 120°C and was allowed to react with stirring for 24 hours.

UV-vis analysis was used to look for disappearance of starting material. This appeared to indicate a small amount of starting material remaining, as the salt solution showed a sharp peak with a wavelength of maximum absorption at 407nm which remained as a slight shoulder in the post-reaction solution (Figure 2.15). To confirm this, particles were collected by centrifuge, washed with ethanol and dried. Isolated yield was not calculated, however, from chlorine elemental analysis a 99.4% conversion was

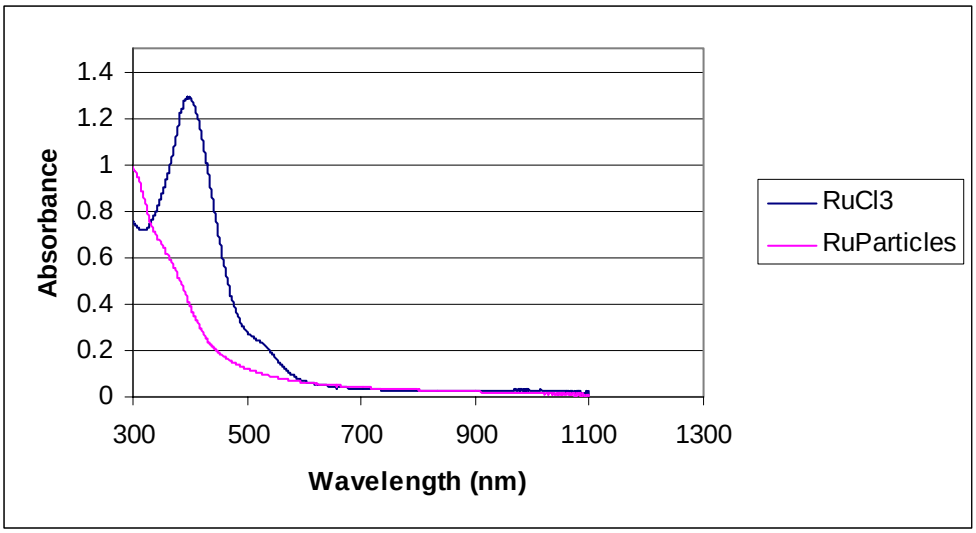

Figure 2.15 UV-vis spectrum of $RuCl_3$ salt solution and Ru nanoparticle solution

calculated (0.65% Cl remaining) consistent with the UV-vis results. These particles were imaged by TEM to look at shape and size distribution (Figure 2.16 A), which is represented by a size histogram (Figure 2.16 B). From this, the Ru particles formed were found to be 1.3nm ± 0.8nm in diameter.

A. 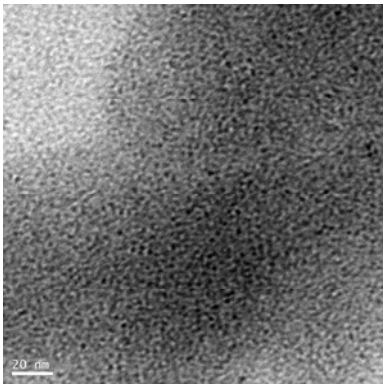

B. 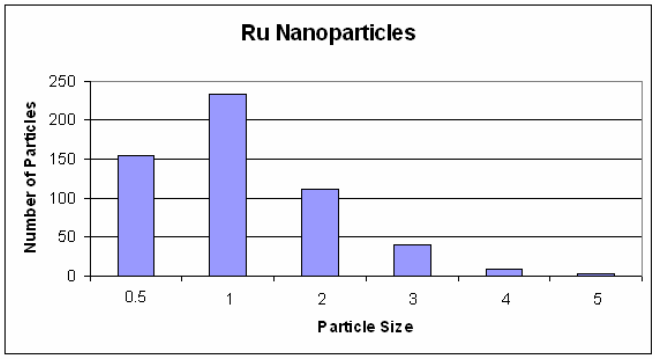

Figure 2.16 A. TEM of Ru nanoparticles and **B.** the resulting size histogram

As with Co, when these particles were analyzed by XRD, only very faint peaks were seen. However, these peaks were consistent with the expected hexagonal ruthenium signal.

To synthesize rhodium nanoparticles, the salt $RhCl_3 \cdot 3H_2O$ was used as a precursor (Equation 2.10). The standard procedure and concentrations were used to carry

$$4RhCl_3 \cdot 3H_2O + 12NaOH + 3N_2H_4 \rightarrow 4Rh + 12NaCl + 15H_2O + 3N_2 \qquad \text{(Equation 2.10)}$$

out this reduction. However, as with ruthenium, the reaction time and temperature were increased. This was not unexpected based on literature where rhodium salt reductions are run anywhere from 90°C to 220°C.[36-37] For this synthesis, temperature was raised to 190°C and reacted for 2 hours. UV-vis analysis was used to check for disappearance of starting material and chlorine analysis indicated 99.2% conversion (0.85% Cl remaining). The particles were isolated in 76% yield. It was believed that the unaccounted for rhodium remained in suspension as nanoparticles.

These particles were also imaged by TEM to look at particle shape and size distribution (Figure 2.17 A). In these images, the individual particles can clearly be seen as the dark spots within an ethylene glycol matrix. From this imaging the size histogram showed a particle size of 2nm ±1nm in diameter (Figure 2.17 B). When analyzed by XRD, though the resulting peaks were broad, they clearly showed the expected pattern for face centered cubic rhodium metal (Figure 2.18).

A.

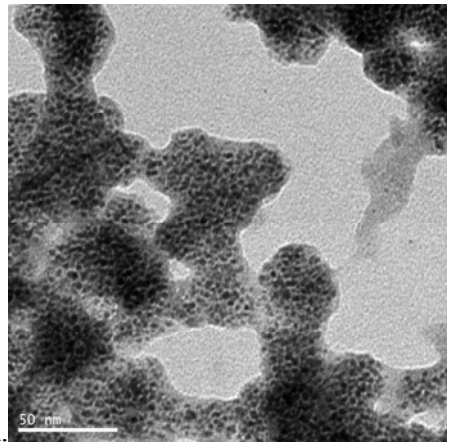

B.

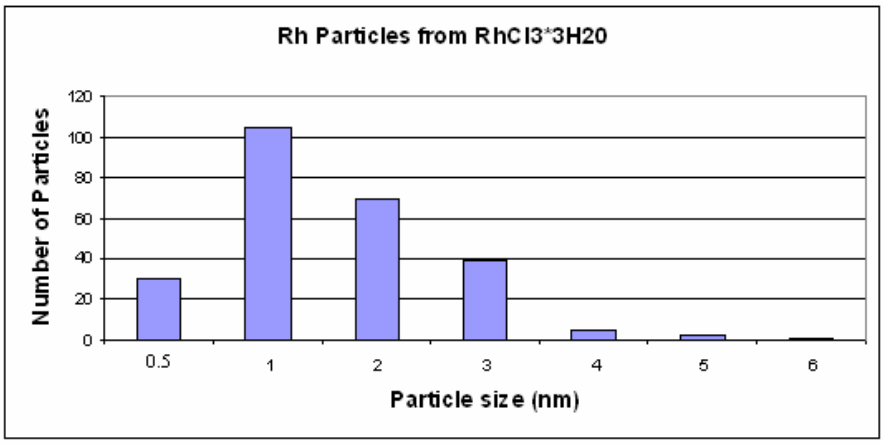

Figure 2.17 A. TEM of Rh nanoparticles and **B**. the resulting size histogram

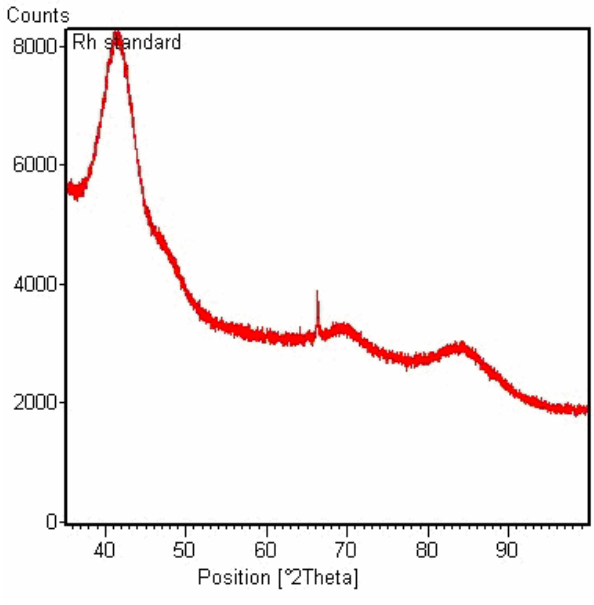

Figure 2.18 XRD of rhodium nanoparticles

To synthesize iridium nanoparticles, the salt $IrCl_3 \cdot 3H_2O$ was used. The reaction and stoichiometry of this reduction are identical to that of the rhodium reaction (Equation 2.11).

$$4IrCl_3 \cdot 3H_2O + 12NaOH + 3N_2H_4 \rightarrow 4Ir + 12NaCl + 15H_2O + 3N_2 \qquad \text{(Equation 2.11)}$$

For this synthesis, the same concentrations and procedure were used as with previous metals, however, the reduction was carried out at 190°C for 3 hours. By UV-vis analysis, complete conversion occurred, as the starting salt solution showed a double humped peak with maxima at 460nm and 499nm, and the product nanoparticle solution showed neither of these (Figure 2.19).

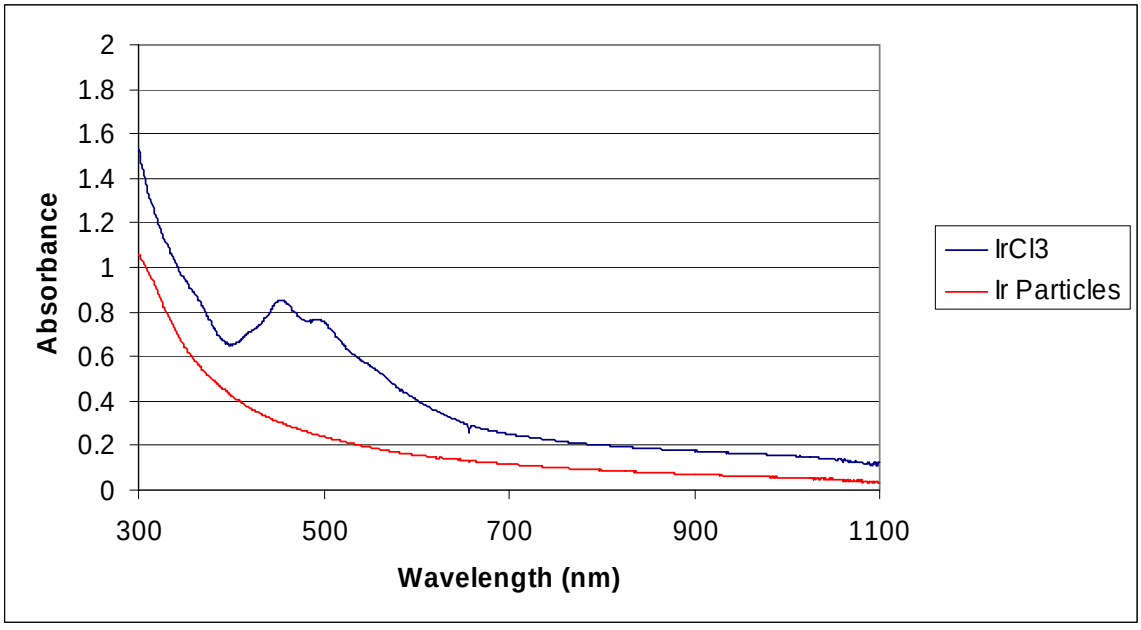

Figure 2.19 UV-vis spectrum of $IrCl_3$ starting salt and the resulting nanoparticle solution

Particles were isolated in 96% yield. Based on chlorine analysis, the reduction occurred with 98.4% conversion (0.91% Cl remaining).

These particles were imaged by TEM to determine particle shape and size distribution (Figure 2.20 A). From this, a size histogram was developed (Figure 2.20 B) which showed the particles to be 2nm ± 1nm in diameter.

A.

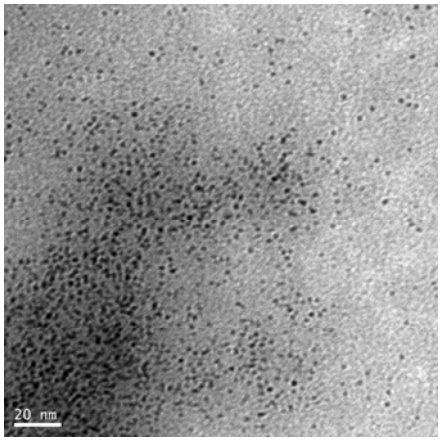

B.

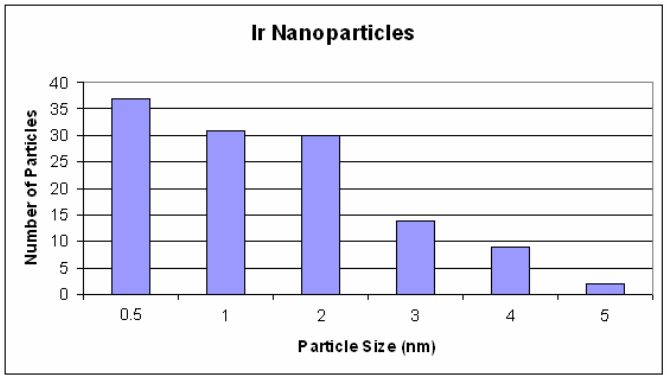

Figure 2.20 A. TEM of iridium nanoparticles and **B.** the corresponding size histogram.

2.3.1.2 Supported Nanoparticle Synthesis

To support the nanoparticles on silica, three methods were initially investigated using nickel as the catalyst metal. These methods were: (1) isolating the nanoparticles and adsorbing them onto a dried silica surface by solvent evaporation at elevated

temperature,[20] (2) adsorbing $NiCl_2$ onto the silica surface, then reducing it with hydrazine monohydrate, and (3) adding silica to the ethylene glycol solution during nanoparticle formation and allowing them to adsorb onto the surface.

In method one, the silica was first dried by heating at 500°C. This silica was stirred with nickel nanoparticles in ethanol solution for 12 hours, then dried for 1 hour in the vacuum oven and 12 hours in a regular oven at 100°C. This produced a tan powder that showed no physical evidence of nickel on the surface. This was confirmed by XRD, in which only a single broad peak was present in the 20-30° range, which is characteristic of amorphous silica.

Method two followed the same basic procedure; however the dried silica stirred with a solution of $NiCl_2$ in water for 12 hours. This was then dried for 4 hours in the vacuum oven and 12 hours in a regular oven at 100°C. The product from this was a pale yellow powder, as the nickel chloride was now baked onto the silica surface. The $NiCl_2$ was then reduced following the same procedure as for nanoparticle formation. The solid was suspended in ethylene glycol, sodium hydroxide and hydrazine monohydrate were added, and the mixture reacted at 60°C for 1 hour with stirring. From this, a pale blue powder was collected by filtration and vacuum drying. This color was consistent with at most, a partial reduction of the $NiCl_2$. XRD analysis was performed on this sample, and as with method one, no metallic nickel was visible. The XRD shows only a characteristic amorphous silica peak (Figure 2.21). This method was repeated with similar results. Due to the low loadings, and reduction issues, as well as the fact that method two would not guarantee production of nanoparticles on the support surface, these two methods were not pursued further.

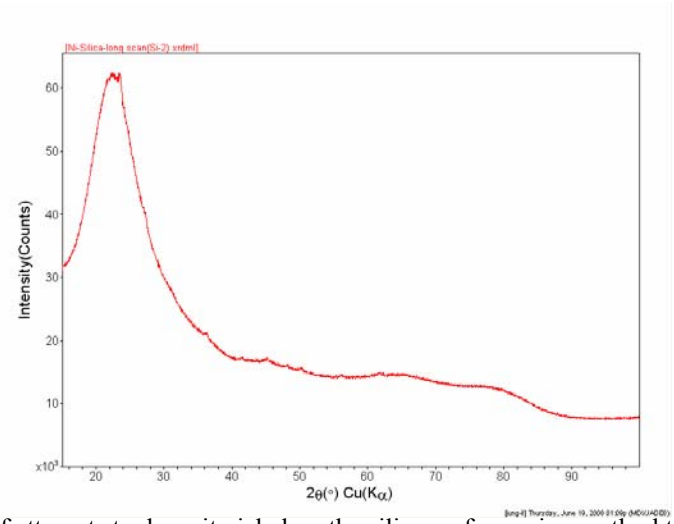

Figure 2.21 XRD of attempts to deposit nickel on the silica surface using method two showing an amorphous silica peak

For initial supported nickel catalyst samples synthesized by the third method, the nanoparticle synthesis was carried out as described in the previous section. However, instead of isolating the nanoparticles after formation, the solution was diluted with a 2:1 volume amount of ethanol (50mL of ethanol for 25mL ethylene glycol), the desired amount of silica was added directly to the mixture, and this was left to stir at room temperature for 4 days. Product was collected by filtration, washed with ethanol and dried overnight in a vacuum oven.

Using this method, a series of samples with 2-50wt.% theoretical loading of nickel were synthesized. These samples were made on both 40-75μM sized silica (Table 2.1) and 75-200μM sized silica (Table 2.2), both with 150Å pores. All were made at the scale described earlier, (0.5mmol of $NiCl_2$ in 25mL of ethylene glycol) unless otherwise noted. These others were made on a five times larger scale (2.5mmol $NiCl_2$, 9mmol NaOH, 31mmol hydrazine monohydrate dissolved in 125mL of ethylene glycol). All samples were analyzed by chlorine analysis to determine the extent of reduction. If no

chlorine was present, as was the case with all samples tested, the reaction was assumed to proceed to 100% conversion. Theoretical percent loading was calculated from the initial amount of nickel introduced into the system as nickel chloride, while nickel metals elemental analysis by atomic absorption (performed by Columbia Analytical Services) was used to determine the actual percent loading after product isolation.

Following the synthesis of these samples, a few modifications were made to the procedure. Nickel chloride and sodium hydroxide were dissolved in ethylene glycol at 60°C. The desired amount of silica was then added to the reaction mixture, with vigorous stirring. Hydrazine monohydrate was added and the entire mixture reacted at 60°C for 1

Table 2.1 Analysis of all samples made on 40-75μM sized silica

Entry	Silica size (μm)	% Ni	% Cl Found	% Ni Found
1	40-75	9	0.0	5.1
2	40-75	17	0.0	7.8
2	40-75	17	0.0	7.3
3	40-75	5	0.0	1.4
4	40-75	50	0.0	8.4
5	40-75	10	0.0	2.7
6	40-75	15	0.0	6.7
7	40-75	20	0.0	6.8

Table 2.2 Analysis of all samples made on 75-200μM sized silica

Entry	Silica size (μm)	% Ni	% Cl Found	% Ni Found
1	75-200	10		2.6
2	75-200	5	0.0	1.1
3	75-200	15	0.0	3.5
4	75-200	10	0.0	2.6
5	75-200	20	0.0	2.7
6[a]	75-200	2	0.0	0.4
7[a]	75-200	10	0.0	2.9
8[a]	75-200	6	0.0	2.2

a. Samples made on larger scale

hour. After an hour, all heating was stopped, and the solution stirred at room temperature overnight. Product was isolated by centrifugation, washed with ethanol, and dried overnight in a vacuum oven at 80°C

This method, with the addition of silica prior to reduction of the metal salt, was used to synthesize supported metal samples of nickel, copper, ruthenium, rhodium, and iridium. Cobalt, however, required a few modifications. Initially $CoCl_2$ (2.5mmol) and sodium hydroxide (9mmol) were dissolved in 125mL ethylene glycol. Silica (1.69g for 8% loading) was added with vigorous stirring. Hydrazine monohydrate (31mmol) was added and the heat raised to 190°C for 12 hours to carry out the reduction. When the reaction was stopped, the product was isolated by centrifugation, however, it was a dark brown powder. This was not the expected color, and it was not magnetic, indicating that metallic cobalt was not formed. In literature it is known that cobalt can form silicate complexes when reduced in the presence of silica.[53-54] To address this, in all further deposition reactions, Co particles were formed first. The desired amount of silica was then added to the system and left to stir for three days at room temperature. Catalyst product was collected by centrifugation, washed with ethanol, and dried overnight in a vacuum oven at 80°C.

All supported samples were made using spherical silica with a range of 75-200μm area and 150Å pores. Supported samples of each metal were analyzed by Cl and metals elemental analysis to determine conversion and actual percent loading, XRD to confirm formation of the desired metal, scanning electron microscopy (SEM) imaging to look at metal distribution on the surface, and with a Brunauer, Emmett and Teller (BET)

machine to determine surface area and pore volume. Table 2.3 shows a comparison of the values found for a representative sample of each of these different metals.

Table 2.3 Comparison of conversion, metal loading, surface area and pore volume

Metal	Metal % Load	% Cl Found[A.]	BET Surface Area (m^2/g)	Pore Volume (cm^3/g)
Ni	3.0%	<0.25%	167 ± 5	0.9 ± 0.1
Cu	2.6%	0%	141 ± 4	0.8 ± 0.1
Co	3.1%	0%	96 ± 3	0.6 ± 0.1
Ru	3.1%	<0.25%	195 ± 5	0.8 ± 0.1
Ir	3.4%	0%	163 ± 5	0.9 ± 0.1
Rh	3.6%	<0.25%	109 ± 3	0.6 ± 0.1

A. 0% - No Cl detected. <0.25% - Trace Cl detected, but below the quantitative analysis limits of the instrument

It was found that supported samples of each metal were synthesized in a narrow actual loading range (2.6%-3.6%). Also, all were found to go to complete or near complete conversion as Cu, Ir and Co showed no remaining Cl present in the system and Ni, Ru, and Rh showed only traces (<0.25%). The uncoated silica was analyzed and found to have a BET surface area of 168 ± 5m^2/g and a pore volume of 0.9 ± 0.1cm^3/g. Compared to this, depositing the nanoparticles on the silica surface did not appear to cause a substantial change in either surface area or pore volume, except in the cases of cobalt and rhodium, where both values decreased. For cobalt, this was a decrease of approximately 50% (57% decrease in surface area, 33% decrease in pore volume) while rhodium showed a decrease of 35% percent in surface area and 33% in pore volume.

As with the nanoparticles themselves, Co, Rh, Ru and Ir were difficult to see by XRD, especially as the amorphous silica support produces such a large peak. However, what peaks were present corresponded with those expected for the respective metals. Cobalt, for example showed peaks that were small, but characteristic of face centered cubic cobalt (Figure 2.22). Nickel and copper samples both clearly showed the peaks

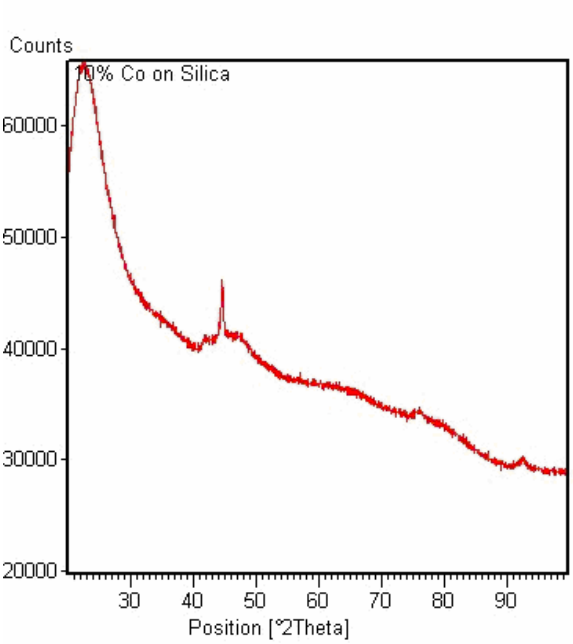

Figure 2.22 XRD of supported cobalt showing characteristic face centered cubic peaks

expected for face centered cubic metal crystals of each of these two species (Figure 2.23 and Figure 2.24), and neither showed any evidence of oxide formation within the detection limits of the instrument.

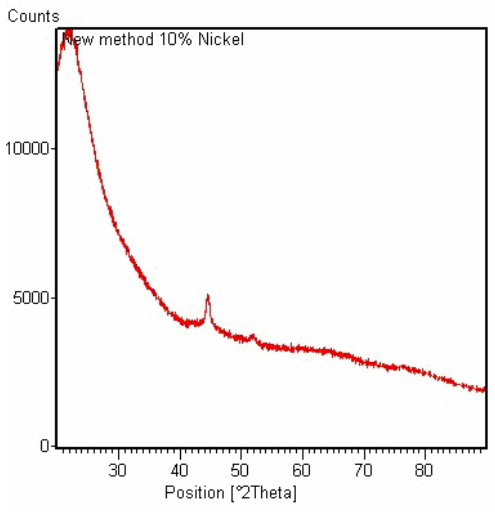

Figure 2.23 XRD of supported nickel sample

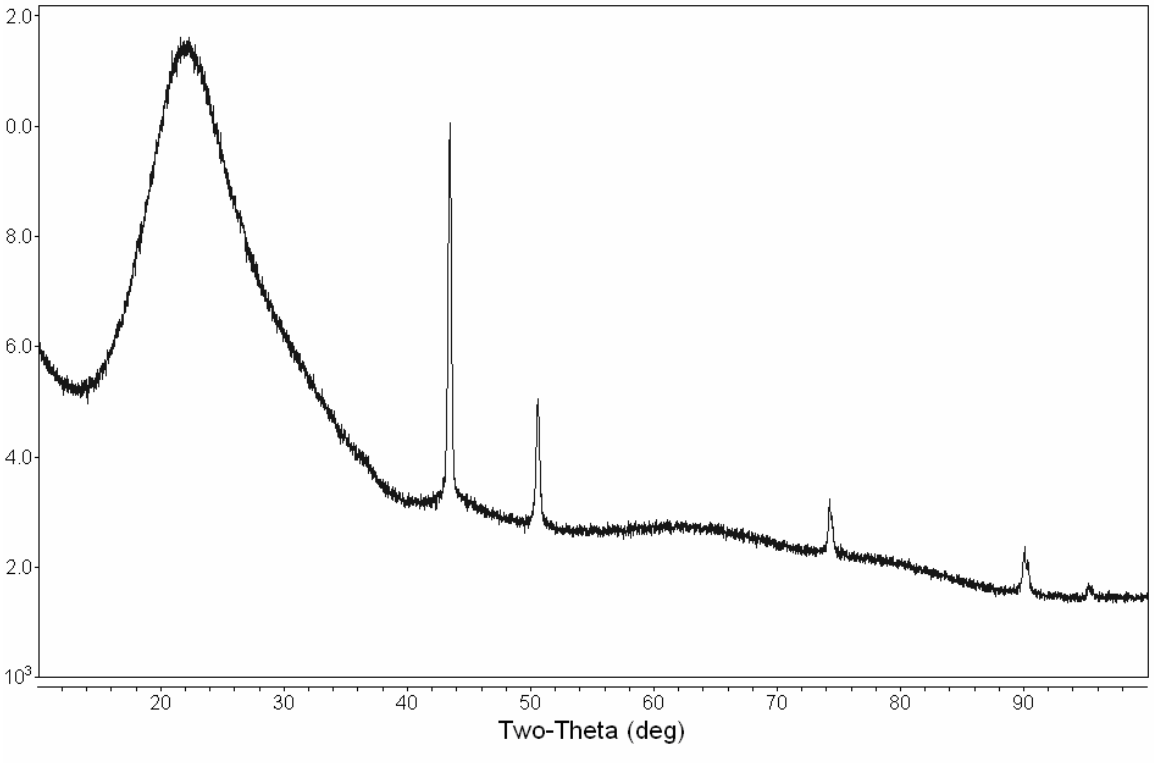

Figure 2.24 XRD of supported copper sample

SEM imaging allowed us to examine whether the different metals retained their nano-scale character on the silica support surface, as well as how the metal particles were distributed on the support surface. In all images, the metals are visible as white or light colored particles on a dark background, which is the surface of the silica support. Nickel (Figure 2.25) and copper (Figure 2.26), showed a very small amount of clustering, but in both the supported particles remained on the nano-scale. The other metals, rhodium, ruthenium, cobalt, and iridium, showed a larger amount of clustering, bringing the metal particles in these cases up to a micrometer size range (Figure 2.27 and Figure 2.28).

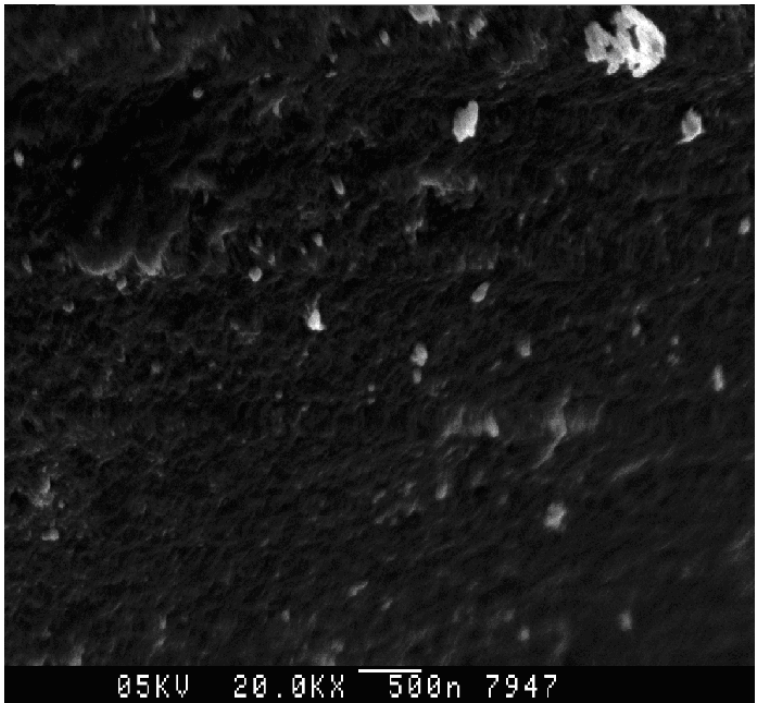

Figure 2.25 SEM of supported nickel catalyst

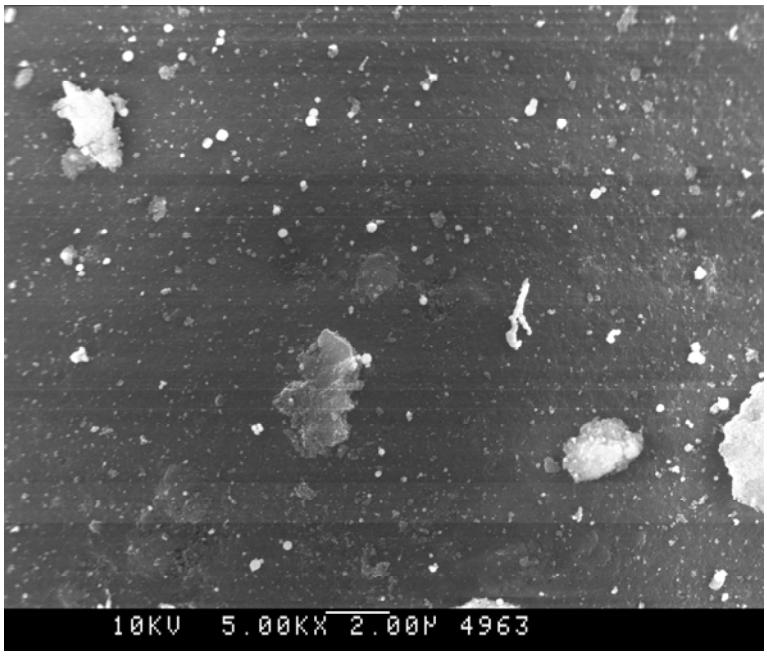

Figure 2.26 SEM of supported copper catalyst

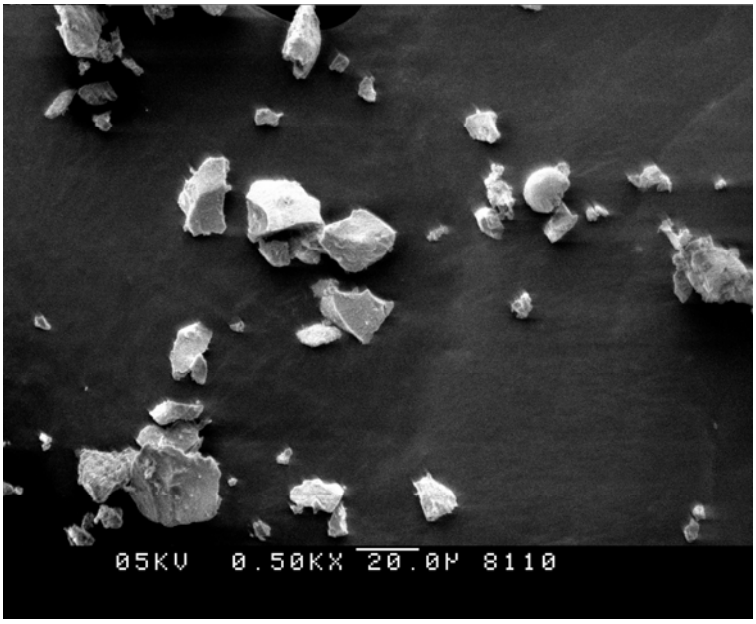

Figure 2.27 SEM image of iridium particles supported on a silica surface

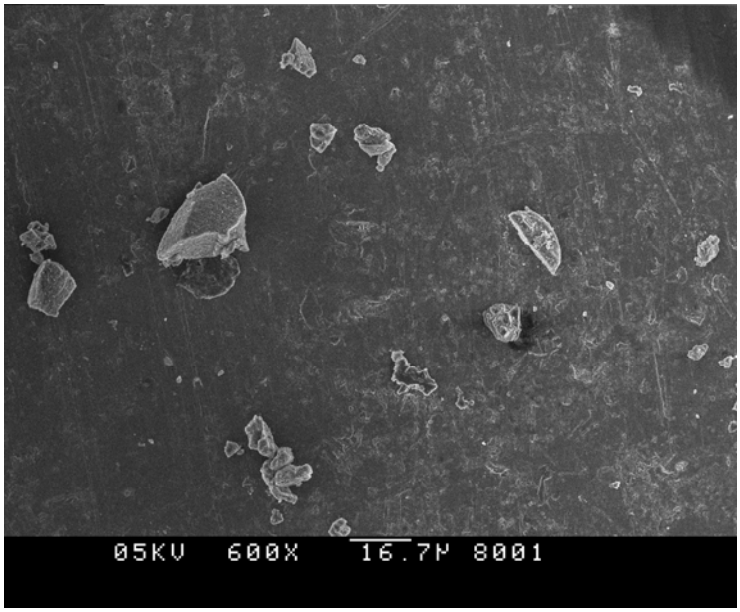

Figure 2.28 SEM image of ruthenium particles on silica surface

Initial work was performed on a method for increasing the total catalyst loading by adding a second layer of nanoparticles to an already synthesized sample. A catalyst sample with 8.4% nickel by weight (Entry 4, Table 2.1) was chosen. The goal was to increase the total loading to 20% by weight, so the necessary amounts of $NiCl_2$ and sodium hydroxide were dissolved in ethylene glycol. The 8.4% sample was added, and reduction was carried out with hydrazine monohydrate. Product was collected by centrifugation, washed with ethanol, and dried in the vacuum oven. Elemental analysis on this sample showed no Cl present in the system, and a new nickel loading of 14%. SEM imaging also showed a visible increase in the amount of nickel present on the surface (Figure 2.29). However, it clustered with the nickel already present on the surface, increasing the metal particle size into the micrometer range. Future work will focus on developing and optimizing this layering method as a way of producing high metal loading catalysts.

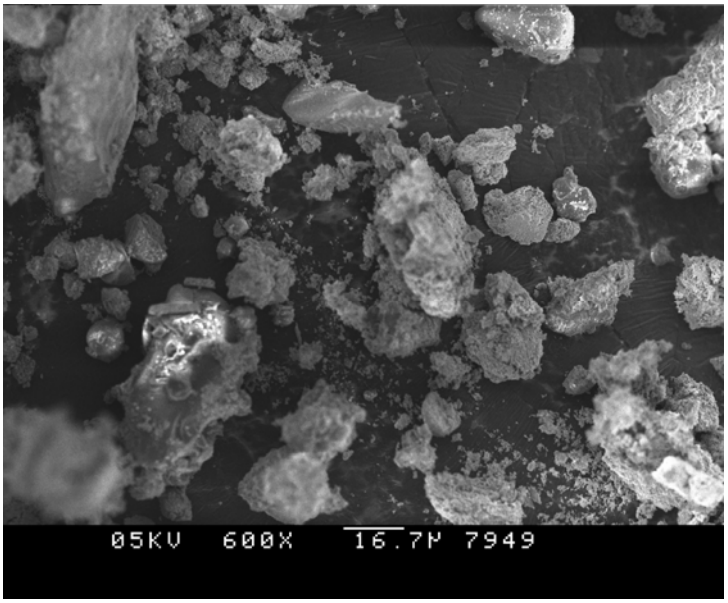

Figure 2.29 SEM image of particle surface with second layer of nickel nanoparticles added

2.3.1.3 Supported Catalyst Synthesis by the Shell Method

The Shell 405 iridium catalyst is commercially available and is the primary catalyst used for chemical propulsion with hydrazine as propellant. Its synthesis was described in a Shell patent in 1978.[24] The patent details the formation of iridium and ruthenium catalysts by reduction of these metals from the corresponding chloride salts. The adsorption of the metal onto the support proceeds step wise. First, the chloride salt is adsorbed by immersion of the support in a basic aqueous solution of the salt. Then, the impregnated-support is dried and reduced using a stream of H_2/N_2 gas at elevated temperature (>400°C). The process is then repeated up to 20 times, forming up to 20 consecutive, metallic layers around the support.

This catalyst contains 31-33% iridium deposited in layers on the surface of the alumina support giving it a BET surface area of 120-121m^2/g and a pore volume of 0.22-0.25cm^3/g. Due to the high loading applied as layers, none of the support surface is exposed. Instead the entire particle is encased in a semi-porous layer of iridium metal, which can be seen with SEM imaging (Figure 2.30).

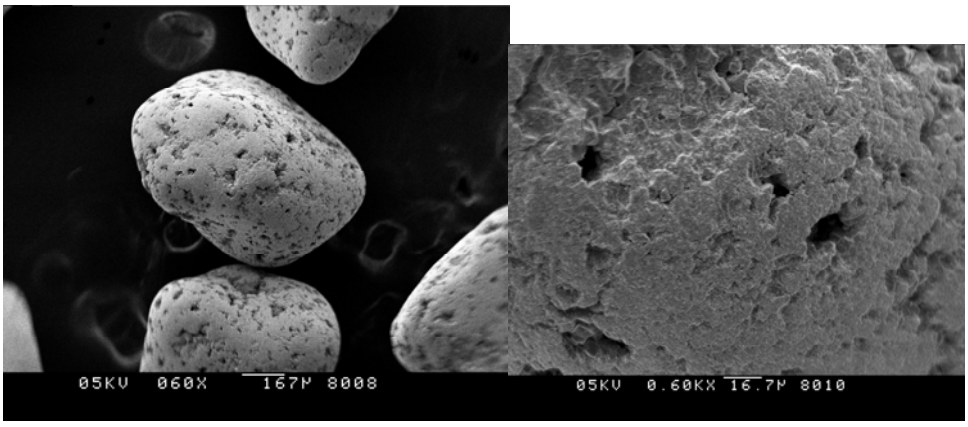

Figure 2.30 SEM images of the surface of Shell 405 commercial catalyst

It should be highlighted that in forming this catalyst, the aqueous solutions of metal chloride are dilute (0.6 M), leading to a single layer coating of metal chloride on the support's surface and yielding to a thin metal layer after reduction. The catalyst loading can be easily adjusted by increasing or decreasing the number of layers applied and the surface area of the silica becomes very important as the aim is to fully cover the support. Reduction occurs simply by reaction of hydrogen gas with the metal chloride to form the metal and HCl gas. For our research, initial syntheses were performed using nickel (Equation 2.12)

$$NiCl_2 + H_2 \rightarrow Ni + 2HCl \qquad \text{(Equation 2.12)}$$

In our initial attempts, a 2.7M basic $NiCl_2$ solution was made and heated to 50°C for 15 minutes. After cooling to room temperature, silica was added to this solution. It stirred for 20 minutes, was filtered, and was dried using a hot plate set at 400°C and a heat gun. The silica was returned to the liquid and this filtering and drying process was repeated twice to ensure complete deposition of all $NiCl_2$ onto the solid surface. Reduction was carried out using a gas mixture of 40:60 H_2:N_2 gas at 250°C for 5 hours. Chlorine elemental analysis was performed on two samples made by this method to study conversion, and they were found to have 30% and 47.5% conversions respectively. The reaction was continued for another 20 hours, however, conversion only increased by another 3.5%.

Most likely only the outermost layer of $NiCl_2$ on the silica surface was being reduced. The Shell method was therefore optimized with nickel chloride (0.7mmol)

being dissolved in distilled water (3mL) to form a 0.2M solution. This was heated to 90°C with stirring. At temperature 30% ammonium chloride solution (2mL) was then added slowly, followed by the addition of silica (2g.) to form a 2 wt.% loading of the nickel. The mixture was stirred at room temperature for 30 minutes, followed by stirring and heating at 150°C until all water was removed from the system. This was then reduced at >300°C in a gas stream of 40:60 hydrogen and nitrogen for 5 hours.

Using this same method, samples were made with 2%, 5%, 10%, 20%, and 50% theoretical loading (Table 2.4) of nickel. Each sample was made using 2 grams of silica as support material, so the loadings were varied by changing the amounts of $NiCl_2$ and water used to make the impregnation solution. Because of this method, the $NiCl_2$ solution molarity increased with each sample (0.225M-1.13M), so it is not surprising that at higher weight loadings (10-50% theoretical weight), and correspondingly higher molarities, not all $NiCl_2$ was reduced as evidenced by chloride elemental analysis (Table 2.4). However, at lower weight loadings (2% and 5% theoretical weight) all $NiCl_2$ has been reduced. Also at lower weight loadings, the actual nickel percent loading is very close to what is expected (1.7% vs. 2% and 4.5% vs. 5%). However, that decreases as the theoretical loading increases up to the 50% theoretical sample actually having only 22% nickel on the surface.

Table 2.4 Supported nickel samples prepared by the Shell method

Entry	$NiCl_2$ (g)	H_2O (mL)	Mol.	30% NH_3OH (mL)	Theoretical % Ni	Actual % Ni	% Cl Found
1	0.088	3	0.226	2	2	1.7	<0.25
2	0.22	5	0.338	5	5	4.5	<0.25
3	0.44	7	0.485	10.1	10	7.2	2.23
4	0.88	10	0.679	20.2	20	13.2	1.23
5	2.2	15	1.13	50.5	50	21.6	9.76

This method was extended to use with CuCl as well as $CoCl_2$. Both can also be reduced with hydrogen gas to form the metal species and HCl gas (Equations 2.13 and 2.14).

$$2CuCl + H_2 \rightarrow 2Cu + 2HCl \quad \text{(Equation 2.13)}$$

$$CoCl_2 + H_2 \rightarrow Co + 2HCl \quad \text{(Equation 2.14)}$$

Samples were made with 17%, 27%, and 50% theoretical copper loading by weight (Table 2.5), as well as 2%, 5% and 10% theoretical cobalt loading by weight (Table 2.6). For all samples, 2g of 75-200μM sized silica with 150Å pores was used and the loading was varied by changing the amount of metal chloride salt and water used in preparation, so molarity of the solution increases from 0.23M-0.48M with higher percent loading (Table 2.5 and 2.6).

Table 2.5 Supported copper samples prepared by the Shell method

Entry	CuCl (g)	H_2O (mL)	Mol.	30% NH_3OH (mL)	Theoretical % Cu	% Cl Found
1	0.62	2	0.31	0.2	17	<0.25
2	1.14	5	0.23	0.5	27	4.08
3	3.12	7	0.45	1	50	11.30

Table 2.6 Supported cobalt samples prepared by the Shell method

Entry	$CoCl_2$(g)	H_2O (mL)	Mol.	30% NH_3OH (mL)	Theoretical % Co	Actual % Co	% Cl Found
1	0.09	3	0.231	0.15	2	1.9	1.13
2	0.22	5	0.339	0.4	5	3.9	0.92
3	0.44	7	0.484	0.9	10	7.6	1.67

As with the nickel, a decrease in conversion is seen with this increase in percent. With copper, only the 17% sample actually went to complete conversion, while no cobalt samples achieved complete conversion.

Though complete conversion was not achieved in all cases, the 5% Ni sample, the 17% Cu sample, and the 5% Co sample were analyzed by XRD. Both the nickel and copper samples showed only the face centered cubic form of the desired metal. No oxide was present in either case. The XRD of the 5% cobalt sample showed formation of cobalt metal with a hexagonal crystal structure (Figure 2.31). This is in direct contrast to the supported nanoparticle cobalt samples which have a face centered cubic cobalt crystal structure. This may have an affect on the catalyst behavior between the two different samples as hydrazine will be interacting with a different metallic face. Though some $CoCl_2$ remained in this sample, it was not seen by XRD most likely because its amount (1.7% of the total sample) was below the detection limit of the instrument.

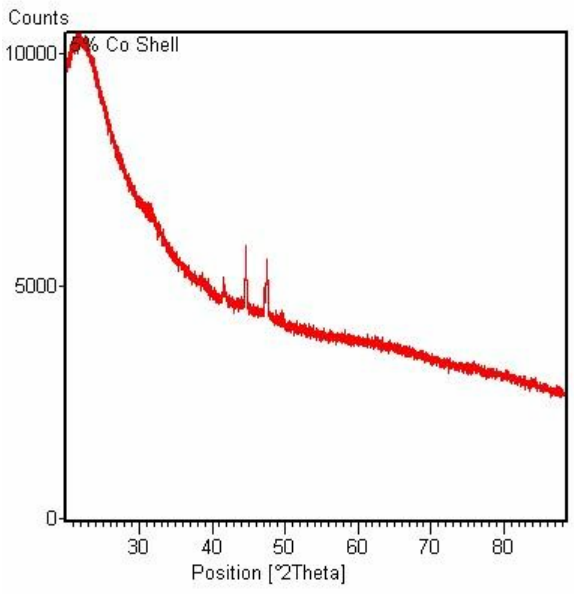

Figure 2.31 XRD of 5% Co sample made by the Shell method

By SEM imaging, both the 5% nickel sample (Figure 2.32) and the 27% copper sample (Figure 2.33) showed the formation of metal crystals in the micro size range. This is a larger metal particle size than was seen for the supported Ni and Cu nanoparticle samples, which retain their nano-scale size even after support. Also, the entire surface of the support is not covered, as is seen with the commercial Shell 405 catalyst, however, this is not unexpected, as our percent loading is an order of magnitude lower than that of Shell 405.

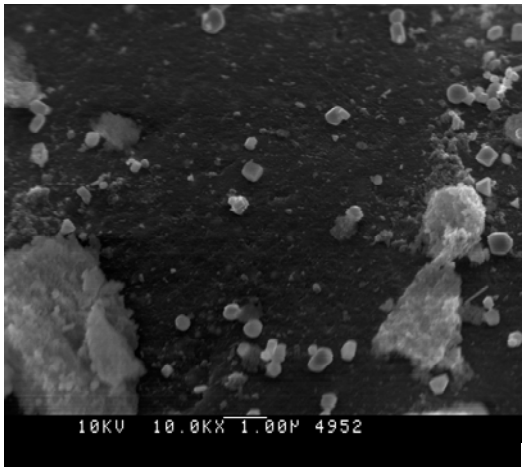

Figure 2.32 SEM image of 5% nickel sample by the Shell method

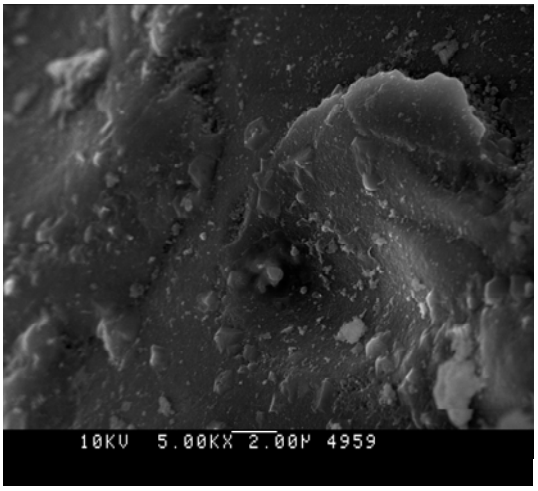

Figure 2.33 SEM image of 27% copper sample by the Shell method

2.3.1.4 Comparison of Supported Nanoparticle and Shell Synthesis Methods

Thus far, the supported nanoparticle method and the Shell method each appear to have their own advantages and disadvantages. The supported nanoparticle method is consistent for the formation of nanoparticles of nickel, copper, iridium, ruthenium, rhodium and cobalt. Complete or near complete conversion (> 95%) has been obtained in all reactions run. It also allows for simple deposition onto a silica surface. For some metals (nickel and copper) the nano-character is successfully retained during this deposition, though there is some agglomeration seen with others such as iridium and rhodium. It can be easily scaled up in size to produce the desired amount of catalyst. However, when supported on silica, the weight percent loadings obtained are much lower than expected due to metal nanoparticle stability in the ethylene glycol solvent.

With the Shell method, much higher loadings are possible with a better surface coverage on the silica and it can also easily be translated to other metals as shown with copper and cobalt. In future work, each type of catalyst will be tested for their hydrazine decomposition abilities to determine which is better suited for our desired purpose of hydrazine decomposition to high ammonia levels.

2.3.2 Hydrazine Safety

Hydrazine is a class 3 explosive and a class 3 health risk chemical, making it a rigorously regulated substance. In coordination with the Environmental Health and Safety department (EHS) at Georgia Tech a standard operating procedure and an emergency procedure were developed for working with hydrazine. The entire reactor system was placed within a hood and is equipped with pressure sensors and pressure relief valves.

The hood ventilation system was adjusted to a flow of 120ft/min, which is the legal requirement for handling Class 3 chemicals. The level of hydrazine in the laboratory is continuously monitored using a Honeywell® ChemCassette system (Figure 2.35). The detection limit of this device was set at the conservative level of 5 ppb. This is the level to which an individual can be exposed for 8 hours without suffering from adverse health issues such as irritation of the eyes, nose, and throat, dizziness, nausea, and in extreme cases pulmonary edema and seizures. In addition, each operator is required to wear a monitoring badge that changes color when exposed to hydrazine (Figure 2.34).

Figure 2.34 ChemCasette hydrazine monitoring system and hydrazine monitoring badges

The intensity of the color is a function of the hydrazine level it has been exposed to. These badges are purchased from DoD Technologies and can be used for 48 hrs before they must be disposed of. Their detection limit is 0.5 ppm. These same badges have been placed within the hood at strategic places as an extra precaution to signal possible hydrazine leaks. If a badge outside the hood or on the body of any operator turns colors, the lab will immediately be evacuated and those involved taken for medical attention.

2.3.3 Hydrazine Reactor and Analysis Design

To study the catalyst activity for the decomposition of hydrazine to ammonia, a reactor was designed and built in our lab. The reactor was divided in three sections: (1) hydrazine introduction, (2) a catalyst bed, and (3) analysis with a Gas Chromatogram coupled with a Thermal Conductivity detector (GC/TCD, Figure 2.35). In the first section, the argon carrier gas passed through a flow meter and pressure check point with relief valve. Then, it bubbled through liquid hydrazine in a containment vessel resulting in a combination hydrazine/argon stream. The amount of hydrazine in the resulting argon

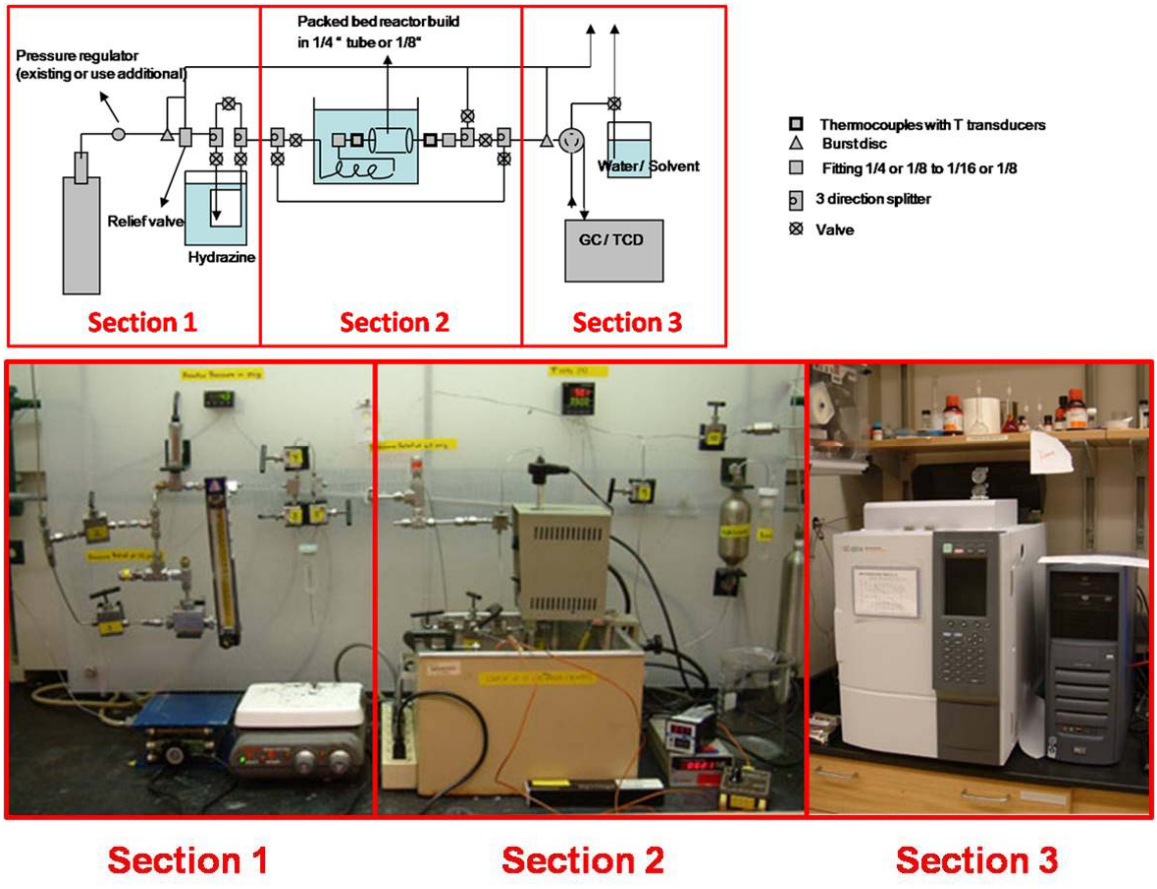

Figure 2.35 Reactor designed and built to test the hydrazine decomposition abilities of metal catalysts supported on silica.

stream contained a fixed percentage of hydrazine that could be altered by changing the temperature and thus the vapor pressure of the hydrazine within the containment vessel. The hydrazine-containing argon stream was then directed through a valve allowing the stream to pass through the second section of the reactor, the temperature controlled catalyst bed. The catalyst bed was constructed from ¼ inch stainless steel tubing. The catalyst powder was kept in place by a piece of mesh and a small piece of glass wool at each extremity. Both vibration and vacuum suction were used to ensure tight packing within the reactor. Originally, the silica particle sizes were 40-75μM. However, when this was tested using a catalyst bed packed with uncoated silica, the resulting pressure drop across the system was too large, and no flow was taking place after the catalyst bed. As a consequence, all catalyst beds studied were packed with samples made with 75-200μM sized silica particles. After passing over the catalyst bed, product stream flowed into the third section, the GC-TCD, for analysis.

Before completely exiting the system and being released into the hood, the gas stream was bubbled through a nitric acid solution of pH 1 to neutralize the ammonia and a bleach solution that is 6.15mol% sodium hypochlorite to neutralize any remaining hydrazine. There were valves installed within the system that allowed the argon stream to bypass the hydrazine or the hydrazine/argon stream to bypass the catalyst bed, the analysis, or both if so desired. This reactor enabled us to study the activity of the catalyst as a function of (1) catalyst bed temperature, (2) hydrazine concentration, (3) percent loading of catalyst, (4) amount of catalyst in the catalyst bed, and (5) the flow rate of the system.

This first generation reactor was used for initial decomposition testing. However, the system was long. As it stretched across an entire hood (Figure 2.35) it contained over 20 feet of stainless steel tubing. The residency time provided by this allowed for a great deal of interaction between the hydrazine and the stainless steel, before it even came into contact with the catalyst bed. It was determined that for more accurate results, a better control of the variables of the system, and greater consistency and repeatability a simpler system was desired.

The second generation reactor incorporated several changes (Figure 2.36). First and foremost, the length of tubing between hydrazine introduction and analysis was shortened, decreasing the amount of stainless steel tubing that the hydrazine passes through to less than one foot between the hydrazine introduction and catalyst bed, and only two feet from catalyst bed to GC-TCD for analysis (Figure 2.37). Second, the quarter inch stainless steel tubing being used for catalyst packed beds was replaced by HPLC columns of 4.6mm inner diameter and 30mm in length. As these columns come with filters on either end, they could now be packed completely with catalyst without the

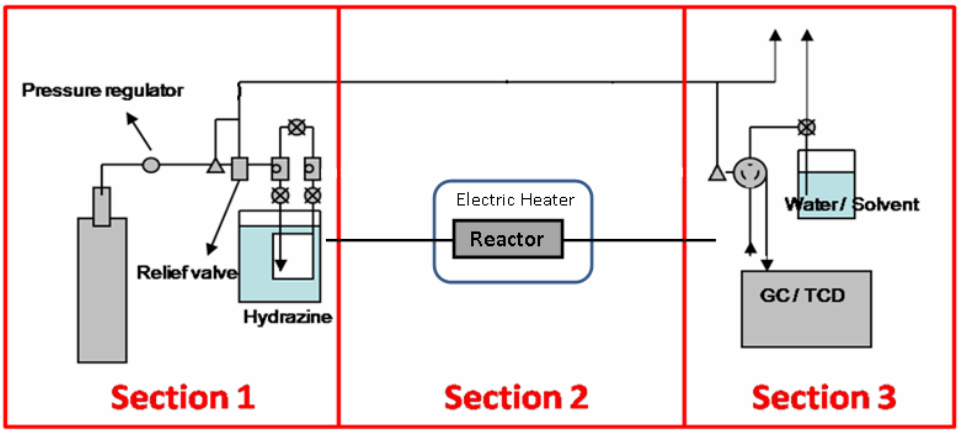

Figure 2.36 Schematic of second generation reactor

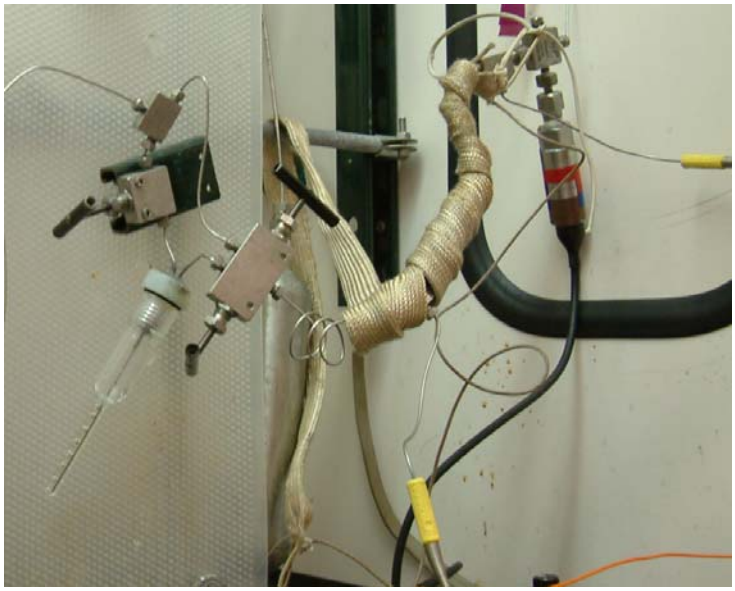

Figure 2.37 Shortened hydrazine pathway in second generation reactor

need for mesh or glass wool inserts. These columns could be packed with ~0.3g of catalyst, and the packing procedure remained the same, with vacuum and vibration used for consistent packing.

The third change was the removal of a bypass system around the packed catalyst bed. This decreased the number of valves and fittings in the system, again making it simpler and decreasing the number of potential leaks or corrosion points between hydrazine and the reactor itself. Finally the fourth change was the removal of the water bath to heat the catalyst bed. This was replaced with electric heating using heating tape and a temperature controller (Figure 2.37). This allowed for better control of the temperature of the gas stream, as this heating was controlled by a probe inserted into the flow of the gas stream itself, rather than by an external temperature probe. All further work has been carried out with this second generation reactor.

2.3.4 Analysis of Product Gas Stream

Gas chromatography was chosen for this analysis as it allows us to easily sample directly from the product gas stream without having to manually sample or isolate any of these hazardous gases. The TCD detector was chosen because it detects gases based on their relative conductivity properties, making it a universal detector. Hence using the GC-TCD, the hydrazine starting material and its three potential decomposition products (hydrogen, nitrogen, and ammonia) can be individually isolated and quantified.

In order to achieve this separation, in the first generation system, the GC was configured with two 6 port sample valves and 3 columns. The first 6 port valve controlled the injection of a metered amount of the product gas stream into the GC-TCD (Figure 2.38). Once inside the GC, the gas stream flowed through a Chromosorb 102 packed column (12 ft. long, 1/8 inch outer diameter), which performed the basic separation of nitrogen and hydrogen from ammonia and hydrazine, as well as the separation of the ammonia and hydrazine from each other. A second 6 port valve was located after the Chromosorb 102 column (Figure 2.38). The switching of this valve

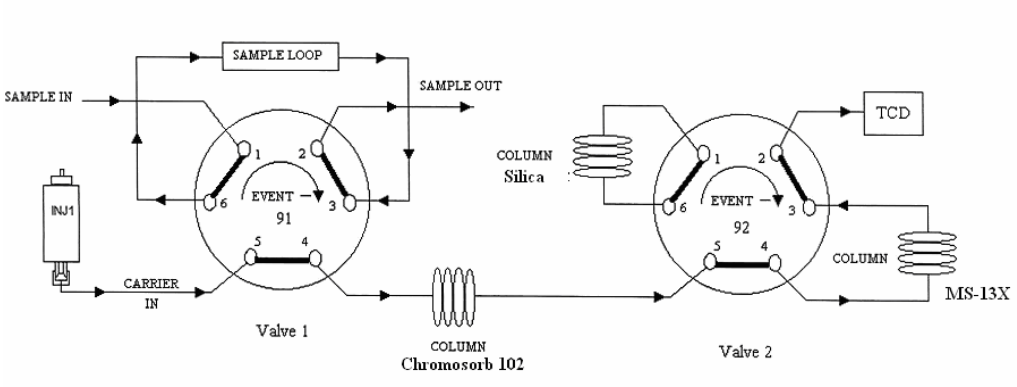

Figure 2.38 Diagram of the 3 columns and two valves necessary for the product stream to be introduced into, separated, and identified using the GC-TCD

allowed the hydrogen and nitrogen to pass over an MS-13X mole sieve column (6 ft. long, 1/8 inch outer diameter), which separated these two gases, and the ammonia and hydrazine to simply pass through a silica column (6 feet long, 1/8 inch outer diameter), so that ultimately four distinct peaks were seen by the TCD detector. The timing of the second valve switch was critical to direct the streams onto the desired columns and needed to be optimized after any change in column configuration for separation to occur correctly.

Calibration curves were prepared for the hydrazine, ammonia, hydrogen, and nitrogen that were used to quantify the decomposition reactions. For ammonia, hydrogen and nitrogen, this was done using calibrating gas mixtures containing 2mol% and 8mol% of the desired gases, with the balance being argon. The area of the peaks obtained from the TCD detector directly correlate to the thermal conductivity of the individual components. Specifically, the thermal conductivity of ammonia is 0.024W/mK, of hydrogen is 0.186W/mK and of nitrogen 0.026W/mK at 300K.[56] A comparison of these numbers suggests that the responses of ammonia and nitrogen should be about the same while the response for hydrogen should roughly be 7 times larger at the same concentration, which corresponds with what is observed experimentally with the calibrating gas (Figure 2.39). In all of the calibration curves, very high R^2 values (0.98-0.99) were obtained which indicate a linear and proportional detector response (Experimental Figures 2.48-2.56).

To prepare a calibration curve for hydrazine, the hydrazine concentration in the argon stream was varied by varying the temperature of the hydrazine reservoir and therefore the vapor pressure.[57] At the constant flow rate of 83.7 mL/min, the

concentration of hydrazine in argon was 1.7 mol% at 25°C and 5.9 mol% at 45°C. The resulting linear calibration curve had an R^2 value of 0.9947 (Figure 2.40).

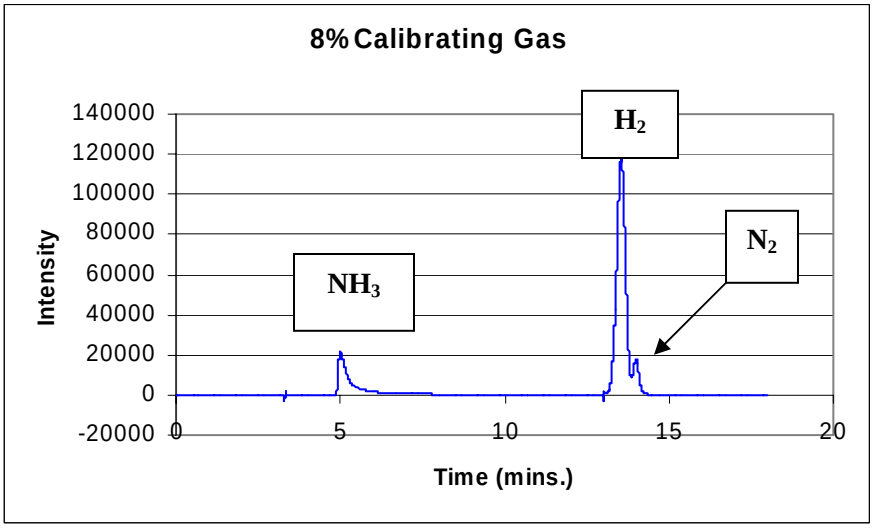

Figure 2.39 Chromatogram of 8% calibrating gas showing the TCD response differences between ammonia, hydrogen, and nitrogen.

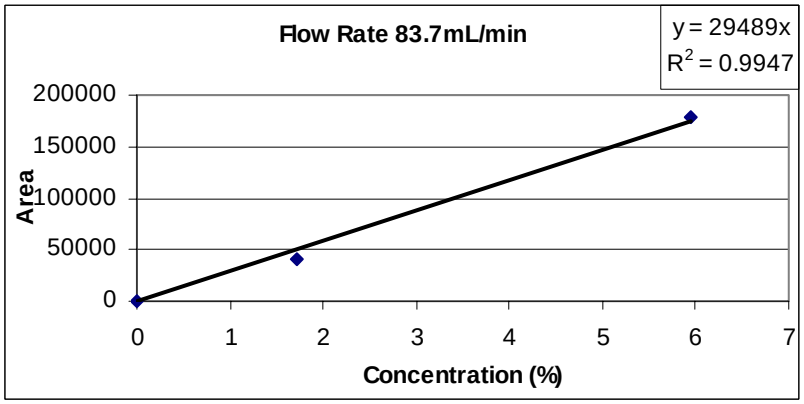

Figure 2.40 Hydrazine calibration curve at 83.7mL/min

By studying the pure compounds, the average retention time for each gas was determined (Table 2.7). These values were used for identification of the products

obtained once hydrazine decomposition testing began. NH_3 and hydrazine show a constant retention time of 5.2 ±0.3 and 7.6 ±0.4 minutes respectively. However, the retention times of H_2 and N_2 are dependent on the timing of the second valve switch, so they changed as the system was optimized. What remained constant however was that the H_2 retention time was 0.52 ± 0.03 minutes after the valve switch and the N_2 retention time was 0.99 ±0.04 minutes after the switch.

Table 2.7 Average retention times of all four pure gas components in minutes

	NH_3	**Hydrazine**	**H_2**	**N_2**
Retention Time	**5.2** ± 0.3	**7.6** ± 0.4	**10.52** ± 0.03	**10.99** ± 0.04
			13.52 ± 0.03	**13.99** ± 0.04

2.3.5 GC-TCD Analysis Modifications

While initially excellent results were obtained with this GC-TCD configuration, over time, problems arose with the analysis. During attempts to calibrate hydrazine at a flow rate of 29.4mL/min, a diminished signal with a gas stream of 7.1% was seen, much lower than what was expected for these conditions (an area of 20,000-30,000 versus 170,000-180,000 expected). The GC was tested at a variety of temperature and flow rates (130°C-200°C and 10-30m/min), however, signal was not consistently seen. Furthermore, hydrazine decomposition was seen with no catalyst bed present (Figure 2.41).

To determine whether this problem was occurring in the reactor system or within the GC-TCD itself, the hydrazine gas stream from the end of the reactor was collected and condensed into a tetrahydrofuran (THF) solution. After an hour of collection, this

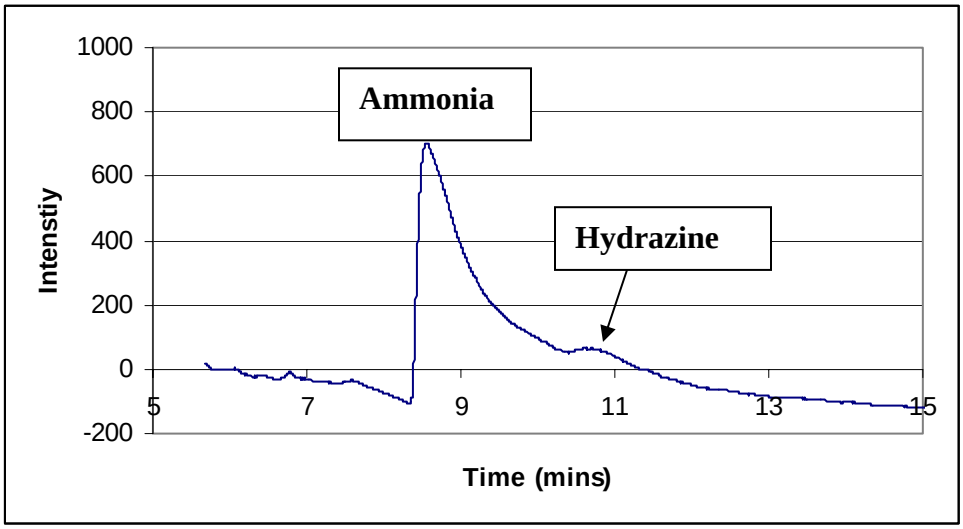

Figure 2.41 Appearance of ammonia peak with no catalyst bed present in the system

solution was injected into a GC-mass spec. For comparison, an independently prepared solution of hydrazine in THF was also injected into the GC-MS. The two solutions gave identical spectra, both clearly indicating the presence of hydrazine. This test showed that the complete decomposition we were seeing and any hydrazine adsorption leading to a diminishing of signal must be taking place inside the GC itself.

The GC columns were replaced with columns containing the same packing, Chromosorb 102, but now glass lined so that the hydrazine did not come into contact with any metal surfaces within the GC. This was done as 316 stainless steel (the column material) is only rated for use with hydrazine up to 70°C.[58] This eliminated the decomposition problem, however, the problem of a diminished hydrazine signal remained.

Two columns, Tenax TA and Carbowax 1500 have been reported in the literature and are used for hydrazine analyses.[59-61] Initially neither column gave promising results, as through the Tenax TA column, the hydrazine peak appeared broad and double

humped, and through the Carbowax 1500 column, no peak at all was seen. However, when the 2% calibrating gas was passed through each of these columns, and no ammonia peak could be seen either, this indicated that a problem caused by something other than column packing material was occurring.

The six port valves were removed and cleaned. Upon opening them up, a black oily liquid was found inside both valves. These valves were made of hastelloy, which can react with hydrazine. It is believed that the black oil was caused by a side reaction with this metal and was both interfering with the passage of hydrazine and ammonia through the system, as well as contaminating the GC columns themselves. The six port injection valve was replaced with an identical valve constructed of Nitronic 60 stainless steel. With this in place, the second generation analysis method was devised.

The second generation analysis system was a simplified version of the first generation system. The product gas stream passes through the injection six port valve (Figure 2.42). Following injection, all products pass over a Carbowax 1500 column (6 ft.

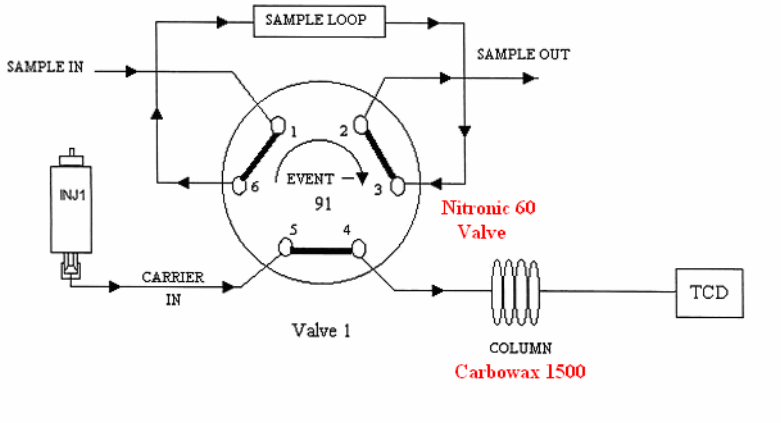

Figure 2.42 Second generation GC-analysis system

long, 1/8 inch outer diameter) at a flow rate of 50mL/min in a GC heated to 130°C and directly to the detector. There is no second valve switch and no passing over either a silica or a mole sieve column. With this method, hydrogen and nitrogen cannot be separated and they elute as a single peak. However, there is good peak separation between the combined H_2/N_2 peak, the ammonia peak, and the hydrazine peak, allowing for analysis of products based on yield of ammonia formed. With this new configuration, the N_2/H_2 peak elutes at 0.2780 ± 0.0005 minutes, the ammonia at 0.41 ± 0.05 minutes, and the pure hydrazine at 2.90 ± 0.03 minutes. It is interesting to note that, in the presence of ammonia, there is a co-elution affect and the hydrazine then elutes at 1.6 ± 0.1 minutes (Table 2.8).

Table 2.8 Average retention times with second-generation configuration in minutes

	N_2/H_2	**NH_3**	**Hydrazine**
Retention Time	**0.2780** ± 0.0005	**0.41** ± 0.05	**2.90** ± 0.03
		In the presence of NH_3	**1.6** ± 0.1

A new calibration was performed for ammonia, nitrogen, and hydrogen, using the calibrating gas mixtures. Both the N_2/H_2 peak and the ammonia peak were found to have the desired linear calibrations with an R^2 value of 0.99 (Experimental Figure 2.58). Hydrazine was calibrated by passing two different concentrations of hydrazine through the system. At a flow rate of 29.4mL/min, a 0.9% hydrazine stream and a 1.4% hydrazine stream were passed through the system. Assuming 0% hydrazine produces 0 response, a linear calibration with an R^2 value of 0.99 was achieved (Figure 2.43).

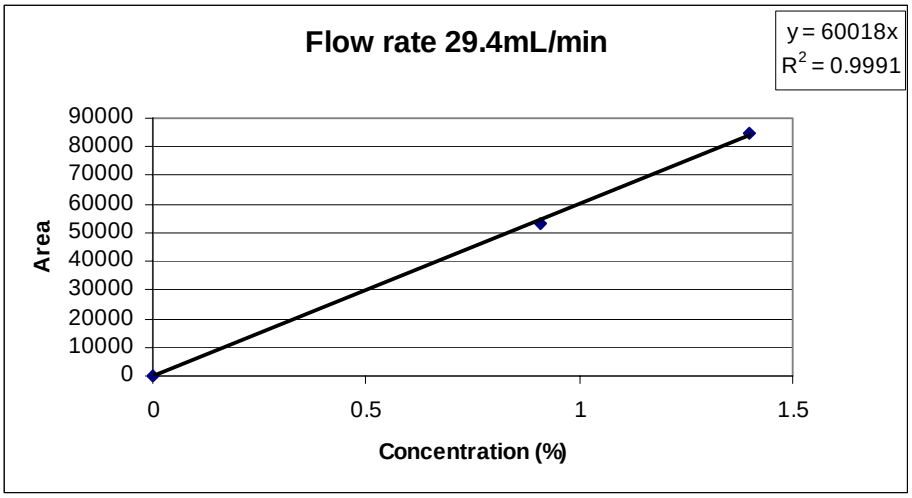

Figure 2.43 Hydrazine calibration with second generation system

2.3.6 Decomposition of Hydrazine – First Generation Reactor

Initial catalyst decomposition testing was performed on a nickel catalyst bed that was 1.06% loading by weight on 75-200μm silica. Hydrazine was kept at room temperature (~25°C) with a system flow rate of 83.7mL/min (~1mol% hydrazine in the gas stream. Hydrazine amount is approximate as an accurate system pressure was not recorded at the time of reaction). The system was tested with the catalyst bed at 25°C, 35°C, 50°C, and 60°C. At each temperature, two samples were taken per data point, which means the system was run at each temperature for 40 minutes. Under these conditions, the system did not reach equilibrium at each condition; however, it allowed us to see general trends.

The areas found for hydrazine, hydrogen and nitrogen were converted to mole percent amounts of the total gas stream using the 83.7mL/min calibration curve (Experimental Figure 2.57). Under these conditions, at all temperatures, a hydrazine peak was seen. The amount of hydrazine seen was highest at 25°C, with 1.32% and

decreased steadily to 0.25% at 60°C indicating 19% of the hydrazine remained unreacted. There was 0% yield of ammonia, but very small quantities of hydrogen (0.005-0.01%) and nitrogen (0.004-0.02%) were present at all temperatures. The hydrogen amount peaked a 35°C with 0.02%, then decreased steadily, while the nitrogen amount was more fluxional, with its highest amount being seen at 35°C (0.02%), and its lowest amount at 50°C (0.004%).

Along with the expected peaks for hydrazine, hydrogen and nitrogen, a new peak appeared with a retention time that varied from 8.9 to 10.4 minutes as the temperature was increased. This peak initially appeared with an area of 973.6 and increased as temperature increased to a final value of 1400 (Figure 2.44).

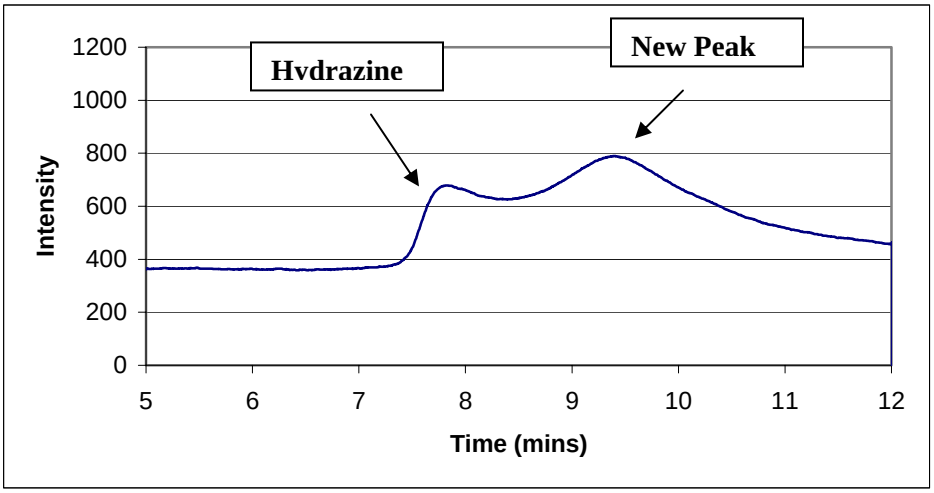

Figure 2.44 New peak appearance during hydrazine decomposition

An investigation began into the identity of the new peak. The first possibility studied was that this peak was water introduced in the system either from the hydrazine or from the silica. To test this, a sample of a 50:50 mixture of water and hydrazine by volume, followed by a sample of pure water were introduced into the GC-TCD. The

mixture displayed a single peak, which is not surprising as water and hydrazine together form a hydrate complex. This peak had a retention time of 7.2, while pure water had a retention time of 6.9 (Figure 2.45), indicating that neither of these species could explain the new unknown peak with a retention time of ~10.3.

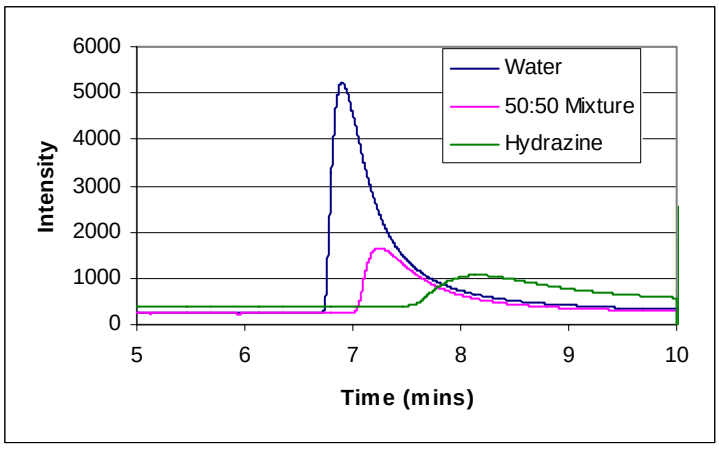

Figure 2.45 Comparison of the retention times of pure hydrazine, pure water, and a 50:50 mixture of the two

Diazene (Figure 2.46) is a well-known intermediate in the decomposition of hydrazine to its final product mixture of ammonia, hydrogen and nitrogen.[62] In our system, if hydrazine was only undergoing partial decomposition, diazene could be formed by the adsorption of hydrogen onto the nickel catalyst surface. The thermal conductivity of diazene is not known, nor is it available as a pure substance which can be calibrated; therefore diazene will be reported as a peak area.

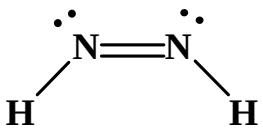

Figure 2.46 Diazene molecule, formed as an intermediate of hydrazine decomposition.

Due to the appearance of diazene, it was conjectured that in the previous catalyst tests the hydrazine was decomposing, but incompletely, forming diazene instead of ammonia. This may have occurred due to the short exposure time between the hydrazine and the catalyst caused by either too high of a flow rate, too small an amount of catalyst packed into the catalyst bed, or a combination of the two. The residency time of the hydrazine within the catalyst bed was increased by addressing both issues simultaneously.

The catalyst bed was packed with 0.7g of catalyst with 2.90% nickel loading by weight. The temperature of the catalyst bed was maintained at 75°C. The hydrazine was kept at room temperature with an argon flow of 29.4mL/min (~1.35 mol% hydrazine). To analyze the data obtained with this catalyst bed, ammonia, hydrogen and nitrogen were converted to mole percents using the 29.4mL/min calibration curves (Experimental Figure 2.55), and hydrazine and diazene amounts were compared as peak areas. The reactor was run at these conditions for 4 hours and 40 minutes. Over that time, the system did not reach equilibrium, however, once initial ammonia formation occurred 1 hour and 20 minutes into the reaction, the ammonia, hydrogen and nitrogen increased steadily, while the hydrazine and diazene both decreased (Figure 2.47). In the final sample of the day, the total gas stream analyzed consisted of 0.55% ammonia, 0.02% hydrogen, and 0.14% nitrogen. There was 73% percent conversion of hydrazine, and 42% yield of ammonia. When just the product stream was examined, the products contained 81% ±3% of the desired ammonia.

The reactor column was stored under argon overnight, and the reaction continued the next day under the same system parameters, (~1.35% hydrazine stream

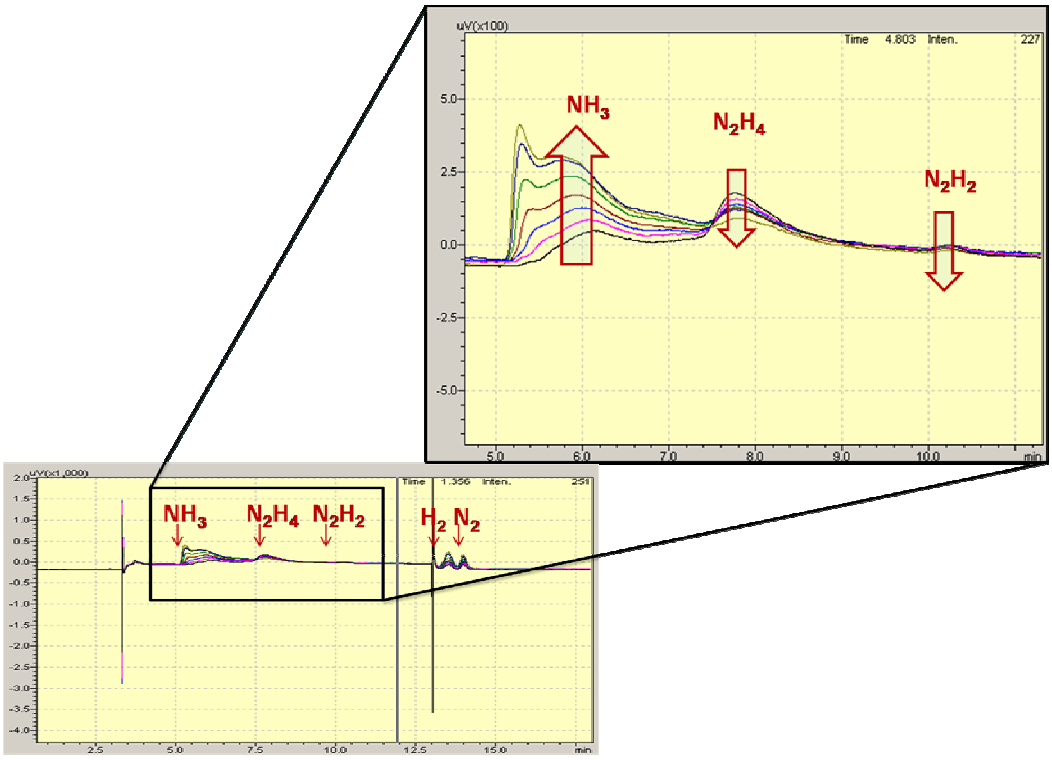

Figure 2.47 Results over time from passing a ~1.35% hydrazine stream over 0.7g of 2.90% Ni loading catalyst at 75°C with a flow rate of 29.4mL/min.

over 0.7g of 2.90% Ni loading catalyst at 75°C with a flow rate of 29.4mL/min). Ammonia, hydrazine, diazene, hydrogen, and nitrogen were all present from the beginning. For 3 hours and 20 minutes, the hydrazine and diazene amounts decreased, and the ammonia and hydrogen amounts increased until equilibrium was reached with 100% conversion of hydrazine, and a total gas stream composed of 1.7% ammonia, 0.05% hydrogen, and 0.40% nitrogen. This is a 96% ± 2% yield of ammonia, and it represents 82% ±3% of the total product stream. The nano-nickel catalyst supported on silica appeared more active toward the formation of ammonia than the nickel thin film reported in the literature, which produced a product stream containing 76.03% ammonia at 90°C.[19]

2.3.7 Decomposition of Hydrazine – Second Generation Reactor

After re-designing the reactor and analytical method, all supported nanoparticle catalysts (Ni, Cu, Co, Ir, Rh, and Ru) were tested for their activity towards hydrazine decomposition and selectivity for ammonia formation. The catalysts were supported on 75-200μm silica particles with 150Å pores. Each catalyst to be tested had between 2.6% and 3.6% actual metal loading (The exception was the repeat Ir catalyst, which had only 1.3% metal loading). For each test, approximately 0.3g of catalyst was packed into the catalyst bed. The catalyst bed was heated to 90°C with flowing argon for 12 hours prior to the decomposition reaction. During the reaction, the bed was heated to 75°C and the flow rate of the system was kept at 29.4mL/min. The hydrazine was kept at room temperature (~ 25°C). Each catalyst was evaluated for activity (amount of hydrazine decomposed at equilibrium) and selectivity (amount of ammonia formed) at system equilibrium. Ammonia formation is reported as a yield based on the complete hydrazine decomposition reaction (Equation 2.15)

$$3N_2H_4 \rightarrow 4NH_3 + N_2 \qquad \text{(Equation 2.15)}$$

For each catalyst, based on the mole percent of hydrazine entering the system, the theoretical 100% yield amount of ammonia was calculated. The actual amount of ammonia formed was determined from the ammonia calibrating curve (Experimental Figure 2.58). The percent yield was determined as the ratio of the two. Each metal was tested twice using fresh catalyst either from the same or a similarly prepared batch of catalyst to confirm reproducibility (Table 2.9).

Table 2.9 Results from supported nanoparticle catalyst decomposition tests

Metal Loading	BET Surface Area (m^2/g)	NH_3 Yield	Conversion
3.0% Ni	167 ± 5	91% ± 3%	100%
2.9% Ni[A]		96% ± 2%	100%
2.6% Cu	141 ± 4	0%	0%
2.6% Cu		0%	0%
3.1% Ru	195 ± 5	67% ± 4%	100%
3.1% Ru		60% ± 6%	100%
3.1% Co	96 ± 3	0%	0%
3.1% Co		0%	0%
3.3% Ir	163 ± 5	67% ± 5%	100%
1.3% Ir		63% ± 3%	100%
3.6% Rh	109 ± 3	60% ± 2%	100%
2.8% Rh		55% ± 4%	100%

A. Results obtained using first generation reactor system

Under these reaction conditions, both copper and cobalt were found to have no measurable activity for hydrazine decomposition. With cobalt, in all tests run, no product formation was observed. With copper, the initial samples showed indications of product formation, however, after half an hour, these disappeared and no product formation was observed. It is possible that the copper surface was being poisoned or corroded by ammonia formation, preventing any further hydrazine from interacting with the catalyst active sites.

With the other four metals (Ni, Ru, Rh, and Ir) 100% conversion of the hydrazine to products is assumed, as no hydrazine was seen within the detection limits of the GC-TCD at equilibrium conditions. In terms of selectivity, nickel was found to have the lowest, corresponding to the highest ammonia yields, as 94% ± 3% yield of ammonia was observed with this metal. Ruthenium and iridium both produced similar yields of ammonia with 67% ± 6% and 62% ± 6%. Under our conditions, rhodium showed the highest selectivity and lowest yields with 57% ± 4% ammonia yield. Prior to reaching

equilibrium, the product stream from rhodium and ruthenium both showed some fluctuations, with ammonia yield ranging from 17%-97%, which may indicate some initial ammonia adsorption onto the metals surface. However, these fluctuations were no longer evidenced once equilibrium was reached.

Based on its excellent ammonia yields, complete conversion of hydrazine to products, and moderate equilibration times, nickel appears to be the most promising catalyst for further study and optimization.

2.4 Conclusions

A method for the synthesis of nickel, copper, cobalt, iridium, ruthenium, and rhodium nanoparticles has been developed. That the particles are of the desired metal and have a nanoscale size has been confirmed by chlorine and metals elemental analysis, XRD, and TEM imaging. A method has also been developed to support these metals on silica for use as catalysts, and samples containing between 2.6% and 3.6% actual loading of all metals have been prepared and analyzed by chlorine and metals elemental analysis, XRD, SEM imaging, and BET surface area analysis. The method is versatile, being easily scaled up in size to produce gram scale quantities of catalyst. However, the actual metal loading amounts on silica are low. Preliminary work has been done on increasing the catalyst loading by adding multiple layers of nanoparticles, and that was successful in increasing the catalyst loading of a nickel sample from 8% to 14%, however the nanoscale of the catalyst was lost in this process. Future work will focus on further ways to increase the supported amount and to better control the actual percent loading compared to the desired theoretical percent loading.

A variation of the method used to produce the commercial catalyst Shell 405 has also been developed for catalyst synthesis. Using this method, samples have been made with theoretical loadings from 2-50% of nickel, copper and cobalt. At low percent loadings (<7% for Ni and <20% for Cu), full reduction to metal is achieved with nickel and copper, however, at higher loadings of these metals and all loading of cobalt, unreduced metal chloride salt remains in the system. This method is also versatile as it can be used for multiple metals and can produce large batches of catalyst at once. However, work must be done to optimize the system and achieve complete reduction to the desired metals.

A reactor to test these catalysts was designed and built in our lab and a safety plan for working with hydrazine was developed and implemented with the aid of Environmental Health and Safety. Product analysis was performed using a GC with TCD detector. Using the first and second generation designs of this reactor and analysis method, supported nanoparticle catalysts of nickel, copper, cobalt, ruthenium, rhodium and iridium have been tested for their activity towards the decomposition of hydrazine and selectivity for the formation of ammonia as a product. Cobalt and copper did not show measurable activity for hydrazine decomposition under the reaction conditions investigated. However, nickel, ruthenium, rhodium, and iridium all showed high activity with complete decomposition of the hydrazine to the production ammonia, hydrogen, and nitrogen. Nickel appears to be the most promising catalyst for further development as it showed the most selectivity for ammonia formation with ammonia yields of 94% ± 3% over repeat runs. Optimization of the use of this catalyst including percent loading and reaction temperature will be pursued in future work. Once the synthesis method has been

optimized for complete reduction, the Shell catalysts will also be tested for their hydrazine decomposition abilities, and their behavior compared to that of the supported nanoparticle catalysts. The overall path forward for this work will be to couple our hydrazine decomposition with the electric propulsion thruster to finalize the design of a dual stage, single propellant engine.

2.5 Experimental

General Methods. Nickel chloride, nickel chloride hexahydrate, copper chloride, ruthenium chloride, rhodium chloride hydrate, iridium chloride hydrate, cobalt chloride amorphous silica, hydrazine, hydrazine monohydrate, sodium hydroxide, and sodium borohydride were purchased from SigmaAldrich and used without further purification. Spherical silica was purchased from Sorbent Technologies (Atlanta, GA). Ethylene glycol was also purchased from SigmaAldrich. Initial reactions were run with untreated ethylene glycol, however, for later reactions, ethylene glycol was treated by refluxing with heptane at 95°C for 10-15 hours to remove water. Calibrating mixtures of ammonia, nitrogen and hydrogen, 2mol% and 8mol% of each with argon as the balance gas were purchased from Scott Specialty Gas Corporation (Augusta, GA). All GC-TCD columns were purchased from and packed by Supelco (Bellefonte, PA).

All UV-vis measurements were performed on a Hewlet Packard 8453 UV-Vis system. Chlorine elemental analysis was performed by Atlantic Microlab (Norcross, GA) and was done by flash combustion followed by ion chromatography. All metals elemental analysis were performed by Columbia Analytical Services (Tucson, AZ) by atomic adsorption spectroscopy. All electron microscopy was done at the Robert P.

Apkarian Integrated Electron Microscopy Core at Emory University. SEM images were taken on a Topcon DS-130F Field Emission Scanning Electron Microscope and TEM images were taken on either a JEOL JEM-1210 Transmission Electron Microscope or a Hitachi H-7500 Transmission Electron Microscope. XRD analysis was performed by the microstructural characterization facility in the materials science and engineering department at the Georgia Institute of Technology. The XRD were run on an X'Pert PRO Alpha-1 diffractometer with a symmetrical incident beam Johansson monochromator, an X'celerator detector, and 1.8 kW Ceramic Copper tube X-ray source. BET surface area analysis was performed by the Koros Research group at the Georgia Institute of Technology on a Micromeritics ASAP 2020.

Synthesis of Nickel Nanoparticles with PVP

Ni nanoparticles were synthesized according to the literature procedure of Couto and co-workers.[26] Stock solutions were made of NiCl2•6H2O and the desired PVP in ethylene glycol ($5.0*10^{-3}$M $NiCl_2 \cdot 6H_2O$ and $1.5*10^{-4}$M PVP in 100mL). Vigorous magnetic stirring was used to dissolve all solid. Stock solution (1, 2, or 4 mL) was diluted in ethylene glycol to give the desired concentrations ($4*10^{-4}$M $NiCl_2 \cdot 6H_2O$ and $1.2*10^{-5}$M PVP or $2*10^{-4}$ M $NiCl_2 \cdot 6H_2O$ and $5.9*10^{-6}$M PVP). The solution was heated to 140 °C. At temperature, sodium borohydride was added (0.180g, 4.76mmol) with stirring. This reacted at temperature for 2 hours. It was cooled to room temperature. Acetone was added to the solution (50mL) to precipitate nanoparticles. It was centrifuged and the supernatant decanted. Particles were stored in 15mL of ethylene glycol and acetone mixture.

Synthesis of Nickel Nanoparticles without PVP - Initial

Ni nanoparticles were synthesized according to the literature procedure of Wu and coworkers.[27] Nickel(II) chloride (26mg, 0.20mmol) was added to dry ethylene glycol (10mL) to make a 20mM solution. Sodium hydroxide solution (0.72mL of 1.0M) was added. This was sonicated until all solid $NiCl_2$ dissolved. Hydrazine monohydrate (0.12mL, 2.5mmol) was added. The reaction mixture was warmed to 60°C and stirred for 1 hour. It was cooled to room temperature. A magnet was placed in solution to remove all Ni particles formed. Particles were washed in ethanol, removed from the magnet, and stored in ethanol solution.

Silica Support – Method One

Nickel particles were adsorbed onto silica using a modification of a literature method.[20] Silica gel (1.2g, amorphous silica) was baked in air at 500°C for 10 hours. The dried silica was stirred with nickel particles (0.1g, 1.7mmol) in ethanol (10mL) at room temperature, under an inert atmosphere for 12 hours. Solvent was removed by vacuum and heat to obtain a fine white powder.

Silica Support – Method Two

Nickel particle precursor was adsorbed onto silica using a modification of a literature method.[20] Silica gel (5.0g, amorphous silica) was baked in air at 500°C for 9 hours. The dried silica was stirred with nickel chloride (0.55g, 4.24mmol) in water (25mL) at room temperature, under nitrogen, overnight. Solvent was removed by vacuum and heat to obtain a pale yellow powder. This powder was placed in ethylene

glycol (212mL) with vigorous stirring. Sodium hydroxide solution (15.2mL of 0.1M) was added followed by hydrazine monohydrate (2.5mL, 51.5mmol). The reaction was warmed to 60°C and stirred for 1 hour. It was cooled to room temperature, diluted with ethanol, and filtered to remove solid product. The solid was collected dried by vacuum. Final product was collected as a pale blue powder.

Silica Support – Method Three

Nickel nanoparticles were made by the non-PVP method described above. Once the reaction was finished, before particle isolation, silica (0.058g, 75-200μm, 150Å pores for 20% loading) was added to mixture with vigorous stirring. Two equivalents of ethanol by volume (50mL of ethanol to 25mL of ethylene glycol) were added. This stirred under an inert atmosphere for 4 days. This was filtered to collect solid product. The solid was collected and dried by vacuum. Product was obtained as a grainy, magnetic, black powder.

Standard Synthesis and Support-Optimized Method

Nickel(II) chloride (0.325g, 2.5mmol) and solid sodium hydroxide (0.36g, 9.00mmol) were dissolved in ethylene glycol (125mL) at 60°C. The desired amount of silica was added (1.32g 75-200μm, 150Å pores for 10% loading) Hydrazine monohydrate (1.5mL, 30.9mmol) was added. This mixture stirred at temperature for 1 hour. It was cooled to room temperature and stirred overnight. Product was collected by centrifuge, washed with ethanol, and solvent was removed with vacuum and heat. Product was obtained as a dark grey powder.

Increasing Catalyst Loading-Second Nanoparticle Layer

Nickel(II) chloride (60.8mg, 0.470mmol) was added to dry ethylene glycol (23.3mL) to make a 20mM solution. Sodium hydroxide solution (1.68ml of 1.0M) was added. This was sonicated until all solid $NiCl_2$ dissolved. Hydrazine monohydrate (0.28mL, 5.77mmol) was added. The reaction mixture was warmed to 60°C and stirred for 1 hour. It was cooled to room temperature. Two equivalents of ethanol by volume (46.6mL) were added. Nickel on silica sample was added (189.7mg of 8.4%Ni on silica). This stirred for four days. Solid was collected by filtration, washed with ethanol and dried with vacuum and heat. Product was collected as a dark grey solid.

Synthesis of Copper Nanoparticles

Copper(I) chloride (49.5mg, 0.5mmol) and solid sodium hydroxide (72mg, 1.8mmol) were dissolved in ethylene glycol (25mL) at 60°C with vigorous stirring. After complete dissolution of solid reactants, hydrazine monohydrate (0.3mL, 6.2mmol) was added, and the mixture continued to react for 1 hour at 60°C. It was then cooled to room temperature. Product was collected by centrifugation, washed with ethanol and dried with vacuum and heat. Product was collected as a dark reddish brown powder.

Synthesis of Supported Copper Nanoparticles

Copper (I) chloride (247mg, 2.5mmol) and sodium hydroxide (360mg, 9.00mmol) were added to dry ethylene glycol (125mL). The solution was warmed to 60°C with stirring until complete dissolution of solid. The desired amount of silica was added (1.43g, 75-200μm, 150Å pores for 10% loading). Hydrazine monohydrate (1.5mL,

30.9mmol) was added. This mixture stirred at temperature for 1 hour. It was cooled to room temperature and stirred overnight. Product was collected by centrifuge, washed with ethanol, and solvent was removed with vacuum and heat. Product was obtained as a reddish brown powder.

Synthesis of Cobalt Nanoparticles

Cobalt(II) chloride (0.325g, 2.5mmol) was added to dry ethylene glycol (125mL). Sodium hydroxide (0.36g, 9.00mmol) was added. The solution was warmed to 60°C with stirring until complete dissolution of solid. Hydrazine monohydrate (1.5mL, 30.9mmol) was added. The reaction was stirred for 1 hour. It was warmed to 190°C and stirred overnight. It was then cooled to room temperature. Product was collected by centrifugation, washed with ethanol and dried with vacuum and heat. Product was collected as a dark grey metallic powder.

Synthesis of Supported Cobalt Nanoparticles

Cobalt nanoparticles were synthesized by the standard method described above. Before centrifugation, the desired amount of silica was added (1.69g, 75-200μm, 150Å pores for 8% loading). This stirred at room temperature under an inert atmosphere for 72 hours. Product was collected by centrifugation, washed with ethanol and dried with vacuum and heat. Product was collected as a dark grey metallic powder.

Synthesis of Ruthenium Nanoparticles

Ruthenium(III) chloride (0.104g, 0.501mmol) was added to dry ethylene glycol (25mL). Sodium hydroxide (0.072g, 1.8mmol) was added. The solution was warmed to 60°C with stirring until complete dissolution of solid. Hydrazine monohydrate (0.3mL, 6.16mmol) was added. It was warmed to 120°C and stirred for 24 hours. It was then cooled to room temperature. Product was collected by centrifugation, washed with ethanol and dried with vacuum and heat. Product was collected as a dark brown powder.

Synthesis of Supported Ruthenium Nanoparticles

Ruthenium(III) chloride (0.259g, 1.25mmol) was added to dry ethylene glycol (75mL). Sodium hydroxide (0.18g, 4.5mmol) was added. The solution was warmed to 60°C with stirring until complete dissolution of solid. The desired amount of silica was added (1.449g, 75-200μm, 150Å pores for 8% loading). Hydrazine monohydrate (0.9mL, 18.5mmol) was added. It was warmed to 120°C and stirred for 24 hours. It was then cooled to room temperature. Product was collected by centrifugation, washed with ethanol and dried with vacuum and heat. Product was collected as a dark brown powder.

Synthesis of Rhodium Nanoparticles

Rhodium(III) chloride hydrate (0.264g, 1.000mmol) was added to dry ethylene glycol (50mL). Sodium hydroxide (0.144g, 3.6mmol) was added. The solution was warmed to 60°C with stirring until complete dissolution of solid. Hydrazine monohydrate (0.6mL, 12.3mmol) was added. It was warmed to 190°C and stirred for 2 hours. It was then cooled to room temperature. Product was collected by centrifugation,

washed with ethanol and dried with vacuum and heat. Product was collected as a dark brown powder.

Synthesis of Supported Rhodium Nanoparticles

Rhodium(III) chloride hydrate (0.264g, 1.000mmol) was added to dry ethylene glycol (50mL). Sodium hydroxide (0.144g, 3.6mmol) was added. The solution was warmed to 60°C with stirring until complete dissolution of solid. The desired amount of silica (1.18g, 75-200μm, 150Å pores for 8% loading) was added. Hydrazine monohydrate (0.6mL, 12.3mmol) was added. It was warmed to 190°C and stirred for 2 hours. It was then cooled to room temperature. It stirred at room temperature overnight. Product was collected by centrifugation, washed with ethanol and dried with vacuum and heat. Product was collected as a dark brown powder.

Synthesis of Iridium Nanoparticles

Iridium(III) chloride hydrate (0.1762g, 0.500mmol) was added to dry ethylene glycol (25mL). Sodium hydroxide (0.072g, 1.8mmol) was added. The solution was warmed to 60°C with stirring until complete dissolution of solid. Hydrazine monohydrate (0.3mL, 6.16mmol) was added. It was warmed to 190°C and stirred for 3 hours. It was then cooled to room temperature. Product was collected by centrifugation, washed with ethanol and dried with vacuum and heat. Product was collected as a dark brown powder.

Synthesis of Supported Iridium Nanoparticles

Iridium(III) chloride hydrate (0.1762g, 0.500mmol) was added to dry ethylene glycol (25mL). Sodium hydroxide (0.072g, 1.8mmol) was added. The solution was warmed to 60°C with stirring until complete dissolution of solid. The desired amount of silica was added (1.1g, 75-200μm, 150Å pores for 8% loading). Hydrazine monohydrate (0.3mL, 6.16mmol) was added. It was warmed to 190°C and stirred for 3 hours. It was then cooled to room temperature. It stirred at room temperature overnight. Product was collected by centrifugation, washed with ethanol and dried with vacuum and heat. Product was collected as a dark brown powder.

Synthesis of Nickel Catalyst – Shell Method

$NiCl_2$ powder (0.22g, 1.70mmol) was weighed into a glass evaporating dish. Distilled water was added (5mL), for a solution molarity of 0.338M. Aqueous ammonium hydroxide (0.2mL of 30% solution) was added to this slowly, with constant stirring. Stirring continued for one hour at room temperature. Spherical silica (2g, 75-200μm, 150Å pores) was added. This mixture stirred at room temperature for 30 minutes. It was heated to 150°C with continued stirring to evaporate all solvent. Solid was calcinated at >300°C in a gas stream of 40:60 hydrogen and nitrogen for 5 hours.

Synthesis of Copper Catalyst – Shell Method

CuCl powder (0.62g, 6.26mmol) was weighed into a glass evaporating dish. Distilled water (2mL) was added for a solution molarity of 0.31M. Aqueous sodium hydroxide (5mL, 30% solution) was added to this slowly, with constant stirring. Stirring continued for one hour at room temperature. Spherical silica (2g, 75-200μm, 150Å

pores) was added. This mixture was stirred at room temperature for 30 minutes. It was warmed to 150°C with continued stirring to evaporate solvent. The solid was calcinated at >300°C in a gas stream of 40:60 hydrogen and nitrogen for 5 hours.

Synthesis of Supported Cobalt Catalyst – Shell Method

$CoCl_2$ powder (0.22g, 1.70mmol) was weighed into a glass evaporating dish. Distilled water (5mL) was added for a solution molarity of 0.339M. Aqueous sodium hydroxide (0.4mL, 30% solution) was added to this slowly, with constant stirring. Stirring continued for one hour at room temperature. Spherical silica (2g, 75-200μm, 150Å pores) was added. This mixture was stirred at room temperature for 30 minutes. It was warmed to 150°C with continued stirring to evaporate solvent. The solid was calcinated at >300°C in a gas stream of 40:60 hydrogen and nitrogen for 5 hours.

UV-vis Analysis

To obtain UV-vis spectra of the starting salts, a few crystals of each metal salt were dissolved in ethylene glycol. To obtain UV-vis spectra of product solution, two drops of solution were removed from the product and diluted in ethylene glycol.

Preparation of XRD Samples

XRD samples were prepared on clean glass plates. A small amount of product powder (plain nanoparticles or nanoparticles embedded on silica) was made into a slurry with ethanol. Pasteur pipette was used to transfer the slurry 2-3 drops at a time onto the slide. Ethanol was allowed to evaporate in between each addition. Sample had to cover

an area 0.5cm by 1cm in the center of the slide to obtain good results. Slides were dried in the vacuum oven overnight.

Preparation of SEM Samples

SEM samples were made on SEM stops covered with black carbon tape. Silica supported nanoparticle powder was dusted onto the carbon tape. Samples were coated with either chromium or a gold/palladium mix prior to imaging.

Preparation of TEM Samples

TEM samples were made on carbon coated copper grids. A few drops of metal nanoparticle solution in ethylene glycol were diluted heavily in ethanol (1mL). The mixture was sonicated to evenly disperse particles. One single drop of solution was placed on each grid and allowed to dry in air followed by vacuum drying for 5 minutes.

Preparation of Calibration Curves: Ammonia, Nitrogen, Hydrogen, and Hydrazine

With the first generation GC analysis, configuration, and settings of 130°C and 10mL/min. flow rate, calibration curves of the product gases were made using calibrating gas mixtures containing either 2 mol% or 8 mol% of ammonia, nitrogen, and hydrogen with argon as the balance gas. The areas obtained from these two calibrating gases were used, along with the assumption that at 0% calibration there will be no area response in the GC-TCD. Calibration curves were obtained at flow rates of 83.7mL/min, 190mL/min, 95mL/min, 43.1mL/min, 29.4mL/min and a flow meter setting of 5, which

does not have a calibrated value, and in all cases, R^2 values were 0.98 or higher (Figures 2.48-2.53).

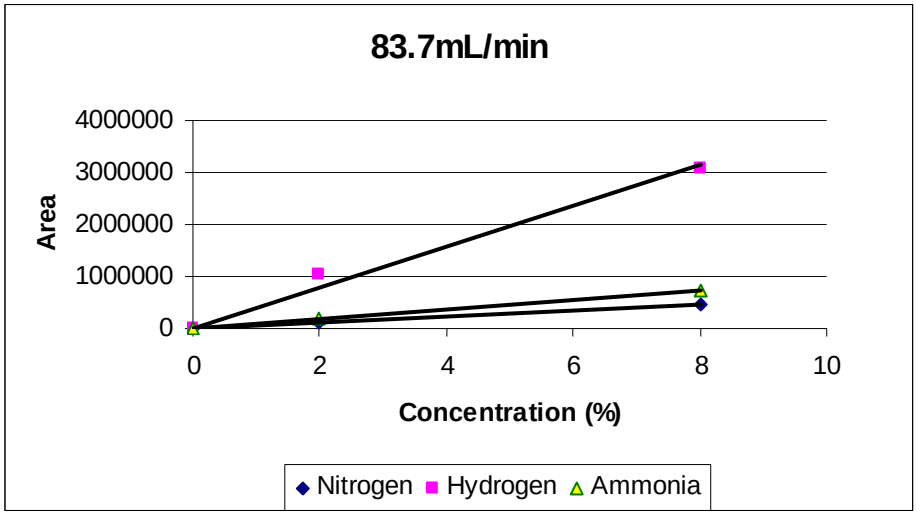

Figure 2.48 Calibration curves of N_2, H_2 and NH_3 at 83.7mL/min

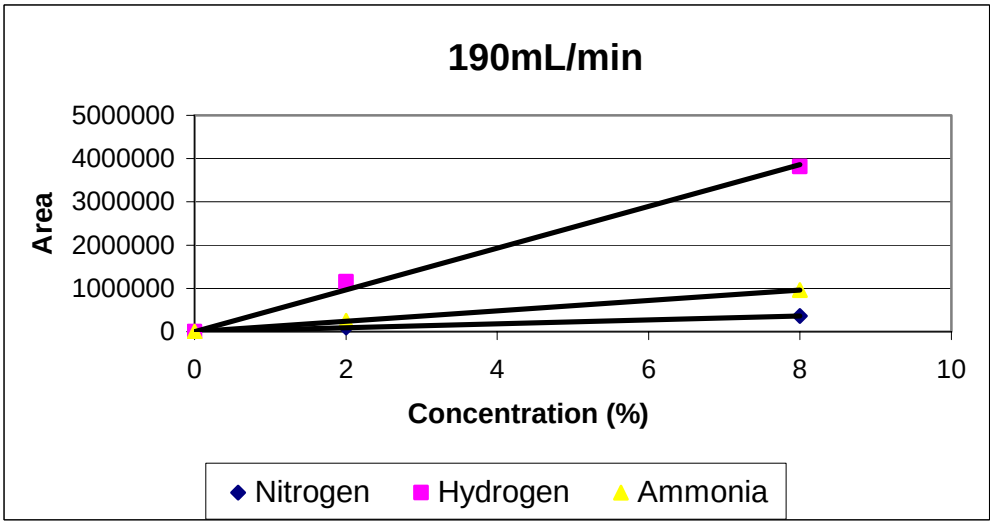

Figure 2.49 Calibration curves of N_2, H_2 and NH_3 at 190mL/min

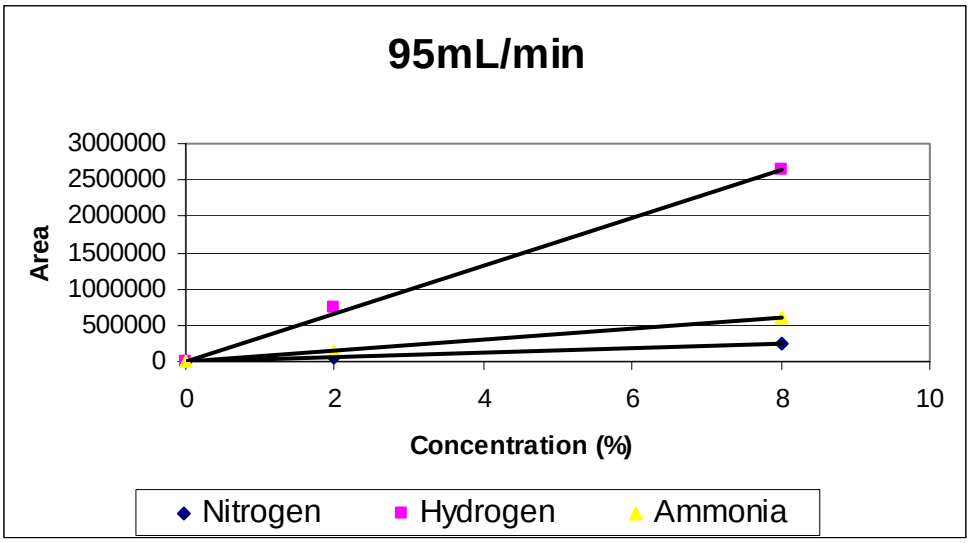

Figure 2.50 Calibration curves of N_2, H_2 and NH_3 at 95mL/min

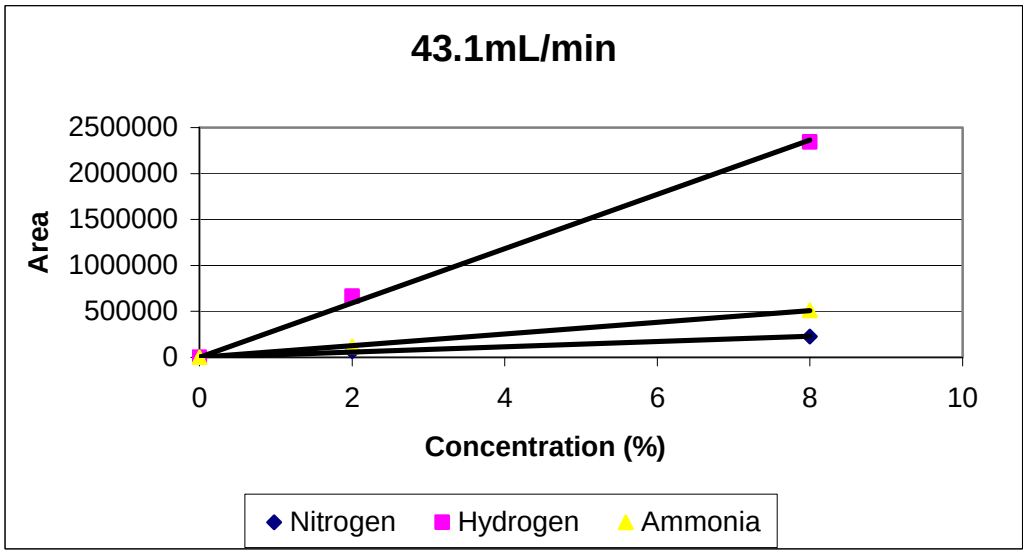

Figure 2.51 Calibration curves of N_2, H_2 and NH_3 at 43.1mL/min

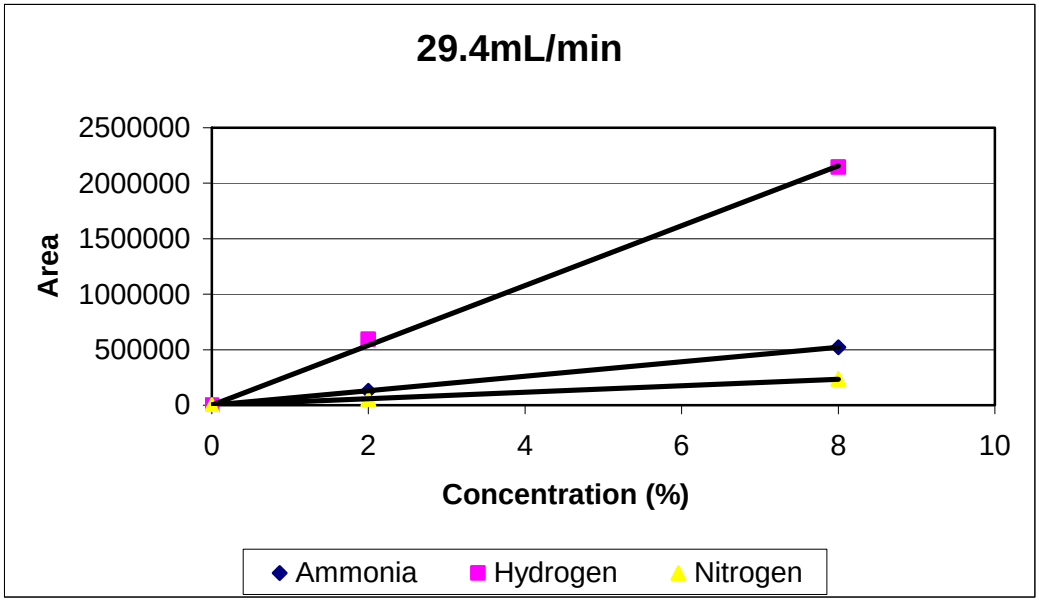

Figure 2.52 Calibration curves of N_2, H_2 and NH_3 at 29.4mL/min

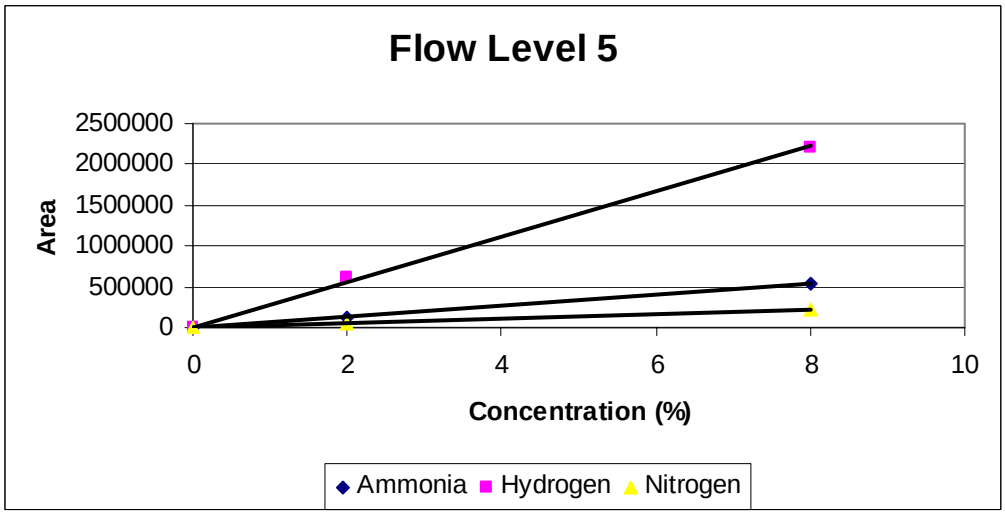

Figure 2.53 Calibration curves of N_2, H_2 and NH_3 at Flow Level 5

With this configuration, the ammonia and hydrazine peaks overlapped with each other due to trailing of the peaks (a common phenomena for compounds containing amine functionality). Therefore, each peak was deconvoluted using the Origin® program. In order for data obtained in Origin to be accurately analyzed, the calibration curves had to be re-done using this program. This was necessary, as the GC software and the Origin software use a substantially different standard area unit. Calibrations at 83.7mL/min, 29.4mL/min, and Flow Level 5 were re-done in Origin (Figures 2.54-2.56).

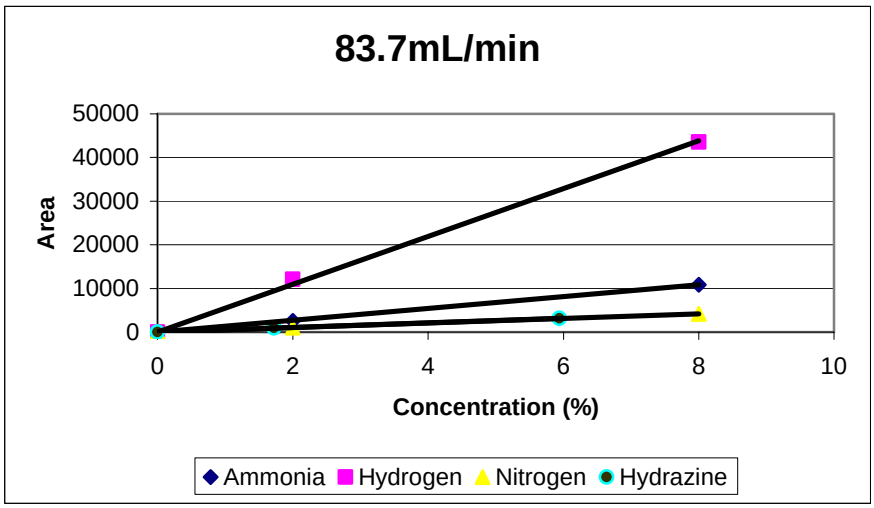

Figure 2.54 Calibration curves of N_2, H_2, NH_3 and N_2H_4 at 83.7mL/min after processing with Origin

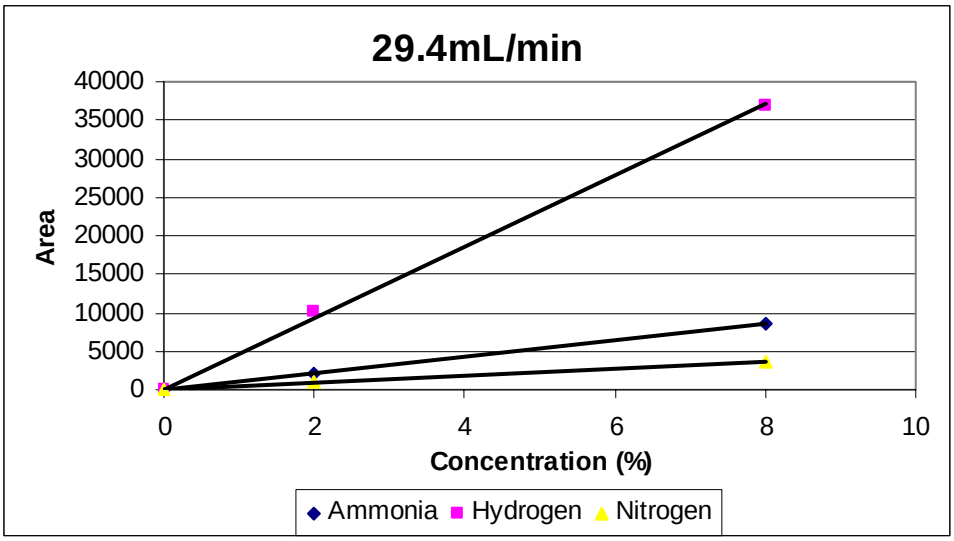

Figure 2.55 Calibration curves of N_2, H_2, and NH_3 at 29.4mL/min after processing with Origin

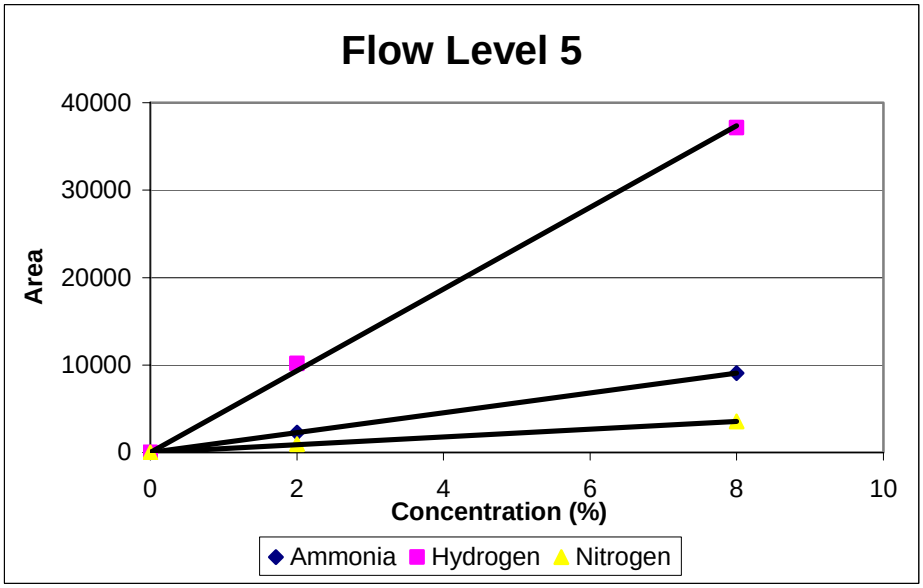

Figure 2.56 Calibration curves of N_2, H_2, and NH_3 at Flow Level 5 after processing with Origin

A calibration curve of hydrazine was also prepared. The hydrazine concentration in the argon stream was varied by varying the temperature of the hydrazine reservoir and therefore the vapor pressure.[57] At the constant flow rate of 83.7 mL/min, the concentration of hydrazine in argon was 1.72 mol% at 25°C and and 5.94 mol% at 45°C. The resulting linear calibration curve with an R^2 value of 0.9947 is shown in Figure 2.57 as well as a comparison of the calibrations for all four gases at a flow rate of 83.7mL/min.

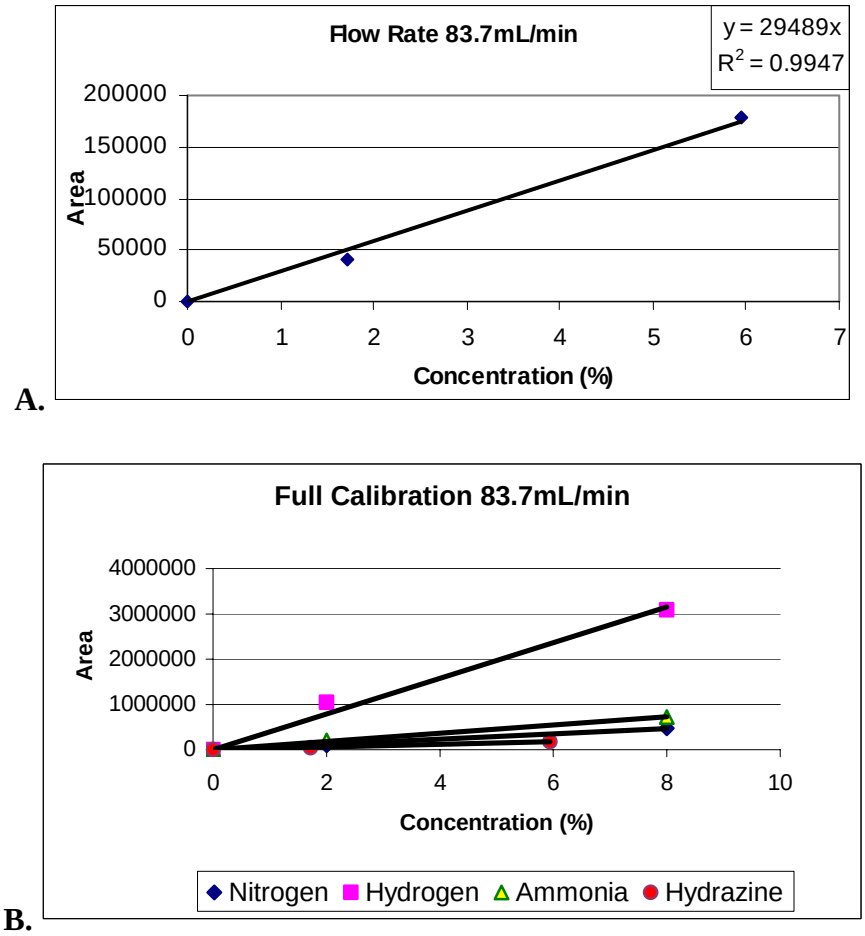

Figure 2.57 A. Calibration of pure hydrazine at 83.7mL/min. **B**. Calibration of all 4 gases at 83.7mL/min

With the second generation GC configuration and settings of 130°C and flow rate 50mL/min, new calibrations were performed. The calibrations of ammonia and the unseparated mixture of N_2 and H_2 gas were performed using 2% and 8% purchased gas mixtures, and assuming a 0 response at 0% calibration for the third point. For each gas, a linear calibration with an R^2 value of 0.99 was obtained (Figure 2.58).

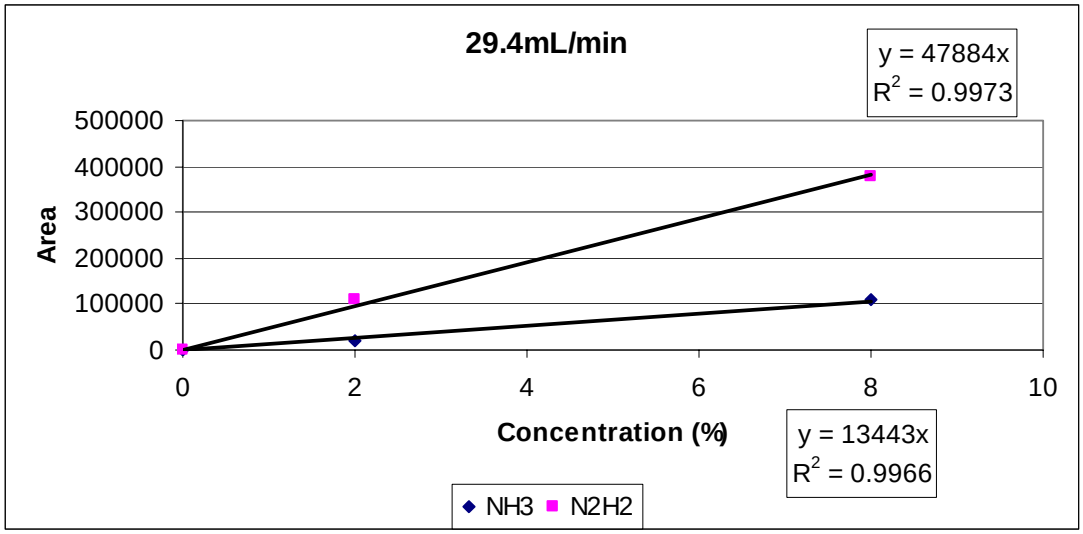

Figure 2.58 Calibration curves of NH_3 and N_2/H_2 mixture at 29.4mL/min

Hydrazine was calibrated at a flow rate of 29.4mL/min by analyzing samples containing 0.9% hydrazine 1.4% hydrazine Assuming 0% hydrazine produces 0 response, a linear calibration with an R^2 value of 0.99 was achieved (Figure 2.59).

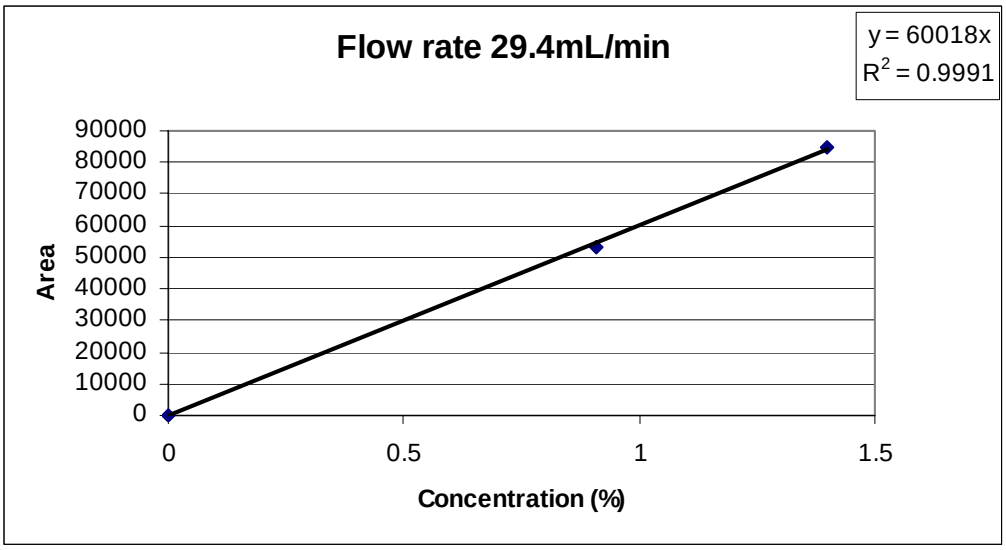

Figure 2.59 Calibration curve for hydrazine at 29.4mL/min

Catalyst Bed Packing Procedure

First Generation: Catalyst was packed in ¼ inch stainless steel 316 tubing (4inches in length). Into one end, 230 mesh size stainless steel mesh, and glass wool were packed. Catalyst powder was added through a funnel. During addition vacuum was pulled (~1mmHg) through the tube, accompanied by vibration to ensure even packing. After the tube was filled, glass wool was inserted in the other end, as well as another piece of 230 mesh size stainless steel mesh.

Second Generation: Catalyst was packed in empty HPLC columns of 4.6mm inner diameter and 30mm in length made of 316 stainless steel. A frit containing 20μm pores was placed at each end of the column. Catalyst powder was added through a funnel. During addition vacuum was pulled (~1mmHg) through the tube, accompanied by vibration to ensure even packing.

Hydrazine Decomposition

For both first and second generation reactors, hydrazine (1mL) was loaded into a glass vessel. Argon carrier gas was flowed through the system. Flow rate was controlled by a flow meter. This carrier gas bubbled through the liquid hydrazine. Based on the temperature of the hydrazine and pressure of the system, a certain percentage of hydrazine vapor was carried into the catalyst bed. The catalyst bed was heated to 75°C. The product stream passed from the catalyst bed into a sample loop heated to 75°C. Rotation of a six-port valve injected the sample from the sample loop into the GC.

GC Troubleshooting

During attempts to calibrate hydrazine at a flow rate of 29.4mL/min, a diminished signal with a gas stream of 7.1% was seen, much lower than what was expected for these conditions (an area of 20,000-30,000 versus 170,000-180,000 expected). To determine where the loss of signal was occurring, the system was tested with the GC at different temperatures and flow rates. The GC oven was set at 130°C and the gas flow rate at 10mL/min. It was found that upon increasing the temperature of the oven to 200°C, while leaving the flow rate at 10mL/min., a consistent hydrazine peak was again obtained. The GC temperature was decreased to 170°C and signal was also detected, so further analyses were run at this temperature.

However, the decomposition of hydrazine to ammonia and nitrogen was seen in the absence of catalyst. This was evidenced by the decrease of the hydrazine peak and the appearance of an ammonia peak, as well a nitrogen peak (Figure 2.41).

To determine whether this problem was occurring in the reactor system or within the GC-TCD itself, the hydrazine gas stream from the end of the reactor was collected

and condensed into a tetrahydrofuran (THF) solution in a dry ice bath. After an hour of collection, this solution was injected into a GC-mass spec. For comparison, an independently prepared solution of hydrazine in THF was also injected into the GC-MS. The two solutions gave identical spectra, both clearly indicating the presence of hydrazine. This test showed that the complete decomposition we were seeing and any hydrazine adsorption leading to a diminishing of signal was taking place in the analysis zone.

The GC-columns were packed 316 stainless steel columns. This stainless steel is rated for use with hydrazine, however, only up to a temperature of 70°C.[58] At higher temperatures and for long exposure time hydrazine decomposition can be catalyzed by these column walls. New glass lined columns were purchased and installed, both of the Chromosorb 102 and the silica column. With these new glass lined columns a 1.6% hydrazine gas stream was passed into the GC, which was set at 170°C and flow rate of 20mL/min. Decomposition of the hydrazine was successfully prevented. However, the hydrazine signal exhibited an area of 20,228±1100 when 44,000±1000 was expected based on previous results. The peak was very broad, trailing over 7 minutes; inconsistent and multi-humped (Figure 2.60). When the temperature was ramped up to 240°C, a single broad peak could be eluted.

The GC system was examined in sections. First, a 1.6% hydrazine stream was injected directly from our reactor into the GC detector. A consistent peak with an area of 133,000±8800 was obtained (Figure 2.61). Next, the hydrazine was passed through the glass lined silica column and to the detector. Once the system stabilized, while the peak shape was now different, it was a consistent peak with an area of 134,000±1500 (Figure

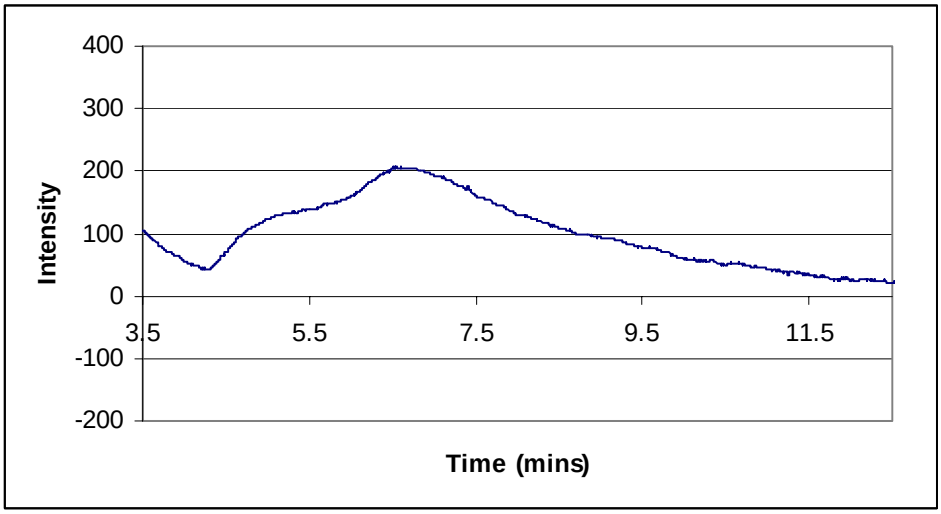

Figure 2.60 Hydrazine peak obtained with glass lined Chromosorb 102 columns

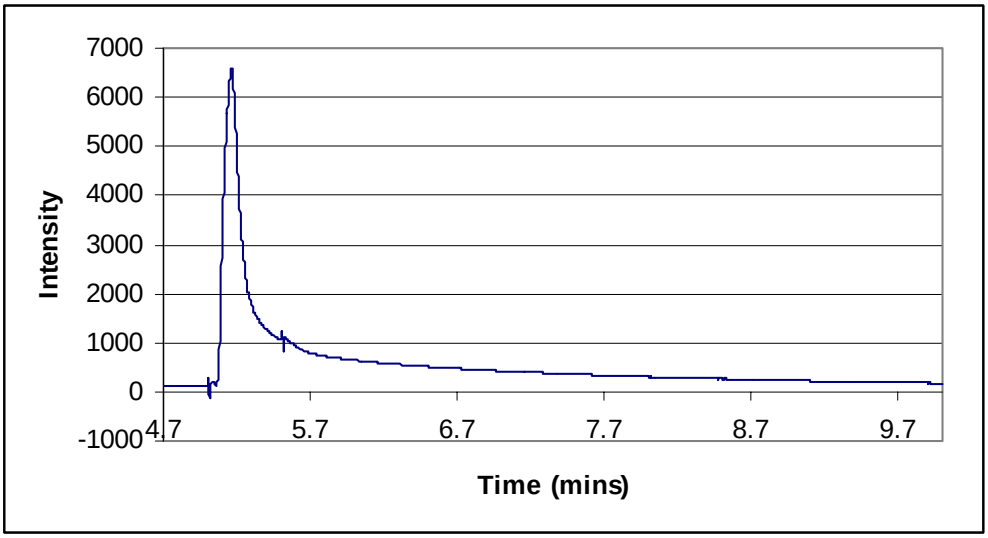

Figure 2.61 Peak obtained from hydrazine passing straight to the detector

2.62). Within error, these are the same value, indicating that the hydrazine problem was not occurring within the silica column either. This implied that the problem could be with the Chromosorb 102 column. To test this, hydrazine was passed straight through this column and to the detector bypassing all other columns and the valve switch.

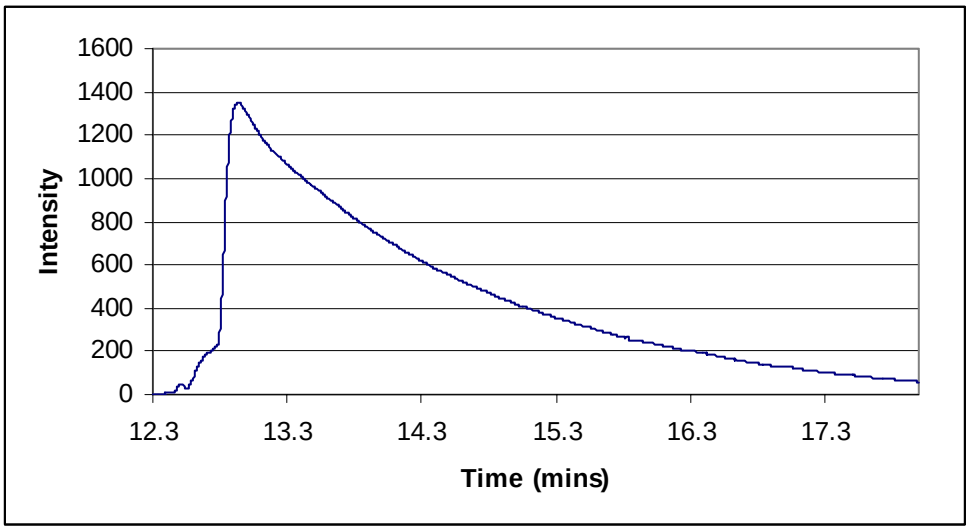

Figure 2.62 Peak obtained from hydrazine passing only through the Supelcoport column

When this was done the peak area diminished considerably, to 44,000. As more samples were run under these conditions, the peak area fluctuated going as low as 34,000 and as high as 46,000. It also broadened from two and half minutes for complete elution to six minutes, and it went from being a single humped peak to having four distinct humps (Figure 2.63). This confirmed that the problem was arising within the Chromosorb 102 column.

Two columns, Tenax TA and Carbowax 1500 were chosen as possible replacements since they are used both in literature as well as by the International Standards Organization to verify the purity of commercially available hydrazine.[59-61]

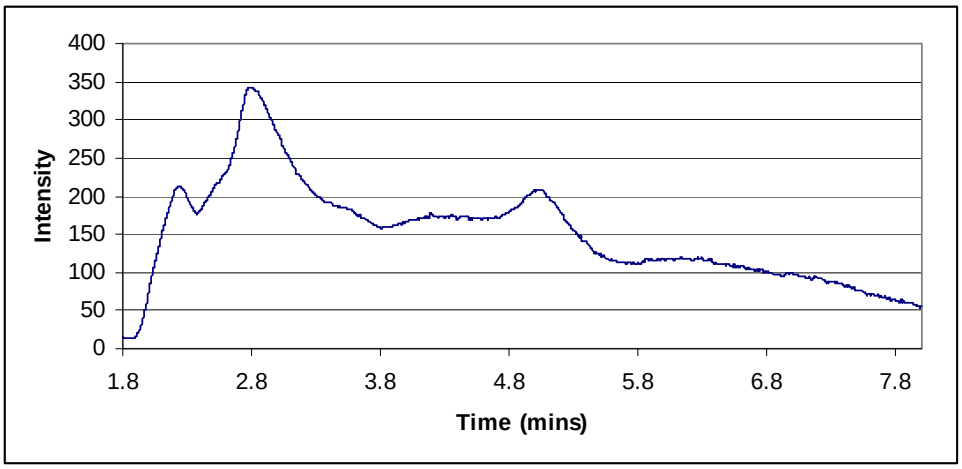

Figure 2.63 Peak obtained from hydrazine passing only through the glass lined Chromosorb 102 column

Initially the Tenax TA column appeared promising. Using this column when a hydrazine gas stream containing 1.6% was passed through the GC at 170°C and a flow rate of 20mL/min a signal with an area of 64,000 ± 3,500 was seen. This signal was broad, taking almost 7 minutes to elute, and double humped, but it was consistent. When the concentration in the gas stream was increased to 9.0%, the signal area increased to 93,000 ± 6,000. Though the peak was still taking 7 minutes to elute, and was double humped, again the peak was consistent (Figure 2.64).

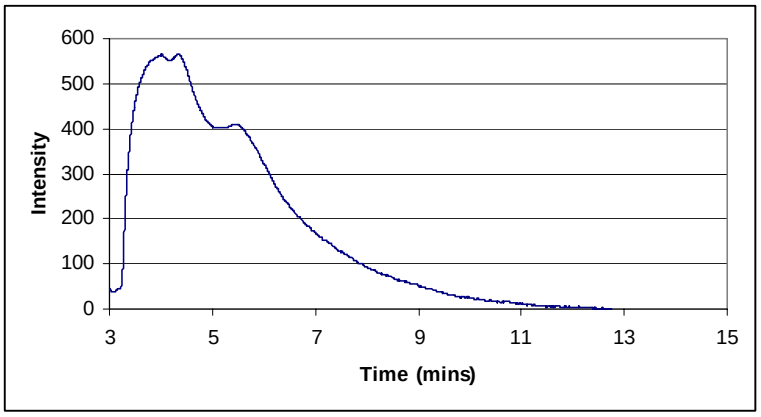

Figure 2.64 Peak obtained from 9% hydrazine passing through Tenax TA

These results were not reproducible, however. When the system was run under the exact same conditions for a second time, the 1.6% hydrazine gas stream gave a signal of only 10,600 ± 280 and the 9% gas stream gave a signal of only 15,400 ± 400. Furthermore, a second unidentified peak appeared down field at a retention time of 8.3 minutes (Figure 2.65).

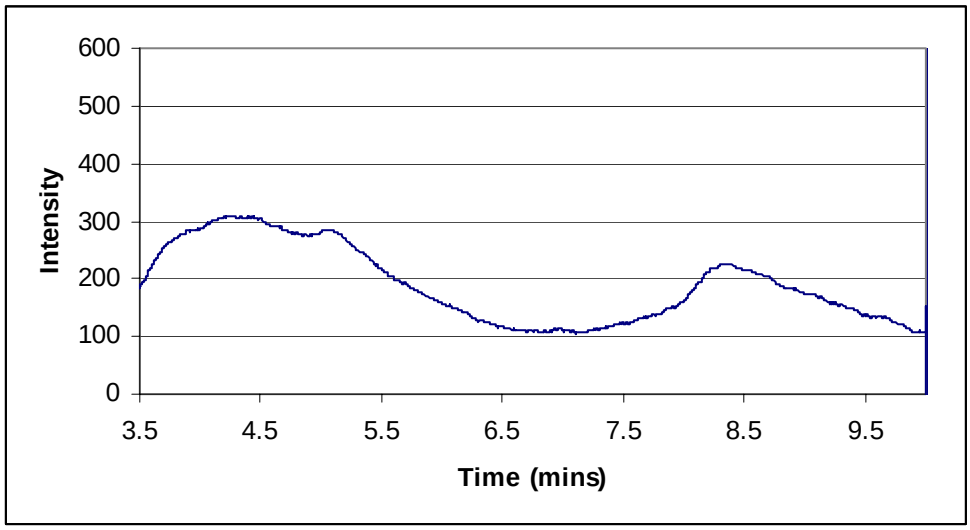

Figure 2.65 Repeat of 9% hydrazine passing through Tenax TA showing a smaller hydrazine peak and new peak

In literature, there are cases where before hydrazine is analyzed, the GC columns are first pre-saturated by a direct injection of liquid hydrazine into the system.[60] That was attempted with the Tenax column by a direct injection of 10µL of liquid hydrazine into the system. After the baseline stabilized, the 1.6% gas stream was again injected from the system. Unfortunately, the saturation did not appear to improve the quality of the resulting hydrazine peak.

The Carbowax 1500 column was installed in the GC. These columns are stable at much lower temperatures than the Chromosorb 102 or the Tenax TA and in literature are

often used at temperature ranges from 100°C-130°C but with high flow rates.[59-60] So, initially the GC was set at 100°C and a flow rate of 40mL/min. Several injections of a 1.6% hydrazine stream produced no peaks. The column temperature was increased to 130°C, and again no peaks were visible. The column saturation was attempted with these columns as well, by direct injection of 30μL of liquid hydrazine per literature method.[60] However, this appeared to have no affect as, after allowing the baseline to stabilize, injections of a 1.6% gas stream from the reactor did not show a signal.

The 2% calibrating gas was passed through this system, and while hydrogen and nitrogen showed the expected peaks, no ammonia signal was visible. The Carbowax 1500 columns were removed and replaced by the Tenax TA columns. 2% calibrating gas was passed through this system with the GC set at 170°C and a flow rate of 20mL/min. Once again, an ammonia signal was not present. This indicated that the problem was not related to the column packing material, as it was seen with two different columns.

By segmenting the GC system, it was found that when calibrating gas was passed only through the injector valve and Tenax column straight into the detector, the ammonia peak was present with the expected area. However, once the calibrating gas was passed through the second six-port valve, that peak disappeared. The valve was removed and opened up for inspection and cleaning. Inside, it was found to contain a black oily liquid. It is likely that this liquid was caused by a reaction between hydrazine the valve material of construction, hastelloy. The six-port injector valve was also opened up and found to contain a similar black liquid. To overcome this problem, the injector valve was replaced by an identical valve constructed of Nitronic 60 stainless steel. The analysis system was also redesigned to only require the use of a single valve, minimizing potential

interaction/decomposition, and the second generation analysis was developed (See section 2.3.5).

2.6 References

1. Vieira, R.; Pham-Huu, C.; Keller, N.; Ledoux, M. J.; *New Carbon Nanofiber/Graphite Felt Composite for Use as a Catalyst Support of Hydrazine Catalytic Decomposition,* Chem. Commun., 2002, **9,** p: 954-955.

2. Chen, X.; Zhang, T.; Zheng, M.; Xia, L.; Li, T.; Wu, W.; Wang, X.; Li, C.; *Catalytic Decomposition of Hydrazine over $\alpha Mo_2C/\gamma$-Al_2O_3 Catalysts,* Ind. Eng. Chem. Res., 2004, **43,** p: 6040-6047.

3. Maurel, F.; Menezo, J. C.; Barrault, J.; *Decomposition of Hydrazine on Group VIII and Group Ib Metals,* J. Chim. Phys., 1973, **70,** p: 1221-1226.

4. Maurel, R.; Menezo, J. C.; *Catalytic Decomposition of ^{15}N-Labeled Hydrazine on Alumnia-Supported Metals,* J. Catal., 1978, **51,** p: 293-295.

5. Cosser, R. C.; Tompkins, F. C.; *Heterogeneous Decomposition of Hydrazine on Tungsten Films,* Trans. Farad. Soc., 1971, **67**, p: 526-544.

6. Contaminard, R. C. A.; Tompkins, F. C.; *Heterogeneous Decomposition of Hydrazine on Molybdenum Films,* Trans. Farad. Soc., 1971, **67**, p: 545-555.

7. Watanabe, K.; Azuma, K.; *Note on the Field Emission Microscopic Observation of Decomposition of Hydrazineon Rhenium,* J. Res. Inst. Catalysis, Hokkaido Univ., Japan, **14(3)**, p: 257-259.

8. Willhoft, E. M. A.; Robertson, A. J. B.; *Mass-Spectrometric Investigation of the Formation of Diimide by the Catalytic Decomposition of Hydrazine at Low Pressures at Platinum,* Chem. Soc. London Chem. Commun., 1967, **1967,** p: 385-387.

9. Wood, B. J.; Wise, H.; *The Interaction of Hydrazine with Polycrystalline Iridium Foil,* J. Catal., 1975, **39**, p: 471-480.

10. Smith, O. I.; Solomon, W. C.; *Kinetics of Hydrazine Decomposition on Iridium and Alumina Supported Iridium Catalysts,* AFRPL-TR-73-59, Aug. 1973, **80**, p: 34.

11. Khomenko, A.; Apelbaum, L. O.; *Study of the Kinetics of the Catalytic Decomposition of Hydrazine Vapors on Paladium,* Kinet. Catal., 1976, **17,** p: 600-607.

12. Rienaecker, G.; Voelter, J.; *Decomposition of Hydrazine Vapor on Copper Single Crystals,* Z. Anorg. Allg. Chem., 1959, **302,** p: 292-298.

13. Block, J.; *Chemisorption and Field Ionization of Hydrazine on Platinum Surfaces,* Z. Phys. Chem. N. F., 1972, **82,** p: 1-10.

14. Grunze, M.; *The Interaction of Hydrazine with and Fe(III) Surface,* Surface Sci., 1979, **81,** p: 603-625.

15. Martignoni, P., et al,; *The Thermal and Catalytic Decomposition of Ammonia and Hydrazine,* U. S. Army Rept. RK-TR-70-2, Jan. 1970, AD-749262, NOFORN, p: 16.

16. Contour, J. P.; Pannetier, G.; *Investigation of Catalytic Properties of Iridium Deposited on γ-Alumina. IV. Investigation of the Adsorption and Desorption of Hydrazine by Thermodesorption and Infrared Spectroscopy,* Bull. Soc. Chim. France, 1970, **1970,** p: 4260-4264.

17. Contour, J. P.; Pannetier, G.; *Hydrazine Decomposition over a Supported Iridium Catalyst,* J. Catal., 1972, **24,** p: 434-445.

18. Escard, J.; Leclere, C.; Contour, J. P.; *The State of Supported Iridium in a Hydrazine Decomposition Catalyst,* J. Catal., 1973, **29,** p: 31-39.

19. Al-Haydari, Y. K.; Saleh, J. M.; Matloob, M. H.; *Adsorption and Decomposition of Hydrazine on Metal Films of Iron, Nickel, and Copper,* J. Phys. Chem., 1985, **89,** p: 3285-3290.

20. Boudjahem, A. G.; Monteverdi, S.; Mercy, M.; Bettahar, M. M.; *Study of Nickel Catalysts Supported on Silica of Low Surface Area and Prepared by Reduction of Nickel Acetate in Aqueous Hydrazine,* J. Catal., 2004, **221**, p: 325-334.

21. Wojcieszak, R.; Zieliński, M.; Monteverdi, S.; Bettahar, M. M.; *Study of Nickel Nanoparticles Supported on Activated Carbon Prepared by Aqueous Hydrazine Reduction.* J. Coll. Int. Sci., 2006, **299,** p: 238-248.

22. Estournès, C.; Lutz, T.; Happich, J.; Quaranta, T.; Wissler, P.; Guille, J. L.; *Nickel Nanoparticles in Silica Gel: Preparation and Magnetic Properties,* J. Mag. Mag. Mater., 1997, **173,** p: 83-92.

23. Trimmel, G.; Lembacher, C.; Kickelbick, G.; Schubert, U.; *Sol-gel Processing of Alkoxysilyl-Substituted Nickel Complexes for the Preparation of Highly Dispersed Nickel in Silica,* New J. Chem., 2002, **26,** p: 759-767.

24. Armstrong, W. E.; Ryland, L. B.; Voge, H. H.; *Catalyst Comprising Ir or Ir and Ru for Hydrazine Decomposition,* US Patent 4124538, **1978.**

25. Chen, X.; Zhang, T.; Zheng, M.; Wu, Z.; Wu, W.; Li, C.; *The Reaction Route and Active Site of Catalytic Decomposition of Hydrazine over Molybdenum Nitride Catalyst,* J. Catal., 2004, **224,** p: 473-478.

26. Couto, G. G.; Klein, J. J.; Schreiner, W. H.; Mosca, D. H.; de Oliveira, A. J. A.; Zarbin, A. J. G.; *Nickel Nanoparticles Obtained by a Modified Polyol Process: Synthesis, Characterization, and Magnetic Properties,* J. Coll. Int. Sci., 2007, **311,** p: 461-468.

27. Wu, S-H.; Chen, D-H.; *Synthesis and Characterization of Nickel Nanoparticles by Hydrazine Reduction in Ethylene Glycol,* J. Coll. Int. Sci., 2003, **259,** p: 282-286.

28. Bai, L.; Yuan, F.; Tang, Q.; *Synthesis of Nickel Nanoparticles with Uniform Size via a Modified Hydrazine Reduction Route,* Mater. Lett., 2008, **62,** p: 2267-2270.

29. Kurihara, L, K.; Chow, G. M.; Schoen, P. E.; *Nanocrystalline Metallic Powders and Films Produced by the Polyol Method,* Nano. Mater., 1995, **5,** p: 607-613.

30. Gao, S.; Zhang, J.; Zhu, Y.-F.; Che, C.-M.; *A Convenient Solvothermal Route to Ruthenium Nanoparticles,* New J. Chem., 2000, **24**, p: 739-740.

31. Xiao, J.; Xie, Y.; Luo, W.; *A Rational Low-Temperature Approach to the Synthesis of Gladiate Ruthenium Nanoparticles,* Chem. Lett., 2002, **31(4),** p: 462-463.

32. Yan, X.; Liu, H.; Liew, K. Y.; *Size Control of Polymer-Stabilized Ruthenium Nanoparticles by Polyol Reduction,* J. Mater. Chem., 2001, **11,** p: 3387-3391.

33. Balela, M. D. L.; Lockman, Z.; *Protective Agent-Free Synthesis of Colloidal Cobalt Nanoparticles,* J. Phys. Sci., 2008, **19(1),** p: 1-11.

34. Kamal, S. S. K.; Sahoo, P. K.; Premkumar, M.; Rao, N. V. R.; Kumar, T. J.; Sreedhar, B.; Singh, A. K.; Ram, S.; Sekhar, K. C.; *Synthesis of Cobalt Nanoparticles by a Modified Polyol Process using Cobalt Hydrazine Complex,* J. Alloys Comp., 2009, **474,** p: 214-218.

35. Gibson, C. P.; Putzer, K. J.; *Synthesis and Charaterization of Anisometric Cobalt Nanoclusters,* Science, 1995, **267,** p: 1338-1340.

36. Hoefelmeyer, J. D.; Niesz, K.; Somorjai, G. A.; Tilley, T. D.; *Radial Anisotropic Growth of Rhodium Nanoparticles,* Nano. Lett., 2005, **5(3),** p: 435-438.

37. Grass, M. E.; Joo, S. H.; Zhang, Y.; Somorjai, G. A.; *Colloidally Synthesized Monodisperse Rh Nanoparticles Supported on SBA-15 for Size and Pretreatment Dependent Studies of CO Oxidation,* J. Phys. Chem. C., 2009, **113,** p: 8616-8623.

38. Bonet, F.; Delmas, V.; Grugeon, S.; Urbina, R. H.; Silvert, P.-Y.; Tekaia-Elhsissen, K.; *Synthesis of Monodisperse Au, Pt, Pd, Ru, and Ir Nanoparticles in Ethylene Glycol,* Nano. Mater., 1999, **11(8),** pp: 1277-1284.

39. Zheng, M.; Chen, X.; Cheng, R.; Li, N.; Sun, J.; Wang, X.; Zhang, T.; *Catalytic Decomposition of Hydrazine on Iron Nitride Catalysts,* Catal. Commun., 2006, **7,** p: 187-191.

40. Goebel, D. M.; Katz, I.; *Fundamentals of Electric Propulsion: Ion and Hall Thrusters,* JPL Space Science and Technology Series, John Wiley and Sons, March 2008.

41. Tsay, M. M.; Martinez-Sanchez, M.; *Simple Performance Modeling of a Radio-Frequency Ion Thruster.,* 30th International Electric Propulsion Conf., Florence, Italy, IEPC-2007-072, 2007

42. Bassner, H.; Killinger, R.; Leiter, H.; Müller, J.; *Development Steps of the RF-ION Thrusters RIT,* 27th International Electric Propulsion Conf., Pasadena, CA, IEPC-01-105, 2001.

43. Groh, K. H.; Loebt, H. W.; *State of the Art of Radio-Frequency Ion Thrusters,* J. Prop. Power, 1991, **7(4),** p: 573-579.

44. Funaki, I.; Kuninaka, H.; Toki, K.; *Plasma Characterization of a 10-cm Diameter Microwave Discharge Ion Thruster,* J. Prop. Power, 2004, **20(4),** p: 718-727.

45. Esker, D. W.; Kroutil, J. C.; Checkley, R. J. *Radiation Cooled MPD Arc Thruster,* NASA CR 72557, Report MDC H296, 1969.

46. Willis, C.; Lossing, F. P.; Back, R. A.; *The Heat of Formation of N_2H_2 and the Proton Affinity of N_2*, Can. J. Chem., 1976, **54(1),** p: 1-3.

47. Martin, J. A.; *Dual-Fuel, Dual-Mode Rocket Engine,* US Patent 4831808, **1989.**

48. Eggers, R. F.; Emmons, D. L.; *Two-Stage Hydrazine Rocket Motor,* US Patent 3695041, **1972.**

49. Park, Y. R.; Kim, K, J.; *Sol-gel Preparation and Optical Characterization of NiO and $Ni_{1-x}Zn_xO$ Thin Films,* J. Cryst. Growth, 2003, **258**, p: 380-384.

50. Savinova, E. R.; Chuvilin, A. L.; Parmon, V. N.; *Copper Colloids Stabilized by Water-Soluble Polymers Part I. Preparation and Properties,* J. Mol. Catal., 1988, **48,** p: 217-229.

51. Sun, X.; Zhang, Y.-W.; Si, R.; Yan, C.-H.; *Metal (Mn, Co and Cu) Oxide Nanocrystals from Simple Formate Precursors,* Small, 2005, **1(11),** p: 1081-1086.

52. Guo, F.; Zheng, H.; Yang, Z.; Qian, Y.; *Synthesis of Cobalt Nanoparticles in Ethanol Hydrazine Alkaline System (EHAS) at Room Temperature,* Mater. Lett., 2002, **56,** p: 906-909.

53. Mankidy, B. D.; Gupta, V. K.; *Novel Composite Particles for Catalysis: Cobalt Nanoparticles on Silica Colloids,* 60th Southeast Regional Metting of the American Chemical Society, Nashville, TN, November 12-15 2008.

54. Kogelbauer, A.; Weber, J. C.; Goodwin, J. G. Jr.; *The Formation of Cobalt Silicates on Co/SiO_2 under Hydrothermal Conditions,* Catal. Lettl, 1995, **34(3,4),** p: 259-267.

55. Viau, G.; Brayner, R.; Poul, L.; Chakroune, N.; Lacaze, E.; Fiévet-Vincent, F.; Fiévet, F.; *Ruthenium Nanoparticles: Size, Shape, and Self-Assemblies,* Chem. Mater., 2003, **15,** p: 486-494.

56. CRC, *Handbook of Chemistry and Physics,* 80th Ed., 1999-2000, editor D. Lide, Washington, DC: CRC Press, p. 6-184.

57. Haws, J. L.; Harden, D. G.; *Thermodynamic Properties of Hydrazine,* J. Space. Rockets, 1965, **2(6),** p: 972-974.

58. Schmidt, E. W.; *Hydrazine and its Derivatives: Preparation, Properties, and Applications,* John Wiley and Sons., New York, 1984.

59. Bighi, C.; Saglietto, G.; *The Gas-Chromatographic Separation of Mixtures of Hydrazine, Methylhydrazine and 1,1Dimethylhydrazine,* J. Chrom., 1965, **18,** p: 297-301.

60. Brull, E. E.; *Improved Column Systems for Gas Chromatographic Determination of Hydrazine Impurities,* J. Chrom. Sci., 1974, **12,** p: 33-35.

61. International Organization for Standardization, *Space Systems-Fluid Characteristics, Sampling and Test Methods-Part 7: Hydrazine Propellant,* ISO/DIS 15859-7, 2002.

62. Huang, S. X.; Rufael, T. S.; Gland, J. L.; *Diimide Formation on the Nickel(100) Surface*, Surf. Sci., 1993, **290(1-2),** p: L673-L676.

CHAPTER THREE
SWITCHABLE ROOM TEMPERATURE IONIC LIQUIDS

3.1. Introduction

Solvents as we traditionally know them have very fixed properties. For example, a polar solvent is always polar, while a non-polar solvent is always non-polar. Some properties, such as viscosity can be modified slightly by altering temperature and pressure of a system, but in general the chemical and physical properties of a given solvent are known and constant. While this can have advantages, there are many cases in which this becomes a disadvantage. In large multi-step syntheses, the solvent may have to be removed and changed between each step, and on an industrial scale, this has a major economic and environmental impact. Having a single solvent whose properties could be easily changed would be a major benefit.

In the past few years, switchable materials have frequently been reported in literature. [1, 2] The first switchable solvent system was published in 2005, by the Eckert-Liotta and Jessop groups. Specifically, bubbling CO_2 through a one-to-one mixture of 1,8-Diazabicyclo[5.4.0]undec-7-ene (DBU) and hexanol led to the formation of a room temperature ionic liquid.[3] Sparging N_2 through the system or heating at only 50 or 60°C reversed it back to the molecular liquid. (Figure 3.1)

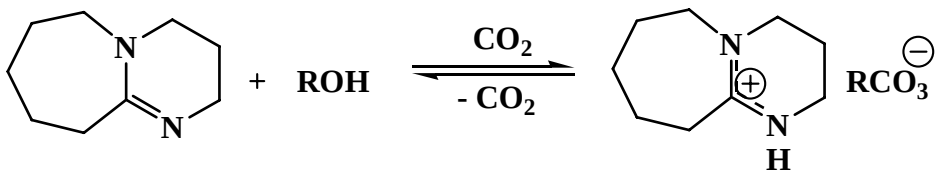

Figure 3.1 Switchable room temperature ionic liquid (RTIL) system based on DBU and an alcohol, controlled by the addition or removal of CO_2

Using the dye Nile Red as a polarity probe, it was measured that with this system, the switch from molecular liquid to ionic liquid is the equivalent of going from the polarity of chloroform to that of dimethylformamide (DMF), a rather substantial switch. In this chapter, other switchable ionic liquid systems are presented, a two component guanidine based system and a one component silylated amine based system, both of which have been studied for their benefits in reactions and separations, as well as other applications such as extraction of pure hydrocarbons from crude oil and bitumen.[4-7]

3.2. Background

3.2.1 Room Temperature Ionic Liquids

In recent years, room temperature ionic liquids, also known as molten salts or RTIL's, have been very popular in literature. They have been touted as the next wave of solvents to fix all the current problems inherent with using standard volatile organic solvents. It is true that RTIL's have many unique and often desirable properties; they generally are conductive, have high solvating properties, and low vapor pressure. It is because of their low vapor pressure that many recognize them as "green" solvents. However, recent studies have shown that, low vapor pressure not withstanding, many RTIL's can be highly toxic to humans and animals and can bioaccumulate easily due to low biodegradability, low volatility, and ease of water solubility.[8-10] This is, however, very structure dependent and often varies according to the chosen anion in the ionic liquid molecule.

3.2.2 Reversible Ionic Liquids

The first known reversible ionic liquid system was published in 2005 by the Eckert-Liotta and Jessop groups.[3] This original work was very basic and focused on a single system, DBU mixed in a 1 to 1 ratio with 1-hexanol. The ionic liquid was formed by bubbling CO_2 through the system, and reversed by sparging with nitrogen. The formation and reversal were confirmed by ^1H NMR. Polarity and miscibility of this single system were also tested. Polarity measurements with Nile Red as the indicator molecule showed that in switching from a molecular liquid to an ionic liquid the solvent switched from a system with the polarity of chloroform to one with the polarity of propanoic acid or the solvent DMF. This polarity change had a major affect on the miscibility of the system as, in the molecular form it was completely miscible with decane, while in the ionic liquid form the two liquids were immiscible. While this publication only gave preliminary information on a single system, and DBU is highly water reactive so the applications of this specific system are very limited, it was a major breakthrough as it opened up the possibilities and potentials available with this type of unique switchable solvent system.

All further ionic liquid work focused on this same type of system using alcohols until, in 2007, Yamada *et al* found that N,N-dimethyl-N'-hexyl ethanimidamide formed a reversible RTIL with n-butylamine and CO_2.[11] (Figure 3.2) With this type of system, when the ionic liquid was exposed to water, there did not appear to be any formation of amidinium carbonates.[11] Unlike the DBU system this was an example of a reversible ionic liquid system which was also water stable, a property which now greatly opened up

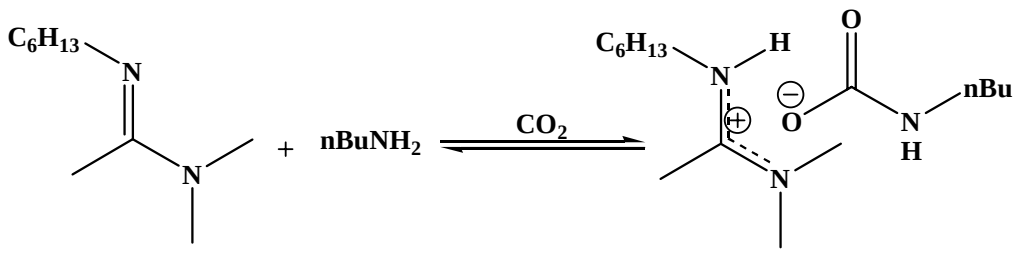

Figure 3.2 Reaction of N,N-dimethyl-N'-hexyl ethanimidamide, n-butylamine, and CO_2 to form RTIL

the number and variety of potential applications for this type of system. However, like the DBU system, this one was still a two component system meaning it relied on two molecular starting components (an amide an amine) that must be kept in an exact 1:1 ratio for the system to be successful. This poses numerous problems from a processing standpoint, and for large scale application, a system with the same beneficial properties, but made from a single starting component, would be much more beneficial.

3.2.3 Two Component Ionic Liquids

Guanidines were chosen for development in a two component ionic liquid system because they are strong bases and are much less reactive to water than amidines. In addition, guanidinium structures have been frequently used as traditional non-reversible ionic liquids.

3.2.3.1 Guanidine Based Ionic Liquids

The first ionic liquids using a non-reversible guanidinium based cation appeared in literature in 2003, when Mateus *et al* synthesized a variety of tetra-alkyl-dimethylguanidinium salts, (Figure 3.3).[12] Of the seventeen different guanidinium salts synthesized, ten were found to be liquids at room temperature. Those that were ionic

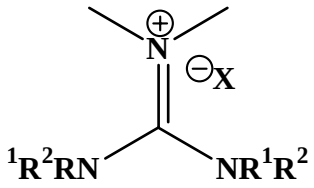

R^1,R^2= Me, Et, n-Bu, n-Hex, n-Oct

X = PF_6, BF_4, Tf_2N, Cl

Figure 3.3 First series of guanidinium based ionic liquids synthesized

liquids showed very good thermal stability (25-150^oC for 24-48h), as well as stability under acidic (HCl), basic (KOH), nucleophilic (NH_3) and oxidative ($NaIO_4$ and O_2) conditions. They also showed low glass transition temperatures. In general, when compared to the common RTIL n-butylimidazolium chloride ([bmim][Cl]), the hexa-alkyl guanidinium salts showed comparable stability.[12]

This study provided the first valuable insight into the affect that the alkyl substitutions on the guanidine have on its physical properties, such as melting point (or glass transition temperature) and miscibility with various solvents, as well as what an important role the anion plays in the system. Ultimately it showed how easy this type of system would be to tailor for specific applications, simply by switching out either the alkyl substitutions on the guanidine (R^1 and R^2, Figure 3.3) or the anion of the ionic liquid (X in Figure 3.3). It provided the first discussion into what a wide range of possibilities there could be for use of these systems due to these unique properties. Soon after this initial publication, three other papers based on hexa-alkyl guanidinium RTILs were published,[13] presenting the possibility of using these novel RTILs for dye-sensitized solar cells[14] and oxidations.[15] Since that time, guanidine based ionic liquids have been successfully used as catalysts for Henry reactions (Figure 3.4)[16] and aldol

condensations[17-18], as solvents for Heck reactions[19], and as immobilized on supports to act as heterogeneous catalysts for olefin hydrogenation[20], just to give a few examples, showing that they are highly versatile.

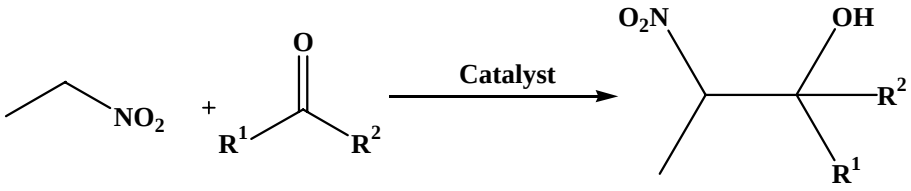

Figure 3.4 Example of guanidinium catalyzed Henry reaction. R^1 and R^2 can be H, aromatic, alkyl

The Liotta-Eckert group recently discovered that guanidines, when mixed in a 1:1 molar ratio with alcohols can reversibly react with CO_2. Specifically, it was found that when an equimolar mixture of methanol and 2-butyl-1,1,3,3-tetramethylguanidine was exposed to gaseous CO_2 at one atmosphere the RTIL 2-butyl-1,1,3,3-tetramethylguanidinium methylcarbonate (TMBG MC IL) was formed.[4] (Figure 3.5) In contrast with other guanidine ionic liquid systems found in literature, TMBG MC IL is easily reversible by bubbling N_2(g), or by heating at 80°C as confirmed by ^{1}H and ^{13}C NMR.

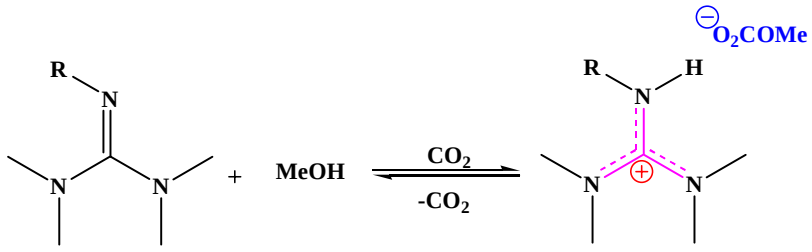

Figure 3.5 Reversible formation of 2-butyl-1,1,3,3-tetramethylguanidinium methylcarbonate ionic liquid

3.2.4 One Component Ionic Liquids

The two component ionic liquids systems have many beneficial characteristics, and maintain an important place as the first reversible ionic liquid systems developed. However, as mentioned previously, to be useful in large scale industrial applications, a reversible ionic liquid system is needed that is based on a single molecular starting component. Primary amines were chosen to study this as they should react with CO_2 in much the same way that guanidine and alcohol mixtures do to form reversible ionic liquids.[5] (Figure 3.6)

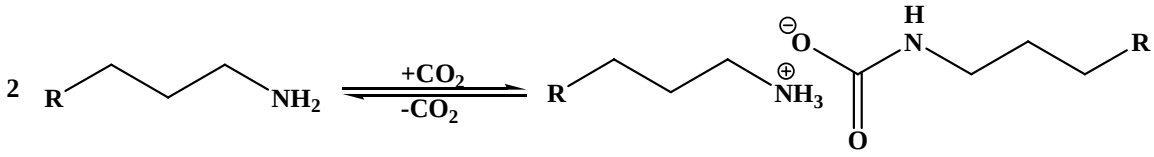

Figure 3.6 Basic scheme of an amine based one component reversible ionic liquid.

It is important to note that this is a unique system unlike anything previously published in literature. It is true that quite a bit of work has been done on the use of amines and amine based ionic liquids to trap CO_2, but that is not what is being presented here. In literature, these so-called task specific ionic liquids are designed specifically for CO_2 capture via mainly chemisorption (Figure 3.7).[21]

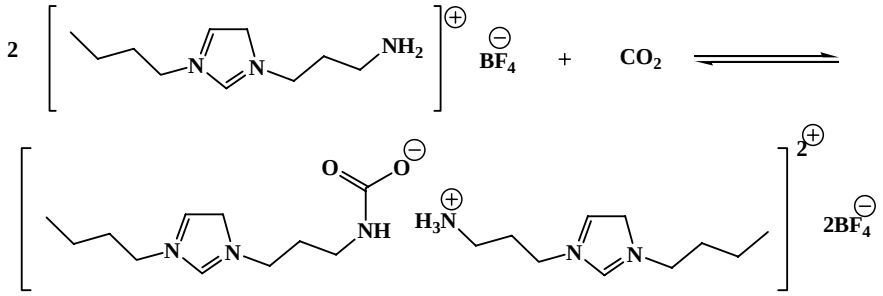

Figure 3.7 Example of task specific amine based ionic liquid for CO_2 capture.

3.3 Results and Discussion

3.3.1 Two Component Ionic Liquids

3.3.1.1 Synthesis of 2-butyl-1,1,3,3-tetramethylguanidine (TMBG)

Tetra-alkylsubstituted ureas are reacted with oxalyl chloride, phosgene, or phosphorus oxychloride producing the intermediate N-(chloro(dimethylamino)methylen)-N-methylmethanaminium chloride (Compound 2, Figure 3.8) which can be reacted with an aliphatic or aromatic primary amine to obtain a penta-substituted guanidine (Figure 3.8).[13,22-25] While there are variations in solvents used, reaction time and reaction temperature, the same basic procedure is always consistent. While this process is successful in producing product, the yields are generally low to moderate, the process is time consuming and involves many solvent changes and highly toxic chemicals (phosgene for example).

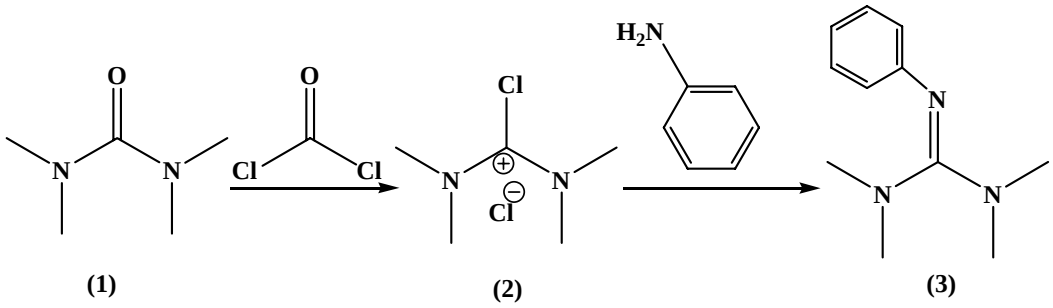

Figure 3.8 Example of the guanidine synthesis method

Basically, no simple straightforward procedure exists in literature for the synthesis of 2-butyl-1,1,3,3-tetramethylguanidine (TMBG) (Figure 3.9). Originally, the method reported by Costa, *et al* for the synthesis of 2-cyclohexyl-1,1,3,3-tetramethylguanidine was modified for our purposes.[23]

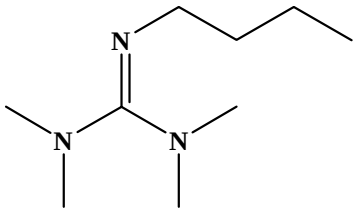

Figure 3.9 2-butyl-1,1,3,3-tetramethylguanidine (TMBG)

In this method, 50mL of dry 1,2-dichloroethane were added to a round bottom flask along 5mL tetramethyl urea. To this, 8mL of oxalyl chloride were added at room temperature. This was allowed to reflux at 60°C for 12 hours, at which point the solvent was removed and the resulting solid dissolved in dry acetonitrile. 8mL of butylamine dissolved in 20mL of dry acetonitrile were slowly added dropwise at 0°C. This was allowed to warm to room temperature, then refluxed at 92°C for 24 hours. Solvent was removed under vacuum, and the resulting oil was treated with 30% NaOH solution, extracted with diethyl ether, dried with magnesium sulphate, filtered, and ether solvent removed under reduced pressure. This resulted in a pale yellow oil. Distillation of this oil led to a clear, colorless product whose structure (Figure 3.9) was confirmed by NMR and elemental analysis.

Results using this method were inconsistent, however, with yields often in the 30% range with large quantities of degradation product in the mixture. To address this, a switch was made to the method published by U. Schuchardt *et al.* for the synthesis of 1,1,2,3,3-pentamethylguanidine.[22] While similar in many respects, this method differed on several key points; these include reaction time and temperature. Specifically, the first step was allowed to react for 2 hours at 70°C instead of 12 hours at 60°C, and in the second stirring was conducted at room temperature overnight then refluxed for only 1

hour as opposed to 24 hours. This method gave better results, improving isolated yields to ~70%. However there was still a substantial amount of unreacted starting material, approximately 15% of the total as seen in ^{1}H NMR (Figure 3.10) and it was believed that 2 hours was not a long enough reaction time for all tetramethylurea to be consumed. Ultimately the chosen reaction method was a combination of the two previously described methods with the first step reacting for 5 hours at 70°C and the second step refluxing for 1 hour at 92°C (Figure 3.11). When fresh reagents were used this method consistently gives yields of 70-75%.

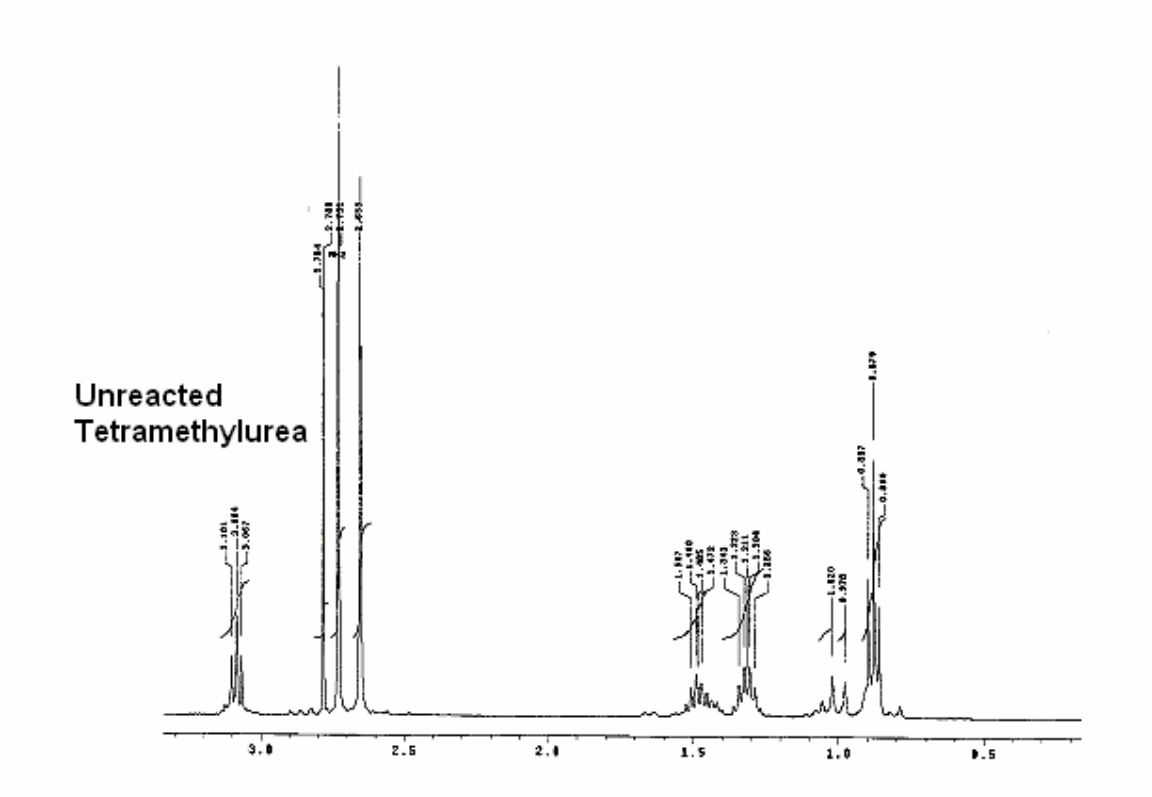

Figure 3.10 ^{1}H NMR of TMBG product from the Schuchardt method, showing the large amount of unreacted tetramethylguanidine remaining in the system

The entire reaction including the product is highly water sensitive, so in all cases all procedures were conducted under strictly anhydrous conditions. Starting materials were

stored in the glove box, all reactions were run under nitrogen or argon, and the final product was also stored in the glove box as soon as it was purified.

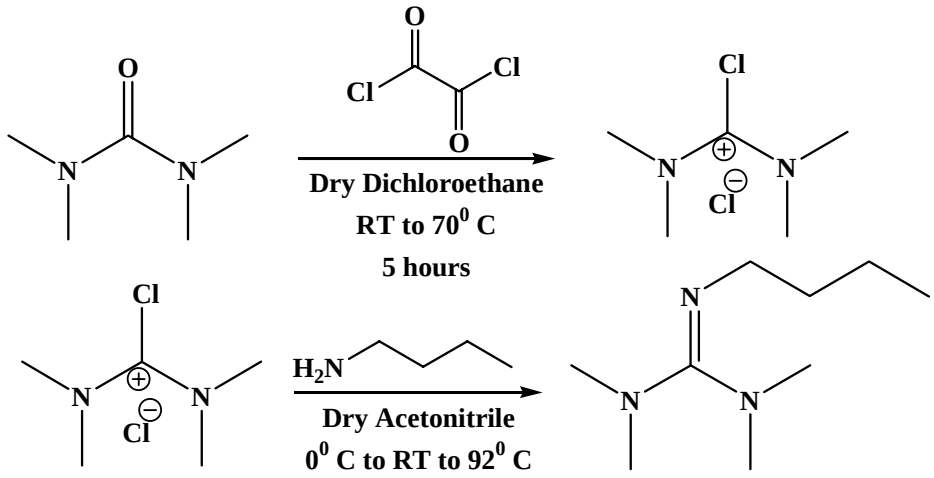

Figure 3.11 Optimized synthesis of 2-butyl-1,1,3,3-tetramethyl guanidine (TMBG)

3.3.1.2 Alternative Approach for the Synthesis of 2-butyl-1,1,3,3-tetramethylguanidine

A simple one pot, one step synthesis method, for penta-substituted guanidines that could be easily scaled up was also investigated. This involved the simple reaction of tetramethylguanidine with n-butylbromide. The first step in this process is the reaction of butylbromide with tetramethyl guanidine to form 2-butyl-1,1,3,3-tetramethyl guanidinium bromide (Figure 3.12).

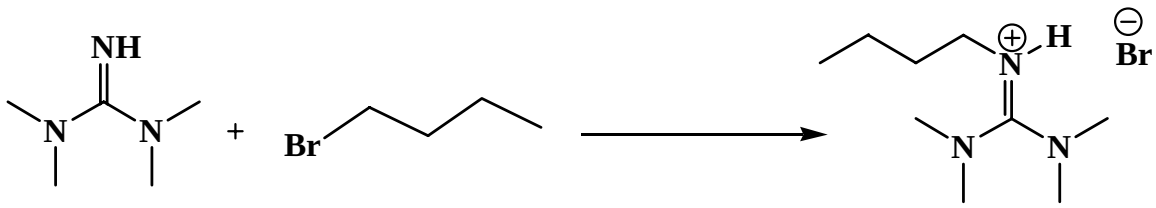

Figure 3.12 Basic reaction scheme for one step TMBG synthesis

As the bromide group is a good leaving group, this salt should form easily. Depending on the reaction conditions, either this salt will crash out of solution, which helps drive the reaction, and it can then be neutralized, or base in the system will perform the neutralization in situ. Either excess TMG in the system (Figure 3.13 A) or the added base NaOH (Figure 3.13 B) has been used for this neutralization.

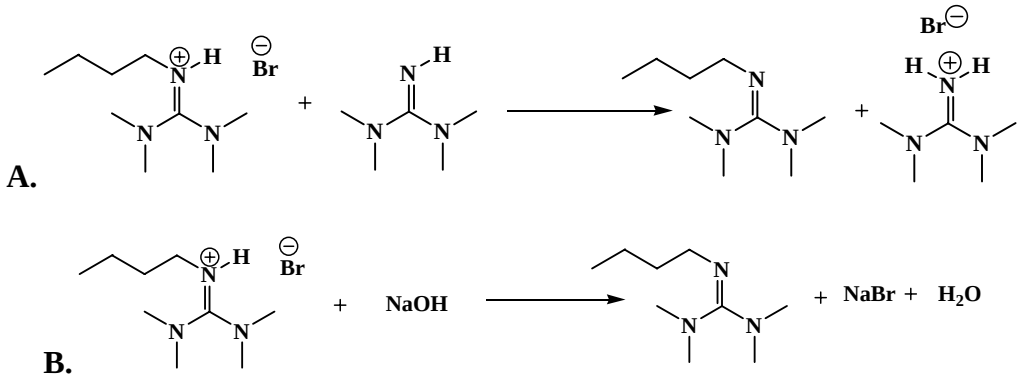

Figure 3.13 A. Neutralization by excess TMG. **B.** Neutralization by NaOH

First attempts at this reaction were done with a 3:1 excess of tetramethylguanidine (TMG) to butylbromide. 25mL of TMG were placed in a three neck flask, and 7.13mL of butylbromide were slowly added dropwise with stirring. This solution was refluxed at 100°C overnight. After reacting overnight a pale yellow solid formed in the bottom of the flask. This was removed by filtration, washed with pentane and treated with 30% NaOH solution. At this point the product existed in an aqueous mixture. All organics were extracted with diethyl ether (3 times, 25mL), dried with magnesium sulphate, filtered, and the ether solvent removed under reduced pressure. The NMR showed a mixture of approximately 4:1 starting material (tetramethylguanidine) and desired TMBG product. This mixture was purified using Kugelrohr distillation, and a large improvement

was seen, as the amount of TMG decreased from 80% of the total solution to 8%. However, that 8% was still too great of an amount for TMBG to be used as a pure product.

In an effort to increase the purity of the product both different separation techniques and different reaction methods were attempted. The different reaction conditions tested are summarized in Table 3.1. For the first five sets of conditions tested (Runs 1-5, Table 3.1) the starting materials were mixed together at room temperature, along with a base if used, then brought to the desired reaction temperature. Of these, the best results were obtained in Run 5, where a 2:1 ratio of TMG to n-BuBr was reacted at 120°C. This method gave 100% yields, as shown by a 1:1 ratio of TMG to TMBG in the NMR.

Table 3.1 Reaction conditions studied for the one pot synthesis of TMBG

	Starting Ratio	**Base**	**Reaction Temp.**	**Reaction Time**
Run 1	3:1 TMG:BuBr	None	100°C	Overnight
Run 2	1:1 TMG:BuBr	Solid NaOH	100°C	1 hour
			Room Temp.	Overnight
Run 3	2:1 BuBr:TMG	50mL DCM	70°C	1 hour
			Room Temp.	Overnight
Run 4	2:1 TMG:BuBr	None	100°C	Overnight
Run 5	2:1 TMG:BuBr	None	120°C	1 hour
			Room Temp.	Overnight
Run 6	2:1 BuBr:TMG	Solid NaOH	TMG at 120°C	1 hour
			Room Temp.	Overnight
Run 7	1:1 BuBr:TMG	None	TMG at 120°C	1 hour
			Room Temp.	Overnight
Run 8	1:1 BuBr:TMG	None	BuBr at 120°C-145°C	Allowed to cool once peak temp. reached

In an attempt to separate the desired product from TMG, three different separation methods were studied. Distillation was the first method attempted; however, it could not get below the 8% TMG impurity level achieved by using the Kugelrohr, and often the

entire sample thermally decomposed. Crystallization was the second method tried; however, it is believed the two substances have freezing points that are too close to together as no clear separation was achieved, even though solid was formed in the solution. The final method attempted was the use of CO_2 and methanol in the system. It is known that CO_2 and a 1:1 mix of TMG and methanol form a solid salt, rather than an ionic liquid (Figure 3.14), and that this would crash out of solution. However, no solid was seen when CO_2 was bubbled through the mixture, which most likely occurred because that solid is soluble in the TMBG MC IL

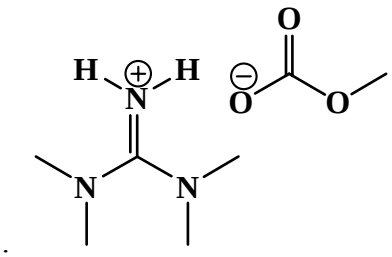

Figure 3.14 Tetramethylguanidinium methylcarbonate salt.

For Runs 6-7 (Table 3.1) the TMG was preheated to 120°C, at which point n-BuBr was added dropwise with vigorous stirring. In Run 8 (Table 3.1) these conditions were reversed; the n-BuBr was preheated to 120°C and TMG was added dropwise. The best results were obtained when the n-BuBr was first heated to 120°C and the TMG was slowly added dropwise with stirring in a 1:1 ratio (Run 8, Table 3.1). The reaction exotherm was allowed to spike to a maximum at approximately 145°C, at which point all heating was stopped and the solution allowed to cool to room temperature. Standard work up procedure, using NaOH solution was performed, and NMR analysis showed formation of TMBG in good yields, with the product mixture containing ~90% of the

desired TMBG product. However 8-9% unreacted TMG starting material remained in the system as seen by ^{1}H NMR.

Based on these promising results, several further attempts were made to improve the reaction yield and decrease the impurity amount. These attempts included running the entire reaction at higher temperatures (145-160°C) and bubbling argon gas through the solution rather than simply having it flowing over the mixture as the reaction was occurring. However, in no case was the amount of TMG present decreased below 8%.

3.3.1.3 Synthesis and Characterization of the Ionic Liquid 2-butyl-1,1,3,3-tetramethylguanidinium methylcarbonate

The ionic liquid 2-butyl-1,1,3,3-tetramethylguanidinium methylcarbonate (TMBG MC IL) was formed by reacting an equimolar amount of methanol and 2-butyl-1,1,3,3-tetramethylguanidine with CO_2. Operationally, CO_2 gas was bubbled through the equimolar solution of methanol and guanidine until the exotherm from the reaction ceased. The salt formed was a viscous oily liquid. It was characterized by NMR (^{1}H, ^{13}C & DEPT-135), IR, elemental analysis, and melting point. The NMR data was run neat, and showed all expected peaks for this structure, including the appearance of a carbonate peak in the $^{13}CNMR$ at 158.15ppm. The elemental analysis data exactly matched that for 2-butyl-1,1,3,3-tetramethylguanidinium methyl carbonate, and the IR clearly showed the appearance of a methyl carbonate peak at 1780cm^{-1}. The melting point was found to be -24 ± 1°C.

The solvatochromic properties of 2-butyl-1,1,3,3-tetramethylguanidinium methylcarbonate were thoroughly investigated. Initially standard Kamlet-Taft

measurements as well as dielectric constant measurements were attempted. However, these were unsuccessful as Reichardt's dye reacted with the solvent, leading to a disappearance of its typical color, and other standard Kamlet-Taft probes absorb at the same wavelength as TMBG. However, it is known that dielectric constants are often difficult to measure for room temperature ionic liquids due to overlapping of signals or reactivity of the ionic liquid with probe molecules.[26] To address these limitations, the solvatochromic probe Nile Red is often used for the polarity determinations of ionic liquids (Figure 3.15).[27] With this probe, the wavelength of maximum absorption is a direct comparative indicator of polarity of a solvent.

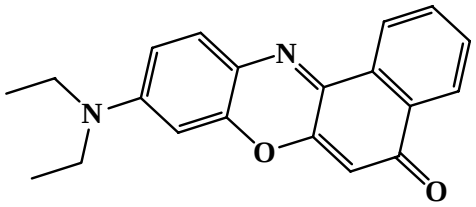

Figure 3.15 Structure of solvatochromic probe Nile Red.

In Table 3.2 the λ_{max}, or wavelength of maximum absorption, obtained for 2-butyl-1,1,3,3-tetramethylguanidinium methylcarbonate (TMBG MC), as well as those for other common solvents and ionic liquids are compared.[28-29] It can be clearly seen that when exposed to CO_2, the system is significantly more polar than the molecular liquid mixture of TMBG and methanol, as evidenced by the change in λ_{max} from 538nm to 554nm. This jump is substantial enough that it is equivalent to going from a solvent with the properties of chloroform (537.6nm) to one with the properties of acetic acid (557.2nm). Upon comparison with λ_{max} values reported in the literature,[28-29] it can also

be seen that the solvent 2-butyl-1,1,3,3-tetramethylguanidinium methyl carbonate has properties comparable to other known room temperature ionic liquids (hexylmethylimidazole tetrafluoroborate ionic liquid, $[C_6mim][BF_4]$, λ_{max} (Nile Red)= 551.9).

Table 3.2 Comparison of common λ_{max} values[28-29] with TMBG and TMBG MC IL.

Solvent	λ_{max}, nm, Nile Red
Ether	504.4
CH_2Cl_2	535.2
$CHCl_3$	537.6
TMBG + MeOH	538.0
DMF	541.2
Propanoic acid	542.4
$[bmim][PF_6]$[1]	547.5
DMSO	549.2
$[bmim][BF_4]$[1]	550.8
$TMBGH^+ + MeOCO_2^-$	554.0
Acetic Acid	557.2

1. bmim = 1-butyl-3-methylimidazonium

3.3.1.4 Relative Polarities of Various Solvents with 2-butyl-1,1,3,3-tetramethylguanidinium alkylcarbonates

Along with methanol, 1-butanol, 1-hexanol, 1-octanol, and 1-dodecanol in combination with TMBG and reaction with CO_2 were all tested for their abilities to form reversible room temperature ionic liquids (Figure 3.16). In each case, an equimolar amount of alcohol was added to 2-butyl-1,1,3,3-tetramethylguanidine. Operationally, CO_2 was bubbled through the solution until the reaction exotherm ceased. Each ionic product was characterized with ^1H and ^{13}C NMR melting point, and elemental analysis. The polarity switch was also examined. The NMR samples were run neat and showed

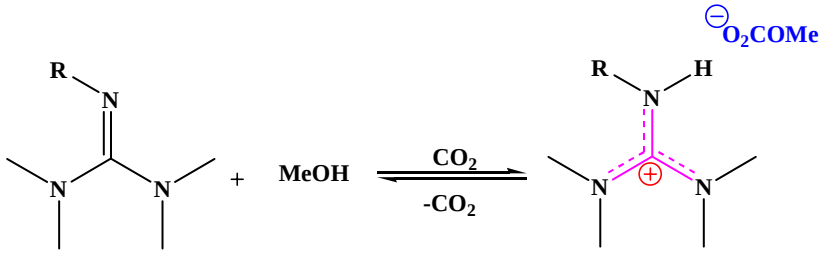

Figure 3.16 Reversible formation of a variety of alkyl carbonate ionic liquids

the expected peaks for these structures. Figure 3.17 shows a few representative examples of these ^{1}H NMR spectra. In these the most important aspect to note is the single large peak at 3.1, which are the four methyls on the TMBG. This will only exist as a single peak if the mixture is in the ionic form due to the charge resonance within the molecule.

The melting points of these ionic liquids as a function of alcohol chain length were also determined (Figure 3.18). As might be expected, the longer chain length alcohols have a higher melting point, following the trend of the alcohols themselves. However, in all cases, the ionic species formed is well within the range of ionic liquid as, even for the longest alcohol, dodecanol, the melting point is still at -10.5°C ± 1°C, well below room temperature.

Nile Red was used as a solvatochromic probe to measure polarity. The polarity of the systems was found to depend on alcohol chain length, with longer chain alcohols leading to both lower polarity (536.6 for dodecanol ionic liquid, versus 554.0 for methanol ionic liquid), indicated by a shorter λ_{max}, and a smaller polarity difference between the molecular and ionic forms. However, even this smaller difference was still a substantial jump, such as changing from the properties of benzene to those of chloroform for the neutral to ionic liquid switch using dodecanol. Table 3.3 shows the relative polarities of these liquids with respect to each other, as well as other common solvents

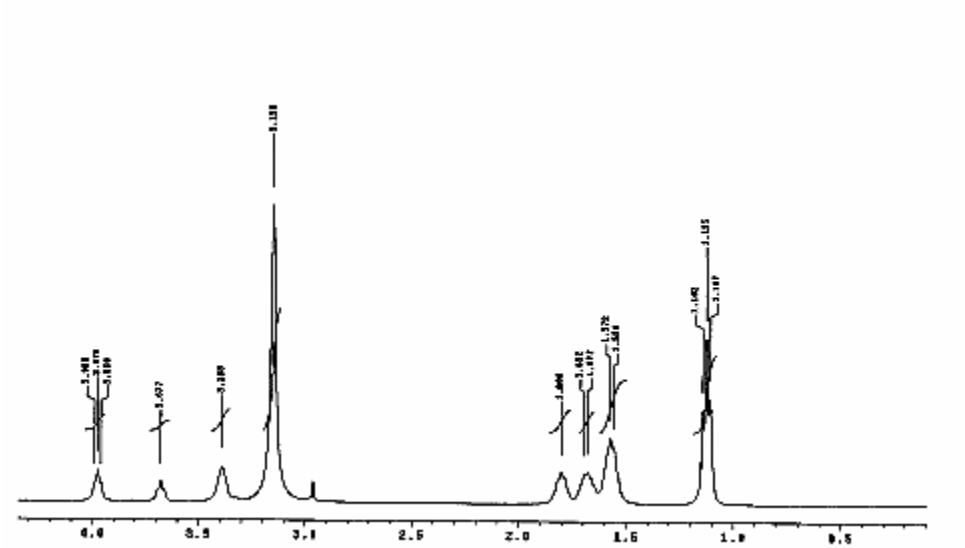

A.

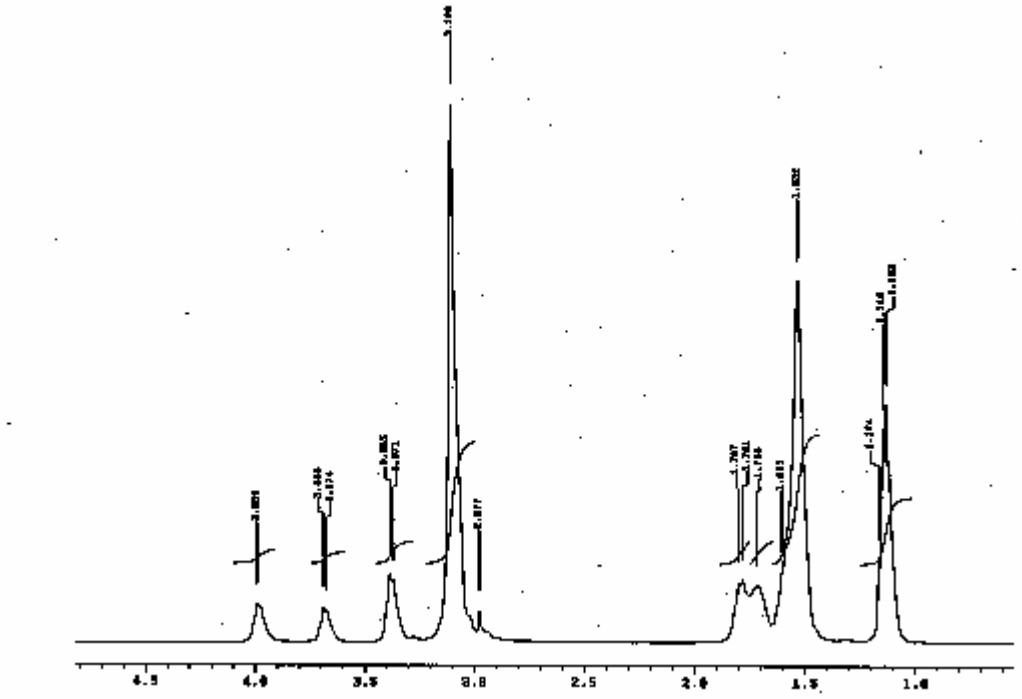

B.

Figure 3.17 A. ^{1}H NMR of 2-butyl-1,1,3,3-tetramethylguanidinium butylcarbonate **B.** ^{1}H NMR of 2-butyl-1,1,3,3-tetramethylguanidinum octylcarbonate

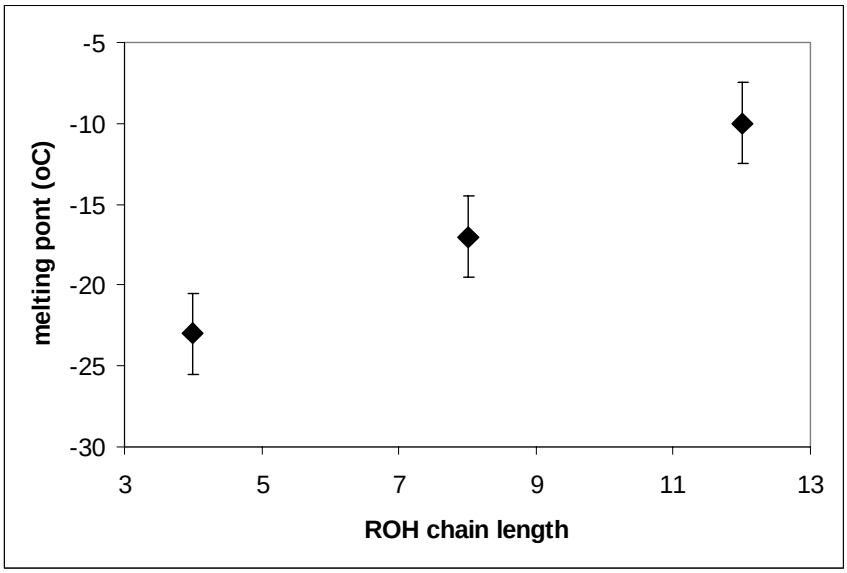

Figure 3.18 Melting points of various alkyl carbonate ionic liquids as a function of chain length.

Table 3.3 Polarity comparison of alkyl carbonate molecular liquids and ionic liquids with standard solvents and ionic liquids[28-29]

Solvent	λ_{max} (Nile Red), nm
Ether	504.4
TMBG (neat)	524.8
Benzene	525.4
TMBG + DodecOH	528.0
TMBG + OctOH	530.1
TMBG + HexOH	531.1
TMBG + BuOH	532.0
CH_2Cl_2	535.2
$TMBGH^+$ + $DodecOCO_2^-$	536.5
$CHCl_3$	537.6
TMBG + MeOH	538.0
$TMBGH^+$ + $OctOCO_2^-$	541.1
DMF	541.2
Propanoic acid	542.4
1-Octanol	544.0
$TMBGH^+$ + $BuOCO_2^-$	544.4
$TMBGH^+$ + $HexOCO_2^-$	545.0
1-Propanol	545.6
[bmim]PF_6[1]	547.5
Methanol	549.6
$TMBGH^+$ + $MeOCO_2^-$	554.0
[eim]BF_4[2]	562.9

1. bmim = 1-butyl-3-methylimidazonium 2. eim = ethylimidazonium

and room temperature ionic liquids.[28-29] As this table indicates, by changing the alcohol used to make the ionic liquid, the properties of this solvent system can be tuned over a wide range, basically from something with the properties of methanol for the methanol ionic liquid system, all the way down to something with the properties of benzene for neat TMBG, making this type of system highly tunable.

3.3.1.5 Structure Property Relationships in all Synthesized 2-butyl-1,1,3,3-tetramethylguanidinium alkylcarbonates

By studying a series of alcohols ranging from one to twelve carbons in length, several trends can be seen in how changing the chain length alters the properties of ionic liquid formed. The lowest boiling point alcohol (methanol, bp 64.7°C) gives the lowest melting point room temperature ionic liquid, the methylcarbonate salt with a melting point of -24°C ± 1°C, while the highest boiling point alcohol (dodecanol, bpt 260-262°C) gives an ionic liquid with a melting point of -10°C ± 1°C.

As mentioned above, the chain length also greatly affects the polarity of the molecular and ionic liquids. This effect is most clearly seen by comparing the polarity of each mixture in its neutral and ionic forms (Figure 3.19). Increasing chain length leads to a sharp decrease in polarity in both forms. There is also a very noticeable difference in the viscosity of the various ionic liquids as the alcohol chain length is increased. While in all cases, the ionic liquid form is more viscous than its neutral counterpart, the long chain alkylcarbonate ionic liquids were noticeably more viscous than, for example, the 2-butyl-1,1,3,3-tetramethylguanidinium methylcarbonate ionic liquid.

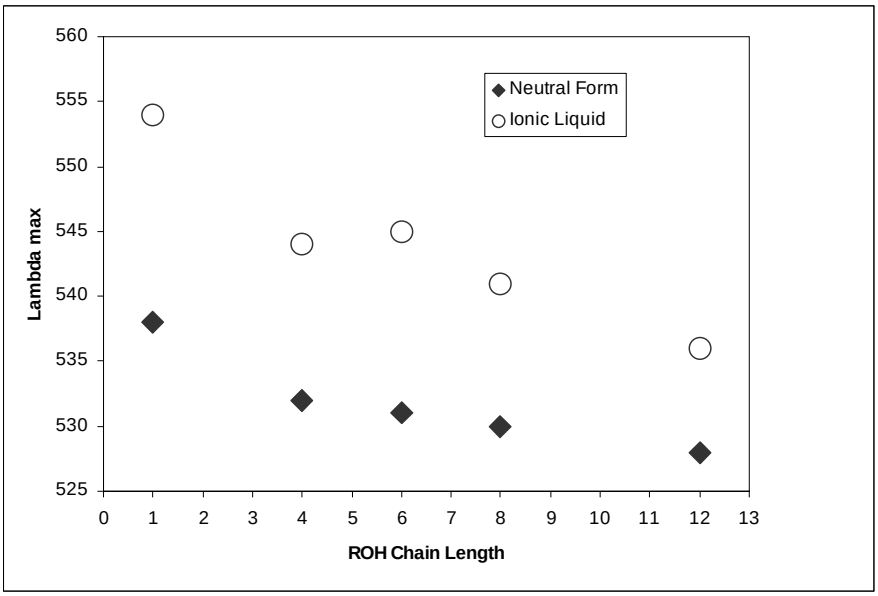

Figure 3.19 Polarities of TMBG based ionic liquids in their neutral and ionic forms

3.3.1.6 Reversibility of 2-butyl-1,1,3,3-tetramethylguanidinium methylcarbonate

The formation and reversal of the 2-butyl-1,1,3,3-tetramethylguanidinium methylcarbonate ionic liquid were studied by ^{1}H and ^{13}C NMR as well as conductivity measurements. For the NMR studies, 2-butyl-1,1,3,3-tetramethylguanidine was mixed in a 1:1 ratio with methanol, and CO_2 was bubbled through the system until the exotherm subsided. The solution was then heated at 80°C for 2 hours with stirring to drive off the CO_2. An NMR sample was taken for comparison in each of these stages, starting mixture, IL formation, and after heating (Figure 3.20).

In the starting mixture (Figure 3.20-A) the expected peaks for TMBG and methanol can be clearly seen. As CO_2 is added to the system, the guanidine is protonated and the methyl carbonate anion is formed. This is indicated by the upfield shift in the aliphatic proton peaks and the collapse of the two N-Me peaks into one single peak in the ^{1}HNMR, (Figure 3.20-B). In the ^{13}C NMR, after CO_2 addition (Figure 3.21) the

appearance of a characteristic carbonate peak is seen at 161ppm. No unreacted CO_2 remains in the system, as no peak is seen at 120ppm in the ^{13}C NMR. After being reversed by heating, the ^{1}H NMR spectrum is identical to the original molecular liquid, indicating complete reversal (Figure 3.20-C). In this specific example the reversal was brought about by heat, but the same results are obtained by stirring under vacuum for 1 hour, or bubbling with nitrogen gas for 16 hours. When reversal is performed by heating or nitrogen bubbling, no or only partial methanol loss is observed. However, when reversal is performed by vacuum, complete methanol loss occurs.

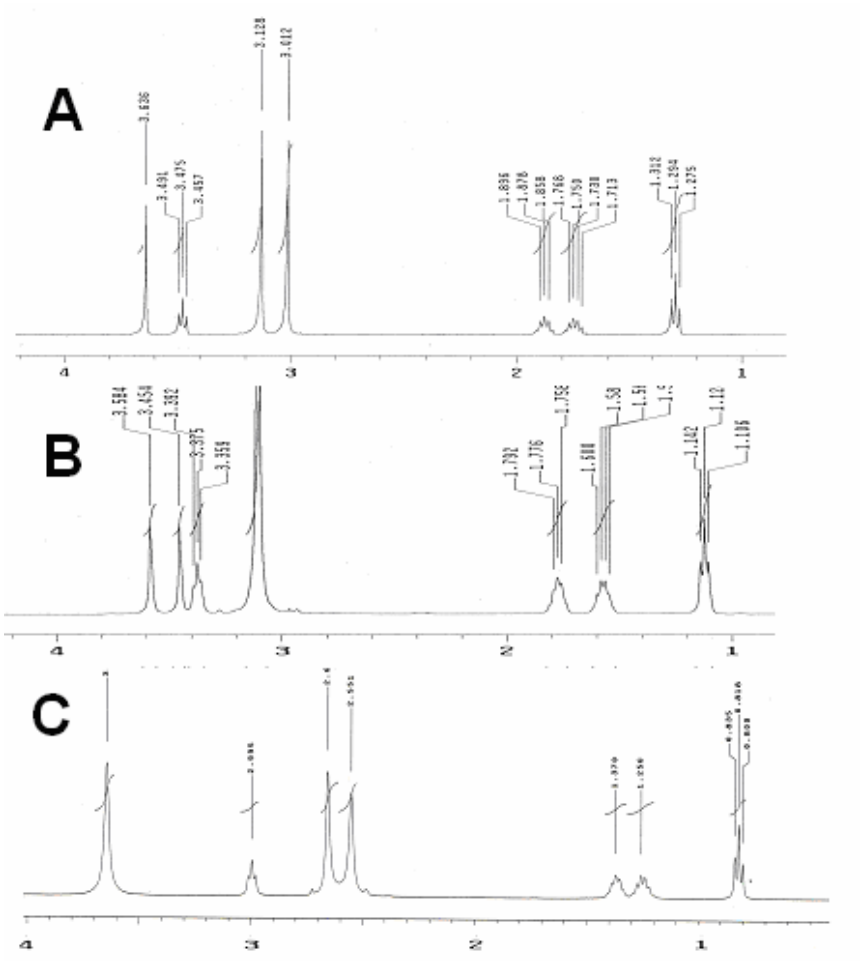

Figure 3.20 NMR spectra of **A**. Neutral mixture of TMBG and methanol **B**. After CO_2 has been bubbled through the system to form the ionic liquid. **C**. Reversal to a neutral mixture

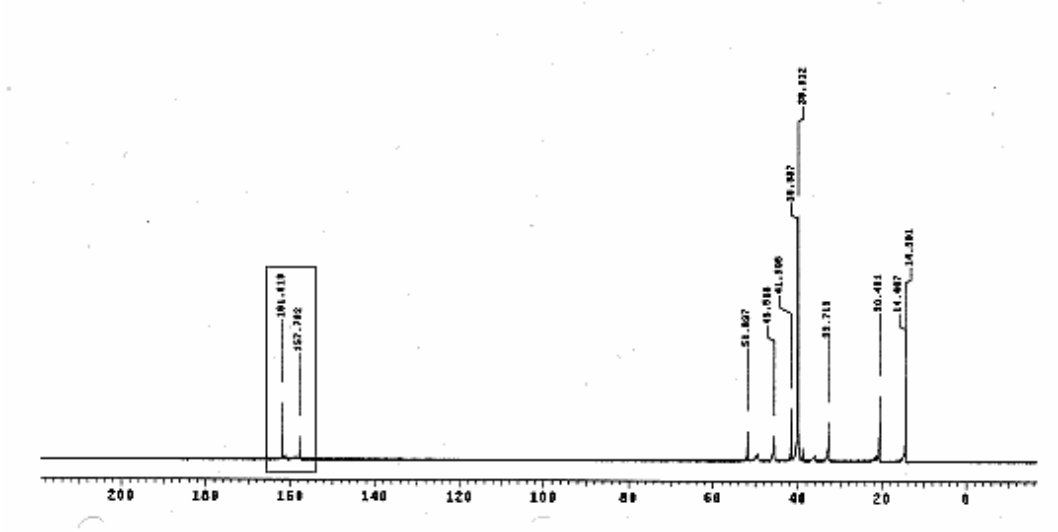

Figure 3.21 ^{13}C NMR of TMBG MC IL, showing formation of the characteristic carbonate peak

Conductivity measurements on the ionic liquid were run in the glovebox to prevent any moisture contamination during the experiment. To carry out these experiments, solvent chloroform was used as the pure ionic liquid was too viscous for neat conductivity measurements. A 1:1 mixture of TMBG and methanol (5.56mmol each) was dissolved in 4mL of deuterated chloroform. The deuterated form was used so that NMR could be run on these samples as well. The molecular liquid does not conduct electricity, reading 0 microSiemens (μS) (Figure 3.22). However, as CO_2 is bubbled through the system, that conductivity jumps to 246μS, with the formation of an ionic species. After reversal conductivity falls back to just above 0 (actually 19μS), again consistent with a return to the molecular liquid. This cycle was repeated three times, with similar results in each case (Figure 3.22).[6]

Thermogravimetric analysis (TGA) as well as differential scanning calorimetry (DSC) were also used to document the reversal of the ionic liquid based solely on heating, (Figure 3.23). Loss of CO_2 from the TMBG MC IL system would be an 18%

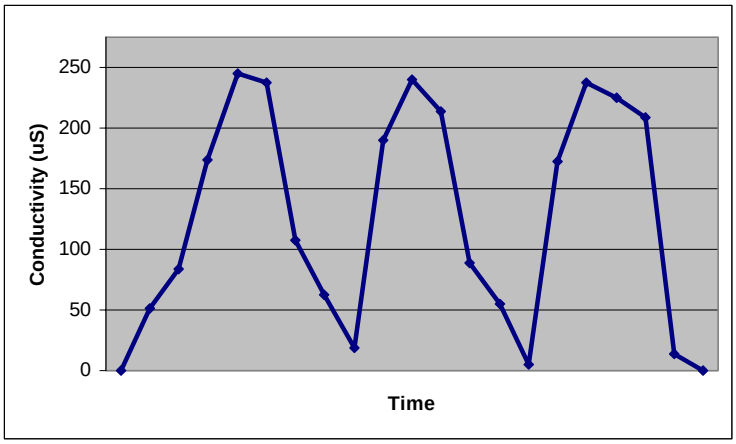

Figure 3.22 Conductivity of 2-butyl-1,1,3,3-tetramethylguanidinium methylcarbonate in chloroform. Reprinted from Tetrahedron, 66(5), Hart, R.; et al. Benign Coupling of Reactions and Separations with Reversible Ionic Liquids, 1082-1090, 2010, with permission from Elsevier[6]

mass loss, while loss of methanol would be a 13% mass loss. The TGA showed mass loss beginning at 50°C which corresponded to 24% by 65°C. This is consistent with the ionic liquid reversal upon loss of CO_2 and methanol. The remainder of the mass loss is speculated to be from evaporation of TMBG prior to decomposition. The DSC is consistent with this interpretation, as it also shows a dip at ~65°C consistent with the boiling point of methanol. A smaller exotherm at approximately 150°C is attributed to the decomposition of any remaining guanidine.

It can be concluded that all experiments run confirm that the 2-butyl-1,1,3,3-tetramethylguanidinium ionic liquid can be reversibly formed by bubbling CO_2 through an equimolar mixture of 2-butyl-1,1,3,3-tetramethylguanidine and methanol. Reversal can take place by three methods including sparging with an inert gas (nitrogen or argon), heating above 50°C with stirring, or application of vacuum on the solution, again with stirring. In all of these methods, some or all, of the methanol is removed along with the CO_2. However, in principle, both the CO_2 and methanol can be collected and recycled.

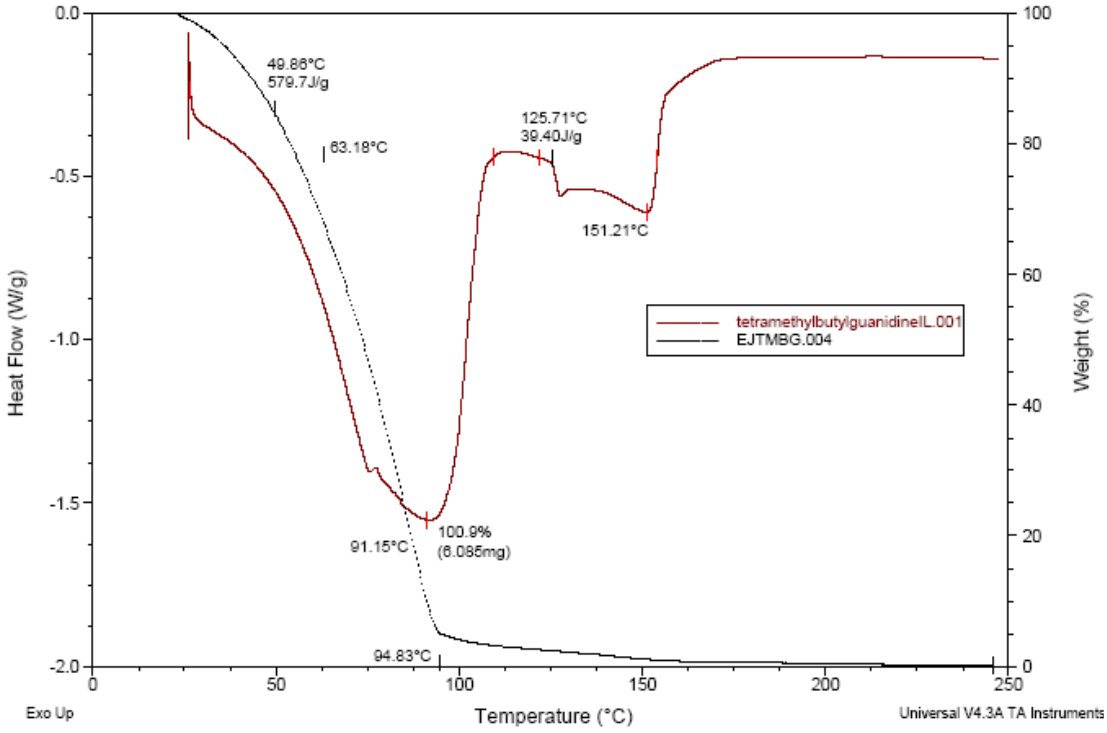

Figure 3.23 Overlayed DSC and TGA spectra of 2-butyl-1,1,3,3-tetramethylguanidinium ionic liquid reversal

3.3.1.7 Reversibility of 2-butyl-1,1,3,3-tetramethylguanidinium alkylcarbonates

The reversibility of other 2-butyl-1,1,3,3-tetramethylguanidinium alkylcarbonates was studied by the same procedure as with the methylcarbonate ionic liquid. All mixtures (butyl, hexyl, octyl, and dodecyl) were examined by ^{1}HNMR and ^{13}CNMR in both ionic and neutral forms. As with the methylcarbonate ionic liquid, changes in ^{1}H NMR spectra best illustrate the formation and subsequent reversal of the ionic liquids (Figure 3.24-3.27).

Ionic liquid formation of the various alkylcarbonate mixtures were indicated in the ^{1}H NMR spectra by an upfield shift in the aliphatic protons, and the collapse of the two N-Me peaks into one. Also in each case in the ^{13}C NMR spectrum a characteristic carbonate peak appeared between 157 and 161ppm. These ionic liquids were also

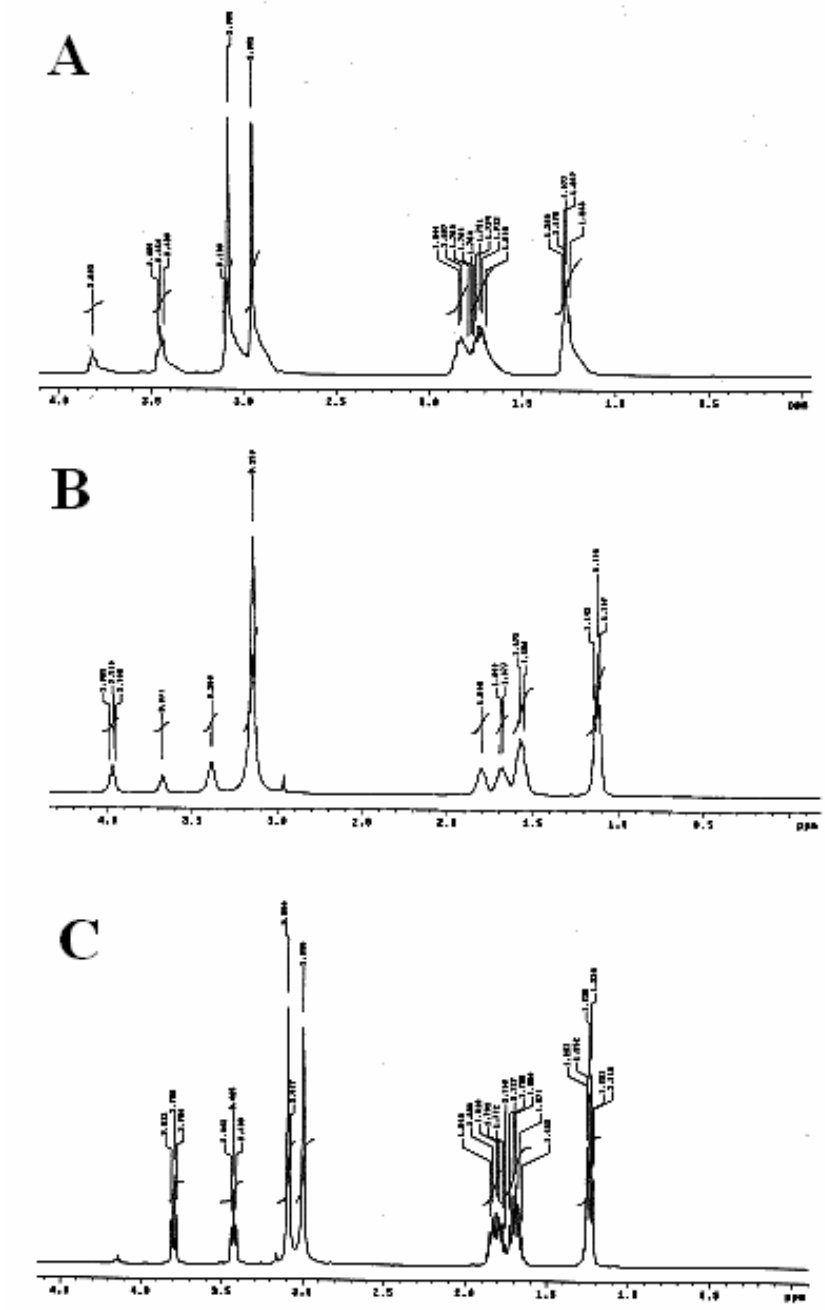

Figure 3.24 ^{1}H NMR spectra of **A.** the starting molecular mixture, **B.** the ionic liquid formation, and **C.** the reversal product of 2-butyl-1,1,3,3-tetramethylguanidinium butylcarbonate ionic liquid.

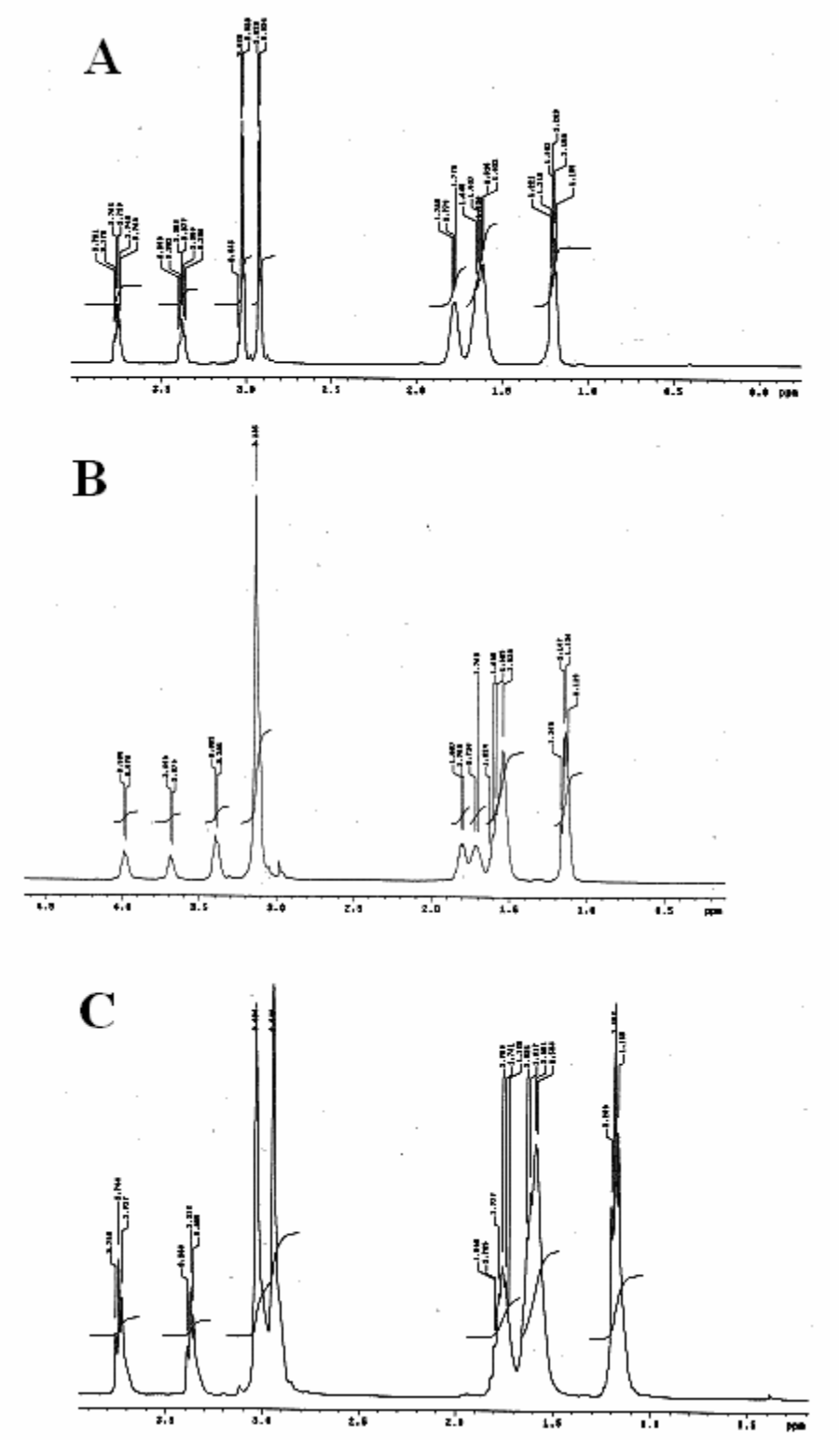

Figure 3.25 ^{1}H NMR spectra of **A.** the starting molecular mixture, **B.** the ionic liquid formation, and **C.** the reversal product of 2-butyl-1,1,3,3-tetramethylguanidinium hexylcarbonate ionic liquid.

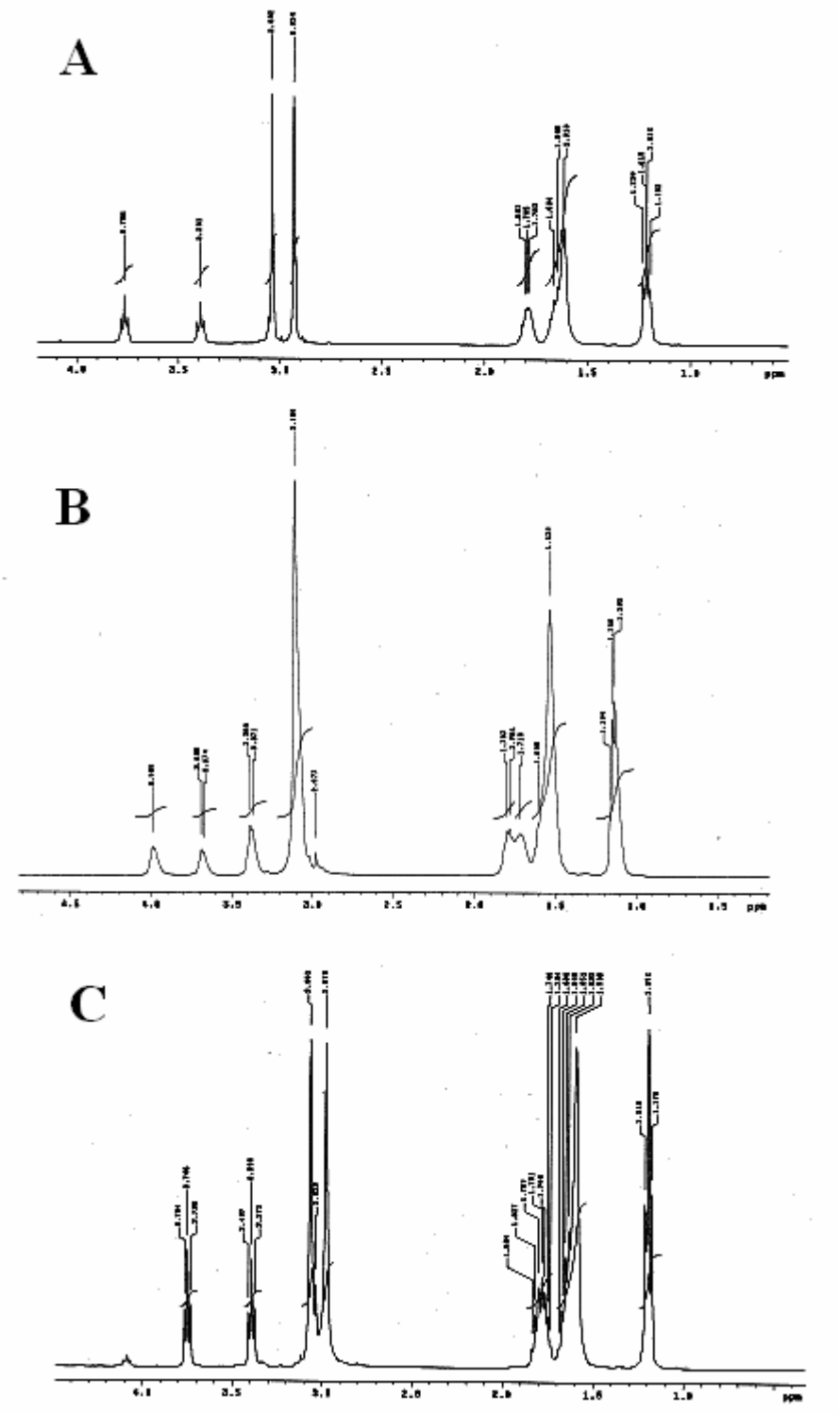

Figure 3.26 ^{1}H NMR spectra of **A.** the starting molecular mixture, **B.** the ionic liquid formation, and **C.** the reversal product of 2-butyl-1,1,3,3-tetramethylguanidinium octylcarbonate ionic liquid.

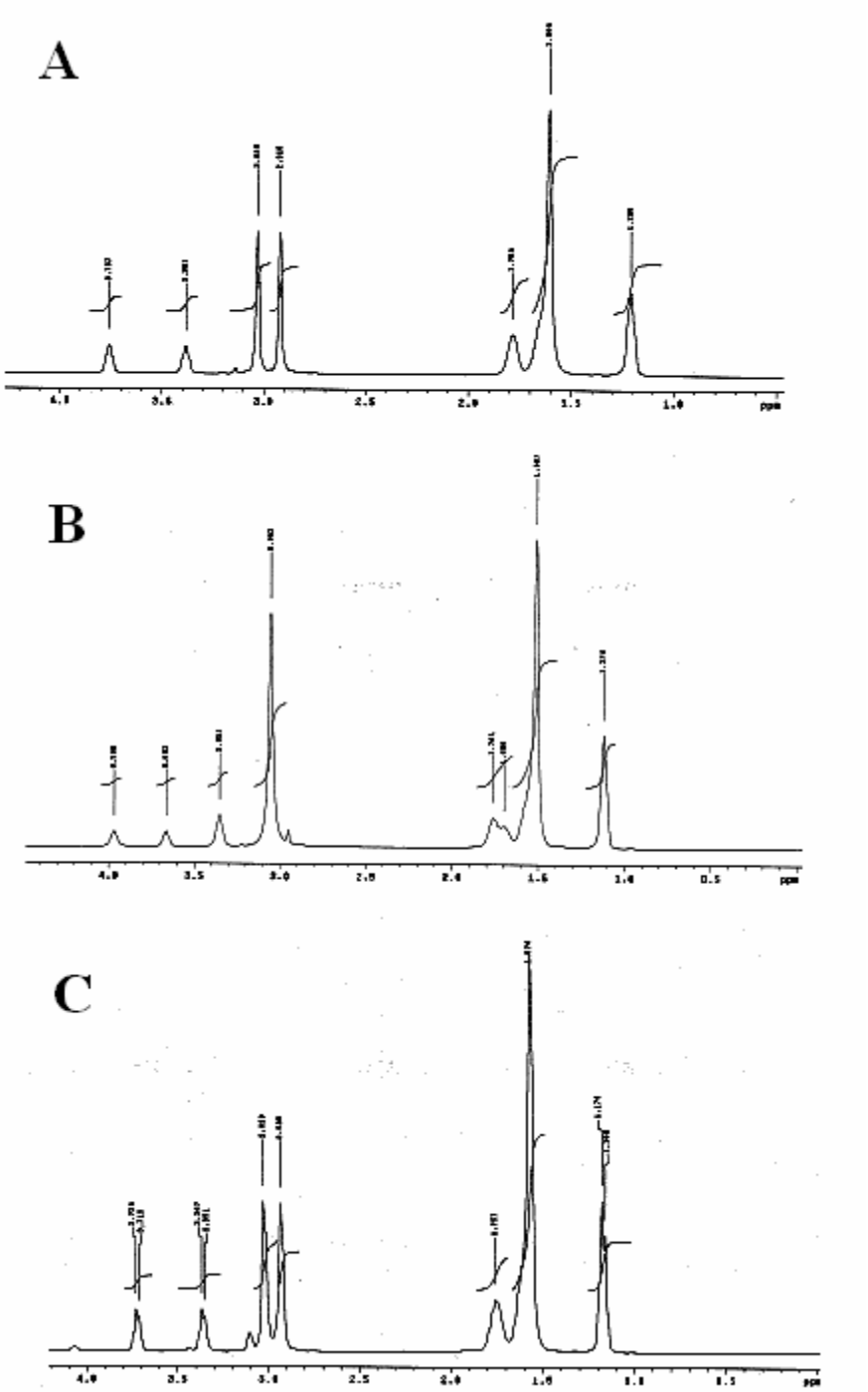

Figure 3.27 ^{1}H NMR spectra of **A.** the starting molecular mixture, **B.** the ionic liquid formation, and **C.** the reversal product of 2-butyl-1,1,3,3-tetramethylguanidinium dodecylcarbonate ionic liquid.

examined by elemental analysis as well as by IR. The ionic liquids were all reversed by heating at or above 80°C with stirring for various amounts of time. All experiments indicate that like the methylcarbonate ionic liquid, they could also be reversed by purging with an inert gas or applying a vacuum on the system.

3.3.1.8 Comparison of 2-butyl-1,1,3,3-tetramethylguanidinium alkylcarbonates

All alcohols tested (methanol, buatnol, hexanol, octanol and dodecanol) when mixed in an equimolar mixture with 2-butyl-1,1,3,3-guanidine and treated with CO_2 easily formed alkylcarbonate ionic liquids, and in each case, heat was found to be the most efficient method of reversal. However, the increase in melting point and viscosity that accompany the increase in alcohol chain length were found to have a noticeable affect on the length of time necessary to cause complete reversal from ionic liquid back to the guanidine/alcohol molecular liquid.

As the alcohol chain increased, the length of time needed for complete reversal at 80°C also increased (Figure 3.28). Reversal time was studied using ^{1}H and ^{13}C NMR. Both types of NMR were run on the starting molecular liquid. CO_2 was bubbled through the system to form the ionic liquid. Simultaneously the process was followed by NMR. The ionic liquid was then heated at 80°C with stirring. After each hour of this heat treatment, a sample was taken and examined by ^{1}H and ^{13}C NMR. When the resulting NMR spectra were identical to the NMR of the initial molecular liquid, reversal was considered complete.

While the 2-butyl-1,1,3,3-tetramethylguanidinium methylcarbonate ionic liquid takes only 3 hours to reverse at 80°C, when the chain length is increased up to twelve

carbons for the 2-butyl-1,1,3,3-tetramethylguanidinium dodecylcarbonate ionic liquid, that time is increased to 7 hours. This difference gives a lot of flexibility in designing and choosing the best ionic liquid solvent based on the specific requirements of a desired application.

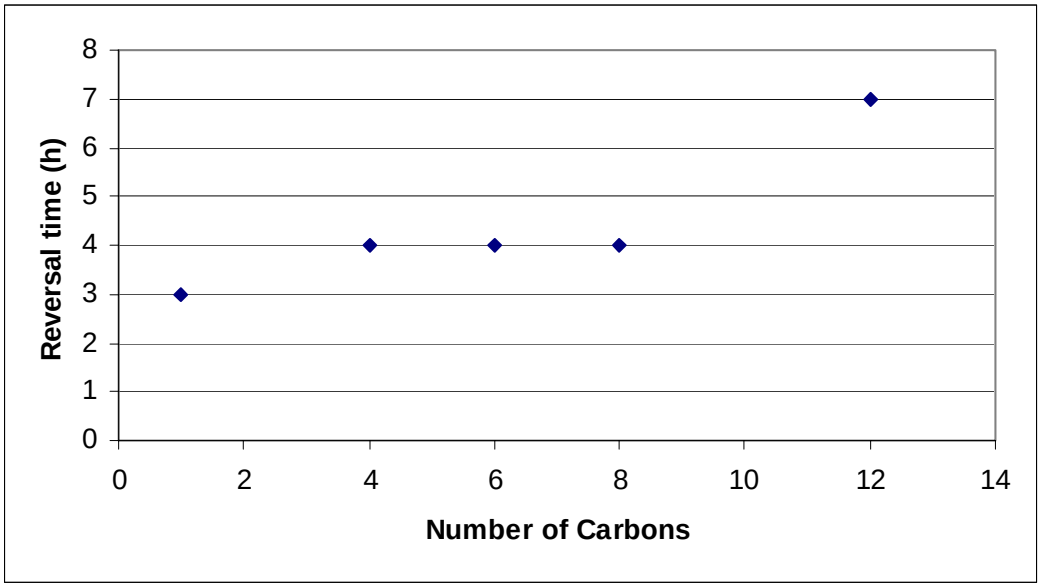

Figure 3.28 Comparison of the reversal time of the various alkyl carbonate ionic liquids at 80°C, as a function of number of carbons in the alkyl chain.

3.3.1.9 Miscibility studies of the 2-butyl-1,1,3,3-tetramethylguanidinium alkylcarbonate ionic liquids.

The miscibility of the various 2-butyl-1,1,3,3-tetramethylguanidinium alkylcarbonate ionic liquids with a variety of solvents was investigated. The solvents employed with 2-butyl-1,1,3,3-tetramethylguanidinium methylcarbonate were pentane, hexane, heptane, octane, DMSO, chloroform, THF, toluene, and ethyl acetate. The other 2-butyl-1,1,3,3-tetramethylguanidinium alkylcarbonates (butyl, hexyl, octyl, and dodecyl)

were tested with hexane, toluene, and ethyl acetate. The results of these experiments are tabulated in Table 3.4.

These miscibility studies were carried out by first forming an equimolar mixture of 2-butyl-1,1,3,3-tetramethylguanidine and the chosen alcohol (0.88-1.23mmol of each). To this mixture, 1.1-1.5mmol of the desired solvent were added. In all cases the solvent was miscible with the neutral guanidine and alcohol mixture. CO_2 was bubbled through the system and ^1H NMR were used to confirm formation of the ionic liquid.

Table 3.4 A comparison of the miscibility of all alkylcarbonate ionic liquids with pentane or hexane, toluene and ethyl acetate

R of guanidinium alkyl carbonate	Pentane or Hexane	Toluene	EtOAc
Me	2 phases	1 phase	1 phase
Bu	1 phase	1 phase	1 phase
Hex	1 phase	1 phase	1 phase
Oct	1 phase	1 phase	1 phase
Dodec	1 phase	1 phase	1 phase

When 2-butyl-1,1,3,3-tetramethylguanidinium methylcarbonate ionic liquid was formed, the solvents octane, heptane, and pentane formed distinct phases, while DMSO, chloroform, THF, and ethyl acetate remained homogeneous, only one phase was visible. In the cases where two phases were formed, ^1H NMR and GC-MS were used to investigate the composition of each of the phases. In all cases, no cross contamination was seen between the ionic liquid and the alkane phase, within the error limits of the analysis techniques (95% purity). When the other 2-butyl-1,1,3,3-

tetramethylguanidinium alkyl carbonate ionic liquids were formed, all solvents tested were miscible and only one phase was observed.

3.3.1.10 2-butyl-1,1,3,3-tetramethylguanidinium bicarbonate

2-butyl-1,1,3,3-tetramethylguanidine reacts with water to form 2-butyl-1,1,3,3-tetramethylguanidinium bicarbonate, which is also an ionic liquid. Preliminary studies indicate that its reversal takes place at higher temperature; therefore its formation and reversal was investigated. The reaction of 2-butyl-1,1,3,3-tetramethylguanidine with water and carbon dioxide was carried out (Figure 3.29).

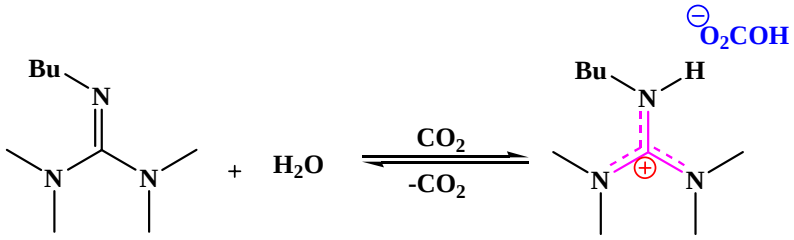

Figure 3.29 Formation of 2-butyl-1,1,3,3-tetramethylguanidinium bicarbonate ionic species

CO_2 was bubbled through an equimolar mixture of 2-butyl-1,1,3,3-tetramethylguanidine and water. As with the alcohol mixtures a noticeable exotherm developed. Formation of the bicarbonate salt was confirmed by ^{1}HNMR and ^{13}CNMR. Unlike the alkylcarbonate ionic liquids, reversal took place by heating at 80°C overnight instead of just a few hours. It was also observed that reversal was not permanent. When left open to the atmosphere, the bicarbonate salt reformed.

3.3.1.11 Modification of the Structure of the Guanidine and its Affect on Physical and Chemical Properties

3.3.1.11.1 Alcohol Attached to Guanidine – 1 Component IL System

In the previously discussed guanidinium alkylcarbonate ionic liquid systems, heating to reverse the ionic liquid often led to loss of alcohol as well as CO_2 from the system; this was especially true in the cases of the shorter chain alcohols. In order to address the problem, an attempt was made to synthesize a guanidine with the alcohol moiety directly attached (Figure 3.30).

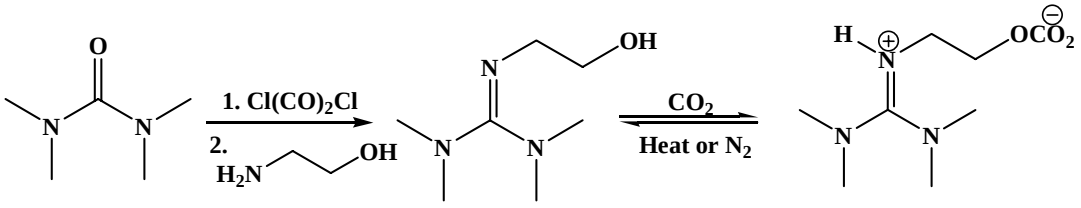

Figure 3.30 Synthesis of 2-[1-hydroxyethyl]-1,1,3,3-tetramethyl guanidine, and potential ionic species formation from this guanidine

2-[1-hydroxyethyl]-1,1,3,3-tetramethyl guanidine was synthesized following the same procedure as 2-butyl-1,1,3,3-tetramethyl guanidine, simply using ethanolamine in place of butylamine in the second synthesis step. Recrystallization in dichloromethane was necessary to isolate solid product 78% yield. Unfortunately, when CO_2 was added to this hygroscopic compound (decomposition point 171^{o}C) an RTIL did not form. Upon examination with ^{1}HNMR and ^{13}CNMR only characteristic peaks for unreacted 2-[1-hydroxyethyl]-1,1,3,3-tetramethyl guanidine were seen.

3.3.1.11.2 Attaching Silicon groups to the Guanidine Core

A silyl group was attached to the guanidine in an attempt to decrease the viscosity that is normally seen with room temperature ionic liquids. High viscosities can limit the

usefulness of a solvent system by making it more difficult to carry out the standard procedures of filtering, and decanting a solution, as well greatly slowing down the rate of reaction in a diffusion controlled reaction. Recent literature has shown that silyl groups may help to decrease the inherent viscosity of the ionic liquid system, and we were attempting to take advantage of that observation.[30-31]

The first attempt was based upon the 2-[1-hydroxyethyl]-1,1,3,3-tetramethyl guanidine synthesized whose synthesis was described above. Attempts to silylate this compound employing standard conditions were unsuccessful (Figure 3.31). Under argon, 2-[1-hydroxyethyl]-1,1,3,3-tetramethyl guanidine was placed in an ice bath, and chlorotrimethylsilane was slowly added. This mixture was then allowed to warm to room temperature, followed by stirring at room temperature for 24 hours.

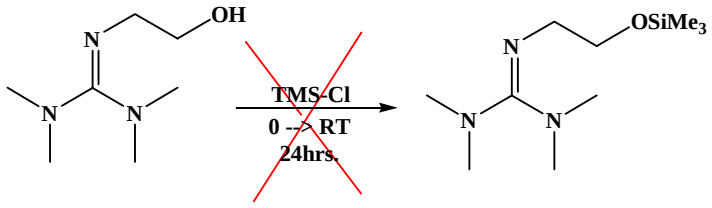

Figure 3.31 Reaction of 2-[1-hydroxyethyl]-1,1,3,3-tetramethyl guanidine with chlorotrimethylsilane to form 2-[trimethylsiloxyethyl]-1,1,3,3-tetramethyl guanidine

^{1}HNMR and ^{13}CNMR were used to examine the isolated products. The desired silylated product was not formed; the isolated product could not be identified.

A second attempted to synthesize the silylated alcohol was then initiated. Trimethylsiloxyethylamine was first synthesized and then used in the standard optimized guanidine reaction method to form the desired guanidine product (Figure 3.32). To carry out this reaction a slight modification was made to the standard tetramethylbutylguanidine synthesis method. During the step involving the addition of

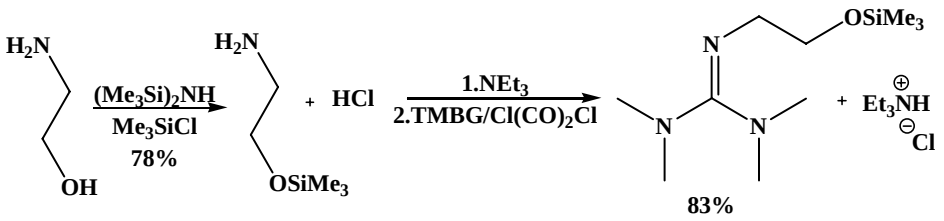

Figure 3.32 Synthesis of 2-[trimethylsiloxyethyl]-1,1,3,3-tetramethyl guanidine from trimethoxysiloxyethylamine

the amine, triethylamine was also added to the reaction system in order to scavenge the HCl formed during the reaction and prevent the decomposition of the silylated oxygen. After a standard workup, the product was isolated as a pale yellow oil in an 83% yield, which was characterized by ^{1}H and ^{13}C NMR. Under argon, the 2-[1-trimethylsiloxyethyl]-1,1,3,3-tetramethyl guanidine was mixed with methanol. Then CO_2 was bubbled through the system. However, NMR analysis did not indicate any formation of the desired salt product. (Figure 3.33)

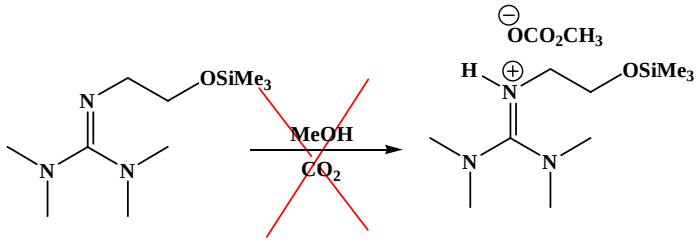

Figure 3.33 Attempts at ionic liquid formation with this guanidine were unsuccessful based on NMR results

The third attempt at silylating the guanidine was done using the commercially available trimethylsilylmethylamine. This molecule was introduced into step two of the standard guanidine formation reaction (Figure 3.34). Though yields were relatively low, only 38%, pure product was isolated as a pale yellow oil. CO_2 was bubbled through an equimolar mixture of 2-[trimethylsilanylmethyl]-1,1,3,3- tetramethylguanidine and

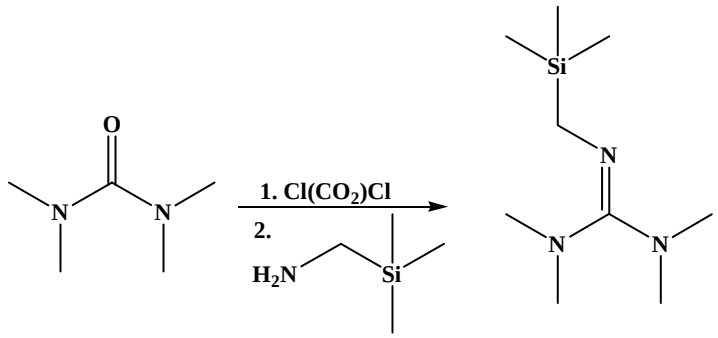

Figure 3.34 Standard synthesis of a penta-substituted guanidine using silylated amine in the second step

methanol, and the ionic species 2-[trimethylsilanylmethyl]-1,1,3,3-tetramethylguanidinium methylcarbonate was successfully formed, (Figure 3.35) however it was found to be not an ionic liquid, but rather a solid at room temperature, with a melting point of 35-40°C. It was difficult to pinpoint an exact melting point as it was also found that reversal from the ionic species back to neutral components occurred simultaneously with melting, making this species unsuitable for running reactions at temperatures above the melting point.

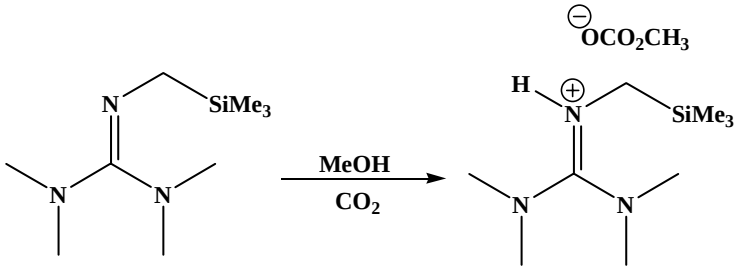

Figure 3.35 Formation of the ionic species 2-[trimethylsilanylmethyl]-1,1,3,3- tetramethylguanidinium methylcarbonate

In an attempt to obtain a liquid rather than a solid ionic species from 2-[trimethylsilanylmethyl]-1,1,3,3- tetramethylguanidine, it was mixed in a 1:1 molar ratio with octanol. It was hoped that the long flexible alcohol chain would prevent crystallization. To some extent this was successful as a liquid ionic species was formed

and confirmed by NMR, but conversion was not complete. At most approximately 50% conversion took place. This could possibly be due to steric affects from that long hydrocarbon chain (Figure 3.36).

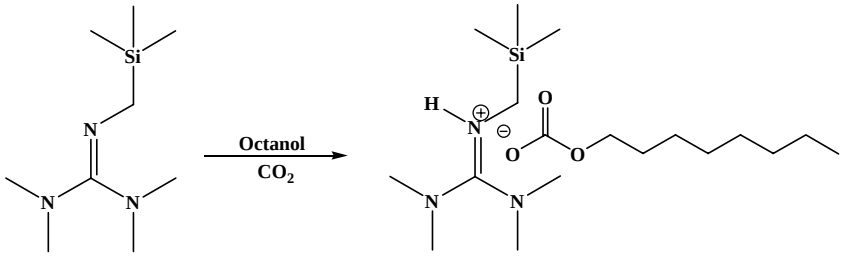

Figure 3.36 Formation of the ionic species species 2-[trimethylsilanylmethyl]-1,1,3,3-tetramethylguanidinium octylcarbonate

The fourth and final attempt to attach a silicon was synthesis of the molecule 2-(propylpentamethyldisiloxane)-1,1,3,3-tetramethylguanidine. In order to carry out this synthesis, pentamethyldisiloxanepropylamine had to first be synthesized. The synthesis was carried out by a literature method found in U. S. Patent 5,654,374 (Figure 3.37).[32]

Figure 3.37 Synthesis of pentamethylisiloxanepropylamine

Allylamine and the platinum catalyst platinum(0)-1,3-divinyl-1,1,3,3-tetramethyldisiloxane were dissolved in heptane. Pentamethyldisiloxane, also dissolved in heptane, was slowly added. The reaction was heated to 70°C and held at that temperature for three hours. After the reaction was complete, heptane was removed. Kugelrohor distillation was subsequently used to isolate and purify the product. GC-MS

analysis confirmed formation of a product with the desired molecular weight, however, NMR analysis actually showed formation of two different isomers, both the desired product and that formed from siloxane attachment to the other end of the allylamine double bond (Figure 3.38).

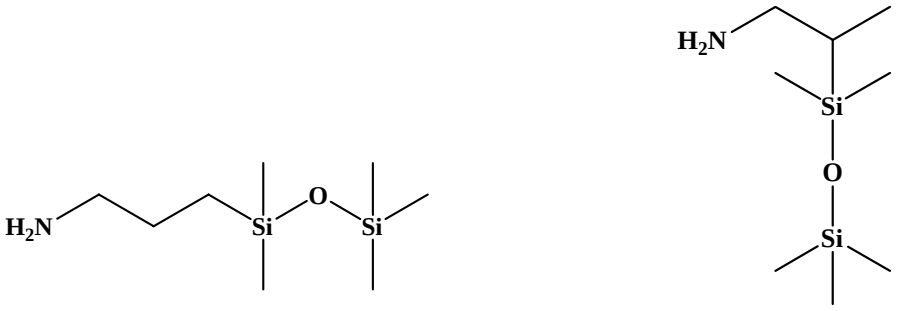

Figure 3.38 Two isomers formed during siloxylamine synthesis

These isomers were formed in an approximately 60:40 ratio of linear to branched amine, and the total overall isolated yield of all products was found to be 40%. Vacuum distillation was attempted to separate the two isomers, however, it was unsuccessful. The isomer mixture was used as is to continue with the standard penta-substituted guanidine synthesis. However, upon completion it was found that while the linear amine does react readily to form 2-(propylpentamethyldisiloxane)-1,1,3,3-tetramethylguanidine,the branched does not. The reaction mixture was a mix of desired product, unreacted branched amine, and unreacted tetramethyl urea. With such a complicated mixture, it was decided not to move on to attempt formation of an ionic species.

3.3.1.11.3 Pentamethyl Guanidine

The next attempted modification was the synthesis of pentamethyl guanidine. We were very curious as to how the properties of pentamethylguanidinium

butylcarbonate ionic species would compare to those of 2-butyl-1,1,3,3-tetramethylbutylguanidinium methylcarbonate ionic species, as they contain an identical number of carbon atoms, just distributed differently between the cation and anion.

It was decided to synthesize this molecule using the same two step synthesis optimized for synthesis of all the penta-substituted guanidines, simply substituting methylamine into the second step of the reaction. A commercially available 2.0M solution of methylamine in tetrahydrofuran (THF) was chosen. (Figure 3.39)

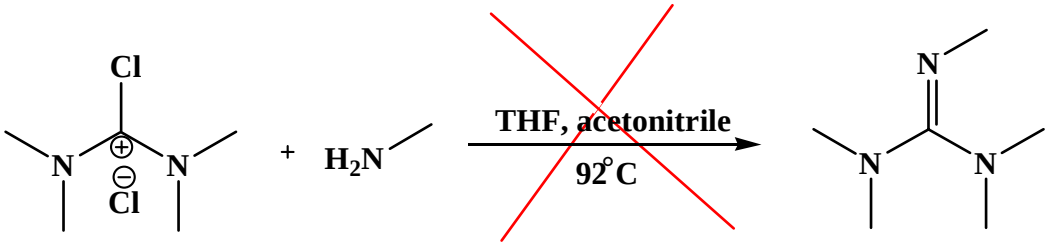

Figure 3.39 Unsuccessful pentamethylguanidine synthesis, using methylamine solution in THF

The previously discussed optimized guanidine synthesis reaction was carried out; however, the desired pentamethylguanidine was not formed. The addition of THF into the system appeared to lead to a variety of unexpected and unknown side reactions, as some sort of white crystals were seen in solution during the second step, and the formation of many unidentified side products was seen in the NMR spectra. In order to address this, it was decided to start with the pure methylamine gas, and dissolve it straight into an acetonitrile solution which could then be used in the second step of the guanidine reaction.[22]

Methylamine gas was condensed on a dry ice condenser and dripped into a graduated collection flask of acetonitrile waiting below. This solution was then used to carry out the second step of the standard guanidine synthesis reaction. (Figure 3.40)

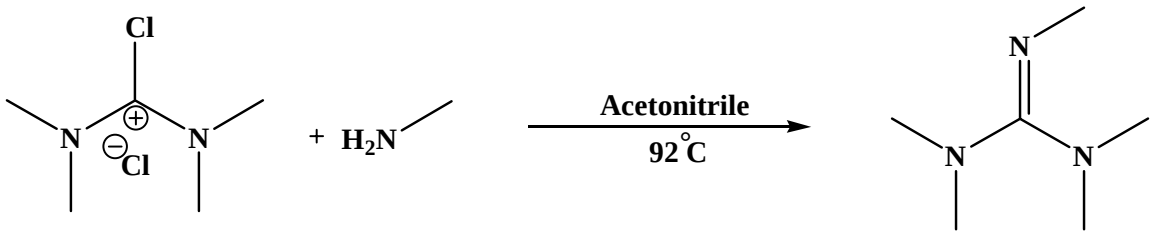

Figure 3.40 Successful synthesis of pentamethylguanidine

Using this acetonitrile solution, the reaction was successful. After the standard work up procedure, pure pentamethylguanidine product, as confirmed by NMR, both ^{1}H and ^{13}C NMR, was isolated in 70-75% yield.

An equimolar mixture of pentamethylguanidine and butanol was prepared and CO_2 was bubbled through the system. (Figure 3.41) A very wet looking white solid formed. NMR analysis showed the formation of the desired ionic species with approximately 70% conversion, with the remaining 30% being unreacted starting materials. A variety of different methods were attempted to increase the conversion during formation of the ionic species. CO_2 bubbling was tried with stirring, without

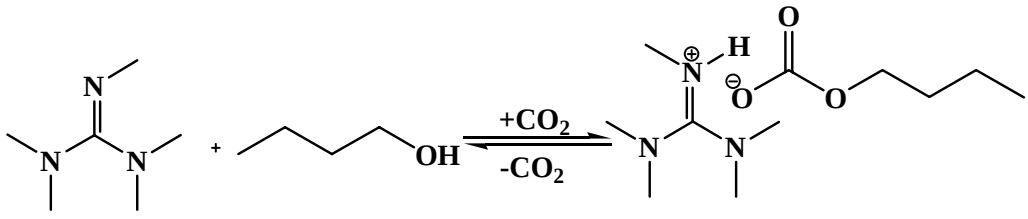

Figure 3.41 Attempted formation of pentamethylguanidinium butylcarbonate ionic liquid

stirring, at room temperature and at temperatures up to 60°C, however, in all cases both ^{1}HNMR and ^{13}CNMR looked the same, indicating approximately 70% conversion. These samples were then washed with pentane and dried in the vacuum oven at room temperature to remove any excess starting material. The melting point of this salt was found to be between 92-96°C, however, as soon as melting began, bubbles of CO_2 could be seen coming off the sample. As was observed with species containing a silicon group, melting occurred simultaneously with reversal to neutral components, making this material unsuitable for higher temperature reactions and processes. It is believed that ultimately, the symmetry of the guanidine molecule allowed for tight packing, hence the formation of a solid salt, rather than the desired ionic liquid.

3.3.1.11.4 2-allyl-1,1,3,3-tetramethylguanidine

An attempt was made to synthesize 2-allyl-1,1,3,3-tetramethylguanidine. This molecule was chosen in order to study how the addition of a double bond would affect the formation of and properties of the ionic species. Once again, it was decided to follow the previously optimized reaction procedure, simply using commercially available allylamine in the second step of the reaction. (Figure 3.42)

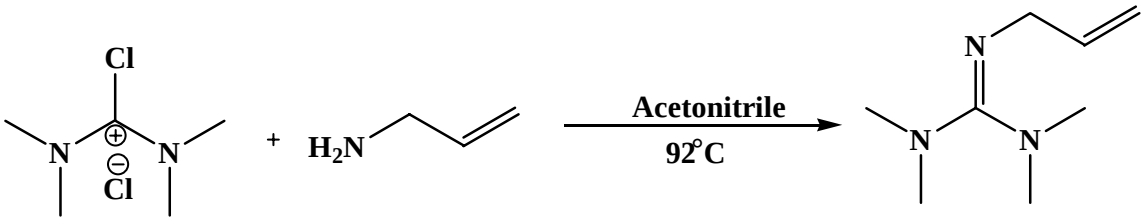

Figure 3.42 Synthesis of tetramethylallylguanidine

The reaction procedure was successful, and after standard work up, the product was isolated in approximately 70% yield as a pale yellow oil. The structure was confirmed by ^{1}HNMR and ^{13}CNMR as well as GC-MS. 2-allyl-1,1,3,3-tetramethylguanidine was mixed in an equimolar mixture with methanol and CO_2 was bubbled through the solution. There was a noticeable viscosity increase, as is typical for ionic liquid formation, and both ^{1}HNMR and ^{13}CNMR showed changes consistent with the formation of an ionic species with 100% conversion to the ionic liquid within the error of the NMR instrument.

The ionic liquid sample was heated at 80°C for 4 hours in an attempt to reverse it back to its neutral components. Though gas could immediately be seen bubbling out of solution, the NMR spectra was not consistent with a clean reversal. Many degradation products could be seen. The sample was left to bubble with nitrogen gas overnight. This did not change the NMR spectrum in any noticeable way, though it did cause a black solid material to settle out of the solution. A sample of the ionic species was diluted in chloroform and bubbled with nitrogen gas to get a closer look at the reversal. Again, by NMR, some reversal was seen, but mostly various degradation products were formed and some type of black solid settled out of solution.

It was speculated that the ionic species is reacting with itself to form allylmethylcarbonate (Figure 3.43). ^{13}C NMR shows peaks consistent with the formation of this compound. Once this occurs, there are a variety of other reactions that could take place with these molecules, leading to the degradation products visible in the NMR. Ultimately, this ionic species can be formed initially, but it is not stable and cannot be reversed to the molecular liquid and recycled.

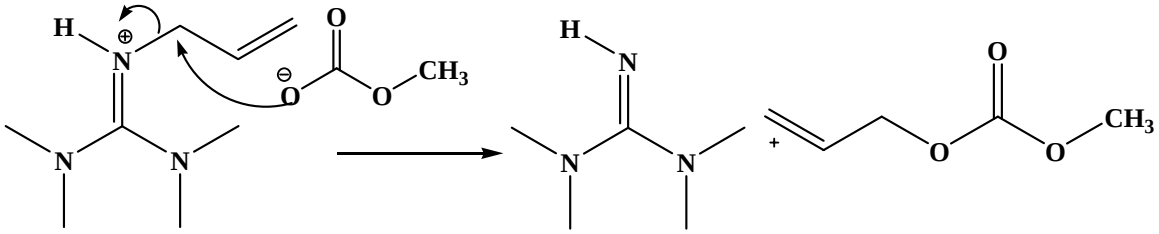

Figure 3.43 One possible degradation pathway of the 2-allyl-1,1,3,3-tetramethylguanidine ionic liquid

3.3.1.12 Applications of TMBG/TMBG MC IL system

3.3.1.12.1 Reaction/Recycle of TMBG-methanol IL systems

Thus far the formation, reversal, and recycle of a variety of tetramethylguanidinium alkylcarbonate ionic liquids has been demonstrated. However, this is just the first step. Their scope as solvents both for reactions and separations, as well as other applications, such as CO_2 capture and oil extraction still remains to be explored. Organic transformations, product separation, and solvent recycle for a variety of base catalyzed organic reactions were studied using the 2-butyl-1,1,3,3-tetramethylguanidine/methanol reversible ionic liquid system.

The following processes were studied: 1) Claisen-Schmidt condensation of 2-butanone and benzaldehyde, 2) cyanosilylation of cyclohexanone, 3) Michael addition between 2-cyclohexenone and dimethyl malonate, 4) addition of aniline to chalcone, 5) Diels Alder reaction between anthrone and N-phenylmaleimide, 6) Suzuki reaction between phenylboronic acid and bromobenzene, and 7) oxidation of benzyl alcohol with hypochlorite.[6]

The goal of each of these studies was to demonstrate the use of TMBG and its ionic liquid in a complete chemical process including reaction, separation of products,

and the reformation and recycle of solvent (Figure 3.44). For the Claisen-Schmidt reaction, for instance, the reaction, A+B, could take place in the neutral guanidine form to produce product C. Pentane or another long chain hydrocarbon can then be added along with methanol to the reaction mixture containing product C followed by the addition of CO_2 to form the ionic liquid which results in a subsequent phase split. The products would most likely be soluble in the alkane phase, which could be removed from the system leaving behind the ionic liquid phase which could be reversed by heat or by sparging with an inert gas, recycled and reformed as the system is used again. In some cases, adding an alkane might not be necessary if the products are insoluble in the ionic liquid. It is also possible to envision this system working, basically in reverse, with A+B

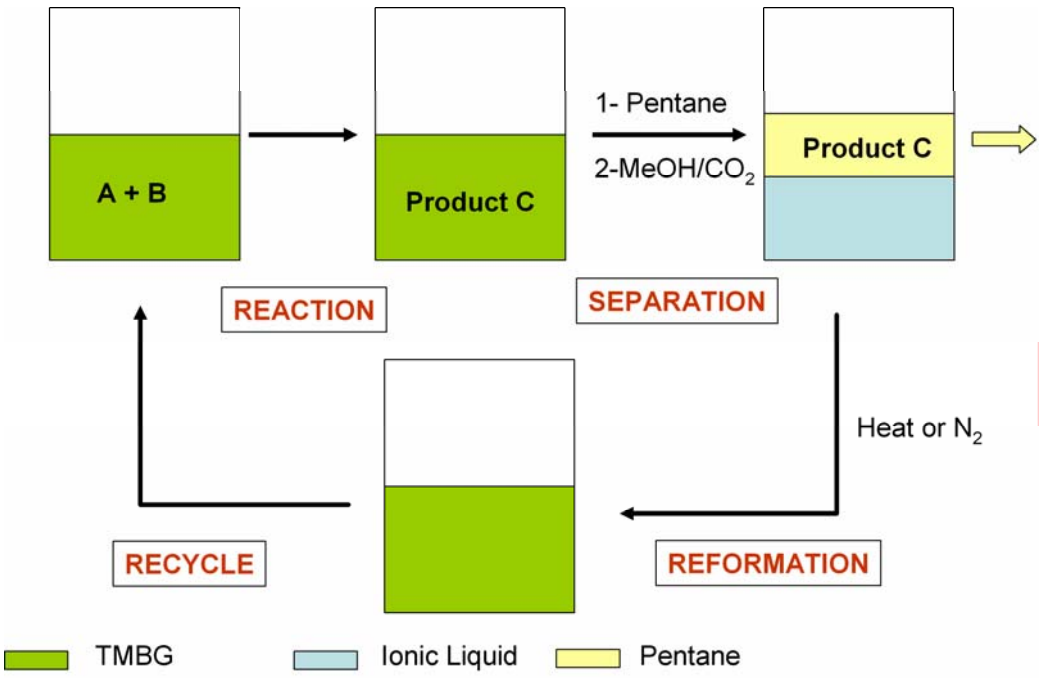

Figure 3.44 A complete chemical process using the TMBG/methanol ionic liquid system

forming C in the ionic liquid phase, and the system being reversed for product separation, and then being reformed and recycled to continue the system in that way.

3.3.1.12.2 Base Catalyzed Reactions in TMBG

The Claisen-Schmidt condensation of butanone and benzaldehyde yields three products: the internal enone (3-methyl-4-phenyl-but-3-en-2-one), the terminal enone (1-phenyl-pent-1-en-3-one) and water (Figure 3.45).[33-34]

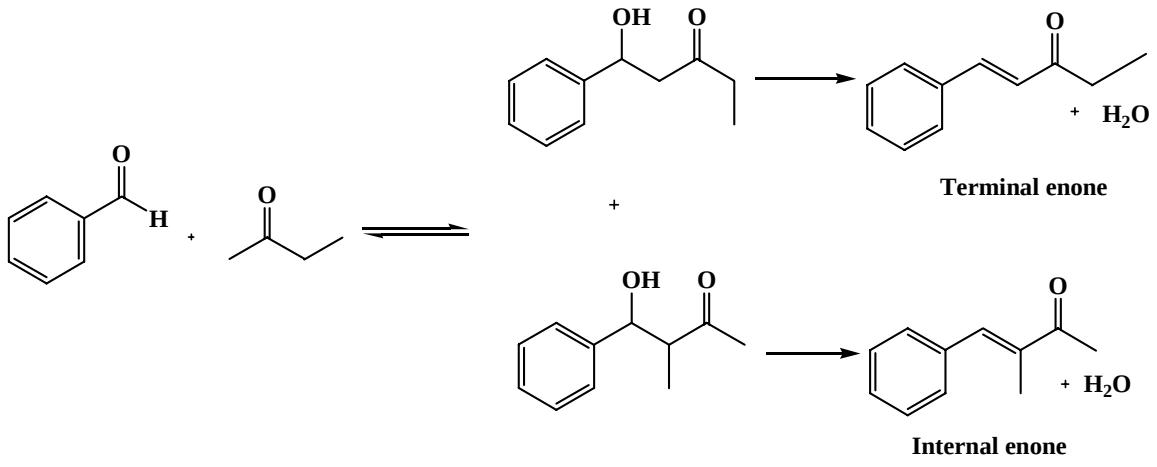

Figure 3.45 Claisen-Schmidt condensation of 2-butanone and benzaldehyde

The reaction of butanone and benzaldehyde was carried out in TMBG. For this reaction, the TMBG acted as both base catalyst and solvent.[23,35] After the reaction was completed, octane and methanol were added to the mixture, followed by the addition of CO_2. This caused ionic liquid formation, an ionic liquid/hydrocarbon phase split, and subsequent product isolation into the hydrocarbon phase. The enone products were predominantly in the octane phase and were easily separated by decantation. Reaction of either 24 hours at room temperature or 3 hours at 80°C, yielded enone products in 48%

and 44% yield, respectively (Table 3.5). The reaction temperature of 80°C was chosen for further tests. At this temperature, the total enone product formation was studied as a function of time. Initially, as the reaction time increased, the yields increased from 13% at 1 hour to 44% at 3 hours. However, a maximum was reached at approximately 4 hours, after which time product yields then decreased (Table 3.5). It is believed that this decrease was caused by competing condensation reactions between the enone products and the benzaldehyde starting material. To maximize formation of the desired products, short reaction times to partial conversions were necessary. This allowed the development of a process in which isolated yields were maximized and solvent recycle was possible[6] (Figure 3.44).

Table 3.5 Effect of reaction conditions on the condensation of 2-butanone and benzaldehyde in the presence of TMBG.

Temp. (C)	Time (h)	Yield (%)
RT	24	48
80	1	13
80	2	24
80	3	44

Initially ionic liquid reversal and TMBG recycle attempts were unsuccessful. This was due to the formation of water, a product of the condensation reaction. As previously discussed, water reacts with TMBG and CO_2 to form the 2-butyl-1,1,3,3-tetramethylguanidinium bicarbonate. With the formation of the carbonate salt, a dramatic increase in ionic liquid viscosity was noted. This visocosity increase, combined with the difficulties inherent in reversing the carbonate salt prevented TMBG MC IL recycling. However, the reversal of the ionic liquid and recycle of TMBG were successful when the water was removed from the reaction mixture via drying with magnesium sulfate prior to

ionic liquid formation. Once the system was dried, the TMBG was successfully recycled three times. Over these three cycles, the isolated yields of enone products were 34%, 32% and 34%. The enones also consistently showed a product distribution of 95% terminal enone and 5% internal enone product.[6]

The cyanosilylation of cyclohexanone with trimethylsilyl cyanide (TMSCN) was carried out in TMBG at room temperature (Figure 3.46). After the reaction was completed, heptane and methanol were added to the reaction mixture, followed by CO_2 addition. This caused ionic liquid formation and a subsequent phase split into ionic liquid and heptane phases. The product 1-trimethylsilyloxy-1-cyclohexanecarbonitrile was found to selectively partition into the heptane phase, where it could be easily removed by decantation.

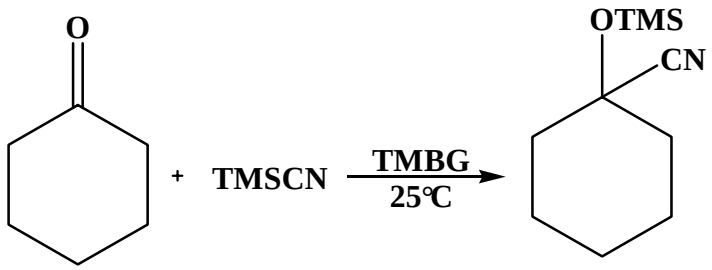

Figure 3.46 Cyanosilylation of cyclohexanone in TMBG

Though reaction times (from 1.5 to 16 hours) as well as molar ratios of TMBG to cyclohexanone (0.02:1 to 1:1) were varied, these changes did not appear to have any effect on reaction yields. In all cases, yields were essentially quantitative. When ^{1}H and ^{13}C NMR were used to analyze the ionic liquid phase, however, there was evidence of the formation of the ionic by-product 2-butyl-2-trimethylsilyy-1,1,3,3-tetramethylguanidinium cyanide (Figure 3.47).[36]

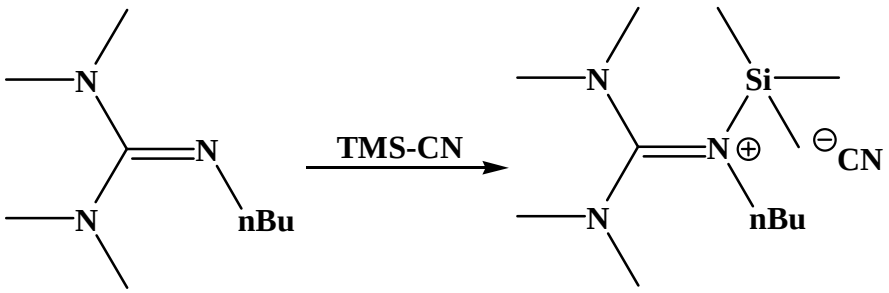

Figure 3.47 Formation of the by-product 2-butyl-2-trimethylsilyl-1,1,3,3-tetramethylguanidinium cyanide

Formation of this by-product was detrimental to the ionic liquid reversal process as this salt was found to be irreversible and its presence dramtically increased the viscosity of the ionic liquid phase, hindering reversal of the TMBG MC IL for recycle. In an effort to minimize formation of this silyl salt, heptane was added prior to the reaction. This did not have any noticeable affect on yields as they remained quantitative (96% and 98%), and the formation of the silyl salt was minimized, but not eliminated. Under these conditions, two different molar ratios of TMBG to cyclohexanone to TMSCN were investigated for ionic liquid formation and reversal; 0,4:1:1.2 and 1:1:2 (Table 3.6).

Table 3.6 Cyanosilylation of cyclohexanone coupled with the recycling of the ionic liquid phase.

Entry	Mole Ratio TMBG/Cyclohexanone/TMSCN	Time (hours)	Yield (%)
1-1	0.4:1:1.2	17	96
1-2	0.4:1:1.2	16	54
2-1	1:1:1.2	16	86
2-2	1:1:1.2	16	56

In the first cycle, the 1-trimethylsilyloxy-1-cyclohexanecarbonitrile product was isolated with 86% and 96 % yields (Table 3.6, entries 1-1 & 2-1 respectively). To reverse the ionic liquid phase, it was then heated at 80°C for 4 hours. The resulting TMBG was

used for a second cycle, yielding the desired product in 54% and 56% yields (Table 3.6, entry 1-2 & 2-2 respectively). It is believed that contamination of the guanidine precursor by the 2-butyl-2-trimethylsilyy-1,1,3,3-tetramethylguanidinium cyanide by-product leads to the decreased yields.[6]

To carry out the base-catalyzed Michael addition of dimethyl malonate to 2-cyclohexenone the reactants were mixed in TMBG in a 1:1:1 ratio of TMBG to malonate to 2-cyclohexanone. Once mixed, they were allowed to react at 80°C for 16 hours (Figure 3.48). Upon completion of the reaction, methanol, hexane and CO_2 were added to form the ionic liquid. As expected, upon ionic liquid formation, two phases, an ionic liquid phase and a hexane phase were obtained. GC-MS was used to analyze the hexane phase, which showed complete disappearance of all starting materials.

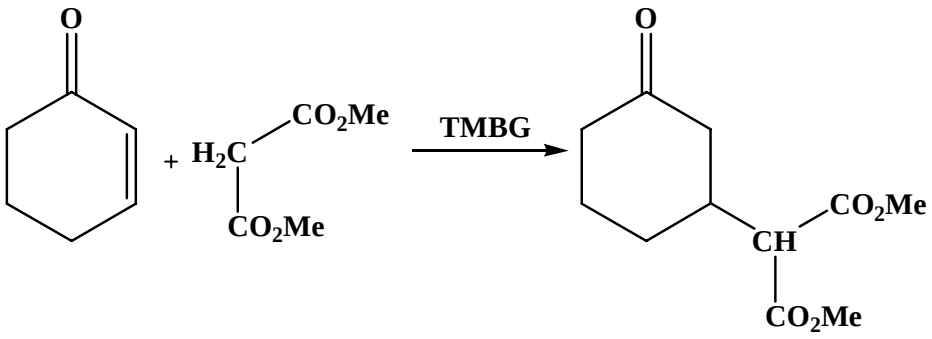

Figure 3.48 Michael addition of dimethyl malonate to 2-cyclohexenone

Both phases were then examined by ^1H NMR analysis. This showed that while the desired product was formed, the α-carbon was deprotonated due to the basic surrounding environment (Figure 3.49). This deprotonation formed an ionic product that existed only in the ionic liquid phase. After an acidic work up with 10% aqueous HCl, the neutral product was recovered and partitioned into the hexane phase. From this phase, it was

subsequently isolated in 86% to 100% yields. While both the product, and the TMBG could eventually be recovered and recycled, the necessity of an acidic work-up defeated the purpose of the overall reaction and separation process. Little advantage was offered over current synthesis methods.[6]

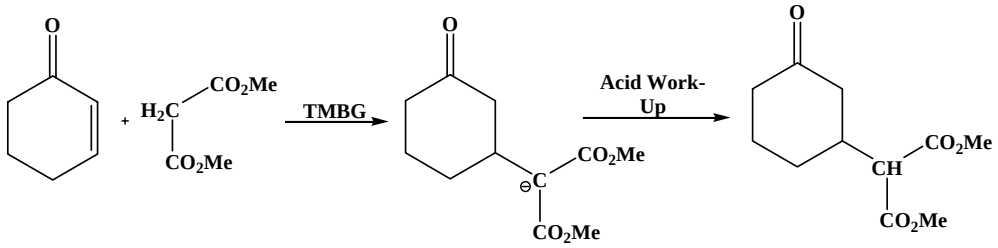

Figure 3.49 Necessary quenching of the β-diester

To react aniline with 1,3-diphenyl-propenone, both reactants were first dissolved in a 1:4 methanol:heptane mixture. TMBG was subsequently added to this in a 1:1 equimolar ratio with the methanol. (Figure 3.50).

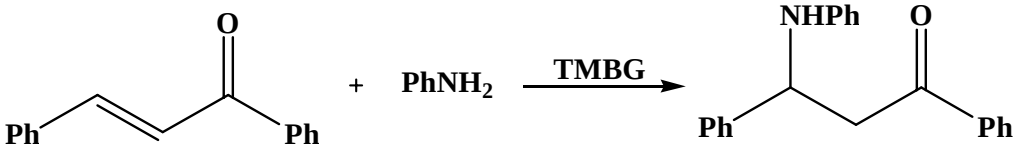

Figure 3.50 Base catalyzed addition of aniline to chalcone, using TMBG as the catalyst

The reaction was run at 80°C for 18 hours. After completion, CO_2 was added to the mixture to form the ionic liquid, and cause the subsequent ionic liquid/heptane phase split. The 1,3-diphenyl-3-phenylamino-propan-1-one product selectively remained in the heptane phase, from which it was isolated in 86% yield and the ionic liquid was reversed by heating at 60°C for 4 hours. A second reaction was carried out, but in this case

isolated yield decreased to 45% and a great deal of both desired product and unreacted starting material remained dissolved in the ionic liquid phase. It was believed that the accumulation of these organic materials in the ionic liquid altered the product partitioning and subsequent ionic liquid reversal.[6]

The base catalyzed Diels Alder reaction between anthrone and N-phenylmaleimide (Figure 3.51) was carried out by first dissolving anthrone in TMBG (a 1:1 mixture), followed by the addition of solid N-phenylmaleimide (also in a 1:1 ratio). After reacting at room temperature from 1 to 48 hours, an equimolar amount of methanol and decane were added to the solution, followed by the addition of CO2 to the reaction mixture. While the desired phase split was seen, the decane layer contained at most 5%

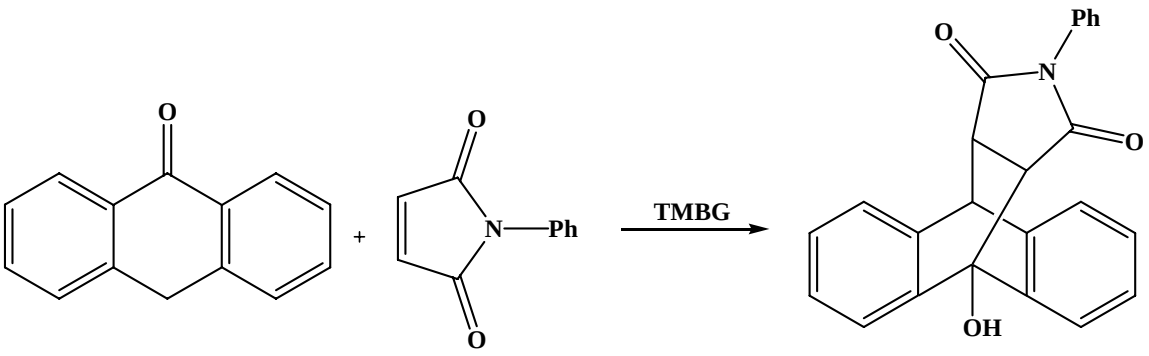

Figure 3.51 Diels Alder reaction between anthrone and N-phenylmaleimide catalyzed by our TMBG system

product when analyzed by GC-MS and ^{1}H and ^{13}C NMR, even after reacting for 48 hours. It is conjectured that the TMBG, being linear was simply not basic enough to catalyze this type of reaction, a finding that is supported by literature.[37]

In order to investigate how a metal catalyzed reaction would behave in the TMBG system, the Suzuki coupling between phenyl boronic acid and bromobenze using $Pd(Ac)_2$

as the catalyst was examined (Figure 3.52). To carry out this reaction, boronic acid, palladium precatalyst and phosphine ligands were mixed and degassed. TMBG was

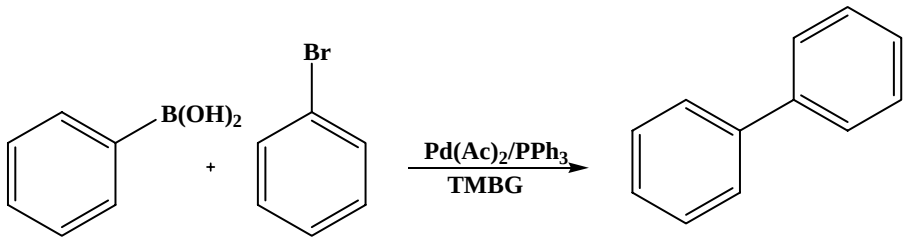

Figure 3.52 Suzuki reaction between phenyl boronic acid and bromobenzene using TMBG as the base catalyst

added with stirring. Finally, bromobenze was added to the reaction mixture. This mixture was heated at 80°C with stirring for sixteen hours. Upon completion, an equimolar amount of methanol and heptane were added, and CO_2 bubbled through the solution to isolate the product. The heptane layer was examined by GC-MS as well as ^{1}H and ^{13}C NMR, and at most was found to contain 25% desired product. Analysis of the ionic liquid layer showed an equal distribution of products between the heptane and the ionic liquid layers. Analysis by ^{1}H NMR showed that the ionic liquid layer contained a mixture of product, unreacted starting material, as well as a variety of byproducts. Attempts at reversing the ionic liquid layer were unsuccessful.

3.3.1.12.3 Base Catalyzed Reactions in TMBG MC IL -Oxidation of benzyl alcohol

We were curious about examining reactions that could take place in the TMBG MC IL, not just in the guanidine phase. It is known in literature that the oxidation of benzyl alcohol in the presence of a room temperature guanidinium based ionic liquid, using sodium hypochlorite and water can be carried out successfully (Figure 3.53).[38] In

this reaction, high yields were obtained by extracting the product out of the ionic liquid into diethyl ether, after which the ionic liquid could easily be dried, recovered and reused. We decided to examine this reaction in the TMBG MC IL using the standard alkane

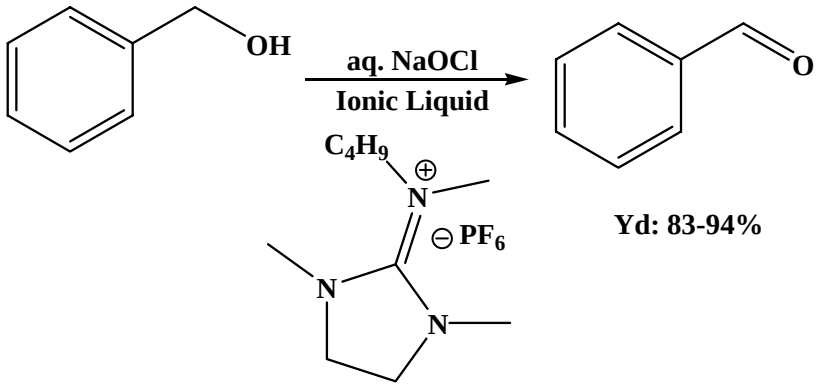

Figure 3.53 Oxidation of benzyl alcohol using sodium hypochlorite in the presence of an RTIL

extraction method to isolate our product. For our reaction, calcium hypochlorite was chosen, instead of sodium. (Figure 3.54)

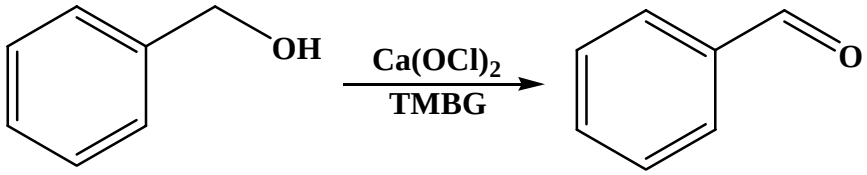

Figure 3.54 Oxidation of benzyl alcohol using calcium hypochlorite in the presence of our TMBG MC IL

To carry out this reaction, a mixture of TMBG MC IL (5.26mmol) and benzyl alcohol (0.526mmol) was employed. Once this was thoroughly mixed, calcium hypochlorite was added to the system (0.789mmol). This mixture was allowed to react at room temperature for 16 hours. A heptane extraction was then used to remove benzaldehyde product. As per usual, GC-MS and NMR were used to analyze the heptane and product

layer and it was found that only benzyl alcohol was recovered from the system. The lack of reaction is believed to be caused by the insolubility of calcium hypochlorite in the TMBC MC IL.

3.3.1.12.4 Summary of Reactions run in TMBG-methanol IL systems

We were able to successfully perform and carry out two reactions with separation and recycle using the TMBG-methanol ionic liquid systems; the Claisen-Schmidt condensation of 2-butanone and benzaldehyde and the cyanosilylation of cyclohexanone. The Claisen-Schmidt reaction was successfully recycled three times with consistent yields (32-35%). Though these numbers may seem low, they are the maximum obtainable to avoid side product formation. The cyanosilation was successfully recycled twice, affording good yields in the first cycle (98% and 85%) but only moderate yields on the second cycle (54% and 56%). This decrease in yield is due to the formation of the TMBG/TMS-CN salt. This salt formation is also the reason why this solvent cannot be recycled further.[6]

Other reactions were successfully run once in the system and afforded high yields (Michael addition between 2-cyclohexenone and dimethyl malonate up to 90% and addition of aniline to chalcone 85%).[6] However, these reactions could only be run once, no recycle was possible, and ultimately they afforded no obvious advantage over systems currently in place.

3.3.1.12.5 Separation of alkanes from tar sands/shale

As demand for oil increases throughout the world, traditional sources, crude oil reservoirs are becoming depleted. This is forcing society to turn to less traditional sources, such as tar sands and shale. However, it is currently very difficult to isolate oil from these sources.[39-40] Materials such as tar sands and shale are mainly made of bitumen, which is composed primarily of clay, inorganic salts such as Mg^{2+} and Ca^{2+} and alkanes.

The ideal process for extracting hydrocarbons from these sources using a reversible ionic liquid system is outlined in Figure 3.55. Bitumen would first be mixed with the tetramethylbutyl guanidine. This would extract the hydrocarbons from the solid components. Filtration would occur at this point to remove those solids from the system. Upon addition of methanol and CO_2 to the system, the TMBC MC IL would be formed, causing the alkanes to phase separate, at which point they can be removed for further purification and refining. It is possible that some purification will also take place during

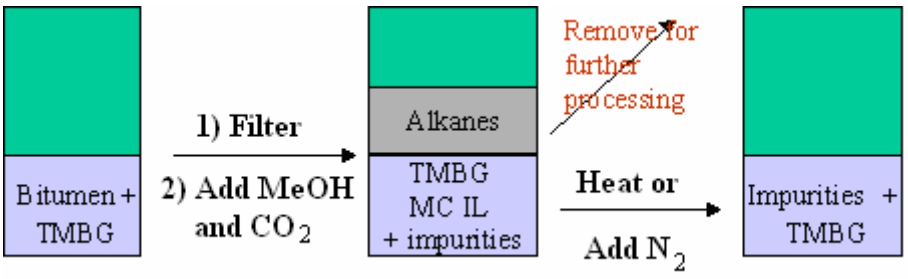

Figure 3.55 Complete process for separation of alkanes from tar sands and shale using formation of the TMBG MC IL

extraction as some ionic impurities should preferentially stay in the ionic liquid phase. The ionic liquid could then be reversed, purified in its neutral form, and recycled.

Miscibility tests with octane and the TMBG MC IL discussed in section 3.3.1.9 showed that octane is miscible with the molecular liquid, but immiscible with the ionic liquid form. This concept was tested on a crude oil sample. The crude oil was first mixed with TMBG, with which it is completely miscible (Table 3.7). At this point an equimolar amount of methanol, relative to the TMBG in the system, was added to the solution, and CO_2 was bubbled through the entire system.

Table 3.7 Composition of TMBG/methanol/crude oil systems used for separation studies

Mol TMBG	Crude Oil (g)	% Crude Oil in Mixture
0.00206	0.1	19.3
0.00199	0.1	19.7

It is important to note that the percentage of oil in the mixture is a volume % based on all liquids in the solution, TMBG, methanol and crude oil. As expected, after CO_2 addition, the crude oil phase separated (Figure 3.56). The experiments began with TMBG and methanol (Figure 3.56-A), to this crude oil was added to form a dark brown homogeneous mixture (Figure 3.56-B) As CO_2 was bubbled through the mixture, a phase separation could be seen as the ionic liquid formed (Figure 3.56-C). Ultimately, after the reaction was completed, two phases existed, a very dark upper layer, which contains the

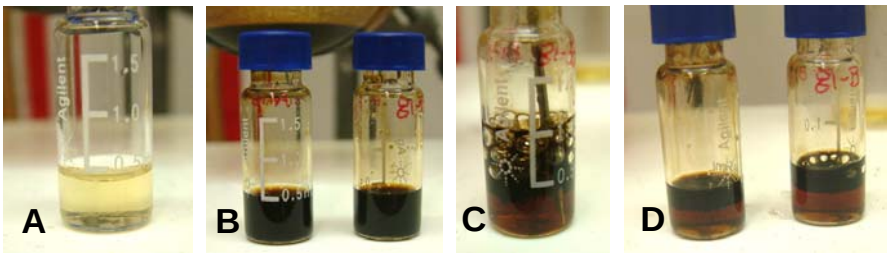

Figure 3.56 Separation of crude oil from TMBG MC IL. **A.** Pure TMBG **B.** TMBG with crude oil – homogeneous mixture **C.** Bubbling CO_2 to form ionic liquid **D.** After IL formation, clear phase split can be seen

hydrocarbons, and a lighter brown lower ionic liquid layer (Figure 3.56-D). Both phases of this mixture were analyzed by GC-MS. This analysis showed only trace amounts of TMBG in the upper crude oil phase, and no evidence at all of hydrocarbon in the ionic liquid phase.

A bitumen sample obtained from Conoco Phillips was also tested. The bitumen sample is known to be a mixture of clays, inorganic alkali metal salts, 1-3 wt% hydrogen sulfide, <2 wt% ethyl benzene, <1 wt% benzene, and crude oil.[41] An NMR run on this sample showed only the expected alkane peaks, though it is known that trace aromatics are present, they are in quantities below the limit of detection for the NMR equipment.

As with the previous test, the bitumen was added to the TMBG. This was vigorously stirred to ensure complete mixing of the bitumen and TMBG. An equimolar amount of methanol was added to the system, and CO_2 was bubbled to form an ionic liquid. As a result, two immiscible liquid phases formed. Both phases were sampled and analyzed using ^{1}H and $^{13}CNMR$. This system was tested with a variety of different amounts of bitumen in the solution. The exact compositions in weight percent of all solutions tested can be seen in Table 3.8.

It was found that there is an upper limit to the amount of bitumen that can be used and still have a successful phase separation occur. In the first two samples tested (Runs 1 and 2, Table 3.8), the amount used was above that limit 14.6 and 10.2% bitumen respectively, and phase separation was not seen. However, when lower amounts of bitumen were used, from 1.07-8.56% (Runs 3-7, Table 3.8) a phase separation was visible (Figure 3.57), so this limit appears to be at or just below 10%. From a visual examination, it could be seen that the ionic liquid phase darkened after separation (Figure

Table 3.8 Separation of bitumen with TMBG MC IL

	Mol TMBG	g bitumen	% bitumen in mixture
1	0.00409	0.142	14.6
2	0.00409	0.103	10.2
3	0.00409	0.009	1.07
4	0.000567	0.003	2.54
5	0.00067	0.006	4.25
6	0.000544	0.007	5.96
7	0.000421	0.008	8.56
8-1	0.00725	0.016	1.07
8-2	0.00772	0.017	1.07
8-3	0.00316	0.007	1.07

3.57-D). However, when examined with NMR analysis, no peaks aside from those expected for the TMBG MC IL were seen. Most likely ionic contaminant species remained in the ionic liquid phase, which could not be detected via NMR or GC-MS. After separation from the TMBG MC IL, the isolated alkane phase was noticeably less viscous. NMR analysis (^{1}H and ^{13}CNMR) was run on the isolated hydrocarbons, and now both the expected alkanes and trace aromatic impurities (benzene, ethyl benzene) could be seen.

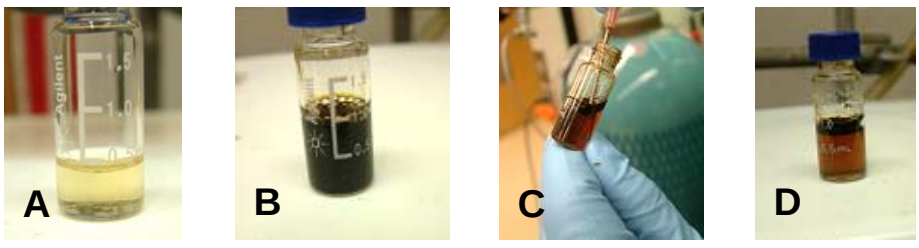

Figure 3.57 Separation of alkanes from bitumen using TMBG MC IL. **A.** Pure TMBG, **B.** TMBG with added bitumen sample, **C.** Bubbling CO_2 to form TMBG MC IL, **D.** Bitumen phase separated from TMBG MC IL

After the alkane layer was removed, the TMBG MC IL was successfully reversed to the molecular liquid, and the entire process was repeated two more times (Runs 8-1 to 8-3, Table 3.8). It is important to note, however, that after the second separation, the TMBG had become almost black. To remedy this situation, the TMBG was run over a pad of silica gel with ethyl acetate. After this cleaning, TMBG MC IL was formed, any impurities that phase separated out at this point were removed, the ionic liquid was reversed, and fresh bitumen was added to successfully carry out the third recycle.

3.3.1.12.6 Summary of other TMBG IL Applications

Aside from being a means of carrying out reactions and separations, due to its unique properties and abilities, the TMBG IL system has proven to be useful in a variety of other capacities which are currently industrially important. Due to its immiscibility with common alkanes, the TMBG MC IL can be used to extract the alkanes in oil from impurities which was successfully shown both in a proof of concept study with crude oil and on a sample of bitumen provided by Conoco Phillips. Not only could the ionic liquid be used for this once, it could also be successfully recycled up to three times.

3.3.2 One Component Ionic Liquids

3.3.2.1 Amine Precursor Molecules

(3-Aminopropyl)trimethoxysilane and (3-aminopropyl)triethoxysilane were chosen as the first precursors to examine for one-component ionic liquid formation (Figure 3.58).

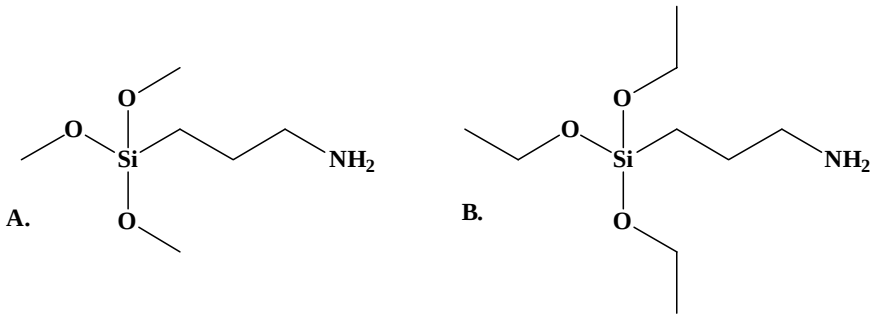

Figure 3.58 One component ionic liquid precursors. **A.** (3-Aminopropyl)trimethoxysilane and **B.** (3-aminopropyl)triethoxysilane

3.3.2.2 Synthesis and Characterization of One Component Ionic Liquids

The neat precursor was placed in round-bottom flask under nitrogen. To form the ionic liquid, carbon dioxide was bubbled through the precursor. (Figure 3.59) An exotherm was observed to take place, and bubbling was stopped only after the solution

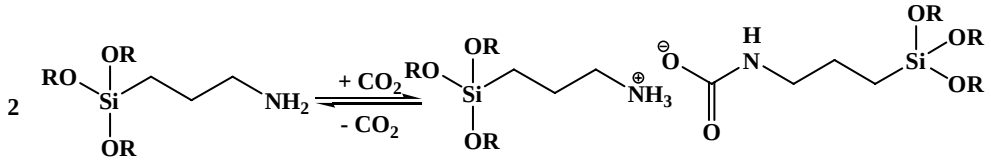

Figure 3.59 One component ionic liquid formation from alkoxy precursor

had cooled to room temperature, at which point, in both cases, a clear viscous oily liquid had formed.

When (3-aminopropyl)triethoxysilane was used as precursor, analysis of the product by ^{1}H NMR, ^{13}C NMR, IR and elemental analysis all confirmed formation of the desired 3-(triethoxysilyl)-propylammonium 3-(triethoxysilyl)-propyl carbamate (TESAC) ionic liquid. This was evidenced in the ^{13}C NMR, with a characteristic carbamate peak that appeared at 162.6ppm. The ^{1}H NMR also showed appearance of the third proton attached to the nitrogen, the IR displayed characteristic NH_3+ stretches at υ_{max}/cm^{-1} 3400-

2400 and CO_2- stretches at υ_{max}/cm^{-1} 1570 and 1481 and the elemental analysis matched the expected element ratios for the desired ionic liquid product.

Using (3-Aminopropyl)trimethoxysilane as the precursor molecule, the same tests were run on the resulting ionic liquid and similar results were found, confirming the formation of 3-(trimethoxysilyl)-propylammonium 3-(trimethoxysilyl)-propyl carbamate (TMSAC) ionic liquid. This was particularly evident by the carbamate peak appearing at 162.5ppm in the ^{13}C NMR. Viscosity tests were run on both ionic liquids using a cup and bob viscometer, temperature controlled at a constant 25°C. The viscosity was found to vary greatly with structure, as TMSAC showed a viscosity of 2,160 cP, and TESAC showed a viscosity of 930 cP. (Figure 3.60) This difference is consistent with what was observed physically and is not unexpected as the larger ethoxy groups can more readily disrupt ionic packing. However, both ionic liquids proved to be Newtonian fluids with no shear thinning observed.

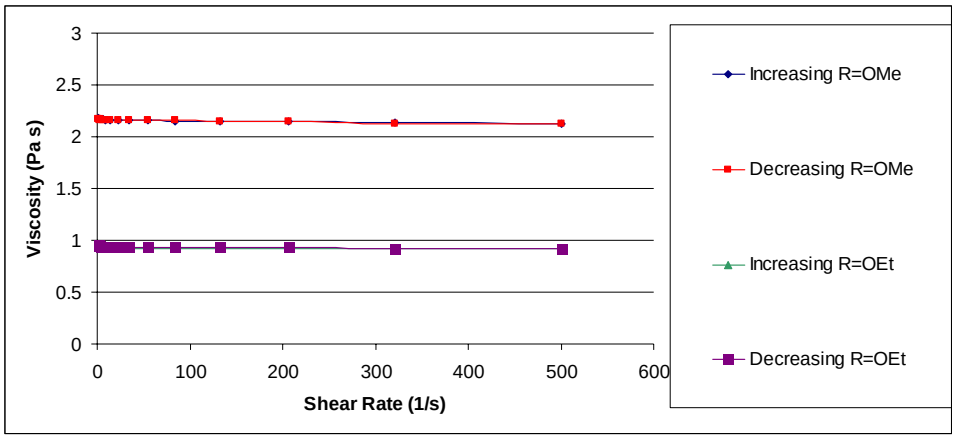

Figure 3.60 Viscosity measurements of TMSAC and TESAC ionic liquids

After basic physical characterization was completed, the solvatochromic properties of TMSAC and TESAC were investigated using the solvatochromic probe Nile

Red and following the same procedure described previously with the two component ionic liquids. As with the two component ionic liquids, a substantial shift in polarity was found when going from neutral precursor molecule to ionic liquid. TMSA showed a 9.0 nm λ_{max} increase (from 528.1 nm to 537.1 nm) when converted to the ionic TMSAC form, while TESA showed a 11.4 nm increase (from 522.6 nm to 534.0 nm) when converted to TESAC. The TMSA is more polar then TESA, however it undergoes less of a polarity switch. In general, these solvents change from a polarity value similar to benzene (525.4 nm) to one similar to chloroform (537.6 nm).[29] In both cases, the polarity change is smaller than for the two component guanidine systems. Figure 3.61 shows the wavelength of maximum absorption found for TMSAC and TESAC, their neutral precursor molecules as well as other common solvents.

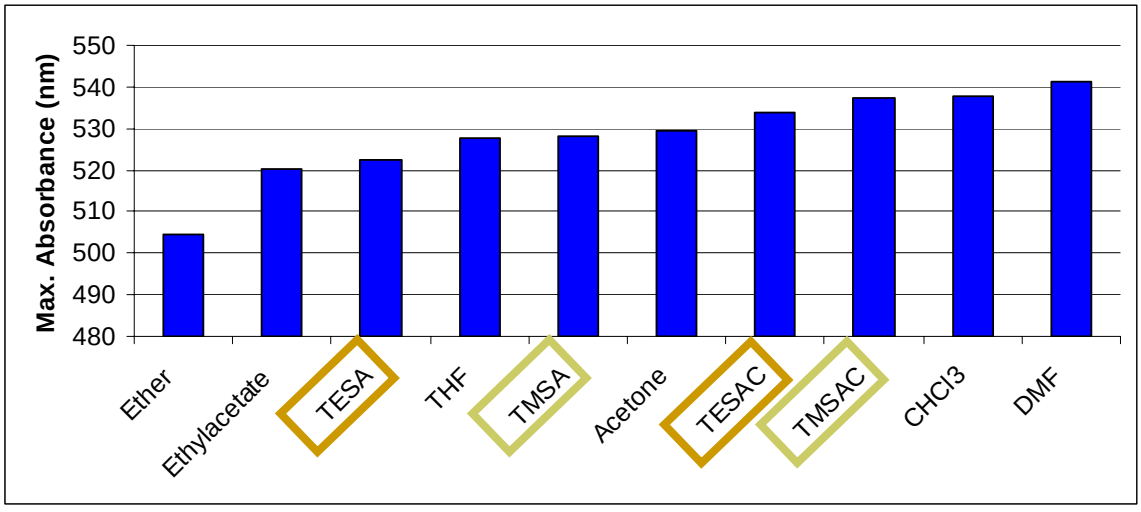

Figure 3.61 Wavelengths of maximum absorption of one component ionic liquids, their precursors and other common solvents

3.3.2.3 Reversibility of One Component Ionic Liquids

The reversibility and reformation of the TMSAC and TESAC ionic liquids were examined using ^{1}H NMR and ^{13}C NMR, as well as DSC and TGA studies. DSC and

TGA were run first to gain an understanding of where reversal may occur. The TGA showed that for the TMSAC ionic liquid, a 13% mass loss was seen by 88°C and for the TESAC ionic liquid, a 9% mass loss was seen by 125°C. In both cases, this corresponds to the loss of CO_2 from the system. These results indicated that complete reversal should be possible at relatively moderate temperatures. These results were confirmed by DSC testing which showed two endotherms present for each ionic liquid, one corresponding to loss of CO_2 from the system, (beginning at 50°C and continuing to 150°C for TESAC and beginning at 75°C and continuing to175°C for TMSAC) and one for the decomposition of the amine precursor, which in both cases took place well over 200°C. The results seen for both ionic liquids can be illustrated by the thermogram obtained for TESAC (Figure 3.62).

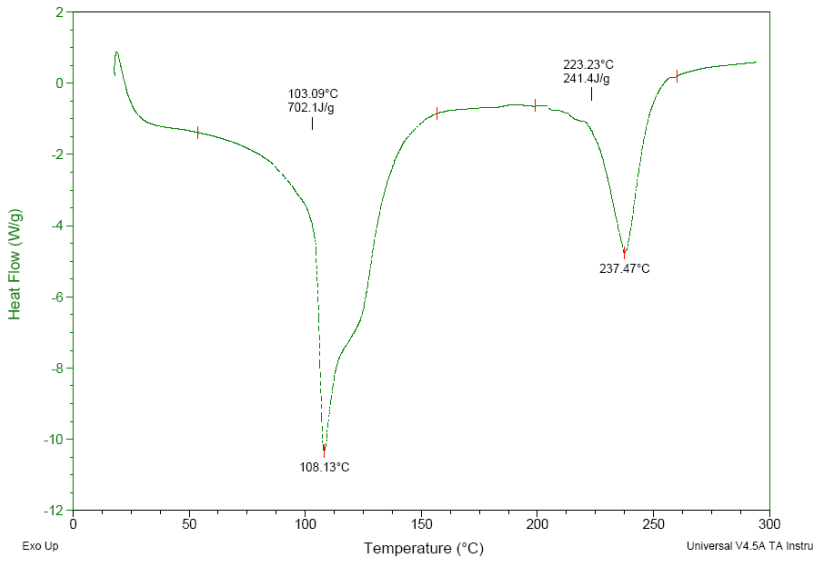

Figure 3.62 DSC thermogram of TESAC ionic liquid, indicating IL reversal between 50°C and 150°C and decomposition of amine precursor over 200°C

After it was determined that reversal was possible at moderate temperatures, NMR studies were performed. For the ^{13}C NMR studies (Figure 3.63)[5], an NMR was taken of the neat starting material (TESA in Figure 3.63-A) which showed peaks at

58ppm and 18ppm from the carbons in the ethoxy groups and peaks at 8ppm, 27ppm, and 45ppm for the carbons on the propyl amine chain. CO_2 was then bubbled through the solution for 20 minutes, and another neat NMR was taken (TESAC in Figure 3.63-B). In this NMR, a peak appeared at 162.6ppm consistent with formation of a carbamate group. In addition, two sets of 5 peaks (for the ethoxy and the propyl chain) are observed in the NMR, one set corresponding to the triethylsilylpropyl carbamate and one set to the triethylsilylypropyl ammonium. Finally, the ionic liquid was heated at 120°C with stirring for 2 hours to reverse (TESA in Figure 3.63-C). After reversal, the carbamate peak disappeared and the peak doubling disappeared, and the five peaks attributed to

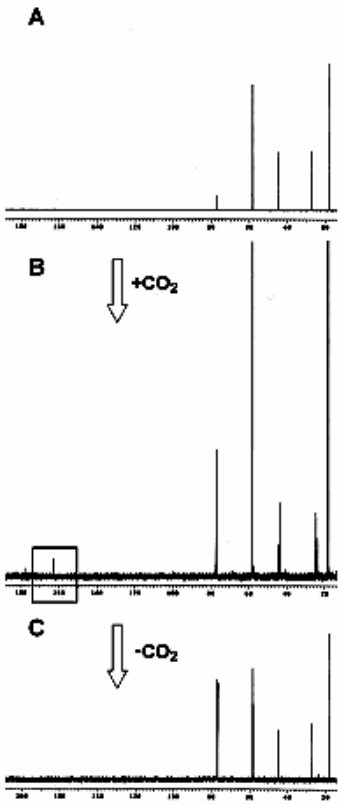

Figure 3.63 ^{13}CNMR taken of **A.** the neat TESA starting material, **B.** newly formed TESAC ionic liquid, and **C.** TESAC ionic liquid after it has been heated at 120°C for 2 hours and reversed to starting material Blasucci, V. et al, *One Component, Switchable Ionic Liquids Derived from Siloxylated Amines*. Chem. Commun. 2009, **1**: p. 116-118. Reproduced by permission of The Royal Society of Chemistry[5] http://dx.doi.org/10.1039/b816267k

TESA were observed at 8ppm, 18ppm, 27ppm, 45ppm, and 58ppm. ^{13}CNMR was the most beneficial tool for tracking the formation and subsequent reversal of the ionic liquid, as appearance and disappearance of the carbamate can clearly be seen.[5]

3.3.2.4 Miscibility Studies of the One Component Amine Based Ionic Liquids

The miscibility of the one component ionic liquids with the hydrocarbons pentane, hexane, and octane was studied. These miscibility studies were carried out by first forming an equimolar mixture of the amine precursor (either TESA or TMSA) and the hydrocarbon. In all cases, the amine precursor and hydrocarbon were completely miscible. CO_2 was bubbled through the mixture for 20 minutes, until the exotherm subsided. At this point two distinct phases were seen, a hydrocarbon phase and an ionic liquid phase. Each phase was analyzed by ^{1}H NMR and GC-MS. This analysis confirmed less than 1 mol % contamination of ionic liquid in the hydrocarbon phase.

3.3.2.5 Applications of One Component Amine Based Ionic Liquids

3.3.2.5.1 Separation of Alkanes from tar sands/shale

The one component ionic liquids may provide easier and more cost effective methods for accessing the oil from non traditional sources such as tar sands than current methods, which frequently involve the energy intensive process of distillation.[7] The TESAC ionic liquid was chosen due to its lower viscosity, lower reversal temperature, and larger polarity switch. Therefore, proof of principle testing with crude oil was done solely with this ionic liquid.

The method followed to carry out these tests is illustrated in Figure 3.64. Crude oil was added in a 50 wt.% amount to the TESA precursor to form a homogeneous mixture. With unconventional oil sources such as bitumen or tar sands filtration can take place at this point to remove solids from the system. However for this test with crude oil no solids were present so filtration was not necessary. CO_2 was bubbled through the mixture for 20 minutes. This produced a single liquid phase with high viscosity. Allowing this mixture to sit overnight, two distinct phases could then be seen. However, centrifuging this mixture for twenty minutes also induced the expected and desired phase split. The need to centrifuge is attributed to the high viscosity of the system and to similar densities between the crude oil and the ionic liquid. The ionic liquid has a density of 1.06 g/mL compared to the crude oil which has a density of 1.03 g/mL. Once the two phases were separated, the top phase was decanted and the bottom phase was heated at 120°C for 2 hours to reverse the ionic liquid back to the molecular liquid. A new oil sample was then introduced in a 50 wt.% amount and the entire process was repeated for three total recycles, and the entire system was run 3 times.[7]

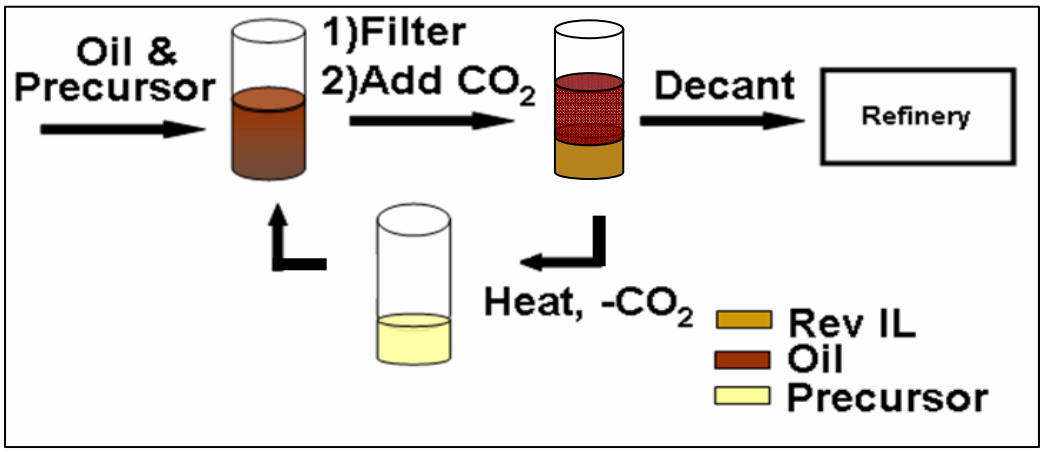

Figure 3.64 Scheme for the use of one component ionic liquid to separate alkanes from crude oil

For each cycle, samples of the top and bottom phases were removed and analyzed using ^{1}H and ^{13}C NMR. This was done by comparing the integrations of the peak from the O-CH_2 protons of the IL or IL precursor to the peak for the terminal CH_3 from the hydrocarbon chains found in the crude oil. The results of ionic liquid contamination in the crude oil phase are shown in Table 3.9.[7] As can be seen here, the product hydrocarbon phase contains less than 4 mol% ionic liquid contamination. The separation efficiency is not altered over each cycle, and is expected to improve with larger scale experiments. The TESAC phase is also expected to contain other impurities such as sulfur, water, and heavy metals like arsenic which are common to crude oil.

Table 3.9 Post cycle amount of TESAC seen in the hydrocarbon product phase

Cycle Number	mol% TESAC
1	3.6
2	3.3
3	2.6

After initial experiments with crude oil, bitumen extractions were also studied. The bitumen sample used for these experiments was of the same type and source as described in section *3.3.1.12.5*. To carry out these tests, the exact same procedure was followed as for the crude oil, however, a smaller amount (18wt.% relative to precursor) was used. The mixture contained a liquid phase and a solid particulate. To remove the solid, the mixture was filtered before CO_2 addition. Once the process was carried out, two clear phases were again seen, however there was no further characterization of the phases.

3.3.2.5.2 Summary of One Component Ionic Liquid Applications

Due to the polarity switch seen when converted from a neutral to an ionic liquid, one component amine based ionic liquids are successful at phase separating from alkanes both in crude oil samples, and from a bitumen sample provided by Conoco Phillips. This indicates that this system should be successful in extracting and separating alkanes from tar sands and oil shale. As these ionic liquids are based on only one component, and loss of a second component is not an issue, this system would ultimately be more practical, from a processing stand point, than that presented previously for two component ionic liquids.

3.4 Conclusions

3.4.1 Two Component Ionic Liquids

A new class of room temperature ionic liquids has been designed and developed. These 2-butyl-1,1,3,3-tetramethylguanidinium alkylcarbonate ionic liquids are unique in that they are part of the first class of ionic liquids that can be formed easily with the addition of CO_2 gas, and readily reversed with either inert gas, mild heating, or vacuum.[4] The properties of the ionic/molecular liquid system can be altered by changing the alkyl substituents on the guanidine as well as by using different alcohols. Many reactions were studied in order to show a complete chemical process that includes reaction, separation, reformation, and recycle. In two of these reactions, the Claisen-Schmidt condensation of butanone and benzaldehyde and the cyanosilylation of cyclohexanone, this was successfully achieved. The TMBG MC IL was reversed and recycled three times and two times, respectively.[6] It has been shown to be successful in

extracting hydrocarbons from bitumen samples, a method that, with optimization, could be used to purify high cost fuel samples for use in oil and gasoline production.

3.4.2 One Component Ionic Liquids

Developed in conjunction with the two component ionic liquids, one component reversible systems are also part of the new class of reversible ionic liquids.[5] These are based on commercially available (3-aminopropyl)-trialkoxysilane precursors, and like two component ionic liquids, the ionic liquid is formed by addition of CO_2 to the system, and reversed by removal of the CO_2 with either inert gas, heating over 100°C or vacuum. The systems properties can be tuned and changed by altering the alkoxy substitution, and they have been found useful for separating hydrocarbons from bitumen samples.[7] Though these ionic liquids have not yet been as extensively studied as the two component variety, they show a great deal of promise, especially as, from a processing stand point, they are more practical to work with and use than the two component ionic liquids.

3.5 Experimental

All chemicals were ordered from Aldrich and used a received, unless noted. The crude oil was analyzed by Chevron for sulphur (combustion followed by infrared detection) and hydrocarbon fractions (gas chromatography and simulated distillation software). The sample contained 1.17 wt% sulphur. The largest hydrocarbon cut was detected between 302ºC and 316ºC. Bitumen was provided by ConocoPhillips and used as received. NMR spectra were obtained from a Bruker DRX 500 and Varian-Mercury VX400 MHz spectrometer. NMRs of neat samples were calibrated to external $CDCl_3$ at

7.24ppm (^{1}H) and 77 ppm (^{13}C). GC-MS analysis was done on a HP GC 6890/ HP MS 5973. Thermal analyses studies were performed on TA instruments Differential Scanning Calorimeter (DSC) Model Q20 and Thermogravimetric Analyzer (TGA) Model Q50. Samples were heated at 5°C/ min for both DSC and TGA analyses. DSC experiments were performed in hermetically sealed pans with a pin-sized hole in the top.

Synthesis of TMBG

2-Butyl-1,1,3,3-tetramethylguanidine was synthesized by a modification of the literature procedure.[22-23] Tetramethylurea (0.08mol) was stirred in dry dichloroethane (80mL) for ~ 5min. Oxalyl chloride (0.18mol) was slowly added. The mixture was then heated at 60^{o}C for 5h. Dichloroethane solvent was removed via vacuum after the mixture cooled to RT. Dry acetonitrile (75mL) was used to dissolve the dichloride intermediate. The reaction vessel was then cooled to 0^{o}C. Butylamine (0.16mol) was dissolved in 15mL of dry acetonitrile and the mixture was added dropwise to the dissolved dichloride intermediate. After the reaction warmed to RT, it was refluxed at 92^{o}C for 1h. Solvent was then removed via the rotary evaporator, and the residue was treated with 30% aq NaOH (30mL). The product was then extracted with diethyl ether (3x20mL), dried with $MgSO_4$, and concentrated to give the desired product as a clear oil in 80 % yield.

2-Butyl-1,1,3,3-tetramethylguanidine: ^{1}H NMR ($CDCl_3$): 0.784 (t, 3H), 1.22 (m, 2H), 1.39 (m, 2H), 2.53 (s, 6H), 2.62 (s, 6H), 2.99 (t, 2H). ^{13}C NMR ($CDCl_3$):13.69, 20.32, 34.26, 38.39, 39.36, 48.69, 161.45. DEPT-135 (neat): up-13, 40, 42, 49; down-23, 36, 50. EA: calculated C, 59.37%; H, 11.96%; N, 20.77% N. Found: C, 59.21%; H, 12.3%; N, 21.5%

Synthesis of TMBG for Easy Scale Up

Synthesis of 2-butyl-1,1,3,3-tetramethylguanidine was carried out in a one pot synthesis. Butyl bromide (0.084mol) was placed in a round bottom flask and heated with stirring to 120C. Once at temperature, slightly less than one molar equivalent of tetramethylguanidines (0.080mol) was dripped in slowly. An exotherm occurred, which was not controlled, but allowed to peak at ~145C and decrease naturally. All heating was stopped and the solution was cooled back to room temperature. The resulting liquid was treated with 30% aq NaOH (30mL). The product was then extracted with diethyl ether (3x20mL), dried with $MgSO_4$, and concentrated on the rotovap to give the desired product as a clear oil, with approximately 8% unreacted tetramethylguanidine remaining in the system as an impurity.

2-Butyl-1,1,3,3-tetramethylguanidine: ^{1}H NMR ($CDCl_3$): 0.67 (t, 3H), 1.11 (m, 2H), 1.27 (m, 2H), 2.42 (s, 6H), 2.52 (s, 6H), 2.88 (t, 2H). ^{13}C NMR ($CDCl_3$):13.63, 20.17, 34.64, 38.38, 39.19, 48.88, 159.44.

1,1,3,3-tetramethylguanidine: ^{1}H NMR ($CDCl_3$): 2.52 (s, 6H). ^{13}C NMR ($CDCl_3$): 38.835

Formation of TMBG ILs

The 2-butyl-1,1,3,3-tetramethylguanidinium alkylcarbonate ionic liquids were synthesized by bubbling CO_2 through equimolar solutions of 2-butyl-1,1,3,3-tetramethylguanidine and the alcohol. The mixture was bubbled with CO_2 an additional 10-15 minutes after the exotherm subsided, indicating full conversion of the neutral mixture to the ionic liquid.

2-butyl-1,1,3,3-tetramethylguanidinium methylcarbonate: ^{1}H NMR (neat): 1.12 (t, 3H), 1.51 (m, 2H), 1.78 (m, 2H), 3.1 (s, 12H), 3.38(t, 2H), 3.45 (s, 3H). ^{13}C NMR (neat): 14.35, 21.05, 33.48, 40, 46.59, 49.12, 51.79, 158.15, 161.16. DEPT-135 (neat): up-13, 39, 49, 51; down-20, 33, 46. EA: Theory 53.42 % C, 10.19% H, 16.99% N. Found 54.64% C, 11.1% H, 17.53% N.

IR (neat) Figure 3.65

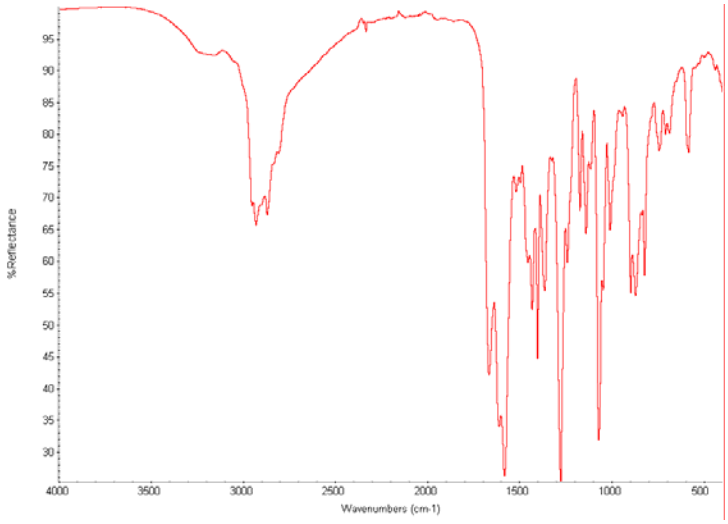

Figure 3.65 IR of 2-butyl-1,1,3,3-tetramethylguanidinium methylcarbonate

2-butyl-1,1,3,3-tetramethylguanidinium butylcarbonate: ^{1}H NMR (neat): 1.11 (br s, 7H), 1.54 (m, 5H), 1.66 (m, 2H),1.8 (m, 2H), 3.1 (s, 12H), 3.39(t, 1H), 3.66 (m, 1H), 3.96 (s, 1H). ^{13}C NMR (neat): 13.6, 13.85, 19.16, 19.93, 32.39, 35.38, 39.27, 45.15, 60.65, 63.35, 157.22, 161.22. EA: Theory: 58.10% C, 10.80% H, 14.52% N. Found: 58.13% C, 11.46% H, 14.31% N.

2-butyl-1,1,3,3-tetramethylguanidinium hexylcarbonate: ^{1}H NMR (neat): 1.03 (br s, 11H), 1.44 (br s, 14H), 1.62 (m, 4H), 1.77 (m, 2H), 3.15 (s, 12H), 3.33(t, 2H), 3.62 (m, 3H), 3.92 (s, 1H). ^{13}C NMR (neat): 13.83, 14.10, 20.16, 22.93, 26.07, 32.16, 33.36,

39.63, 61.38, 157.91, 161.81. EA: Theory: 60.53% C, 11.11% H, 13.24% N. Found: 60.79% C, 11.90% H, 12.69% N.

2-butyl-1,1,3,3-tetramethylguanidinium octylcarbonate: ^{1}H NMR (neat): 1.1 (t, 6H), 1.46 (br s, 12H), 1.65 (m, 2H), 1.75 (m, 2H), 3.08 (s, 12H), 3.33(t, 2H), 3.62 (m, 1H), 3.92 (s, 1H). ^{13}C NMR (neat): 13.9, 14.09, 20.3, 22.84, 26.45, 29.65, 29.72, 30.54, 32.13, 32.97, 39.46, 46.04, 61.27, 63.95, 157, 160.9. EA: Theory: 62.57% C, 11.38% H, 12.16% N. Found: 62.55% C, 11.96% H, 11.98% N.

2-butyl-1,1,3,3-tetramethylguanidinium dodecylcarbonate: ^{1}H NMR (neat): 1.1 (t, 7H), 1.49 (br s, 20H), 1.68 (m, 2H), 1.77 (m, 2H), 3.1 (s, 12H), 3.35(t, 2H), 3.65 (m, 1H), 3.95 (s, 1H). ^{13}C NMR (neat): 14.32, 14.49, 20.7, 23.25, 27.11, 30.03, 30.35, 32.55, 33.42, 39.85, 46.5, 61.69, 64.30, 157.74, 161.15. EA: Theory: 65.79% C, 11.80% H, 10.46% N. Found: 66.52% C, 12.66% H, 11.66% N.

2-butyl-1,1,3,3-tetramethylguanidinium bicarbonate: ^{1}H NMR (neat): 0.84 (t, 3H), 1.26 (m, 2H), 1.4 (m, 2H), 2.67 (s, 12H), 3.02 (t, 2H), 3.38 (br s, 2H). ^{13}C NMR (neat): 13.67, 19.50, 31.46, 39.28, 44.26, 158, 160.62.

Nile Red Measurements

Polarity was measured using Nile Red dye on a Hewlet Packard 8453 UV-Vis system. Samples were measured at three different concentrations of dye, three times each, for a total of nine measurements per sample. For each sample the dye was added the system was allowed to stir for 20 minutes before measurements were taken to ensure complete dissolution

Reversal of IL using inert gas

TMBG MC IL (1g) was placed in a small vial. N_2 gas was sparged through the solution overnight (12 hours). NMR indicated reversal to TMBG as well as some methanol loss

Reversal of IL using heat

TMBG MC IL (1g) was placed in a small vial or NMR tube. A small stir bar was placed in the bottom. This whole set up was placed in an oil bath set at 80°C. This was allowed to heat with stirring at 80°C for 3 hours. Bubbles could be seen leaving the system. After three hours, NMR indicated reversal to TMBG and some small amount of methanol loss

Reversal of IL using vacuum

TMBG MC IL (1g) was dissolved in chloroform (10mL) and rotovapped for 1 hour. NMR indicated reversal to TMBG (methanol had evaporated).

Melting Points

A round bottomed flask was filled with isopropanol. A thermometer and an NMR tube were placed in the flask. Freshly formed ionic liquids was placed in the ionic liquid, which was sealed with an NMR septum and covered with parafilm. The flask was then cooled with a dry ice/acetone bath, and then allowed to warm up until the ionic liquid melted. The cool-heat cycle was performed three times for each sample.

Conductivity study

Conductivity was measured using a ThermoOrion Model 115 Meter. An equimolar solution of *2*-butyl-1,1,3,3-tetramethylguanidine and methanol (5.56 mmol) was dissolved in 4mL of deuterated chloroform. CO_2 was then slowly bubbled into the solution and measurements were taken until equilibrium was reached. After formation of the ionic species, the solution was heated and conductivity measurements were again taken until equilibrium was reached, indicating the reversal of the ionic species and reformation of the neutral species. This procedure was repeated for three cycles.

Water content

Water content was measured by injecting 1mL of solution into a Mettler Toledo DL31 Karl Fischer titrator.

Miscibility studies

Mixtures of solvent (3.5-5.84 mol) and TMBG (1.75-2.92 mol) were stirred together for ~15min. They were observed for miscibility. Methanol and CO_2 were then added to the samples to form TMBG MC IL. These samples were left overnight. If the solvent phase separated, both phases were analyzed with GC-MS and NMR (^{1}H).

Modifications to structure

2-[1-hydroxyethyl]-1,1,3,3-tetramethyl guanidine: The same reaction conditions were used as for the synthesis of TMBG, with a few exceptions: 1) 0.12mol of monoethanolamine was dissolved in Et_3N (23mL) and acetonitrile and added dropwise to

the dichloride. 2) In the work-up, an acid-base procedure was used: 5% HCl (20mL) was added to the mixture, and extracted with CH_2Cl_2 (3x15mL). Residue from the organic extraction was then dissolved in water and basified using 30%NaOH (30mL). The organics were extracted with CH_2Cl_2 (3x15mL) to yield a yellow solid. Recrystallization gave the desired solid product in 78% yield; decomposition point 171°C; ^1H ($CDCl_3$): 1.09 (t, 2H), 2.27 (1H), 2.73-2.78 (m, 14H). ^{13}C ($CDCl_3$): 35.98, 44.51, 45.59, 59, 159.

2-[trimethylsiloxyethyl]-1,1,3,3-tetramethyl guanidine: The same reaction conditions were used as for the synthesis of TMBG, with one exception: 1) 0.12mol of 1-trimethylsiloxyethyl-2-amine was dissolved in Et_3N (23mL) and acetonitrile and added dropwise to the dichloride. Product was obtained as light yellow oil in 83% yield. ^1H NMR(d_6-DMSO): 0.03 (s, 9H), 2.75 (s, 4H), 2.78 (s, 8H), 3.58 (t, 2H), 4.18 (t, 2H) . ^{13}C NMR (d_6-DMSO): 1.5,38, 39, 52, 67, 161.

1-trimethylsiloxyethy1-2-amine:[42] To 0.5mol ethanolamine, 0.28mol of hexamethyldisilizane was slowly added dropwise. One drop of Me_3SiCl was added and the mixture was heated to 130°C for 2hours. Distillation under vacuum gave the liquid product in 78% yield. ^1H NMR(d_6-DMSO): 0.06 (s, 9H), 2,59 (t, 2H), 3.46 (t, 2H). ^{13}C NMR (d_6-DMSO): -0.66, 43.89, 64.63.

2-[1trimethylsilylmethyl]-1,1,3,3-tetramethyl guanidine: The same reaction conditions were used as for the synthesis of TMBG, except that 1-trimethylsilylmethyl amine was added to the dichloride intermediate. 38% yield as a light yellow oil. ^1H NMR($CDCl_3$): -0.07 (s, 9H), 2.57 (s, 6H), 2.65 (s, 6H), 2.69 (s, 2H). ^{13}C NMR ($CDCl_3$): -2.48, 38.78, 39.63 40.81, 159.23.

2-[trimethylsilanylmethyl]-1,1,3,3- tetramethylguanidinium methylcarbonate: CO_2 was bubbled through an equimolar mixture of 2-[1trimethylsilylmethyl]-1,1,3,3-tetramethyl guanidine and methanol to yield solid at room temperature (mp= 36^oC) ^1H NMR(d_6-DMSO): -0.02 (s, 9H), 2.69 (s, 12H), 3.15 (s, 2H).

2-[trimethylsilanylmethyl]-1,1,3,3-tetramethylguanidinium octylcarbonate: CO_2 was bubbled through an equimolar mixture of 2-[1-trimethylsilylmethyl]-1,1,3,3-tetramethyl guanidine and octanol to yield ionic liquid, but with very low conversions.

Pentamethyldisiloxanepropylamine: The amine was synthesized following a procedure from U. S. Patent 5,654,374. Allylamine (0.047mol) was dissolved in heptane (20mL). This solution was heated to 75C with stirring and refluxing. Once temperature stabilized, platinum(0)-1,3-divinyl-1,1,3,3-tetramethyldisiloxane catalyst was added in the amount of 1% by weight (1.34mL of 2% in xylene catalyst solution). Pentamethyldisiloxane (0.047mol) was also dissolved in heptane (20mL) and this mixture was placed in an addition funnel. Heat on the allylamine solution was raised to 85C and the pentamethyldisiloxane solution was dripped in slowly, maintaining the temperature at a constant 85C. Heat was then decreased to 70C and reacted for 3 hours. 2 scoops of Celite were added and the solution was left to stir overnight at room temperature. Celite was removed by filter, and heptane was removed from the solution by rotovap and vacuum oven. The resulting dark brown solution was purified to a clear liquid in 40% yield using Kugelrohr distillation, however, NMR analysis showed this product to actually be a mixture of the linear and branched products. ^{1}HNMR ($CDCl_3$): -0.007 (m, 15H), 0.431 (t, 2H), 1.377 (m, 2H), 2.594 (t, 2H). ^{13}CNMR ($CDCl_3$): 1.861, 15.242,

27.570, 45.313. EA: Theory: 46.77% C, 11.28% H, 6.82% N. Found: 46.72% C, 11.38% H, 6,76%N.

2-(propylpentamethyldisiloxane)-1,1,3,3-tetramethylguanidine: The same reaction conditions were used as for the synthesis of TMBG, except that pentamethyldisiloxanepropylamine was added to the dichloride intermediate. ^{1}HNMR indicates that some reactions has occurred to form the desired product, however, unreacted tetramethylurea and silylamine can be seen in the mixture, indicating that the linear silylamine reacts to form the guanidine, while the branched does not. Most peaks overlap with unreacted materials, however those that indicate product formation are: ^{1}HNMR ($CDCl_3$): 2.525 (s, 6G), 2.562 (s, 6H), 2.93 (t, 2H). ^{13}CNMR ($CDCl_3$) 37.985, 38.243, 159.27.

Pentamethylguanidine: Liquid methylamine was collected by flowing gas through a dry ice condenser and dripped into a flask of acetonitrile. At least 6mL collected, enough to have excess in reaction of at least 8:1 methylamine:chloride intermediate. The same procedure was then followed as in TMBG synthesis, only methylamine in acetonitrile was added for the second step. After reaction completion, normal work up was followed and product was collected as a yellow oil in 70-75% yields. ^{1}HNMR ($CDCl_3$): 2.473 (s, 6H), 2.586 (s, 6H), 2.739 (S, 3H). ^{13}CNMR ($CDCl_3$): 38.350, 39.033, 161.279.

Pentamethylguanidinium butylcarbonate: CO_2 was bubbled through an equimolar mixture of pentamethylguanidine and butanol to form a wet looking white solid (mp 92-96C) with 70% conversion. Heating, increasing stirring during formation, and washing with pentane were all unsuccessful in increasing conversion.

2-allyl-1,1,3,3-tetramethylguanidine: The same reaction conditions were used as for the synthesis of TMBG, except that allylamine was added to the dichloride intermediate. Product was isolated as a pale yellow oil in 70-75% yield. ^{1}HNMR ($CDCl_3$): 2.583 (s, 6H), 2.650 (s, 6H), 3.697 (s, 2H), 4.894 (d, 1H), 5.131 (d, 1H), 5.897 (m, 1H). ^{13}CNMR ($CDCl_3$): 38.698, 39.517, 112.708, 139.631, 160.394.

2-allyl-1,1,3,3-tetramethylguanidinium methylcarbonate: CO_2 was bubbled through an equimolar mixture of 2-allyl-1,1,3,3-tetramethylguanidine and methanol. NMR indicated formation of an ionic species (appearance of peak at 158.179 in ^{13}CNMR), however other species are present as well, and no reversal is possible upon heating at 80C or bubbling of CO_2

Base-catalyzed reactions

Reagents were first mixed in TMBG. After reaction completion, hexane (or another non-polar alkane) and methanol were added. CO_2 was bubbled through the mixture to cause the formation of two separate phases: hexane/product and TMBG MC IL. Each phase was analyzed by GC-MS to quantify the concentrations of reactants and products. Standard calibration curves of all starting materials and most of the products were prepared. If the reaction was recycled, the desired products were isolated, characterized by NMR and compared to literature values. The TMBG MC IL was then reversed, more reagent was added, and the reaction started again.

1-phenyl-pent-1-en-3-one[43]: ^{1}H NMR: ($CDCl_3$): 1.16 (3H, t), 2.7 (2H, q), 6.7 (1H, d), 7.37-7.4 (3H, m), 7.5-7.6 (3H, m)

4-phenyl-3-methyl-3-buten-2-one[44-45]: 66.5mL acetic acid was added to a round-bottomed flask over ice. 13.5mL 37wt% HCl was then added. Next, 7.88mL

benzaldehyde was added. Finally, 13.95mL 2-butanone was added to the mixture and it was stirred until it returned to room temperature, and then for 36 more hours. The solution was neutralized with 125mL 10M NaOH after the addition of 50mL H_2O. The organics were separated with diethyl ether, washed again with 10 wt% $NaHCO_3$, and dried over $MgSO_4$ to give the desired product in 95% yield. $^1H(d_6$-DMSO): 1.87 (d, 3H), 2.37 (s, 3H), 7.3-7.45 (m, 4H), 7.59 (s, 1H).

1-trimethylsilyloxy-1-cyclohexanecarbonitrile. ^1H (d_6-DMSO): 0.2 (s, 9H), 1.48-1.7 (m, 8H), 1.9 (m, 2H). ^{13}C (d_6-DMSO): 1.4, 22.4, 23.8, 38.6, 70.5, 121.

TMBG/TMS-CN salt: ^1H (d_6-DMSO): 0.1 (s, 9H), 0.82 (t, 3H), 0.98 (m, 2H), 1.25 (m, 2H), 2.8 (s, 12H). ^{13}C (d_6-DMSO): 1.1, 13.9, 18.8, 19.7, 31.7, 39.1, 123.4, 161.3.

3[bis(methoxycarbonyl)methyl]cyclohexanone. ^1H ($CDCl_3$): 1.4-1.55 (m, 1H), 1.65-1.8 (m, 2H), 1.9-2.0 (m, 1H), 2-2.15 (m, 1H), 2.3-2.55 (m, 5H), 3.3 (d, 1H), 3.75 (s, 6H).

3-(N-phenylamino)-1,3-diphenyl-1-acetone. ^1H ($CDCl_3$): 3.46 (d, 1H), 3.49 (d, 1H), 5.02 (m, 1H), 6.57 (d, 2H), 6.67 (m, 1H), 7.05 (m, 2H), 7.25 (d, 1H), 7.3-7.34 (m, 2H), 7.78-7.59 (m, 5H), 7.92 (d, 2H).

Separation of alkanes from tar sands/shale

Mixtures of TMBG and either crude oil or bitumen were stirred together. Addition of CO_2 into the mixture caused the formation of two separate phases: crude oil and TMBG MC IL. Each phase was analyzed by GC-MS or NMR for purity.

Bitumen before treatment with TMBG MC IL: ^1H NMR ($CDCl_3$): 0.87 (m), 1.26 (m). ^{13}C NMR ($CDCl_3$): 14.29, 22.83, 29.82

Bitumem after treatment with TMBG MC IL (TMBG peaks withheld for clarity): ^{1}H NMR ($CDCl_3$): 0.1 (s), 1.17 (s), 4.15 (p), 7.45 (m), 7.65 (m). 13C NMR ($CDCl_3$): 12.56, 23.47, 24.32, 29.51, 30.83, 30.97, 67.88, 129.43, 132.34, 132.83, 158.15, 165.43, 167.71, 206.

Formation of Amine Based One Component IL's

Carbon dioxide was bubbled through the pure precursor molecule. Though the necessary time varied slightly based on the amount of precursor being used, it was always bubbled until the exotherm was felt, recorded and cooled back down to room temperature. On average, this was twenty minute for most samples. To confirm ionic liquid formation, neat NMR's were run using a capillary tube containing $CDCl_3$ placed inside the sample in the NMR tube.

3-(trimethoxysilyl)-propylammonium 3-(trimethoxysilyl)-propyl carbamate (TMSAC): ^{1}H NMR (neat): 6.0 (3H, br, NH_3^+), 4.5 (1H, br, NH), 3.5 (18H, br, OCH_3), 3.0 (2H, br, CH_2N), 2.6 (2H, br, CH_2N), 1.6 (2H, br, CH_2), 1.5 (2H, br, CH_2), 0.6 (4H, br, CH_2Si), ^{13}C NMR (neat): 50.0 (OCH_3), 43.9 (CH_2N), 42.8 (CH_2N), 23.8(CH_2), 23.2 (CH_2), 5.8 (CH_2Si); Elemental Analysis Theory: C, 38.78%; H, 8.51%; N, 6.96 %; Found: C, 38.34%; H, 8.57%; N, 6.95%.

IR (neat)(Figure 3.66).

3-(triethoxysilyl)-propylammonium 3-(triethoxysilyl)-propyl carbamate (TESAC): ^{1}H NMR (neat): : 9.6 (3H, br, NH_3^+), 6.0 (1H, br, NH), 4.0 (12H, br, OCH_2), 3.2 (2H, br, CH_2NH), 3.0 (2H, br, CH_2NH), 1.9 (2H, br, CH_2), 1.7 (2H, br, CH_2),1.4 (18H, br, CH_3), 0.8 (4H, br, CH_2Si), ^{13}C NMR (neat): 57.7 (OCH_2), 44.1 (CH_2NH), 41.5 (CH_2NH), 23.7

(CH_2), 21.3 (CH_2), 17.9 (CH_3), 7.6 (CH_2Si), 7.4 (CH_2Si); Elemental Analysis Theory: C, 46.88%; H, 9.53%; N, 5.76%; Found: C, 46.66%; H, 9.49%; N, 5.77%.

IR (neat)(Figure 3.67)

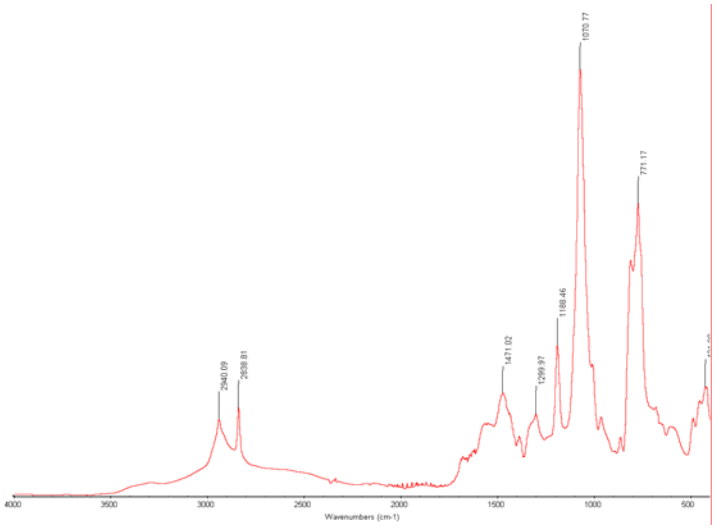

Figure 3.66 IR of 3-(trimethoxysilyl)-propylammonium 3-(trimethoxysilyl)-propyl carbamate

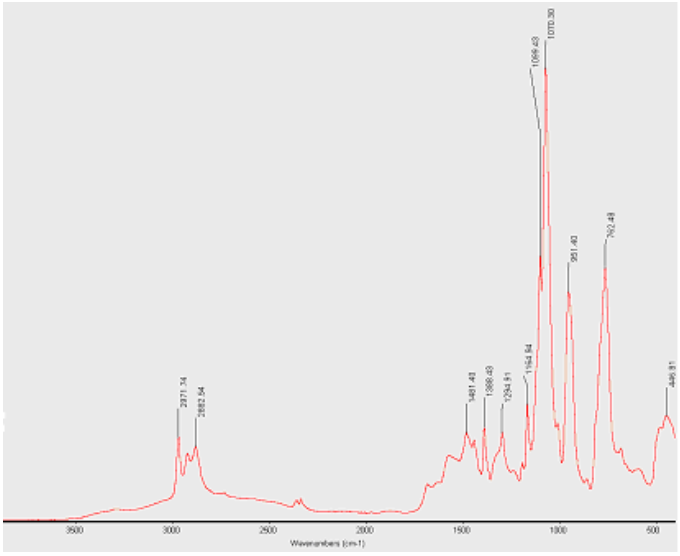

Figure 3.67 IR of 3-(triethoxysilyl)-propylammonium 3-(triethoxysilyl)-propyl carbamate

Viscosity Measurements

Viscosity measurements were made on a Anton Paar MCR 300 rheometer using a 0.97mL coquette geometry sample holder with Peltier temperature control. Shear rates were increased from 0-100 sec^{-1} and then decreased from 100-0 sec^{-1}. The reported values are the average of all data points from 10-100 sec^{-1}.

Differential Scanning Calorimetry (DSC) Measurements

DSC was run from 20ºC to 300ºC or 400ºC (for higher boiling point precursors) at 20ºC/min or 30ºC/min on a Q20 TA Instruments machine. The nitrogen flow for these tests was set at 50 mL/min. The reversal temperature was taken as the average of three repeats.

Thermalgravimetric Analysis (TGA)

TGA on the ionic liquids was run from 20ºC to 500ºC at 20ºC/min on a Q50 TA Instruments machine. The nitrogen flow was set at 40mL/min. Residual mass left at the end of the run (~10wt%) is due to decomposition products.

Nile Red Measurements

UV-Vis spectra were collected using a HP 8453 UV-Vis Spectrophotometer using a quartz cuvette. The indicator dye Nile red was added to the liquids at a concentration that kept the UV absorbance lower than a value of 1.5 to ensure there was no saturation of the detector. The wavelength of maximum absorption was then determined. Tests were repeated three times and averaged to determine the Nile red λ_{max}. For the ionic

liquid samples, Nile red was not added directly to the ionic liquid. Instead it was first added to the molecular liquids, which were then converted to the ionic liquids by bubbling CO_2 through the cuvette.

Reversal of IL Using Heat

TMSAC or TESAC IL (1g) was placed in a small vial or NMR tube. A small stir bar was placed in the bottom. This whole set up was placed in an oil bath set at 120C. This was allowed to heat with stirring at 120C for 2 hours. Bubbles could be seen leaving the system. After two hours, NMR indicated complete reversal to known amine starting material.

Separation of Alkanes from Crude Oil/Bitumen

Mixtures of TESA precursor and either crude oil or bitumen were stirred together to form a homogeneous mixture. In the case of bitumen, this mixture was then filtered to remove any solid particulates. CO_2 was bubbled through the mixture for 20 minutes. The mixture was then centrifuged on high for 20 minutes to form two separate phases, an alkane phase and TESAC IL. Each phase was analyzed by ^1H NMR for purity.

Top alkane layer: ^1H NMR ($CDCl_3$): 3.85 (m, ethoxy), 1.26 (m, CH_2), 0.88 (m, CH_3).

Bottom IL later: ^1H NMR ($CDCl_3$): All peaks as standard TESAC IL plus 1.17 (m, CH_2), 0.82 (m, CH_3).

3.6. References

1. Launay, J.-P.; Coudret, C., *Chemical Approaches of Molecular Switches* Annals of the New York Academy of Sciences, 1998. **852**: p. 116-132.

2. Mendes, P. M.; Flood, A. H.; Stoddart, J. F., *Nanoelectronic devices from self-organized molecular switches* App. Phys. A: Mat. Sci. & Process., 2005. **80**(6): p. 1197-1209.

3. Jessop, P.G., et al., *A Reversible Ionic/Non-Ionic Switchable Solvent.* Nature, 2005. **436**: p. 1102.

4. Phan, L.; Chiu, D.; Heldebrant, D. J.; Huttenhower, H.; John, E.; Li, X.; Pollet, P.; Wang, R.; Eckert, C. A.; Liotta, C. L.; Jessop, P. G., *Switchable Solvents Consisting of Amidine/Alcohol or Guanidine/Alcohol Mixtures.* Ind. Eng. Chem. Res. 2008, **47** (3) p. 539-545.

5. Blasucci, V.; Dilek, C.; Huttenhower, H.; John, E.; Llopis-Mestre, V.; Pollet, P.; Eckert, C.; Liotta, C.; *One Component, Switchable Ionic Liquids Derived from Siloxylated Amines*. Chem. Commun. 2009, **1**: p. 116-118.

6. Hart, R.; Pollet, P.; Hahne, D.; John, E.; Llopis-Mestre, V.; Blasucci, V.; Huttenhower, H.; Leitner, W.; Eckert, C.; Liotta, C.; *Benign Coupling of Reactions and Separations with Reversible Ionic Liquids*. Tetrahedron. 2010, **66**(5): p. 1082-1090.

7. Blasucci, V.; Hart, R.; Llopis-Mestre, V.; Hahne, D.; Burlager, B.; Huttenhower, H.; Thio, B. J. R.; Pollet, P.; Liotta, C.; Eckert, C.; *Single Component Reversible Ionic Liquids for Energy Applications*. Fuel. 2010, **89:** p. 1315-1319.

8. Gathergood, N.; Scammells, P. J.; Garcia, M. T.; *Biodegradeable ionic liquids Part III. The first readily biodegradeable ionic liquids.* Green chemistry, 2006. **8**: p. 156-160.

9. Garcia, M. T.; Gathergood, N.; Scammells, P. J.; *Biodegradeable ionic liquids Part II. Effect of the anion and toxicology.* Green chemistry, 2005. **7**: p. 9-14.

10. Docherty, K. M.; Hebbeler, S. Z.; Kulpa Jr., C. F.; *An assessment of ionic liquid mutagenicity using the Ames Test.* Green chemistry, 2006. **8**: p. 560-567.

11. Yamada, T.; Lukac, P. J.; George M.; Weiss, R. G.; *Reversible, Room-Temperature Ionic Liquids. Amidinium Carbamates Derived from Amidines and Aliphatic Primary Amines with Carbon Dioxide.* Chem. Mater., 2007, **19**: p. 967-969.

12. Mateus, N. M. M.; Branco, L. C.; Lourenço, N. M. T.; Afonso, C. A. M.; *Synthesis and properties of tetra-alkyl-dimethylguanidinium salts as a potential new generation of ionic liquids.* Green chemistry, 2003. **5**: p. 347-352.

13. Gao, Y.; Arritt, S. W.; Twamley, B.; Shreeve, J. M., *Guanidinium-Based Ionic Liquids.* Inorg. Chem. 2005. **44**(6): p. 1704-1712.

14. Wang, P.; Zakeeruddin, S. M.; Gratzel, M.; Kantlehner, W.; Mezger, J.; Stoyanov, E. V.; Scherr, O.; *Novel room temperature ionic liquids of hexaalkyl substituted guanidinium salts for dye-sensitized solar cells.* Applied Physics A: Materials Science & Processing, 2004. **79**: p. 73-77.

15. Xie, H.; Zhang, S.; Duan, H.; *An ionic liquid based on a cyclic guanidinium cation is an efficient medium for the selective oxidation of benzyl alcohols.* Tet. Lett, 2004. **45**: p. 2013.

16. Jiang, T.; Gao, H.; Han, B.; Zhao, G.; Chang, Y.; Wu, W.; Gao, L.; Yang, G.; *Ionic liquid catalyzed Henry reactions.* Tet. Lett, 2004. **45**: p. 2699-2701.

17. Zhu, A.; Jiang, T.; Wang, D.; Han, B.; Lui, L.; Huang, J.; Zhang, J.; Sun, D.; *Direct aldol reactions catalyzed by 1,1,3,3-tetramethylguanidine lactate without solvent.* Green chemistry, 2005. **7**: p. 514-517.

18. Zhu, A.; Jiang, T.; Han, B.; Huang, J.; Zhang, J.; Ma, X.; *Study on guanidine-based task-specific ionic liquids as catalysts for direct aldol reactions without solvent.* New Journal of Chemistry, 2006. **30**: p. 736-740.

19. Li, S., Lin, Y., Xie, H., Zhang, S., Xu, J. , *Guanidine Acid-Base Ionic Liquids: Novel Reaction Media for the Palladium-Catalyzed Heck Reaction* Org Lett, 2006: p. 391-394.

20. Huang, J.; Jiang, T.; Gao, H.; Han, B.; Liu, Z.; Wu, W.; Chang, Y.; Zho, G.; *Pd Nanoparticles Immobilized on Molecular Sieves by Ionic Liquids: Heterogeneous Catalysts for Solvent-Free Hydrogenation.* Angewandte Chemie, Int Ed, 2004. **43**: p. 1397-1399.

21. Bates, E. D.; Mayton, R. D.; Ntai, I.; Davis Jr., J. H.; *CO_2 Capture by a Task-Specific Ionic Liquid.* J. Am. Chem. Soc., 2002, **124**: p. 926-927.

22. Schuchardt , U.; Vargas, R.M.; Gelbard, G., *Alkylguanidines as catalysts for the transesterification of rapeseed oil* J. Mol. Cat. A: Chem., 1995. **99**(2): p. 65-70.

23. Costa, M.; Chiusoli, G. P.; Taffurelli, D.; Dalmonego, G., *Superbase catalysis of oxazolidin-2-one ring formation from carbon dioxide and prop-2-yn-1-amines under homogeneous or heterogenous conditions.* J. Chem. Soc., Perkin Trans. 1, 1998 **9**: p. 1541-1546.

24. Mobinikhaledi, A.; Forughifar, N.; Mohtasabi, S.; Shalbaf, H., *Synthesis of Some new substituted 2-(phenyl)-1,3-dimethyl- and -1,1,3,3-tetramethylguanidines.* Phosphorus, Sulfur, and Silicon, 2003. **178**: p. 2235-2240.

25. Pruszynski, P., Synthesis and properties of phenyl substituted derivatives of 2-phenyl-1,1,3,3-tetramethylguanidine. Can. J. Chem. **65**: p. 626-629.

26. Crowhurst, L.; Mawdsley, P. R.; Perez-Arlandis, J. M.; Salter, P. A., Welton, T., *Sovent-solute interactions in ionic liquids.* Phys. Chem. Chem. Phys., 2003. **5**: p. 2790-2794.

27. Ogihara, W.; Aoyama, T.; Ohno, H., *Polarity Measurement for Ionic Liquids Containing Dissociable Protons.* Chem. Lett., 2004. **33**(11): p. 1414-1415.

28. Carmichael, A.J., & Seddon, K. R., *Polarity Study of Some 1-Alkyl-3-Methylimidazolium Ambient-Temperature Ionic Liquids with the Solvatochromic Dye, Nile Red.* J. Phys. Org. Chem., 2000. **13**: p. 591-595

29. Deye, J.F.; Berger, T. A.; Anderson, A. G., *Nile Red as a Solvatochromic Dye for Measuring Solvent Strength in Normal Liquids and Mixtures of Normal Liquids with Supercritical and Near Critical Fluids.* Anal. Chem., 1990. **62**: p. 615-622.

30. Shirota, H.; Castner Jr., E. W., *Why Are Viscosities Lower for Ionic Liquids with -CH2Si(CH3)3 vs -CH2C(CH3)3 Substitutions on the Imidazolium Cations?* J. Phys. Chem. B., 2005. **109**(46): p. 21576-21585.

31. Crosthwaite, J.M.; Muldoon, M. J.; Dixon, J. K.; Anderson, J. L.; Brennecke, J. F., *Phase transition and decomposition temperatures, heat capacities and viscosities of pyridinium ionic liquids.* J. Chem. Thermodynamics, 2005. **37**(6): p. 559-568.

32. Arren, D. H. C.; Coggio, W. D.; Parker, D. S.; U. S. Patent 5,654,374, 1997.

33. Nolen, S. A.; Liotta, C. L.; Eckert, C. A.; Gläser, R., *The catalytic opportunities of near-critical water: a benign medium for conventionally acid and base catalyzed condensations in organic synthesis.* Green Chem., 2003. **5**: p. 663-669.

34. Carey, F.A. and R.J. Sunberg, Advanced Organic Chemistry, Part B: Reactions and Synthesis. 3rd ed. 1990, New York, NY: Plenum Press.

35. Isobe, T.; Fukuda, K.; Ishikawa, T., *Modified Guanidines as Potential Chiral Superbases. 1. Preparation of 1,3-Disubstituted 2-Iminoimidazolidines and the Related Guanidines through Chloroamidine Derivatives* J. Org. Chem. 2000. **65**(23): p. 7770 - 7773.

36. Wang, L.; Huang, X.; Jiang, J.; Liu, X.; Feng, X., *Catalytic cyanosilylation of ketones using organic catalyst 1,1,3,3-tetramethylguanidine.* Tetrahedron Lett, 2006. **47**: p. 1581-1584.

37. Ye, W.; Xu, J.; Tan, C.-T.; Tan, C.-H.,*1,5,7-triazabicyclo[4.4.0]dec-5-ene (TBD) catalyzed Michael reactions.* Tetrahedron Lett, 2005. **46**(40): p. 6875-6878.

38. Xie, H.; Zhang, S.; Duan, H., *An ionic liquid based on a cyclic guanidinium cation is an efficient medium for the selective oxidation of benzyl alcohols.* Tet. Lett, 2004. **45**(9): p. 2013-2015.

39. L., P.F., *Supercritical tar sand extraction*, U.P. Office, Editor. 1980, Phillips Petroleum Company (Bartlesville, OK) USA.

40. N., H.P., *Oil shale extraction process*, U.S. Patent, Editor. 1984, Union Oil Company of California (Los Angeles, CA) US.

41. ConocoPhillips, *MSDS for bitumen sample (general).* 2007.

42. Mormann, W.; Leukel, G., *A simple and versatile synthesis of trimethylsiloxy-substituted isocyanates.* Synthesis, 1988 **12**: p. 990-2.

43. Peach, P.; Cross, D. J.; Kenny, J. A.; Mann, I.; Houson, I.; Campbell, L.; Walsgrove, T.; Wills, M., *Asymmetric transfer hydrogenation of alpha,beta-unsaturated, alpha-tosyl and alpha-substituted ketones.* Tetrahedron, 2006. **62**(8): p. 1864-1876.

44. Kawai, Y.; Saitou, K.; Hida, K.; Dao, D. H.; Ohno, A., *Sterochemical Control in Microbial Reduction XXVIII. Asymmetric Reduction of alpha-beta-Unsaturated Ketones with Bakers' Yeast.* Bull. Chem. Soc. Jpn, 1996. **69**(9): p. 2633-2638.

45. Nolan, S.A., *Environmentally Benign Chemical Processing Using Supercritical Carbon Dioxide and Near-Critical Water*, in *School of Chemical Engineering*. 2001, Georgia Institute of Technology: Atlanta.

CHAPTER FOUR
A STUDY OF SILANE GRAFTING TO MODEL POLYETHYLENE COMPOUNDS

4.1 Introduction

Low density polyethylene (LDPE) possesses very good electrical and mechanical properties, which have long made it useful for the wire and cable industry, where it is used to insulate and sheath telecommunications cables.[1,2] However, LDPE also has relatively low thermal and chemical stability.[3] Over the years, those limitations have been overcome by inducing cross-linking in the material, which enhances the impact strength, increases both thermal performance and chemical resistance, and gives the material superior wear behavior.[4]

The most common cross-linking strategy for LDPE polymers involves 1) the radical-promoted grafting of a cross-linker precursor such as vinyl trimethoxysilane (VTMS) and 2) exposure to moisture which induces cross linking via the reactive VTMS sites. (Figure 4.1 & 4.2). [5] While VTMS is the most common grafting material, other compounds such as maleic anhydride and various acrylates have been studied for their grafting and cross-linking abilities, however, they tend to exhibit unwanted side reactions such as self polymerization.[6-13]

Some studies have investigated the radical initiated grafting reaction between VTMS and polyethylene or its model compounds such as long chain hydrocarbons or squalane.[1,3-4,14-21] While these studies have examined how different factors such as reactant concentration, peroxide initiator concentration, reaction temperature, and additives to the reaction affect the mechanical properties of the grafted

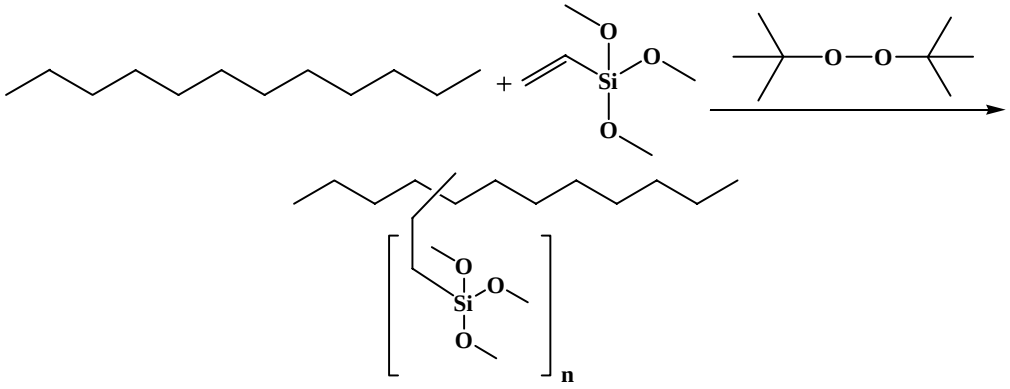

Figure 4.1 Grafting of VTMS onto a hydrocarbon backbone

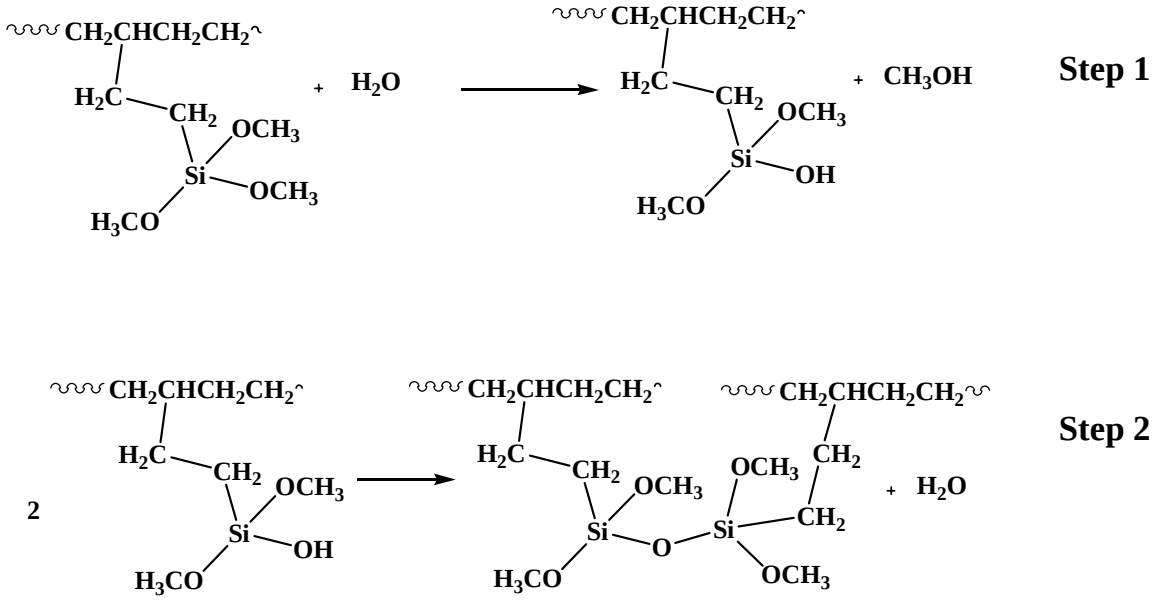

Figure 4.2 Moisture cross-linking of grafted hydrocarbon chains.

and cross-linked final polymer, very little work has been done with regard to the reaction mechanism and the resulting selectivity of the grafts (grafting on primary, secondary, or tertiary carbons) and grafting distribution (the number of grafts per chain). The scope of this project has been to investigate the fundamental aspects of this reaction; specifically the selectivity, graft distribution, effect of small molecules, such as CO_2, on the reaction, and the mechanism or mechanisms by which this grafting takes place.

4.2 Background

4.2.1 LDPE Cross-linking and Grafting

Currently, there are three methods that are commonly used to prepare cross-linked LDPE. The first is the peroxide initiated radical method in which cross-linkers such as VTMS are grafted onto the hydrocarbon chains. Cross-linking then occurs by a moisture induced reaction of these grafted molecules (Figures 4.1 and 4.2). The second method involves irradiation of solid LDPE with ultraviolet (UV) radiation.[5] This high energy bombardment of the polymer chains excites the LDPE polymer molecules, which then leads to radical formation. These radicals come together to form branches and cross-linking in the solid material (Figure 4.3).[22]

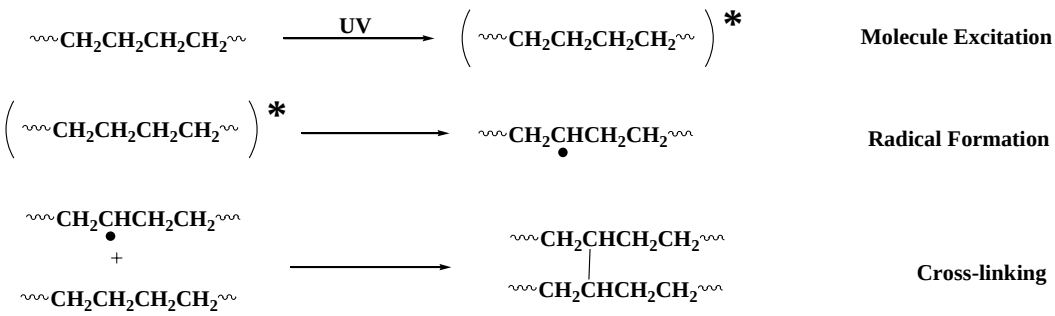

Figure 4.3 UV induced polyethylene cross-linking.

The third method is thermochemical cross-linking.[5] In this method, a peroxide initiator is added to the hydrocarbon, either in solution or in the melt. Heating to 160°C or higher induces peroxide initiation and propagation of the resulting radicals, yielding cross-linking (Figure 4.4).[23]

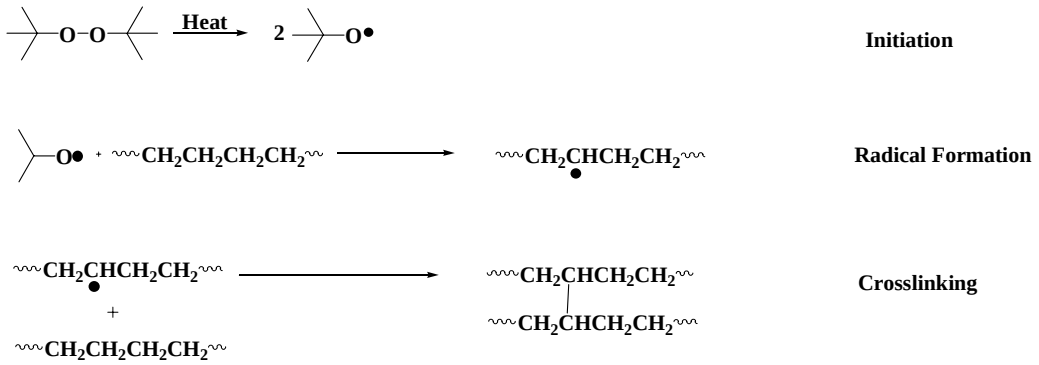

Figure 4.4 Thermochemical polyethylene cross-linking.

Of these three methods, the peroxide initiated radical grafting of small reactive molecules followed by moisture cross-linking of these molecules is of the most industrial importance and interest, due to low investment cost as cross-linking can be performed at room temperature and pressure.[5] However, this method is currently not well controlled and the products are not uniform as the crude product contains a mixture that is mono-grafted, di-grafted, tri-grafted etc. For example, in work done by Forsyth, *et al* VTMS grafting to dodecane produces an average of 2.37 grafts per chain, but this manifested itself as a mix of grafted products containing anywhere from one to six grafts per chain.[15] A better understanding of this reaction leading to better control of the grafted products could make this method more efficient for industrial use.

The reaction initiation occurs when an alkoxy radical formed from the decomposition of the peroxide initiator (Figure 4.5, Step 1) abstracts a hydrogen from the hydrocarbon chain (Figure 4.5, Step 2). This hydrocarbon radical reacts with VTMS to form a single grafted radical intermediate. (Figure 4.5, Step 3). Radical propagation can then occur by one of three methods: 1) intermolecular abstraction in which a hydrogen atom is abstracted from a second hydrocarbon chain, 2) intramolecular abstraction, in

which a hydrogen atom is abstracted from another location on the same hydrocarbon chain, or 3) oligomeric grafting in which the first VTMS continues to reacts with more vinyl rather than a hydrocarbon chain (Figure 4.5, Step 4).

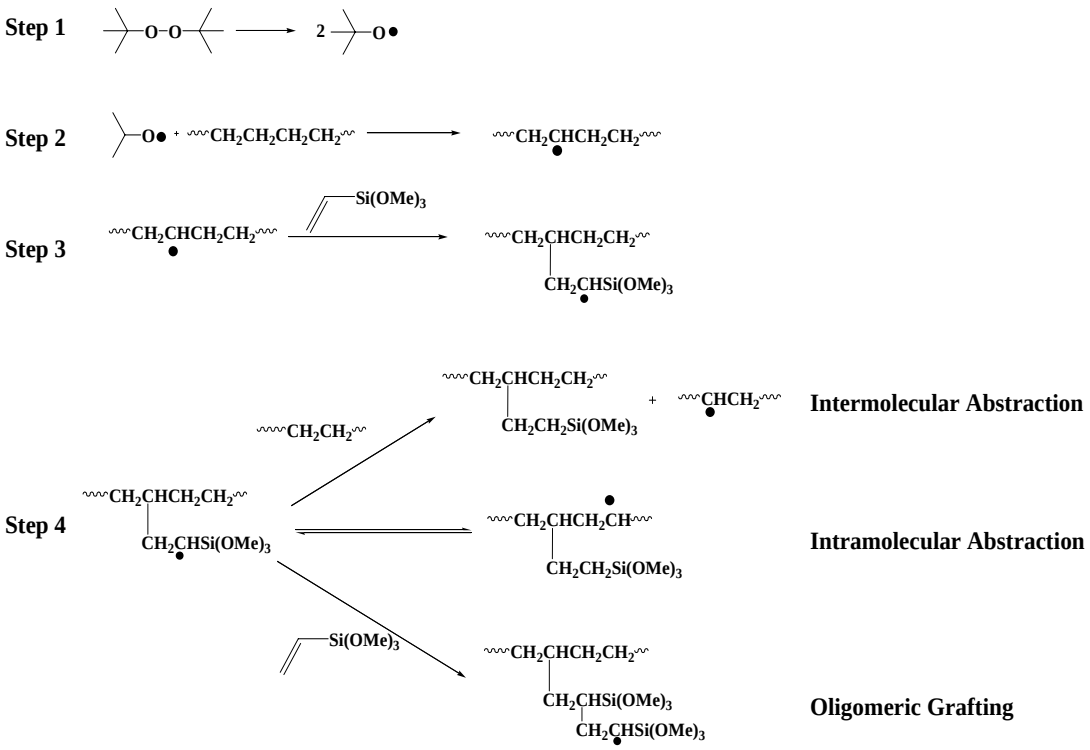

Figure 4.5 Vinyl trimethoxysilane grafting onto a hydrocarbon chain by the peroxide initiated radical method[18]

In literature, two common assumptions are made about the vinyltrimethoxy grafting reaction as it proceeds by this mechanistic scheme: 1) an intramolecular abstraction process is preferred and 2) this process occurs via a 1,5 hydrogen shift mechanism.[15,18,24] Intramolecular propagation can proceed by either a 1,3-hydrogen shift, a 1,4-hydrogen shift, or a 1,5-hydrogen shift (Figure 4.6). However, by the 1,5-mechanism, grafts can only be placed on every other carbon, so for example, on a dodecane chain, the maximum number of grafts possible would be six, assuming only

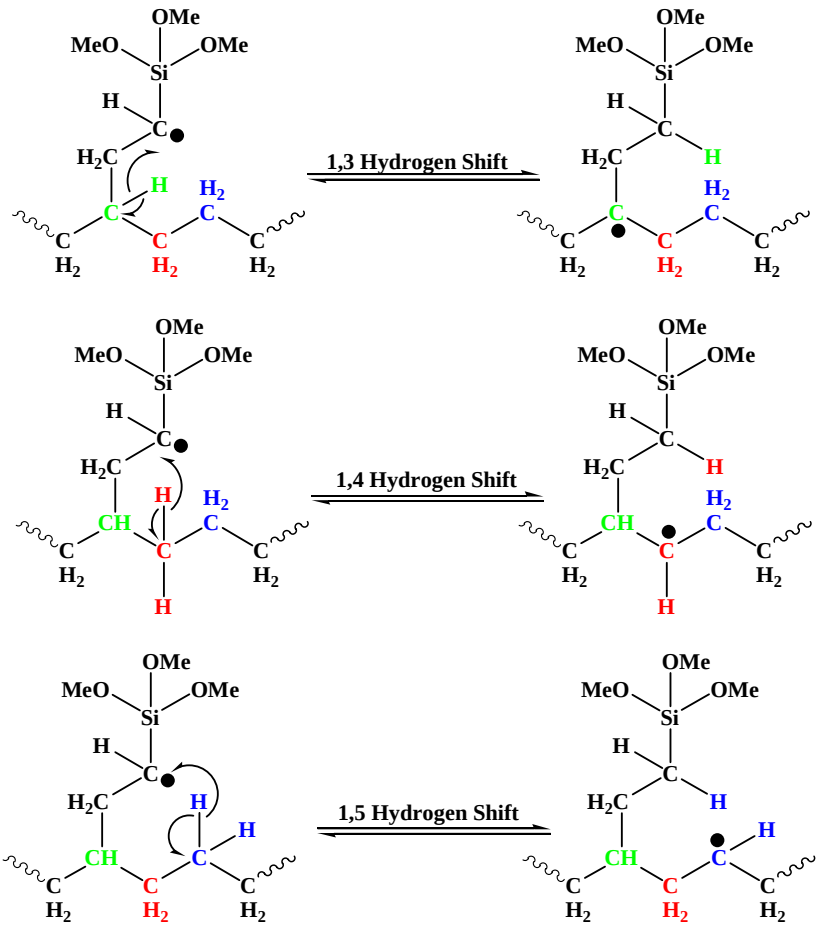

Figure 4.6 1,3-, 1,4-, and 1,5- hydrogen shift mechanisms possible in VTMS graft propagation

one graft per carbon atom. In previous work where grafting number was studied, no more than six grafts were reported.[15,18] The goal of this current research is to study this grafting mechanism.

4.3 Results and Discussion

4.3.1 VTMS Grafting to Dodecane

Dodecane was chosen to serve as a model compound for LDPE. Before being used it was treated with strong acid to remove any potential alkene impurities. Removal

of impurities was confirmed by ^{1}H NMR analysis. This was then stored under a N_2 atmosphere in the glove box.

To carry out the grafting reaction (Figure 4.7), dodecane (50mL, 37.5g) was placed in a round bottom flask with 5% by weight VTMS. These additions were done in the glove box. After removal from the glove box, but under an argon atmosphere, 750ppm *tert*-butylperoxide initiator was added, and the mixture was heated at 150°C for 90 minutes. The crude product was then sampled and analyzed by ^{1}H NMR. A comparison was made between the integration of the vinyl peaks at 6ppm in the spectra obtained at the start of the reaction and at the end of the reaction (Figure 4.8). In each spectrum the area of the vinyl integration was set at a value of 1 and all other integration values were scaled accordingly. This value of 1 was compared to the integration value of the CH_3 peak from dodecane to determine the change in the vinyl to dodecane ratio as the reaction progressed. The results indicated that a 15% conversion was achieved.

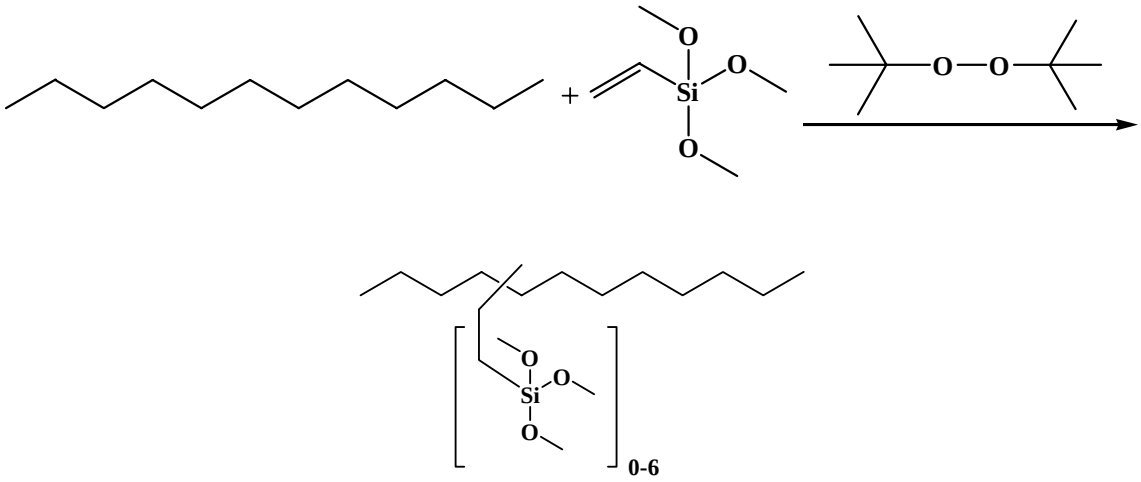

Figure 4.7 Reaction of VTMS with dodecane model compound using *tert*-butylperoxide as initiator.

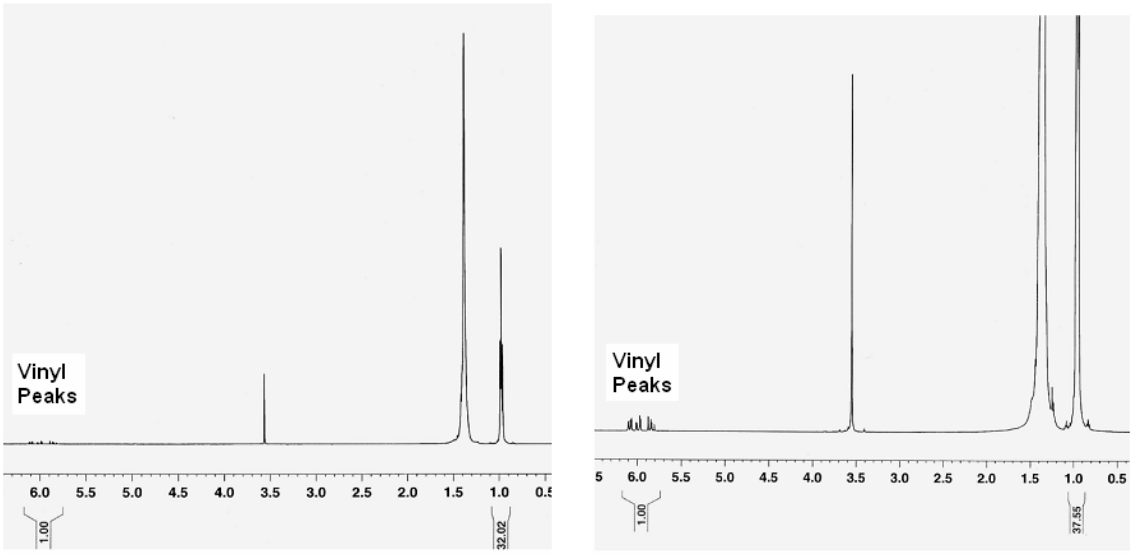

Figure 4.8 ^{1}H NMR spectra of starting material (left) and product mixture (right) from the first VTMS dodecane graft reaction

This is the maximum amount of conversion that may have occurred. Actual conversion may have been less than that as the boiling point of VTMS is 123°C, which is less than the reaction temperature of 150°C, and some vinyl may have been lost during the reaction.

The low percent conversion was attributed to a lack of activity of the radical initiator, *tert*-butyl peroxide. At 150° its half life is 90 minutes so in this initial reaction it only had time to complete a single half life. To increase conversion for this reaction, the reaction was repeated with the same amounts of dodecane, VTMS, and initiator and at the same temperature, 150°C, but allowed to run for 12 hours. In this time the completion of 8 peroxide half lives can occur. This modification increased the conversion to 45%, based on ^{1}H NMR integration.

In an effort to obtain a more concentrated sample of grafted material for analysis, 5mL of the product solution was distilled using a Kugelrohr distillation apparatus under

vacuum at ~1mmHg. Two fractions were collected and analyzed by ^{1}H and ^{13}C NMR. The first fraction, a clear liquid which was collected at 60°C was identified as unreacted dodecane. The second liquid fraction was the bottoms solution remaining after distillation, and it was also a clear liquid. However, analysis showed it contained grafted product, as a methoxy peak was present in the ^{1}H NMR at 3.5. This fraction appeared to contain a mixture of grafted product and unreacted dodecane. Integration showed 1 graft per 6.5 dodecane chains. During distillation, a third sample, a white solid crashed out of the bottoms solution. It was theorized that this material was cross-linked polymer. This may have formed from moisture being introduced into the reaction when it was removed from the argon atmosphere. Cross-linking occurs readily at room temperature and pressure with only small amounts of water present. However, no analysis of this sample was performed.

The grafting reaction was repeated, this time at 200°C for 7 hours. The temperature was increased so that the same amount of peroxide half lives could occur in a shorter time period. After reaction, 5mL of sample were distilled via Kugelrohr at a pressure of ~1mmHg. Similar results were obtained, as confirmed by ^{1}H and ^{13}C NMR analysis. A clear liquid fraction was obtained at 60°C, which was pure dodecane. A bottoms fraction remained, which contained a mix of grafted material and unreacted dodecane (1 graft per 15 dodecane chains). A white solid also formed in the bottoms fraction, which was collected by filtration. This solid was partially soluble in $CDCl_3$ and examined by ^{1}H NMR. Multiple peaks were observed in the methoxy region between 3 and 4 ppm, consistent with cross-linked material (Figure 4.9). In order to allow for a wide range of analyses to be carried out, such as liquid chromatography with ultraviolet

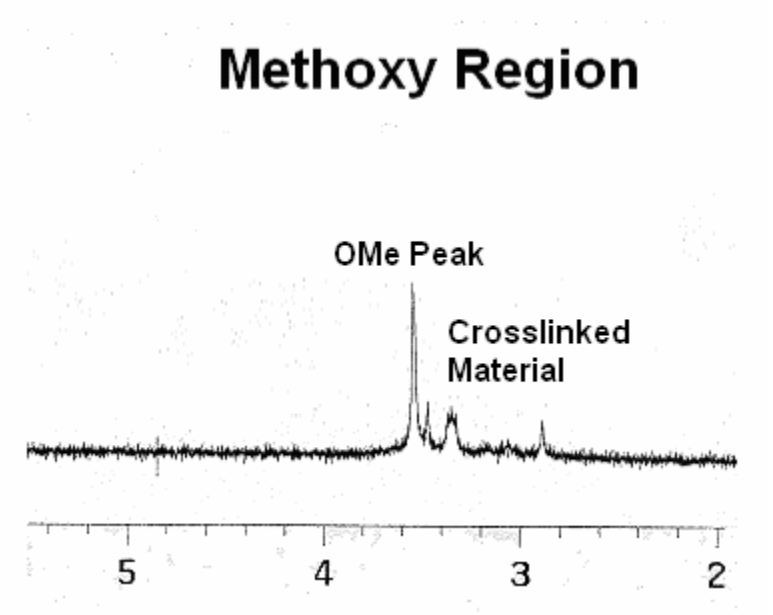

Figure 4.9 ^{1}H NMR of the solid product methoxy region.

and mass spec detection (LC-UV-MS), MS [electron impact (EI), chemical ionization (CI), matrix assisted laser desportion/ionization (MALDI)], NMR, and gel permeation chromatography (GPC), the reaction mixture was treated with phenyl lithium in order to replace the reactive mehoxy groups with unreactive phenyl groups.

4.3.2 Stabilization of VTMS Grafts

4.3.2.1 Phenyllitihium as Stabilization Agent

For preliminary experiments, the method reported by Spencer and co-workers was used (Figure 4.10).[18] After the VTMS grafting onto dodecane was carried out at 200°C for 7 hours, the solution was cooled to room temperature. Phenyllithium (PhLi, 1.5M solution in 70:30 cyclohexane:ether) was added in a 4:1 ratio with the amount of VTMS present in the system. Addition caused the solution to change from clear and colorless to a milky orange color. This mixture stirred at room temperature for 24 hours. After 24

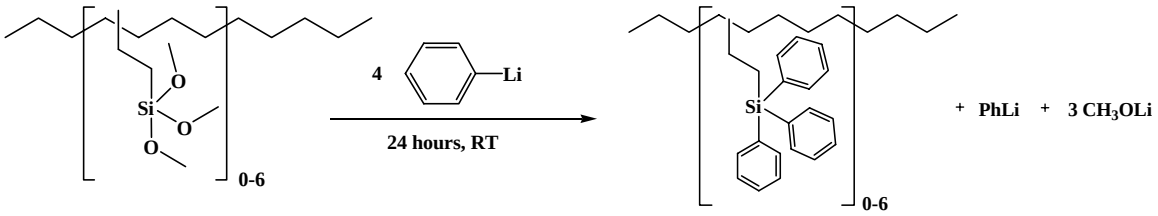

Figure 4.10 Phenyllithium stabilization reaction.

hours, saturated ammonium chloride solution was added. Hexane extraction was used to remove all product from the aqueous layer. After extraction the hexane phase was dried with magnesium sulfate and filtered.

The resulting solution was concentrated on the rotovap which removed all of the light weight, volatile organic solvents as well as any unreacted VTMS, leaving behind a mixture of grafted material and dodecane. Unlike in the previous reactions, no solid formation was observed, even after sitting for several days at room temperature. To remove excess dodecane from the system Kugelrohr distillation at ~1mmHg was used on 5mL of sample producing an unreacted dodecane fraction (60°C) and a bottoms fraction. The resulting bottoms fraction was examined by ^{1}H NMR, ^{13}C NMR, GPC and MALDI-MS. Using ^{1}H NMR, an average of 2.2 grafts per chain was obtained by comparing the integrations of the aromatic peaks, between 7 and 8 ppm, and the aliphatic CH_3 peak of the dodecane at 0.79ppm (Figure 4.11).

To obtain graft distribution information, the bottoms material was examined by GPC and MALDI-MS. The GPC analysis showed peaks consistent with one, two, and three grafts per chain as well as dodecane and vinyltriphenylsilane (VTPS, Figure 4.12). While the masses seen in the GPC were not exact, they are within the 20% error expected from the polystyrene calibration curve that was used. Higher grafting fractions were not

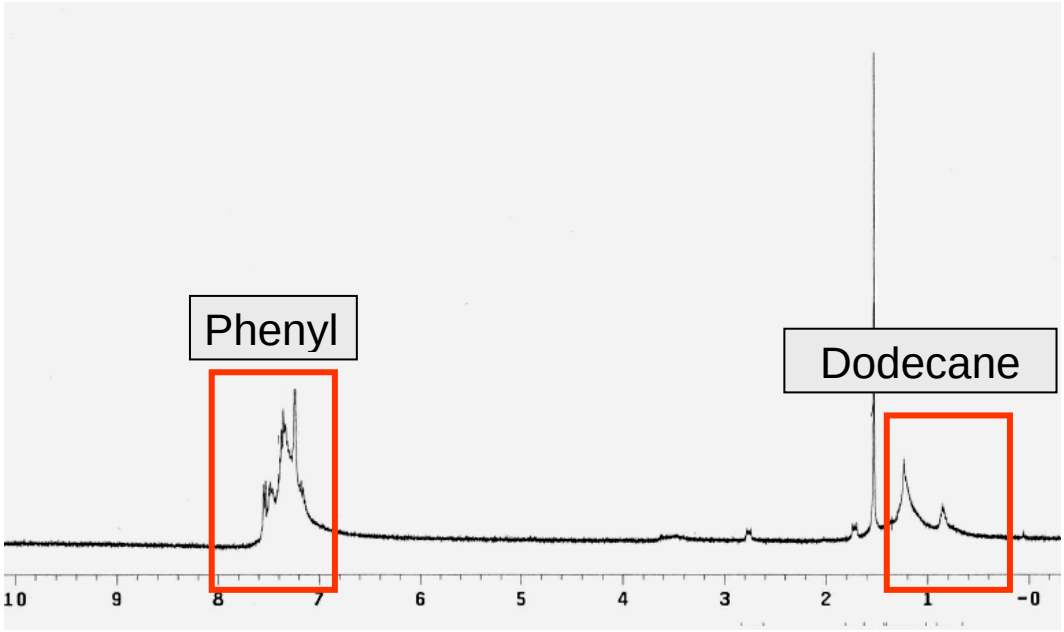

Figure 4.11 [1]HNMR spectrum of kugelrohor bottoms after stabilization.

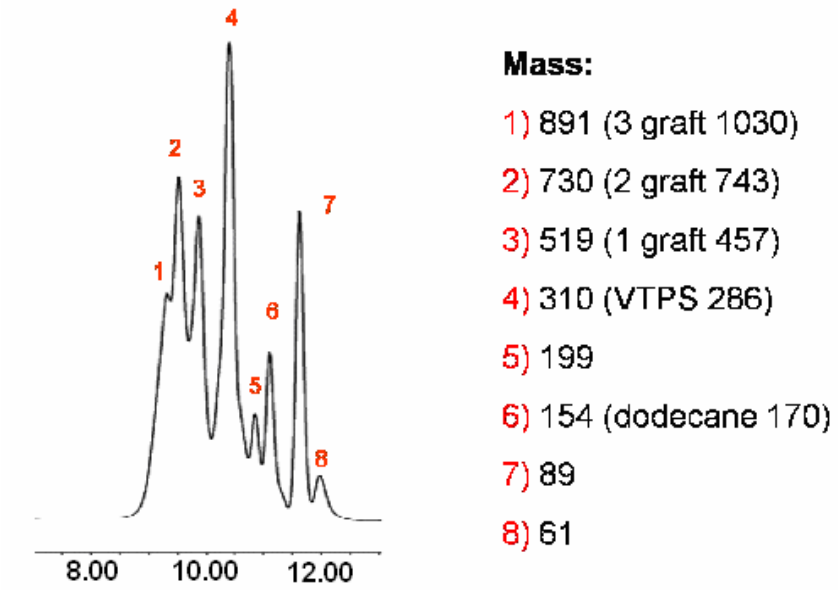

Figure 4.12 GPC chromatogram of PhLi stabilization products showing starting material and up to three grafted product molecules

seen, however, this may be due to peak overlap or they simply exist in such small quantities that they were below the detection limit of the instrument.

The MALDI-MS analysis was performed using a dithranol matrix in combination with silver trifluoroacetate (AgTFA) to aid in ionization. The spectrum showed between 1 and 6 grafts per dodecane molecule (Figure 4.13). As MALDI-MS intensities give a semi-quantitative picture of the sample, this also indicated that the major functionalized product has two VTPS grafts per dodecane molecule (Figure 4.13).

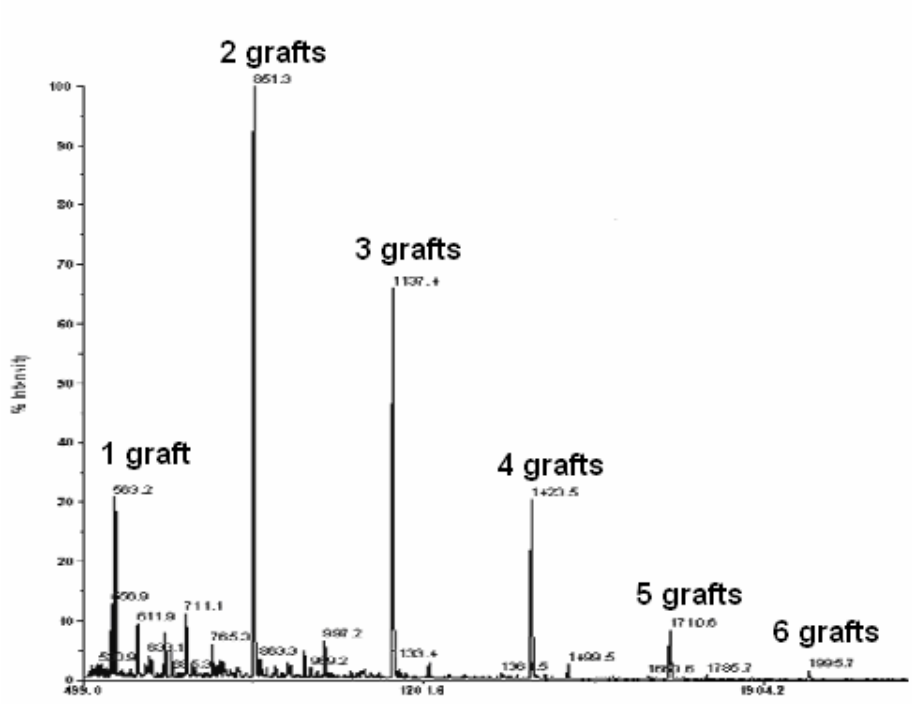

Figure 4.13 MALDI-MS of PhLi stabilized product showing molecules with up to six grafts per chain.

The reaction was repeated with similar results, as the MALDI-MS consistently showed molecules with up to 6 grafts per chain. Several grafts on one chain is consistent with literature, and supports radical propagation proceeding by an intramolecular chain transfer mechanism (Figure 4.5). In some reactions, a sticky, yellowish solid formed in

the bottoms flask. This solid did not physically resemble the white solid cross linked material that was formed before the phenyllithium reaction was employed. Analysis by ^{1}H NMR and MALDI-MS confirmed its identity as the desired product, vinyl triphenylsilane (VTPS) grafted dodecane containing up to six grafts per chain.

4.3.2.2 Optimization of Phenyllithium Stabilization Reaction

^{1}H NMR of crude products (after quenching with phenyllithium for 24 hours) showed a small peak still present in the methoxy proton region (3.5ppm, Figure 4.14). This was consistent with not all methoxy groups being successfully substituted in that time period, possibly due to the steric bulk of the phenyl groups.

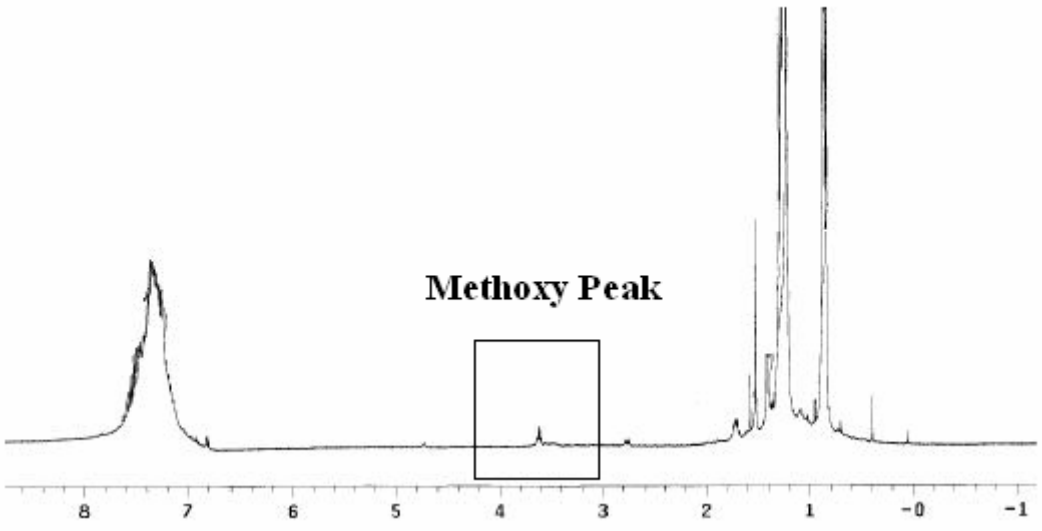

Figure 4.14 ^{1}H NMR of 24 hour PhLi stabilization reaction, with a visible methoxy peak

Reactions were then run in which the phenyllithium was reacted for 48 hours. Other than the increase in reaction time, all of the other parameters of the reaction were unchanged.

A 5mL sample of the product mixture underwent a distillation by Kugelrohr at ~1mmHg. As was seen previously, along with the unreacted dodecane fraction (60°C), both a liquid and a sticky solid bottoms fraction were obtained. Both samples were analyzed by ^{1}H NMR as well as MALDI-MS. In the ^{1}H NMR of the liquid sample (Figure 4.15) a larger average number of grafts per chain was observed, 2.9 grafts per chain for the 48 hour capping reaction versus the 2.2 grafts per chain for the 24 hour capping reaction.

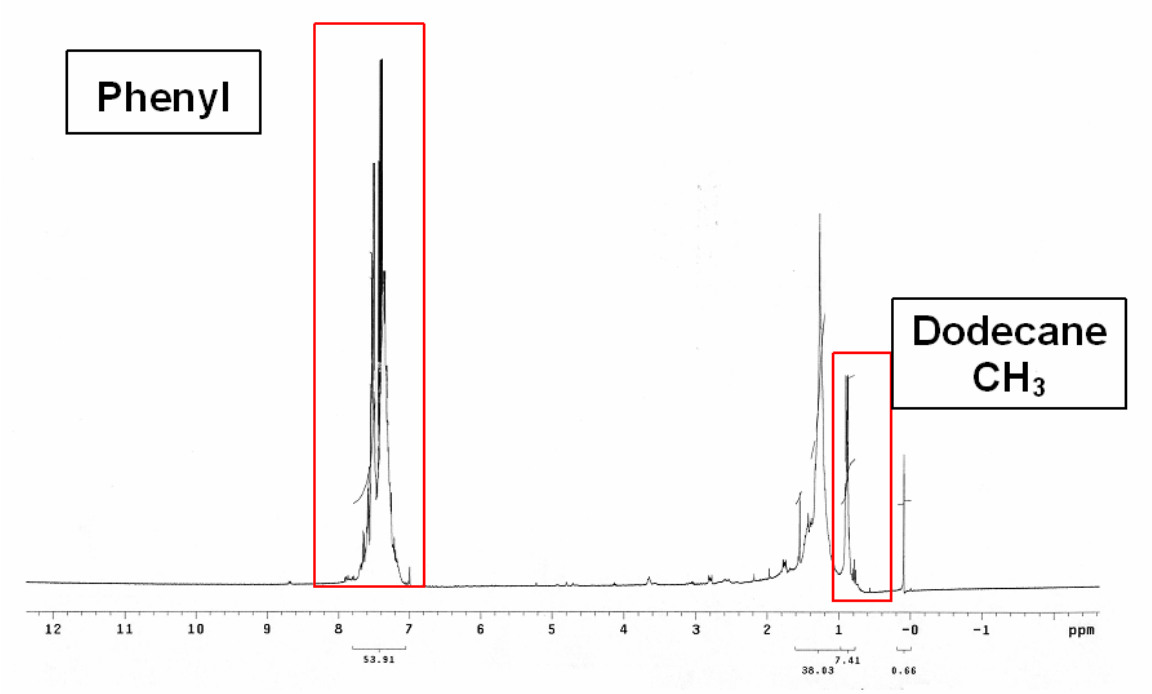

Figure 4.15 ^{1}H NMR spectrum of liquid product from 48 hour stabilization reaction with PhLi

By MALDI-MS, the liquid fraction appeared as expected containing up to 6 grafts per chain with 2 grafts being the most abundant. The sticky yellow solid fraction, however, was different. In this spectrum molecules with 2 to 8 grafts per chain were present with 5

grafts per chain being the most abundant (Figure 4.16). It appeared that a longer phenyllitihium reaction increased the number of grafts that were successfully substituted.

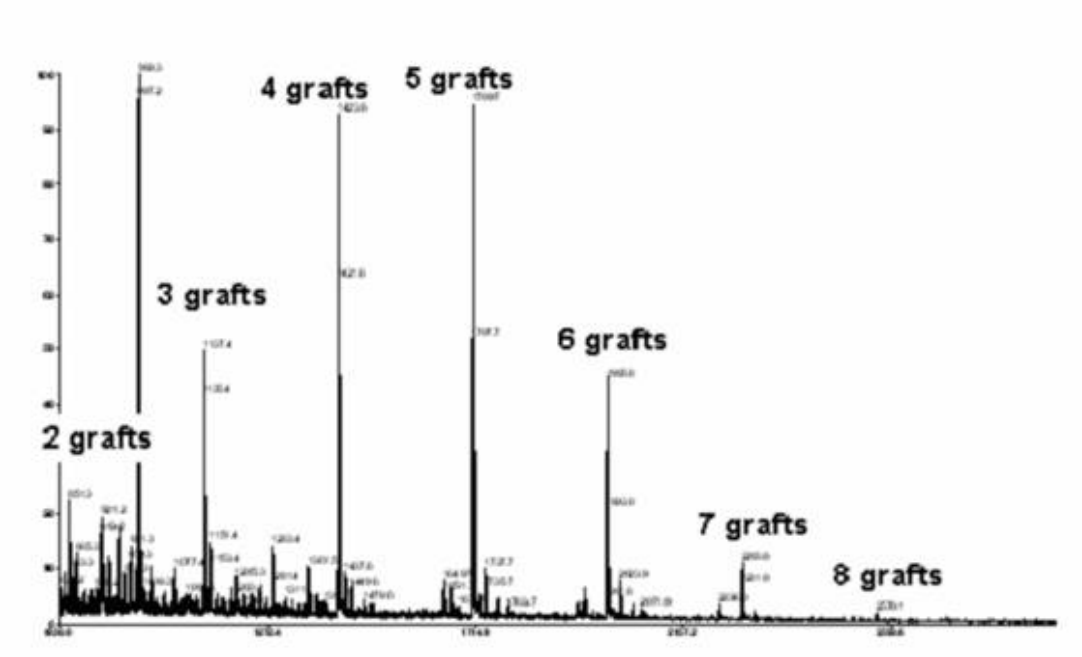

Figure 4.16 MALDI-MS of solids formed in 48 hour PhLi stabilization reaction

This is not consistent with only a 1,5-hydrogen shift mechanism occurring, as that would allow at most 6 grafts per chain assuming one graft per carbon. Instead, it is more consistent with a competing 1,4-hydrogen shift mechanism which allows the placement of grafts on adjacent carbons along the hydrocarbon chain, or, what is more likely, some combination of these two mechanisms as well as possibly the 1,3-hydrogen shift mechanism occurring simultaneously.

Even after 48 hours of the phenyllithium stabilization reaction, a small methoxy peak was present in the ^{1}H NMR. In an effort to achieve total substitution of the methoxy groups by phenyl groups, the stabilization reaction was allowed to react for one week (168 hours). All other parameters of the experiment remained the same. The products

from this experiment were analyzed by ^{1}H NMR and MALDI – MS. No methoxy peak was observed in the ^{1}H NMR and up to 8 grafts per chain were observed in the MALDI-MS (Figure 4.17) consistent with a combination of the 1,3- 1,4- and 1,5- hydrogen shift mechanisms.

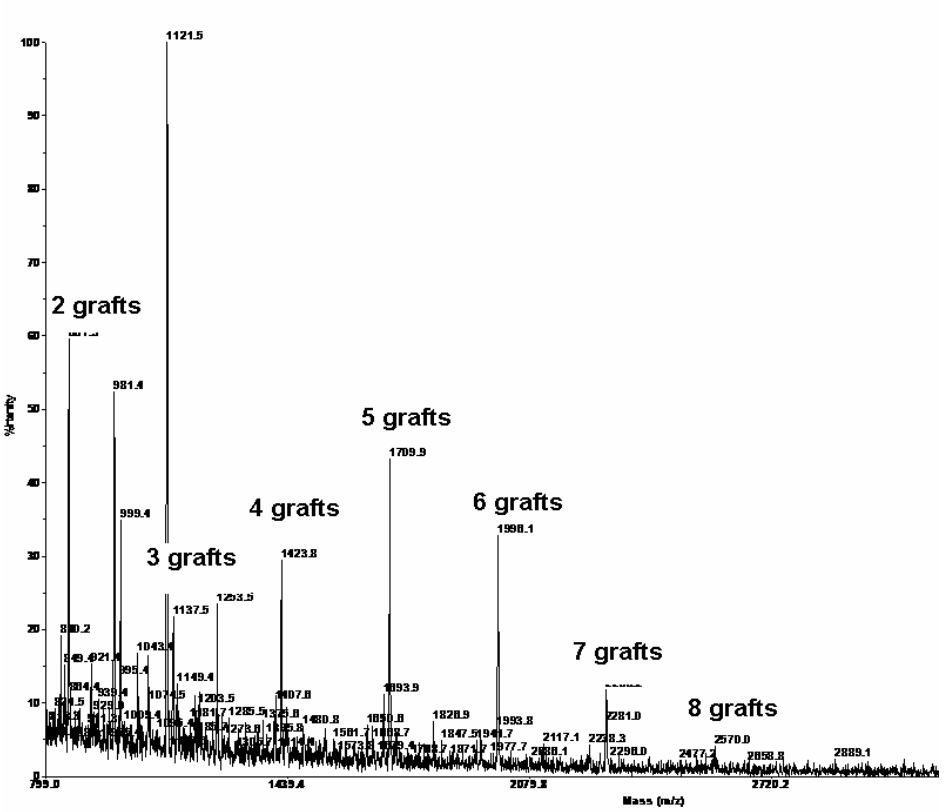

Figure 4.17 MALDI-MS of solids formed in 1 week PhLi stabilization reaction

To determine exactly where in the time period between 48 and 168 hours complete phenyl substitution occurred an experiment was carried out in a Radley's Carousel 12 Reaction Station. The carousel allows up to twelve reactions to be run simultaneously under identical conditions. It removes the need for sampling as each day a separate individual reaction can be stopped and quenched. For this experiment, six PhLi stabilization reactions were begun using standard reaction conditions. The first was

stopped after two days, another after three days, and so on for a week. Both physical observation and ^{1}H NMR were used to track the extent of reaction. From physical observation, solid cross-linked material precipitated out in experiments that were carried out for less than 72 hours of reaction. By ^{1}H NMR tracking of the methoxy peak, complete substitution occurred between 96 and 120 hours (4 and 5 days) of reaction time (Figure 4.18).

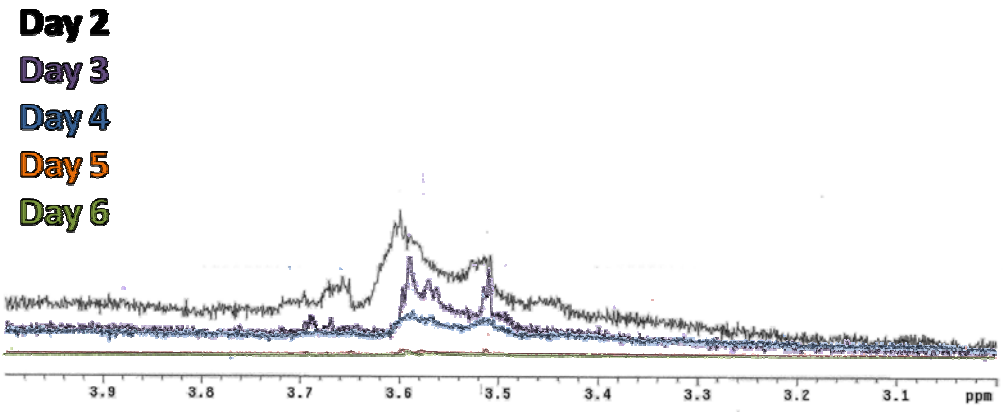

Figure 4.18 Loss of methoxy peak over time of PhLi stabilization reaction

4.3.2.3 Methyllithium as Stabilization Agent

The less bulky organo-lithium, methyllithium (MeLi), was investigated for its capping ability (Figure 4.19). As with phenyllithium, after the VTMS grafting procedure was complete, methyllithium (1.6M solution in diethyl ether) was added in a 4:1 ratio with the amount of VTMS present in the system. This mixture stirred at room temperature for 24 hours. After 24 hours, saturated ammonium chloride solution was added. After extraction, the hexane layer was dried over magnesium sulfate and filtered. The resulting solution was concentrated on the rotovap which removed all of the light

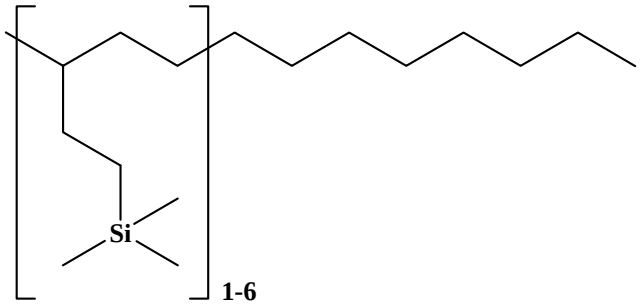

Figure 4.19 Product from VTMS grafting stabilized with MeLi.

weight, volatile organic solvents as well as any unreacted VTMS. A sample of crude product (5mL) was then distilled via Kugelrohr at ~1mmHg. A clear liquid fraction (80°C) and a highly viscous liquid bottoms fraction were obtained. Each was analyzed by ^{1}H NMR, and the 80°C fraction was found to be unreacted dodecane.

The ^{1}H NMR spectra of the bottoms fraction showed grafted product. This included peaks for dodecane at 1.13 and 0.84ppm, the CH_2 groups adjacent to silicon at 0.39ppm, and the methyl groups adjacent to silicon at 0.05 (Figure 4.20). By comparing the area of the peak for methyl adjacent to the silica to the CH_2-Si peak, a nine to two proton ratio was obtained, which is what would be expected for complete substitution. However, by comparing the ratio of the graft methyls to the CH_3 of the dodecane molecule, a grafting ratio of only 1.15 grafts per chain is obtained, much lower than the 2.2-2.9 grafts per chain expected from previous reactions.

Further analysis was needed to determine the specific number of grafts per chain, rather than the average, and how these grafts were distributed. However, this was complicated by the fact that the molecular weight of the grafted products was too low for MALDI-MS and complete fragmentation was seen when analyzed by Fast Atom Bombardment (FAB-MS) and GC-MS. The loss of aromatic groups prevented analysis

using UV-detection. The complications encountered in the analysis stopped the use of methyllithium as a capping molecule despite its size advantages over phenyllithium.

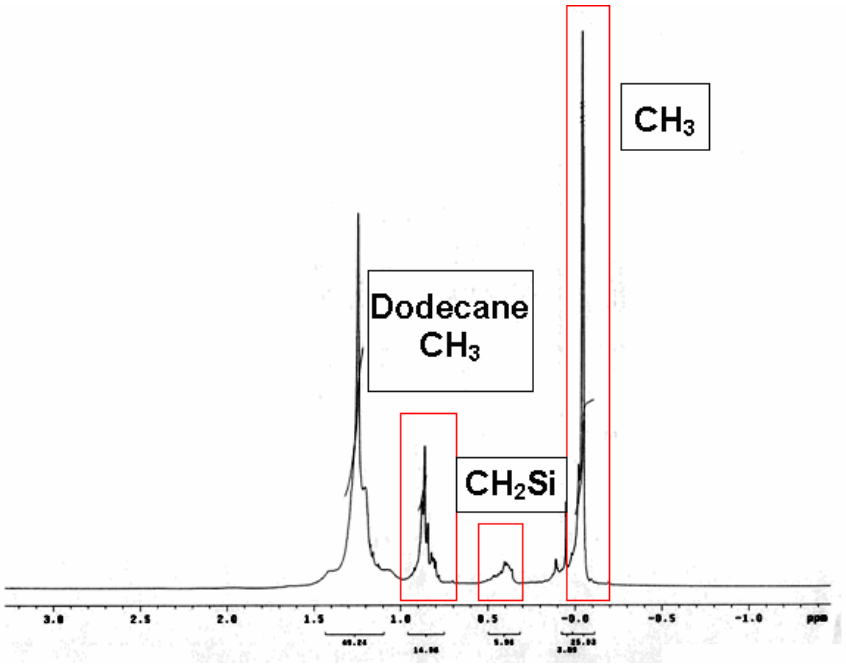

Figure 4.20 ^{1}H NMR spectrum of VTMS reaction with dodecane stabilized with MeLi

4.3.3 Effect of CO_2 Pressure on the Grafting Reaction

The effect of CO_2 pressure on the radical grafting of VTMS onto hydrocarbons was investigated. This reaction was of interest as CO_2 may have both a chemical and physical affect on the reaction, which may change and/or control the grafted product distribution (the number of grafts per chain). From a chemical standpoint, CO_2 can react with the radicals present in the system, which could alter the grafting mechanism. If the mechanism is altered, this may change the amount of grafting which occurs, and the graft distribution along the hydrocarbon chain.

From a physical standpoint, when grafting is performed on the LDPE polymer, CO_2 addition should increase the mass transport of VTMS throughout the polymer by lowering its viscosity. CO_2 is a known polymer swelling agent which has been shown to aid molecule transport through a polymer matrix.[25-29] Further, silanes have a high affinity for CO_2 which should increase their polymer solubility upon CO_2 addition.[30]

The efficiency of silane grafting as a function of CO_2 pressure has not been examined previously. By tuning CO_2 pressure it was hoped that one would be able to change and possibly control the grafting mechanism along the hydrocarbon chain. CO_2 is soluble in dodecane and heptane as well as in LDPE. The solubility of CO_2 at 200ºC (temperature for our reaction) in LDPE is 5 wt%.[31] The solubility of CO_2 in dodecane has not been determined at 200°C, however, at 45ºC it is 0.3 wt%.[32] The phase equilbria for dodecane/CO_2 shows that the dodecane phase is 38 wt% CO_2 and the vapor phase is 99% CO_2 at 70ºC and 100 bar.[33]

4.3.3.1 Dodecane as Model Compound

To carry out these reactions, a 316 stainless steel 100 mL Parr autoclave was used. The same reactant concentrations and reaction conditions as the glassware experiments were used. The Parr was placed under vacuum, and dodecane (25mL) and 5% by weight of VTMS were introduced to the Parr reactor. 750ppm of *tert*-butyl peroxide were added. The desired gas pressure was added. The reactor was heated to 200°C with stirring for 7 hours. The reactor was then cooled to room temperature. PhLi was added in a 4:1 ratio with respect to the amount of VTMS. After PhLi stabilization,

the solution was quenched with saturated ammonium chloride solution, and products were extracted with hexane.

For the initial reactions, the Parr was not pressurized; only one atmosphere of nitrogen (1 bar) was introduced. This was done to confirm that the Parr's materials of construction had no affect on the reaction of products obtained. Both MALDI-MS and GPC analysis were run on the resulting product. The MALDI-MS showed product containing from 1-6 grafts per chain, with two grafts being the most prevalent. By GPC, unreacted dodecane, vinyltriphenylsilane (VTPS) and product containing up to three grafts per chain were visible (Figure 4.21). As these results were consistent with those obtained in the glassware reactions, this showed that the Parr's material of construction, 316 stainless steel, did not affect the reaction.

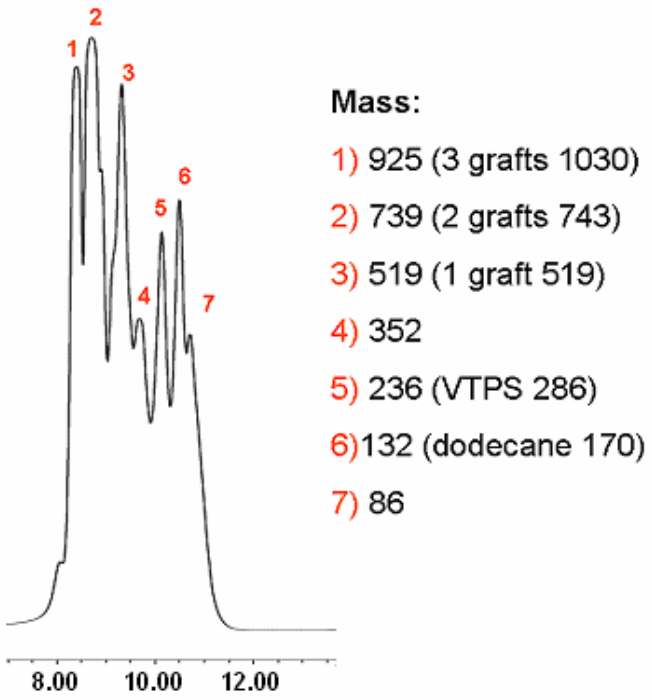

Figure 4.21 GPC chromatogram of dodecane Parr control reaction, 1 bar N_2

For the next reactions, carbon dioxide was added to the reactor. CO_2 pressures of 100 bar and 150 bar were tested. After the grafting reaction was carried out as described above, the reactor was cooled to room temperature. The reactor was then placed under vacuum to remove all CO_2 gas from the system. While under vacuum, PhLi was added in a 4:1 ratio with respect to the amount of VTMS in the system. After PhLi reaction, saturated ammonium chloride solution was added to quench excess PhLi. After quenching, the reaction was opened to the atmosphere, and products were extracted into hexane and analyzed by MALDI-MS. Using this analysis, both the 100 bar and 150 bar reactions showed a decrease in the number of grafts per chain. At 150 bar, a maximum of only 5 grafts per chain were seen (Figure 4.22), and at 100 bar, the maximum of grafts per chain was 4 (Figure 4.23).

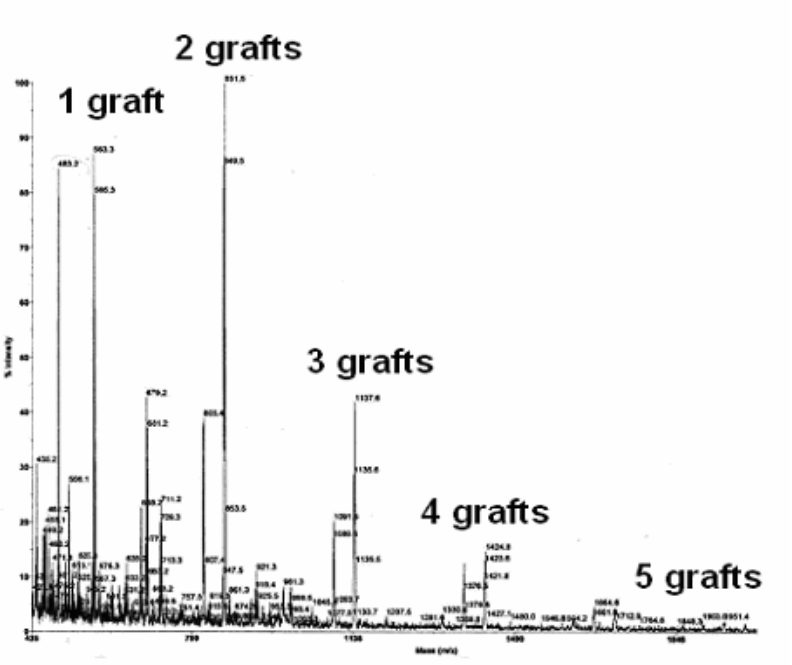

Figure 4.22 MALDI spectrum of VTPS grafted dodecane reaction in Parr autoclave at 150 bar of CO_2

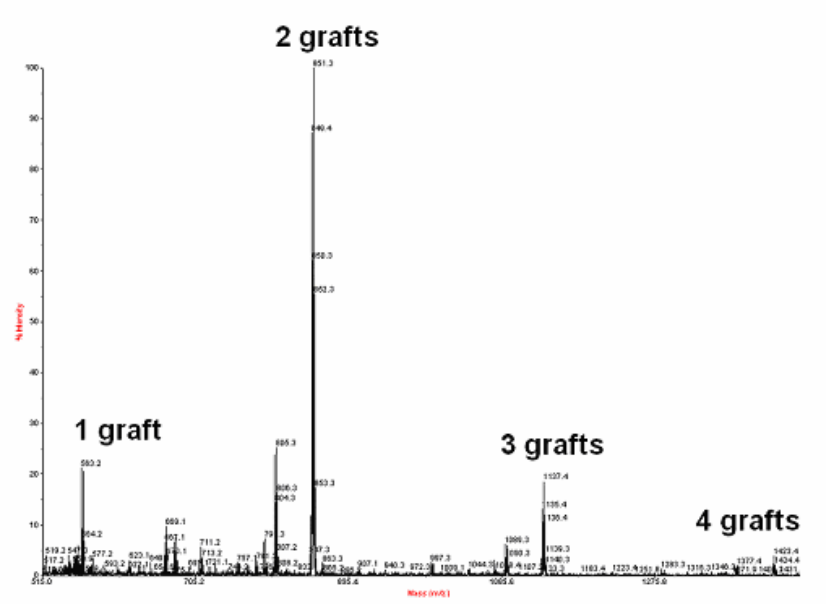

Figure 4.23 MALDI spectrum of VTPS grafted dodecane reaction in Parr autoclave at 100 bar of CO_2

The GPC analysis of these samples detected molecules containing 1, 2, and 3 grafts per chain, as well as dodecane and VTPS. As with previous experiments, higher grafting fractions were not visible by GPC analysis, so by GPC, no change was detected between the CO_2 reactions (Figure 4.24) and the Parr control (Figure 4.21) or the glassware experiments (Figure 4.12).

The change in the polarity of dodecane as a function of CO_2 pressure was explored using Nile Red as a polarity probe (Figure 4.25). With this probe, the wavelength of maximum absorption is a direct comparative indicator of polarity of a solvent. No substantial polarity change was expected with the addition of CO_2, as both are non-polar molecules. When Nile Red has been used in the past to examine the polarity of supercritical CO_2 and hexane, CO_2 was found to be only slightly less polar than hexane as there was only a 4nm difference in wavelength of maximum absorption. Dodecane should show an even smaller change as its longer chain length makes it even

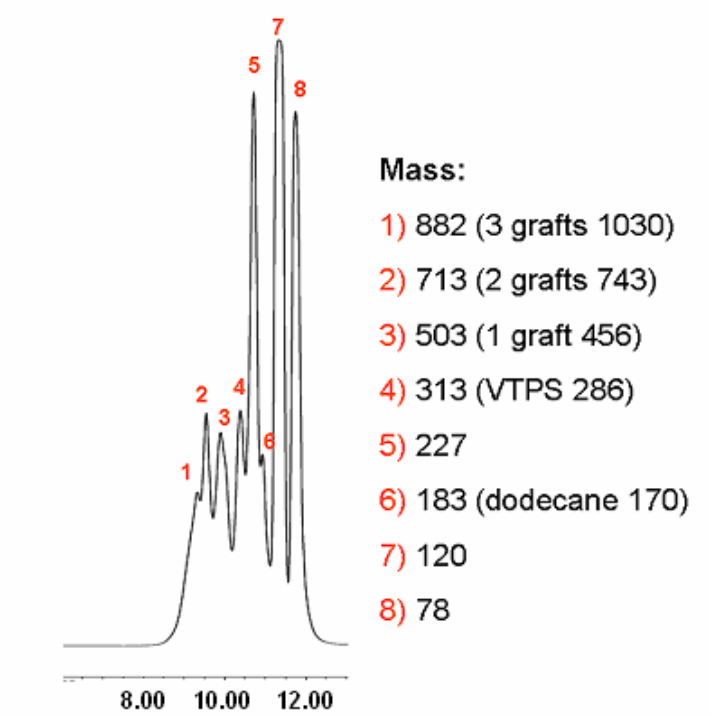

Figure 4.24 GPC chromatogram of dodecane reaction in Parr autoclave with 150 bar CO_2

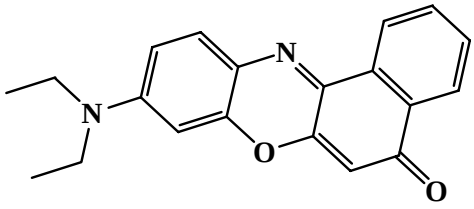

Figure 4.25 Structure of the solvatochromic probe Nile Red

less polar than hexane.[34] However, this was an important factor to examine and rule out in the current research.

Dodecane and Nile Red were mixed and charged into a high pressure UV-Vis cell equipped with quartz windows. While the concentration of Nile Red clearly decreased with increasing pressure, due to the expansion of the dodecane/Nile Red phase and subsequent dilution of the dye, no shift in the wavelength of maximum absorption (492 nm) was observed (Figure 4.26). If the polarity shift at the temperatures and pressures

tested (25°C-40°C, 60-110bar) is too small to be detected by the probe, it is unlikely that it is causing the observed changes in grafting distribution. Other possible causes of the product's change are still under investigation.

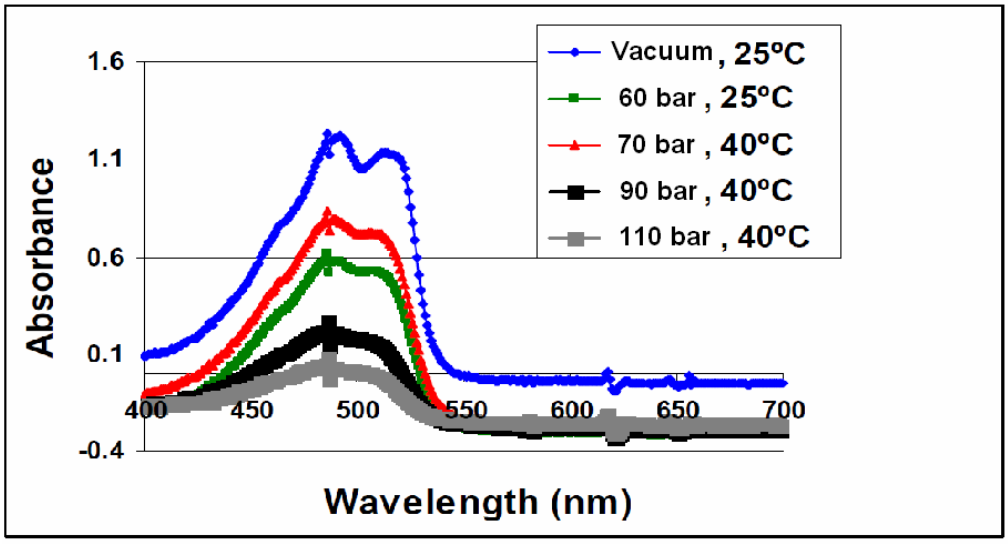

Figure 4.26 Nile Red absorbance in CO_2 expanded dodecane

4.3.4 Heptane as Model Compound

Heptane was used as a model for polyethylene in order to simplify the analysis of the grafted products. These reactions were run in the Parr reactor due to the boiling point of the reagents (heptane 98°C, VTMS 123°C) being lower than the reaction temperature (200°C). The same procedure was followed as for the dodecane reactions. The Parr was evacuated. Using an air tight syringe heptane (25mL), 5 wt.% of VTMS and 750ppm of di-tertbutyl peroxide initiator were introduced. One atmosphere (1 bar) of N_2 gas was introduced and the system was heated to 200°C. After reacting for seven hours with stirring, the reactor was cooled, placed under vacuum and PhLi solution was introduced. The work up was the same as with the glassware reactions. The crude product mixture

was analyzed by MALDI-MS. This analysis showed grafted products containing up to 5 grafts per heptane molecule (Figure 4.27). As with the results of 48 hour phenyllithium stabilization of the dodecane product, which showed up to 8 grafts per dodecane chain, this is not consistent with only the 1,5-hydrogen shift mechanism, but instead suggests a competing 1,4 hydrogen shift mechanism is also occurring.

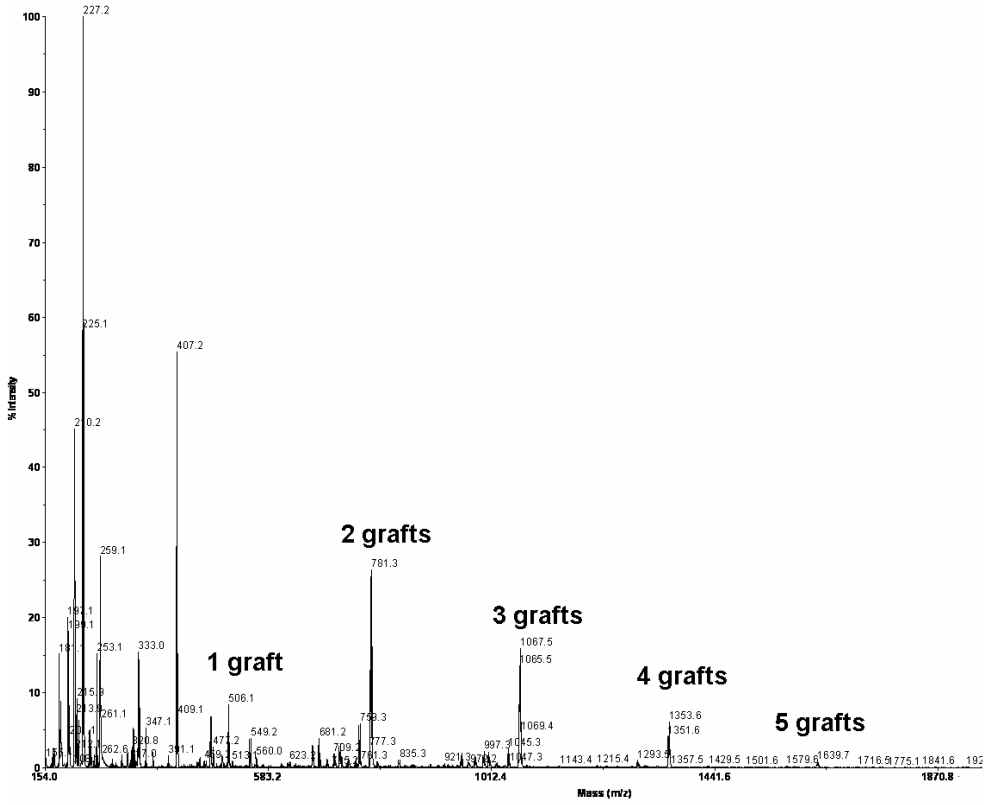

Figure 4.27 MALDI MS spectrum of VTPS grafted heptane showing up to five grafts per chain.

4.3.5 Regio-Chemical Analysis

In the work of Spencer *et al*, tetradecane was used as a model compound to study the VTMS grafting reaction.[18] The grafting reaction was carried out by heating a 5wt.% VTMS mixture with dicumyl peroxide as initiator at 170°C for 45 minutes, with

agitation. After grafting, the product was stabilized by a 24 hour reaction with PhLi. By ^{1}H NMR analysis, their product was found to contain an average of 4.2 grafts per chain. However, they took their analysis a step further. Using semi-preparative high performance liquid chromatography (HPLC) with a Supelcosil PLC-Si column, and 10% ethyl acetate:90% hexanes as the solvent, their mixture of grafted products was successfully separated into fractions containing 1, 2, 3, 4, 5 , and 6 grafted products. Any products containing more than 6 grafts per chain that may have existed could not be separated by this method. That each fraction contained only a single graft content was confirmed by CI-MS analysis, and ^{1}H NMR. From this the amounts of each grafted product, 1-6, was determined, and similar to our results with 24 hour PhLi stabilization, the two graft was found to be the most abundant (Figure 4.28).[18]

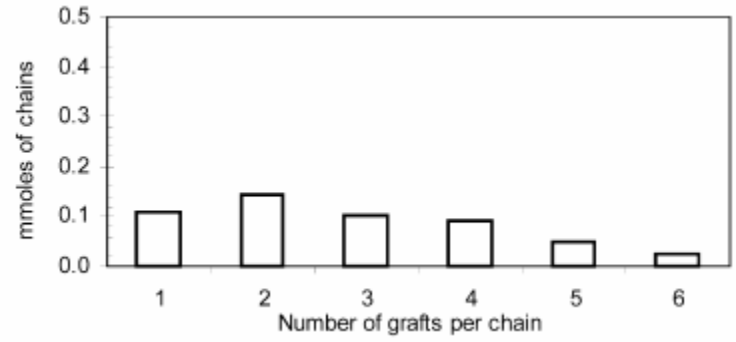

Figure 4.28 Relative distribution of grafted products found by Spencer and co-workers.[18] Reprinted from Polymer, 44, Spencer, M.; Parent, J.; Whitney, R Composition distribution in poly(ethylene-graft-vinyltrimethoxysilane), 2015-2023, 2003, with permission from Elsevier

Use of HPLC was an excellent method to separate grafted fractions and quantitatively determine proportions of grafting distribution. However, by simply using CI-MS and ^{1}H NMR analysis, structural isomers cannot be differentiated. There is no

way of knowing for example, in the single grafted fractions where the graft is located on the carbon chain. This situation is even more complicated for a two grafted fraction.

For the current research, Distortionless Enhancement by Polarization Transfer (DEPT) NMR has been selected as a possible method for determining graft location. In standard ^{13}C NMR the system is broadband decoupled and all carbons present in the sample molecule show up as positive peaks in the NMR spectra. Using DEPT NMR, variations are made in the selection angle parameter (the tip angle of the final ^{1}H pulse), which allows differentiation between primary, secondary, tertiary, and quaternary carbons. When the angle is set at 45°, primary, secondary, and tertiary carbons appear as positive signals, but signals for quaternary carbons are absent. With the pulse angle set at 90° only tertiary carbons are present and give a positive signal. And finally, with the pulse angle set at 135°, primary and tertiary carbons give a positive signal, secondary carbons give a negative signal, and quaternary carbons are absent (Figure 4.29).

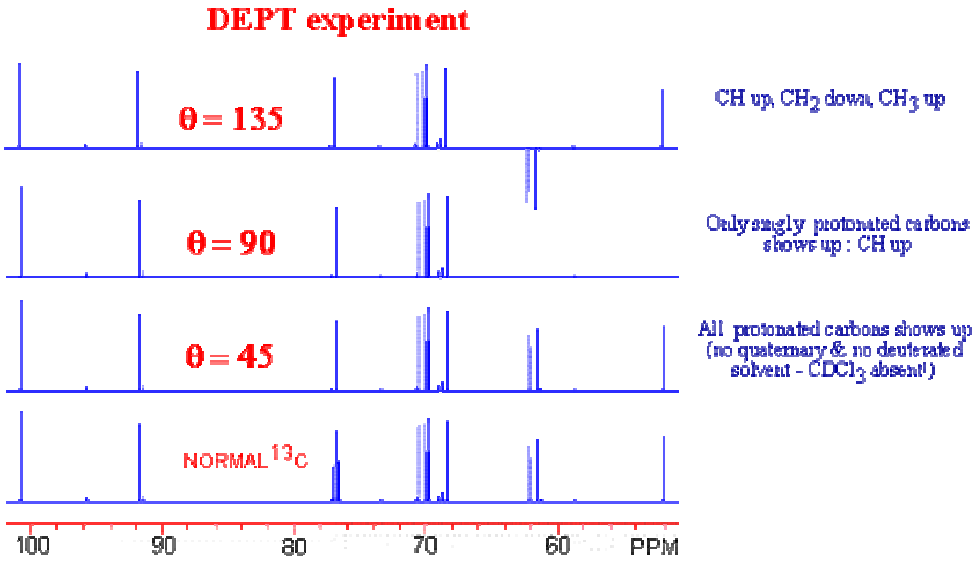

Figure 4.29 Comparison of the spectra seen during a regular ^{13}C NMR and the DEPT experiments as the pulse angle is changed

The starting unreacted hydrocarbon chain contains only primary and secondary carbons, however, after grafting takes place, tertiary carbons are formed. The SPARTAN program was used to predict the expected NMR shifts for these CH carbons in heptane using Hartree-Fock 6.31G* calculations. The NMR shift estimated with Spartan will be used as a guide during the DEPT spectra elucidation (Figure 4.30).

As discussed previously, heptane was chosen as the model compound for the regio-selective analysis experiments due to its simple structure. The reaction was run in the Parr reactor using 5wt.% VTMS with 750ppm di-tert butyl peroxide initiator. The reactants were introduced to the reactor under vacuum, 1 atmosphere of N_2 gas was introduced and the reactor was heated to 200°C. After 7 hours, the reactor was cooled to room temperature, and PhLi stabilization was carried out. The crude product mixture was examined both by ^{13}C NMR as well as by DEPT 135. While unreacted heptane is present in this product mixture (Figure 4.31 A), new peaks indicating the formation of new CH and CH_3 groups during the reaction are also clearly visible (Figure 4.31 B).

With a mixture of grafted products, the spectrum was still too complex to carry out a regio chemical analysis. The grafting products must first be separated. A Chromatotron was used for chromatographic separation. A Chromatotron is essentially preparative thin layer chromatography that spins (Figure 4.32). Pure hexane was used as the eluent to remove lighter compounds. This was switched to a 95:5 hexane:ethyl acetate mix to elute heavier compounds (compounds larger than the di-grafted heptane). Using this method, from 500 mg of crude product mixture, seven individual compound bands were separated and collected. ^1H NMR, DEPT NMR, and MALDI-MS were used to identify these compounds.

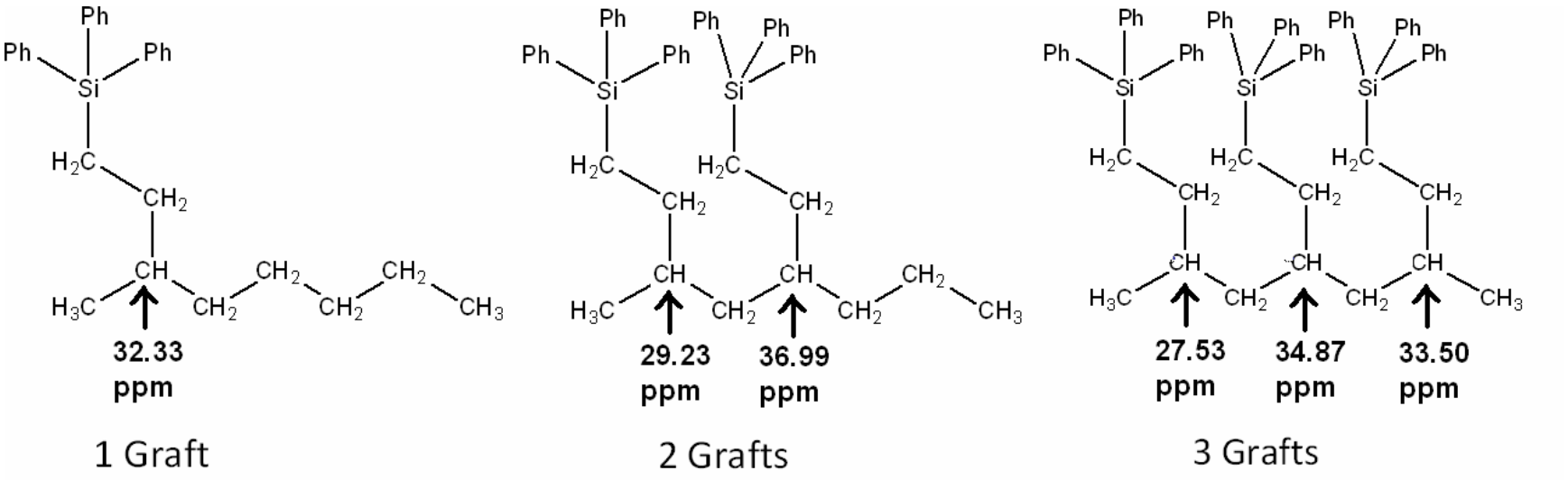

Figure 4.30 Calculated chemical shifts for the tertiary carbons in molecules with one, two, and three grafts per chain

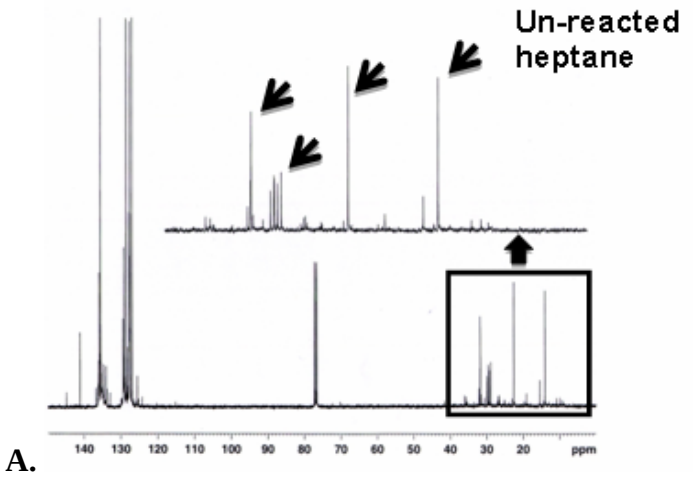

A.

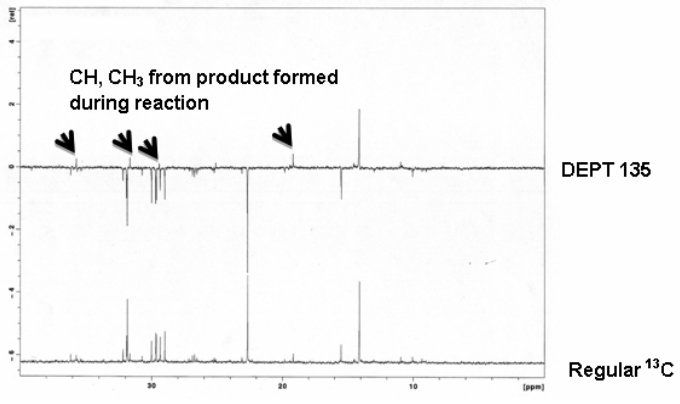

B.

Figure 4.31 A. DEPT NMR of crude heptane product mixture **B.** Zoom in showing product formation

The first band, of which 29.7mg were isolated, contained a single pure compound, the di-heptane monograft (Figure 4.33). This was confirmed by comparison of the integration of the aromatic peaks in the 7.3-7.5ppm range of the ^{1}H NMR to the aliphatic peak for the CH_3 group of heptane, as well as by MALDI-MS, which showed a clear peak at 591 (molecule mass plus Ag+ ion). The second band was isolated in 20.3mg quantities, and appeared to be a mixture of three different compounds, the di-heptane monograft, a single grafted heptane chain, and VTPS.

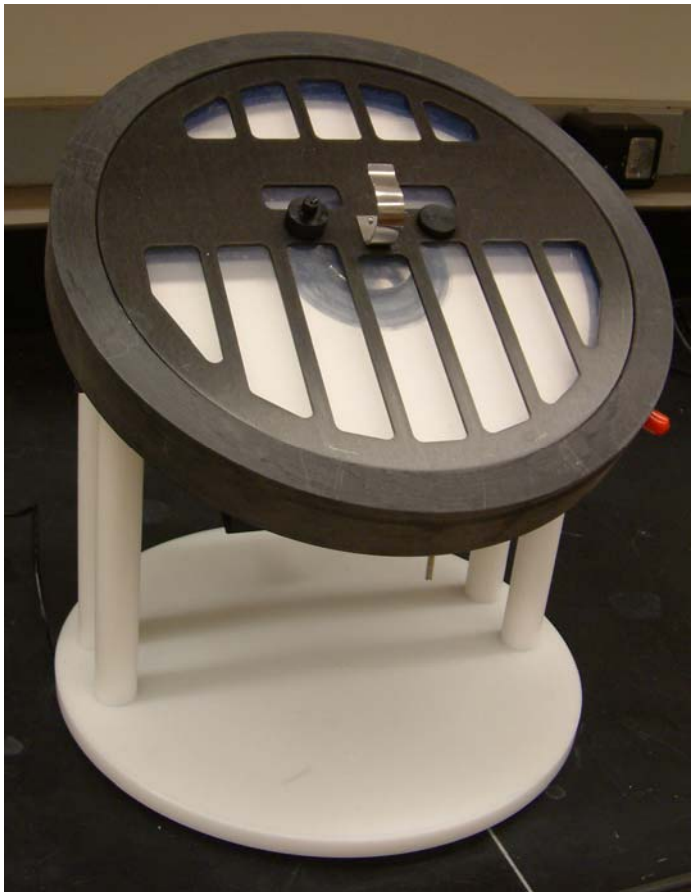

Figure 4.32 Chromatotron separation system

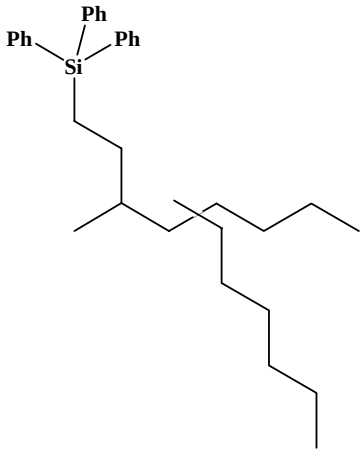

Figure 4.33 Di-heptane monografted material

This was determined by a combination of: ^{1}H NMR, which clearly showed the vinyl peaks from vinyltriphenysilane in the 5.8-6.5ppm range, DEPT NMR, which showed peaks consistent with monograft formation, and MALDI-MS, which showed a peak with mass of 495, representing the singly grafted heptane chain.

The analysis of the third band isolated (26.3mg isolated) is consistent with the side product, triphenyl(2-phenylethyl)silane (Figure 4.34). The MALDI-MS showed only a compound with the corresponding mass (473 for molecule plus Ag+, Figure 4.35), and both ^{1}H and DEPT NMR confirmed this structure.

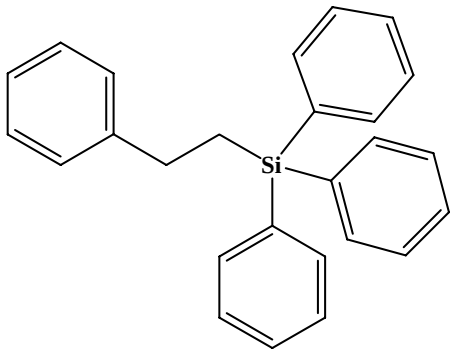

Figure 4.34 Triphenyl(2-phenylethyl)silane

The fourth and fifth bands isolated proved to be the same compound, the di-grafted heptane. Combining these two fractions, 46.0mg were isolated. The formation of the di-grafted heptane was evidenced in the ^{1}H NMR (Figure 4.36), which showed a 2:1 ratio between the aromatic protons and the aliphatic CH_3 protons of heptane. This formation was then confirmed by MALDI-MS which showed only a peak at 779 (molecule plus Ag+).

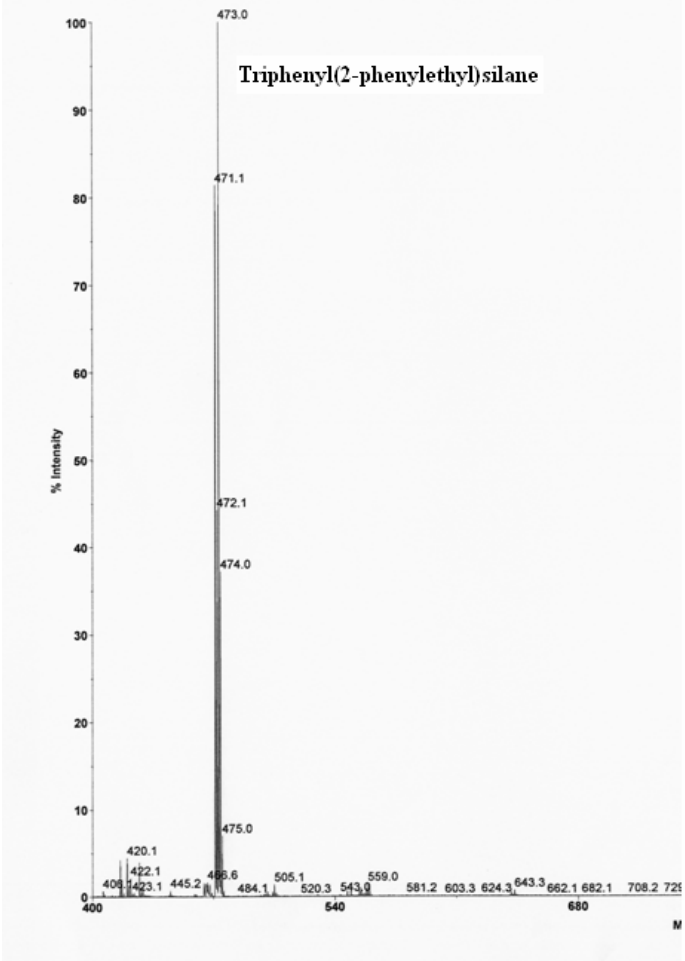

Figure 4.35 MALDI-MS confirming formation of Triphenyl(2-phenylethyl)silane

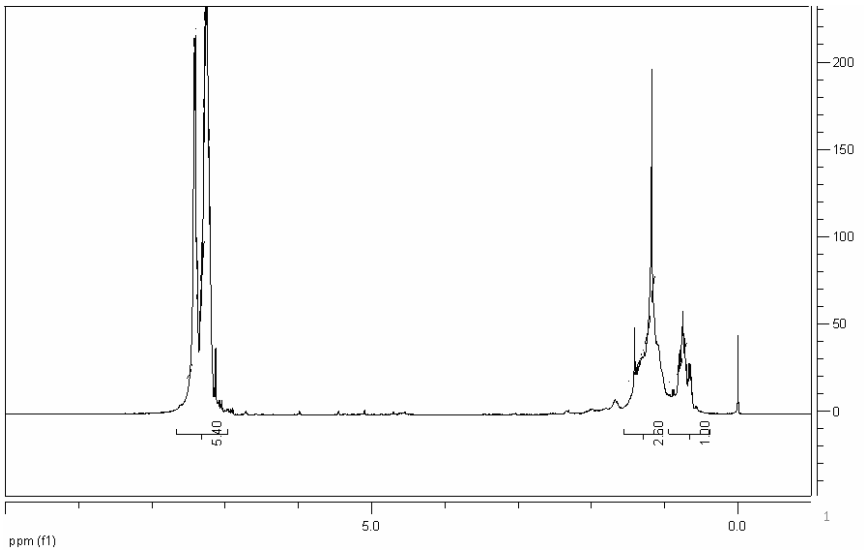

Figure 4.36 ^{1}H NMR of pure di-grafted heptane

The sixth band obtained was found to be the tri-grafted heptane (22.7mg isolated). Comparison of the aliphatic to aromatic protons in the ^{1}H NMR indicated this, and it was confirmed by MALDI-MS, which showed as the largest mass, 1068 (molecule plus Ag+) and no mass peaks corresponding to the double or singly grafted product (Figure 4.37).

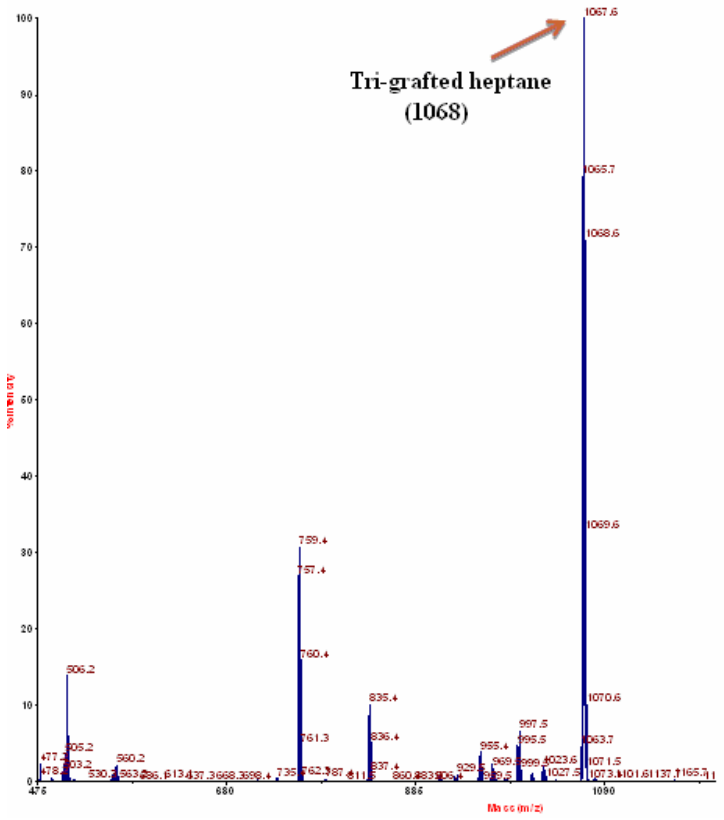

Figure 4.37 MALDI-MS of sixth band, tri-grafted heptane

As in literature[18], the higher grafted fractions could not yet be successfully separated by this method. The seventh and final band obtained (44.7mg isolated) contained a mixture of tri, tetra, and penta grafted heptane, as confirmed by MALDI-MS (Figure 4.38).

By this separation method, pure grafted fractions can be obtained in measurable quantities. Most importantly for determination of the grafting reaction mechanism, pure

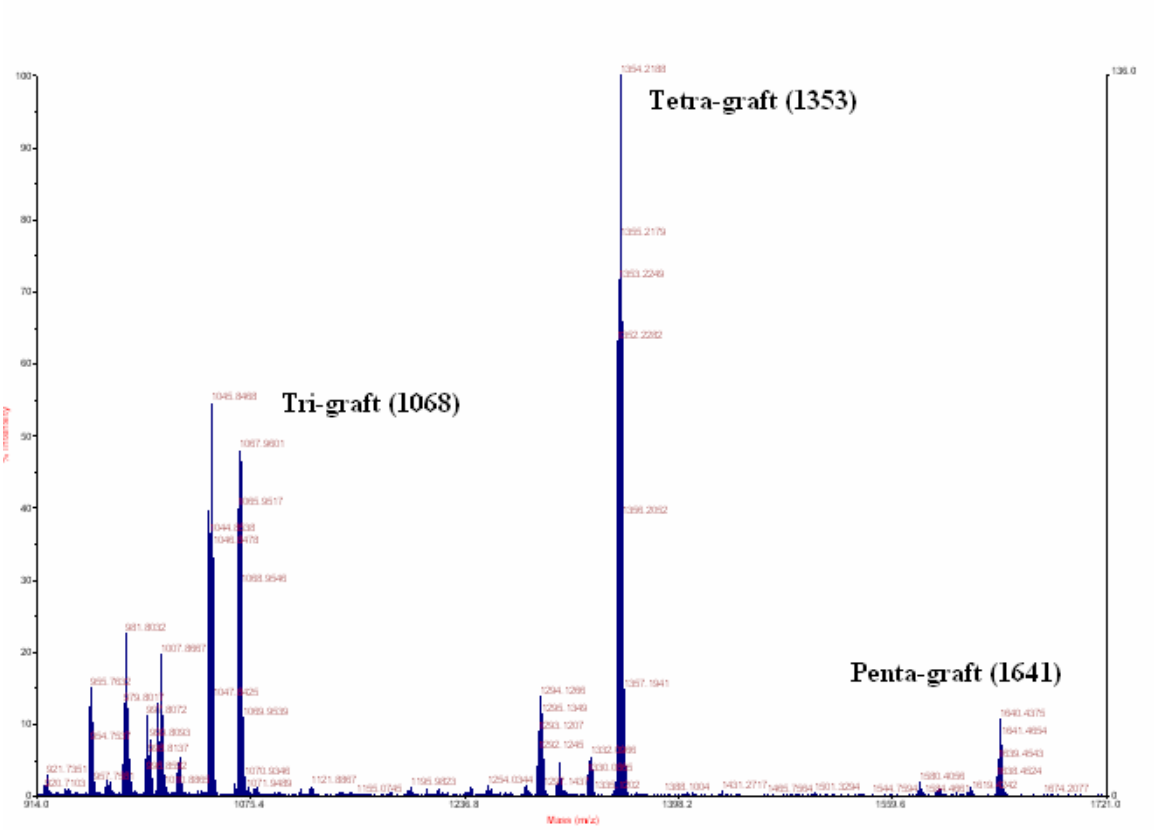

Figure 4.38 MALDI-MS of seventh band, showing a mixture of tri, tetra, and penta grafted heptane

di-grafted heptane has been isolated consistently and repeatedly. Work is in progress to analyze this di-grafted heptane using the DEPT NMR method described previously, in combination with 2-dimensional correlation spectroscopy (COSY) NMR and heteronuclear single quantu m coherence (HSQC) to determine the location of these two grafts along the heptane chain and in relation to each other. A combination of electron impact (EI) and CI MS are presently being used to study the fragmentation patterns, as different stereo-isomers should fragment in different ways. By using these analysis methods, we should be able to definitively answer the question of what hydrogen shift mechanism, or combination of mechanisms the grafting reaction follows.

4.3.6 Reaction Mechanism

As discussed previously, literature makes two basic assumptions about the grafting of VTMS to polyethylene other hydrocarbon chains: 1) grafting occurs by an intramolecular abstraction method in which a hydrogen is abstracted from within the same hydrocarbon chain and 2) the propagation of the grafting reaction proceeds by a 1,5 hydrogen shift mechanism. While all results obtained on this study support intramolecular abstraction (in all cases, multiple grafts per hydrocarbon chain are observed), the idea of a 1,5 hydrogen shift mechanism is called into question by the dodecane results in which between 1 and 8 grafts per chain were observed, and the heptane results where between 1 and 5 grafts per chain were observed.

There are two possible explanations for these results; 1) either the hydrogen shift mechanism is not exclusively a 1,5 mechanism ,or 2) oligomeric grafting is occurring, in which the VTMS is self polymerizing after it grafts onto the hydrocarbon backbone. In order to differentiate between the two possibilities, a reaction was run in glassware using dodecane as the model compound with 10% VTMS by weight, which is twice as much as had been previously used. With an elevated level of VTMS in the system, if the reaction was taking place by intramolecular abstraction, the same results would be seen with1-6 and possibly up to 8 grafts per chain, there would simply be more chains containing this number of grafts. However, if the mechanism was oligomeric grafting, with more VTMS available in the system, a markedly higher amount of VTMS per carbon chain would be seen. There would be the same number of grafting sites per hydrocarbon molecule, however, each graft would contain multiple VTMS molecules self polymerized.

The reaction was performed as before except that the amount of VTMS in the reaction was doubled. Dodecane (25mL) and VTMS (10wt.%) were mixed. To this, 750ppm of di-tert butyl peroxide were added. This mixture reacted at 200°C for 7 hours. After grafting was completed, PhLi was added and allowed to react at room temperature for 3 days. This solution was quenched with aqueous ammonium hydroxide, and products were extracted into hexane, dried, and concentrated on the roto-vap. A sticky solid layer formed in this flask, along with the liquid. ^{1}H NMR and MALDI-MS analysis were run on the solid, as that could be directly compared to the solid formed in previous reactions. The ^{1}H NMR showed an average grafting of 3.37 grafts per chain by comparing the integration of the aromatic peaks (7-8ppm) to the aliphatic CH_3 peak (0.79ppm) (Figure 4.39).

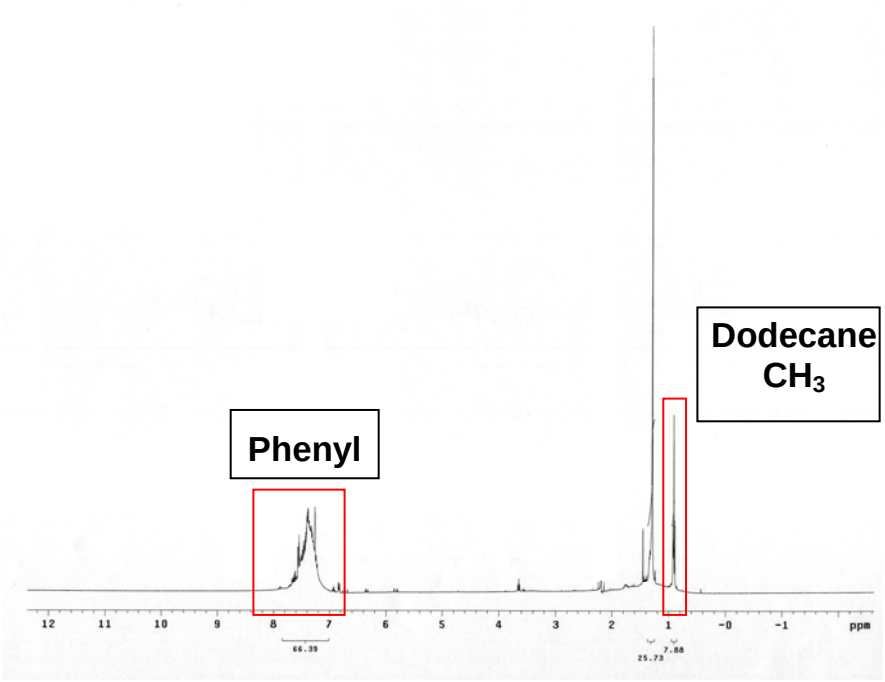

Figure 4.39 ^{1}H NMR spectrum of 10wt% VTMS reactions showing 3.37 grafts per chain

The MALDI-MS spectrum was the convincing piece of evidence that oligomeric grafting was not taking place. The solid material showed compounds containing between 1 and 6 grafts per chain, which is the same as previously seen, and is much lower than would be expected of oligomers of the VTMS were forming (Figure 4.40). These results indicated that the possibility VTMS self-polymerization as a major means of reaction propagation was unlikely.

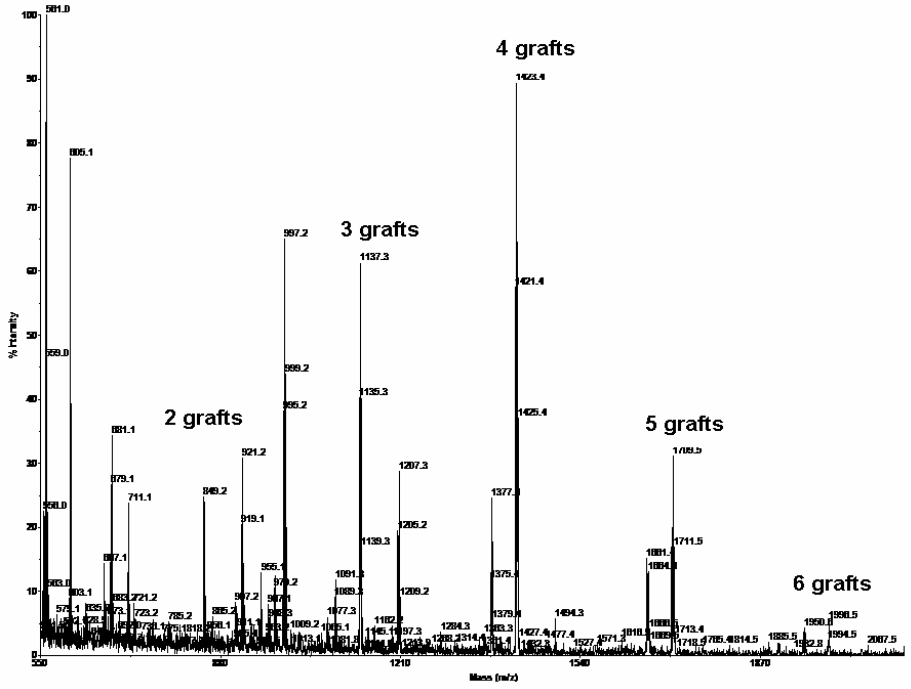

Figure 4.40 MALDI-MS of solid formed in 10wt% VTMS reaction

The lowest energy configuration of the monograft radical in the two position on the dodecane chain was determined by SPARTAN modeling (Figure 4.41). The radical had pre-geometry minimization with a multiscale modeling framework, and calculations were performed using an HF-3.21G*

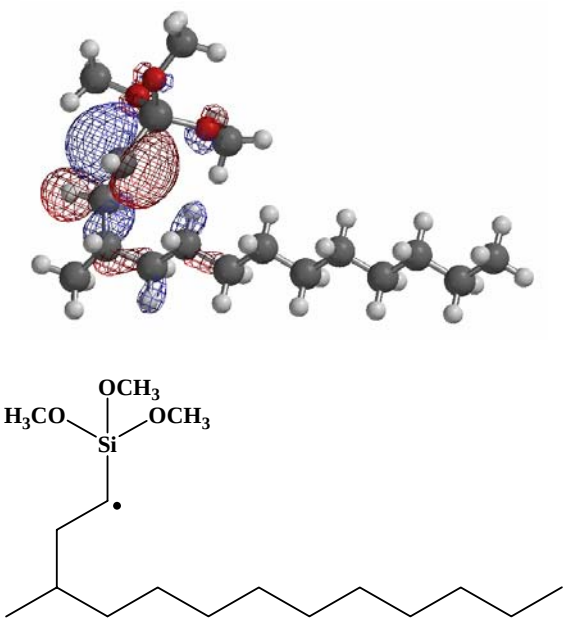

Figure 4.41 VTMS-g-dodecane radical in 2-position. The orbitals shown correspond to the single occupied molecular orbital (SOMO)

basis set. The energy associated with this molecule is -739778 kcal. As discussed previously, from this position, the radical can propagate through a 1,3-hydrogen shift, a 1,4-hydrogen shift, or a 1,5-hydrogen shift. The energy associated with each of these possible configurations was also determined, and it was found that while a 1,3-hydrogen shift is unfavorable as it involves an energy increase of 0.05kcal, both the 1,4-hydrogen shift, and 1,5-hydrogen shift are possible as they require 4kcal and 3kcal less energy respectively (Table 4.1) While the 1,4-hydrogen shift radical is more stable, making this pathway more likely, both propagation pathways may occur. This is consistent with our experimental findings thus far.

Table 4.1 Energy change with radical propagation

Intermediate	Energy Change (kcal)
1,3-shift radical	-0.05
1,4-shift radical	4
1,5-shift radical	3

4.4 Conclusions

Over the course of this project, the successful grafting of vinyl silanes onto polyethylene model compounds has been carried out. It was shown that a one day reaction with phenyllithium is not sufficient for complete stabilization of the grafted model compound, most likely due to steric hindrance. It was also shown that more than one intramolecular hydrogen shift mechanism is taking place, possibly a combination of the 1,3-, 1,4- and 1,5-hydrogen shift mechanisms. By Chromatotron chromatography, the heptane grafted material has been successfully separated. From this, what appears to be pure di-grafted material has been isolated. Full analysis of this material by DEPT NMR in combination with 2-dimensional NMR and EI and CI MS will provide information as to the reaction mechanism that is being followed and what stereo and region-isomers are being formed. Having a clear understanding of how this grafting reaction occurs will allow industry to design a more efficient process.

It was also found the presence of CO_2 appears to affect the reaction. At moderate pressures of CO_2 a shift to less VTMS grafting per single hydrocarbon chain occurs. We have discovered that this change does not arise from a polarity effect.

4.5 Experimental

The following chemicals were used as received and stored in a nitrogen filled glovebox until use: VTMS (Sigma Aldrich, 98%) and dodecane (Acros, 99%). Dodecane was further purified by washing with a concentrated mixture of sulfuric and nitric acids followed by postassium permanganate in sulfuric acid and copious water. The dodecane was then dried with magnesium sulfate and distilled. *Tert*-butyl

peroxide (Aldrich, 98%), phenyllithium (Alfa Aesar, 1.5-1.7M in cyclohexane/ether), methyllithium (Sigma Aldrich, 1.6 M in diethyl ether), anhydrous heptane (Sigma Aldrich, 99%), tetrahydrofuran CHROMASOLV Plus for HPLC inhibitor free (Sigma Aldrich, >99.9%), ethyl acetate (VWR), hexane (VWR), silica gel (Merck, $60PF_{254}$) and magnesium sulfate anhydrous (EMP Chemicals, >98%) were used as supplied. Carbon dioxide was SFC grade (Airgas, 99.999%) and further purified to remove trace water and other impurities via a Matheson gas purifier and filter cartridge (Model 450B, Type 451 filter). Nitrogen (Airgas, Ultra high purity > 99.999%) was used as supplied.

NMR spectra were obtained from a Bruker DRX 500 and Varian-Mercury VX400 MHz spectrometer. NMRs of neat samples were calibrated to external $CDCl_3$ at 7.24 ppm (^1H) and 77 ppm (^{13}C). Polarity testing using Nile Red was done using a Hewlett Packard 8453 UV-Vis system. All mass spectroscopy analyses were performed by the Georgia Institute of Technology Mass Spectroscopy facilities. MALDI-MS was performed on an Applied Biosystems 4700 Proteomics Analyzer with a 200Hz laser, while both FAB and GC-MS were run on a VG Instruments 70SE instrument. Finally the GPC tests were run on a Waters 2690 with two Varian Inc. columns PLgel 5μm and PLgel 3μm using a UV detector (Waters 996) with tetrahydrofuran (THF) as the mobile phase (calibrated using polystyrene).

Glassware Dodecane Reactions

Optimized Experimental Conditions: Dry distilled dodecane (25mL, 18.75g) and 5% by weight of VTMS (0.94g, 6.3mmol) were charged into a round bottom flask inside the glove box. The flask was sealed and removed from the glove box. The flask was topped

with a dry ice condenser and an argon inlet. 750ppm of di-tert butyl peroxide were added. Argon was flowed through the system for 5 minutes to ensure an inert atmosphere, after which time it was stopped and the system was left under static argon pressure. The mixture was then heated at 200°C for 7 hours with stirring. After 7 hours, all heating was stopped.

Mixture of grafted dodecane products: ^{1}H NMR ($CDCl_3$): 3.84 (S, O-CH_3), 1.68 (S, CH_2), 1.25 (M, CH_3); ^{13}C NMR ($CDCl_3$): 49.58, 32.09, 29.76, 22.74, 13.82

Phenyllithium Stabilization Reaction

After reaction cooled from 200°C to room temperature, PhLi was added in a 4:1 ratio with respect to the amount of VTMS (17 mL of a 1.5M solution of PhLi in 70:30 cyclohexane: ether, 25mmol PhLi). The mixture stirred at room temperature for the desired length of time (24 hours to 1 week, depending on the reaction). The system was then quenched with saturated ammonium chloride solution (20mL). Hexane (25 mL) was added, and the organic layer was isolated. The organic layer was then dried with magnesium sulfate and filtered. The mixture was then rotovapped to remove all light weight volatile organics and the product collected as a clear oil mixture of grafted products and unreacted dodecane.

Mixture of grafted dodecane products: ^{1}H NMR ($CDCl_3$): 7.26 (M, Phenyl rings), 1.27 (S, CH_2), 0.79 (M, CH_3); ^{13}C NMR ($CDCl_3$): 135.39, 129.01, 127.52, 31.75, 29.55, 22.49, 13.816; MALDI-MS (108 from AgTFA): 563 (1 graft), 851 (2 grafts), 1137 (3 grafts), 1423 (4 grafts), 1710 (5 grafts), 1995 (6 grafts), 2283 (7 grafts), 2570 (8 grafts); GPC: 891 (3 grafts), 730 (2 grafts), 519 (1 grafts), 310 (VTPS), 154 (dodecane)

Methyllithium Quenching Reaction

Grafting reaction was run by the procedure described above. After the reaction cooled from 200°C to room temperature, MeLi was added in a 4:1 ratio with the amount of VTMS present in the system (25mmol MeLi). This mixture stirred at room temperature for 24 hours. After 24 hours, the system was quenched with saturated ammonium chloride (20 mL). Hexane (25 mL) was added. The organic layer was extracted and dried with magnesium sulfate. This mixture was rotovapped to remove all light weight volatile organics.

Mixture of grafted dodecane products: ^{1}H NMR ($CDCl_3$): 1.13 (M, dodecane CH_2), 0.84 (M, dodecane CH_3), 0.39 (M, CH_2Si), 0.05 (M, CH_3); ^{13}C NMR ($CDCl_3$): 39.89, 36.50, 35.59, 33.10, 31.95, 30.89, 30.19, 29.86, 29.72, 29.68, 27.05, 25.32, 23.2, 22.71, 19.27, 14.59, 14.13, 13.44, 12.53

Reactions in Parr

To carry out these reactions, a 316 stainless steel 100 mL Parr autoclave was used. The same reactant concentrations and reaction conditions as the glassware experiments were used. The Parr was placed under vacuum prior to reagent addition. Reactants were then added using an air tight syringe. The reactor was heated to the desired reaction temperature. If necessary, pressure was added to reach the desired reaction pressure. After the reaction was completed, the reactor was cooled to room temperature. Pressure was vented, and the vapor was bubbled through THF to coolect any possible vabor-soluble reaction products. The reactor was then placed under vacuum to ensure removal of all possible gases. Experiments were twice repeated.

Dodecane: Dry distilled dodecane (25mL, 18.75g) and 5% by weight of VTMS (0.94g, 6.3mmol) were introduced to the Parr reactor. 750ppm of di-tert butyl peroxide were added. The desired gas pressure was added. The reactor was heated to 200°C with stirring for 7 hours. The reactor was then cooled to room temperature. PhLi was added in a 4:1 ratio with respect to the amount of VTMS (17 mL of a 1.5M solution of PhLi in 70:30 cyclohexane: ether, 25mmol PhLi). The mixture stirred at room temperature for 3 days. The system was then quenched with saturated ammonium chloride solution (20mL). Hexane (25 mL) was added, and the organic layer was isolated. The organic layer was then dried with magnesium sulfate and filtered. The mixture was then rotovapped to remove all light weight volatile organics and the product collected as a mixture of grafted products and unreacted dodecane.

Dodecane reaction products: Without CO_2, all analyses the same as glassware experiments. With CO_2 at 150 bar, MALDI-MS: 563 (1 grafts), 851 (2 grafts), 1137 (3 grafts), 1424 (4 grafts); GPC: 882 (3 grafts), 713 (2 grafts), 503 (1 graft), 313 (VTPS), 183 (dodecane). With CO_2 at 100 bar, MALDI-MS: 563 (1 graft), 851 (2 grafts), 1137 (3 grafts), 1424 (4 grafts).

Heptane: Heptane (25 mL) and VTMS (5 wt%, 0.93 mL) were introduced to the Parr reactor. 750ppm of di-tert butyl peroxide were added. One atmosphere of N_2 gas was added. The reactor was heated to 200°C with stirring for 7 hours. The reactor was then cooled to room temperature. PhLi was added in a 4:1 ratio with respect to the amount of VTMS (17 mL of a 1.5M solution of PhLi in 70:30 cyclohexane: ether, 25mmol PhLi). The mixture stirred at room temperature for 3 days. The system was then quenched with saturated ammonium chloride solution (20mL). Hexane (25 mL) was added, and the

organic layer was isolated. The organic layer was then dried with magnesium sulfate and filtered. The mixture was then rotovapped to remove all light weight volatile organics. *Heptane reaction products:* ^{1}H NMR ($CDCl_3$): 7.5 (M, Phenyl rings), 1.27 (S, CH_2), 0.8 (M, CH_3); ^{13}C NMR ($CDCl_3$): 136, 129, 127, 42, 36, 35, 31, 32, 29, 27, 25, 22.5, 22, 20, 19, 14.2, 14, 11, 10, 9; MALDI – MS: 491 (1 graft), 781 (2 grafts), 1067 (3 grafts), 1353 (4 grafts), 1639 (5 grafts)

Chromatotron Separation

The chromatotron plate was prepared using a slurry of silica gel (61.6812 g) in distilled water (130mL). After drying, the plate was scraped to a height of 2mm. Crude grafted heptane product (0.5283 g) was introduced to the plate. Pure hexane solvent was used to elute and collect 82 test tubes of sample. The solvent was switched to a 95:5 mix of hexane:ethyl acetate by volume. Five hundred milliliters of this solvent were run and collected. Thin layer chromatography testing was used to confirm different bands eluting. Like test tubes were combined and concentrated by roto-vap.

4.6 References

1. Barzin, J.; Azizi, H.; Morshedian, J.; *Preparation of Silane-Grafted and Moisture Crosslinked Low Density Polyethylene. Part II: Electrical, Thermal and Mechanical Properties*, Polym,-Plast. Tech. Eng., 2007, **46**: p. 305-310.

2. Dufton, P. W.; *Recent Development in Polymer for Wire and Cable: An Insulation Report,* Raptra Technology Ltd.: UK, 1995.

3. Jiao, C.; Wang, Z.; Gui, Z.; Hu, Y.; *Silane Grafting and Crosslinking of Ethylene-Octene Copolymer,* Eur. Polym. J., 2005, **41:** p. 1204-1211.

4. Barzin, J.; Aziz, H.; Morshedian, J.; *Preparation of Silane-Grafted and Moisture Cross-lInked Low Density Polyethylene: Part I: Factors Affecting Performance of Grafting and Cross-Linking,* Poly.-Plast. Tech. Eng., 2006, **45:** p. 979-983.

5. Venkatraman, S.; Kleiner, L.; *Properties of Three Types of Crosslinked Polyethylene,* Adv. Polym. Tech., 1989, **9:** p. 265-270.

6. Russell, K. E.; Kelusky, E.C.; *Grafting of Maleic Anhydride to n-Eicosane*. J. Polym. Sci., 1988; **26**: p. 2273-2280.

7. Russell, K. E.; *Grafting of Maleic Anhydride to Hydrocarbons below the Ceiling Temperature*. J. Polym. Sci. 1995; **33**: p. 555-561.

8. Sipos. A.; McCarthy, J.; Russell, K. E.; *Kinetic Studies of Grafting of Maleic Anhydride to Hydrocarbon Substrates*. *Journal of Polymer Science: Part A: Polymer Chemistry* 1989; **27**: p. 3353-3362.

9. Ranganathan, S.; Baker, W. E.; Russell, K. E.; and Whitney, R. A.; *Peroxide-Initiated Grafting of Maleic Anhydride onto Linear and Branched Hydrocarbons*. J. Polym. Sci. 1999, **37**: p. 3817-3825.

10. Heinen, W.; Erkens, S. W.; VanDuin, M.; Lugtenburg, J.; *Model Compounds and ^{13}C NMR Increments for the Characterization of Maleic Anhydride-Grafted Polyolefins*. J. Polym. Sci. 1999; **37**: p. 4368-4385.

11. Dokolas, P.; Looney, M. G.; Musgrave, S.; Poon, S.; Solomon, D. H.; *Graft copolymerization studies Part 1. Models related to polyolefins*. Polymer 2000; **41**: p. 3137-3145.

12. Shing, J. B. W.; Baker, W. E.; Russell, K. E.; Whitney, R. A.; *Effect of Reaction Conditions on the Grafting of 2-(Dimethylamino) ethyl Methacrylate onto Hydrocarbon Substrates.* J. Polym. Sci. Part A 1994; **32**: p. 1691-1702.

13. Shing, J. B. W.; Baker, W. E.; Russell, K. E.; *Kinetics and Mechanim of the Grafting of 2-(Dimethylamino) ethyl Methacyrlate onto Hydrocarbon Substrates.* J. Polym. Sci. Part A 1995; **33**: p. 633-642.

14. Isac, S.; George, K. E.; *Silane Grafting of Polyethylenes,* Int. J. Polym. Mater., 2005, **54:** p. 397-413.

15. Forsyth, J. C.; Baker, W. E.; Russell, K. E.; Whitney, R. A.; *Peroxide-Initiated Vinylsilane Grafting: Structural Studies on a Hydrocarbon Substrate*. J. Polym. Sci., 1997; **35**: p. 3517-3525.

16. Sen, A. K.; Mukherjee, B.; Bhattacharyya, A. S.; De, P. P.; Bhowmick, A. K.; *Kinetics of Silane Grafting and Moisture Crosslinking of Polyethylene and Ethylene Propylene Rubber*, J. Appl. Polym. Sci., 1992; **44**: p. 1153-1164.

17. Weaver, J. D.; Chowdhury, A. K.; Mowery, D. M.; Esseghir, M.; Cogen, J. M.; Chaudhary, B. I.; *Structural Comparison of Products from Peroxide-Initiated Grafting of Vinylsilane and Silane-Functionalized Nitroxyl to Hydrocarbon and Polyolefin Substrates*. J. Polym. Sci. 2008; **46**: p. 4542-4555.

18. Spencer, M.; Parent, J. S.; Whitney, R. A.; *Composition distribution in poly(ethylene-graft-vinyltrimethoxysilane)*. Polymer 2003; **44**: p. 2015-2023.

19. Shieh, Y.-T.; Hsiao, K.-I.; *Thermal Properties of Silane-Grafted Water-Crosslinked Polyethylene*. J. Appl. Polym. Sci., 1998; **70**: p. 1075-1082.

20. Parent, J. S.; Parodi, R.; Wu, W.; *Radical Mediated Graft Modification of Polyolefins: Vinyltriethoxysilane Addition Dynamics and Yields*. Polym. Eng. Sci. 2006; **46**: p. 1754-1761.

21. Parent, J. S.; Tripp, M.; Dupont, J.; *Selectivity of Peroxide-Initiated Graft Modification of Ethylene Copolymers*. Polym. Eng. Sci. 2003; **43**: p. 234-242.

22. Ivanov, V. S.; *Radiation Chemistry of Polymers*, VSP – BV, The Netherlands, 1992, Chapter 3.

23. Anbarasan, R.; Babot, O.; Maillard, B.; *Crosslinking of High-Density Polyethylene in the Presence of Organic Peroxides,* J. Appl. Polym. Sci., 2004, **93,** p: 75-81.

24. Freidlina, R. Kh.; Terent'ev, A. B.; *Free-radical Rearrangements in Telomerization.* Acc. Chem. Res., 1977, **10(1)**: p. 9-15.

25. Wang, Y.; Yang, C.; Tomasko, D.; *Confocal Microscopy Analysis of Supercritical Fluid Impregnation of Polypropylene*. Ind. Eng. Chem. Res. 2002; **41**: p. 1780-1786.

26. Li, D.; Han, B.; Liu, Z.; *Grafting of 2-hydroxyethyl methacrylate onto isotactic poly(propylene) using supercritical CO_2 as a solvent and swelling agent.* Macromo. Chem. Physic. 2001; **202**: p. 2187-2194.

27. Liu, Z.; Song, L.; Dai, X.; Yang, G.; Han, B.; Xu, J.; Preparation *of nanometer dispersed polypropylene/polystyrene interpenetrating network using supercritical CO_2 as a swelling agent.* Polymer 2002; **43**: p. 1183-1188.

28. Dorscht, B. M.; Tzoganakis, C.; *Reactive Extrusion of Polypropylene with Supercritical Carbon Dioxide: Free Radical Grafting of Maleic Anhydride.* J. Appl. Polym. Sci. 2003; **87**: p. 1116-1122.

29. Manke, C. W.; Gulari, E.; Smolinski, J. M.; Kwag, C.; *Rheology of polymer melts swollen with dissolved supercritical fluids.* Polym. Mater. Sci. Eng. 2001; **84**: p. 279.

30. Madkour, T. M.; Mohamed, S. K.; Barakat, A. K.; *Molecular Level Investigation into Selective Permeability of Silicon Based Membranes with Potential Use in gas Separation Processes.* Mater. Sci. Tech., 2002, **18**: p. 1235-1240.

31. Chaudhary, B. I.; John, A. I.; *Solubilities of Nitrogen, Isobutane, and Carbon Dioxide in Polyethylene*. J. Cell. Plast. 1998; **34**: p. 312-328.

32. Hayduk, W.; Walter, E.; Simpson, P.; *Solubility of Propane and Carbon Dioxide in Heptane, Dodecane, and Hexadecane.* J. Chem. Eng. Data 1972; **17**: p. 59-61.

33. Adams, W. R.*; A new apparatus for measuring supercritical fluid-liquid phase equilibria and results for the systems carbon dioxide+ decane, carbon dioxide+ dodecane, carbon dioxide + methyl linoleate, and ethane + methyl linoleate.* PhD dissertation, Cornell University, 1986.

34. Deye, J.F.; Berger, T. A.; Anderson, A. G., *Nile Red as a Solvatochromic Dye for Measuring Solvent Strength in Normal Liquids and Mixtures of Normal Liquids with Supercritical and Near Critical Fluids.* Anal. Chem., 1990. **62**: p. 615-622.

CHAPTER FIVE
SYNTHESIS OF THE NOVEL HYDRAZINE REPLACEMENT FUEL MOLECULES 1,1-DIMETHYL-2-[2-AZIDOETHYL]HYDRAZINE AND 1,1-DIMETHYL-2-[2-AZIDOETHYL]HYDRAZONE

5.1. Introduction

For many years, an ongoing search has been underway for a liquid fuel molecule to replace hydrazine and its derivatives (Figure 5.1), due to the inherent human and environmental hazards associated with working with these chemicals. They are carcinogens with high vapor pressures.[1] However, they are very attractive as fuels due to their high specific impulse (impulse obtained per mass unit of propellant), the large quantity of hot expanding gases produced from a very small amount of liquid hydrazine, and low cost manufacturing. Though extensive work has been done[2-10], it has proved difficult to find a liquid fuel that is less toxic but can still compete with hydrazine's high specific impulse and low cost.

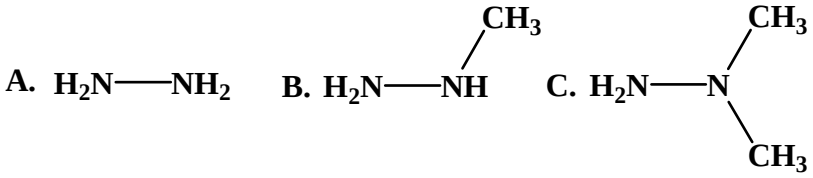

Figure 5.1 A. Hydrazine and its derivatives, **B.** monomethylhydrazine and **C.** 1,1-dimethylhydrazine.

The molecule 2-dimethylaminoethylazide (DMAZ) (Figure 5.2 A) is a suitable hydrazine replacement because it is simple to prepare and less toxic to handle than hydrazine.[2] However, it does not ignite as a monopropellant, and when igniting it with red fuming nitric acid, there is a time lapse or ignition delay of 26 milliseconds between the mixing of the liquids and the actual onset of fuel combustion.[11] While this does not

seem substantial, any delay longer the 25 milliseconds can cause damage to a rocket engine.[11] This delay is believed to be caused by an intramolecular interaction between N2 and N4 within the DMAZ molecule (Figure 5.2 A).[12] Ignition takes place when DMAZ acquires an acidic proton from nitric acid at the N4 nitrogen. This intramolecular interaction decreases the basicity as well as the nucleophilicity of the N4 nitrogen, thereby hindering its ability to pick up this proton. To overcome this, the molecule 1,1-dimethyl-2-[2-azidoethyl]hydrazine (DMAEH) was proposed (Figure 5.2 B).

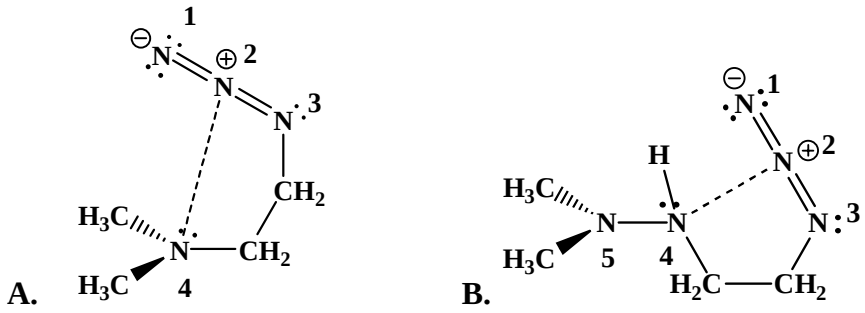

Figure 5.2 A. Structure of DMAZ, a dotted line indicates unfavorable interaction. **B**. Structure of DMAEH, a dotted line indicates the interaction we believe will occur.

DMAEH is anticipated to have lower vapor pressure than hydrazine. Another advantage compared to DMAZ is that lowest energy confirmation calculations have shown that DMAEH will have a "free" terminal nitrogen (N5) that can interact with an acidic proton for improved ignition characteristics. Furthermore, using the NASA Lewis Research Center's Chemical Equilibrium with Applications computer program, the specific impulse of this molecule has been calculated and found to be as good as, or better than that of DMAZ (282s vs. 280s at the optimum oxygen to fuel ratio). [13]

Previous attempts at synthesizing this molecule have been pursued with limited success, as at most only traces of product were seen.[13-14] The process used involved

reacting either 2-chloroethylazide or 2-azidoethyl-p-toluenesulfonate with 1,1-dimethylhydrazine neat at 25°C in the presence of the base 1,4-diazabicyclo-[2-2-2]-octane (DABCO). Unfortunately, the desired product could not be successfully isolated.[13] In the current work a synthetic strategy starting from chloroacetaldehyde, 1,1-dimethlyhydrazine and sodium azide was investigated (Figure 5.3).

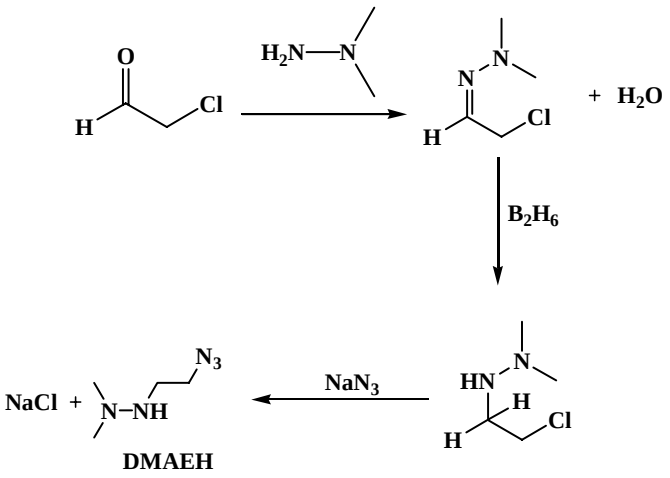

Figure 5.3 DMAEH synthesis from chloroacetaldehyde, 1,1-dimethlyhydrazine, and sodium azide

It should be pointed out that the intermediate 1,1-dimethyl-2-[2-azidoethyl]hydrazone or De-DMAEH (Figure 5.4) is also attractive from a propulsion standpoint. Its synthesis, structure, and possibilities as a fuel molecule were explored since it was anticipated to have comparable ignition and fuel characteristics and benefits as DMAEH.

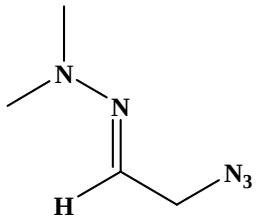

Figure 5.4 Structure of 1,1-dimethyl-2-[2-azidoethyl]hydrazone, De-DMAEH

5.2. Background

5.2.1 Hydrazine

Hydrazine (Figure 5.1 A) has a variety of industrial uses, from acting as a chain extender in the production of spandex fiber[15] to being used as a reducing agent in chemical reactions such as the reduction of metal chloride salts to form metallic nanoparticles. It is produced commercially using the two step Olin Raschig process (Figure 5.5).[16]

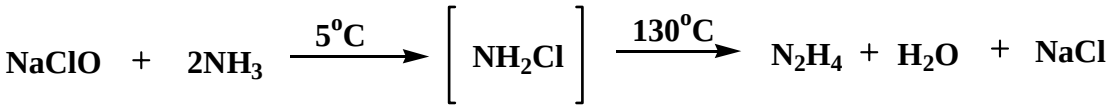

Figure 5.5 Synthesis of hydrazine by the Olin Raschig process

Since World War II one of its most common uses has been as rocket fuel for vehicles such as the German Messerschmitt and NASA's space shuttle maneuvering thrusters. Its rapid ignition (3-10 millisecond time frame),[17] and highly exothermic decomposition to large volumes of hydrogen, nitrogen and ammonia[18] make it an efficient liquid propellant with a specific impulse of 245 seconds.[19] However, it is toxic and a known carcinogen. Due to these problems, the Occupational Safety and Health Administration (OSHA) has set safe exposure limits at 1 ppm over 8 hours, while the recommended limit for the National Institute for Occupational Safety and Health (NIOSH) is lower, at 0.3 ppm for 120 minutes. Replacements for hydrazine as a fuel that can alleviate the problems with both the toxicity and reactivity have been investigated.

5.2.2 2-Dimethylaminoethylazide (DMAZ)

One of the compounds which has been studied as a hydrazine replacement is the molecule 2-dimethylaminoethylazide (DMAZ)[2-3,5,7 9-10] (Figure 5.2 A). When compared to hydrazine it is simple to prepare as it can be formed in a one step process from commercially available starting materials (Figure 5.6)[5]

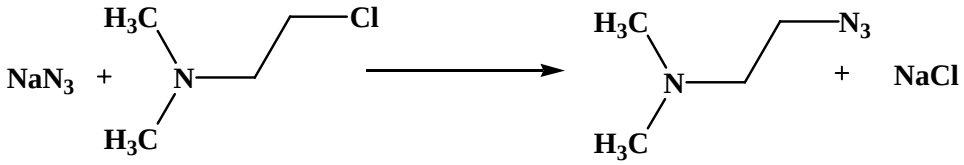

Figure 5.6 Synthesis of DMAZ

The properties of DMAZ are often compared to those of monomethylhydrazine (MMH), and while it has a lower specific impulse (281s) than MMH does (285s), it has a higher density. This gives it, ultimately a density impulse of 13.77lbfsec/in.^{3} that is on the same level as that of MMH (13.36 lbfsec/in^3).[2] With all of these benefits, however, the implementation of DMAZ has been limited mainly due to the longer ignition response. There are currently no adequate catalysts available to ignite DMAZ as a monopropellant and while it is hypergolic with inhibited red fuming nitric acid the delay of 26 milliseconds before ignition remains a limitation for some applications.[11]

Testing has shown that the key step in ignition is the transfer of an acidic proton from the acid to the amine nitrogen N4 of DMAZ (Figure 5.7).[12] Density functional theory calculations show that the most stable conformation of DMAZ has a shape like that of a scorpion's tail (Figure 5.8).[1,12-14]

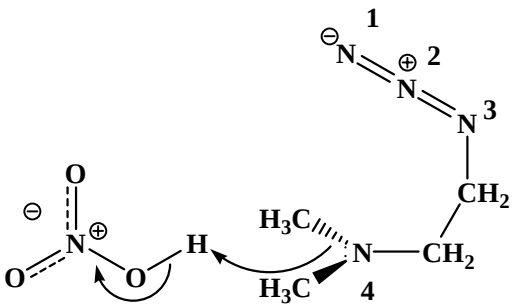

Figure 5.7 Ignition mechanism of DMAZ by fuming nitric acid

The linear azide nitrogens fold up and over the amine nitrogen. This confirmation potentially presents a twofold problem for protonation of the amine nitrogen. First, as it is located directly over the amine group, the azide group could be sterically blocking protonation of amine nitrogen (N4) due to its size. Second, this confirmation allows an intramolecular interaction between N2 and N4 (Figure 5.8). This interaction makes the amine nitrogen, N4, both less basic and less nucleophilic which in turn decreases the ability of N4 to attack the acidic hydrogen of fuming nitric acid, delaying ignition.[1,5,12-14]

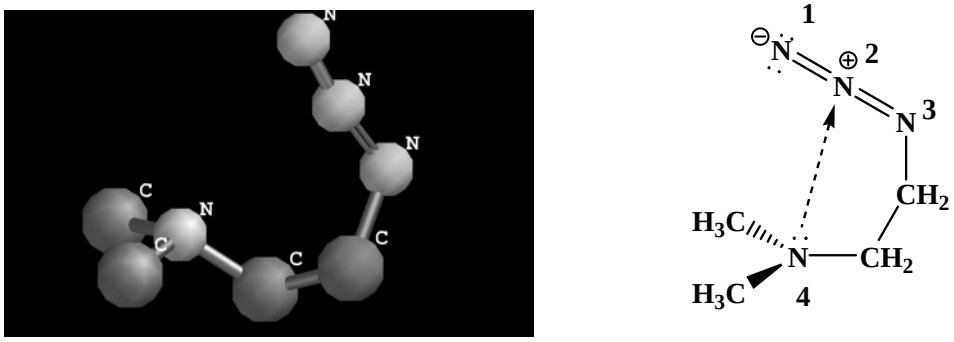

Figure 5.8 Calculated most stable conformation of DMAZ structure showing suspected intramolecular interaction[13]

From this information it has been determined that an adequate replacement molecule will require either an altered electron distribution which does not decrease the

nucleophilicity of the amine nitrogen, an altered physical conformation that prevents the azide group from sterically blocking the active site, or both.[1, 12-14]

5.2.3 DMAEH and its Synthesis

In order to address both the steric and electron distribution problems found in DMAZ, the molecule1,1-dimethyl-2-[2-azidoethyl]hydrazine (DMAEH) was proposed. Density functional theory calculations were performed on this molecule using a Hybrid Density Functional Model (B3YLP) with a polarized split valence basis set (6-31G*) to determine the most stable conformer. From these calculations it was determined that in its lowest energy conformation, the steric affects found with DMAZ are no longer an issue as the azide group is no longer located directly over the terminal amine nitrogen (N5, Figure 5.9) [13-14]

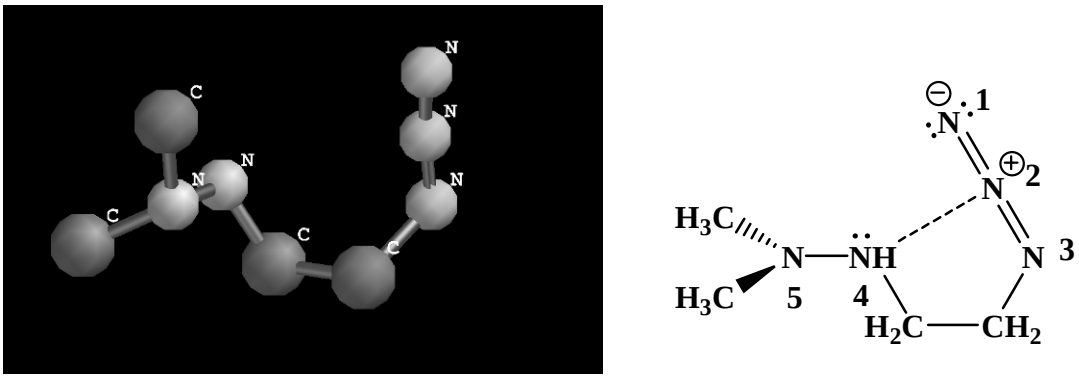

Figure 5.9 Calculated most stable confirmation of DMAEH structure, showing the new intramolecular interactions taking place[13]

Also, while there is still an intramolecular chemical interaction, it is now between the azide group and the N4 nitrogen, leaving the terminal nitrogen (N5) free for protonation during the ignition process (Figure 5.9).[1]

A simple two step synthesis method that involved the reaction of 2-chloroethyl-p-toluenesulfonate with 1,1-dimethyl hydrazine, followed by reaction of that intermediate with sodium azide to produce DMAEH was proposed (Figure 5.10).

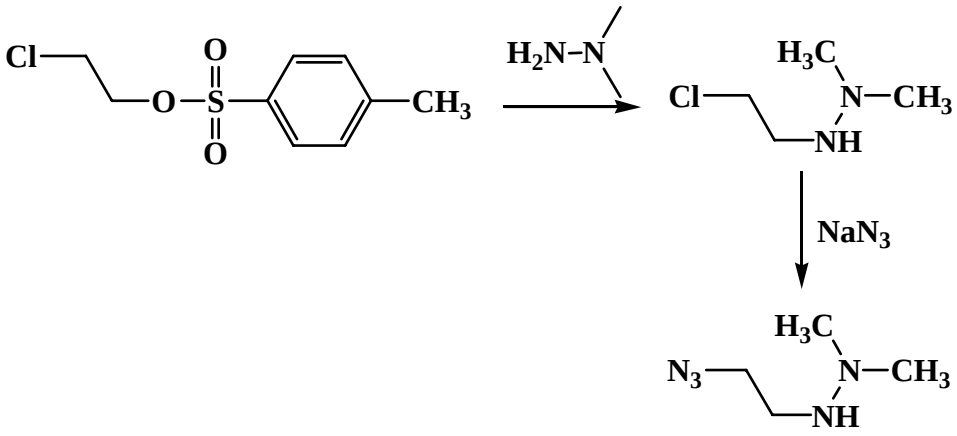

Figure 5.10 Two step synthesis of DMAEH

Unfortunately, the first step of this reaction produced a beige solid. Routine analyses (^{1}H and ^{13}C NMR) performed on this solid indicated two possible isomers (Figure 5.11) which could not be separated and did not react with sodium azide to form DMAEH.[13]

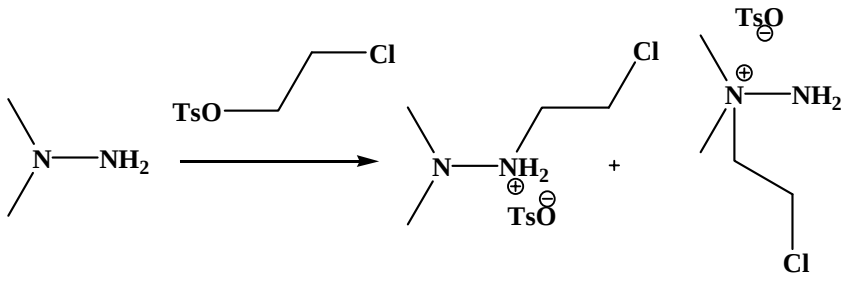

Figure 5.11 Isomers formed during DMAEH synthesis

To address this problem, 2-chloroethylazide and 2-azidoethyl-p-toluenesulfonate were synthesized. These were each then reacted with 1,1-dimethylhydrazine at different

temperatures (0°C and 25°C), different reaction times (1.5-72 hours), in different solvents (neat, in toluene, in ether, and in THF) and in the presence of different bases (triethylamine, sodium hydride, butyllithium, and DABCO). Although the desired product was detected by ^{1}H NMR, it was formed as one of two isomeric quaternary salts, which was confirmed by X-ray crystallography (Figure 5.12).[13] Isolation of the desired product was not successful.

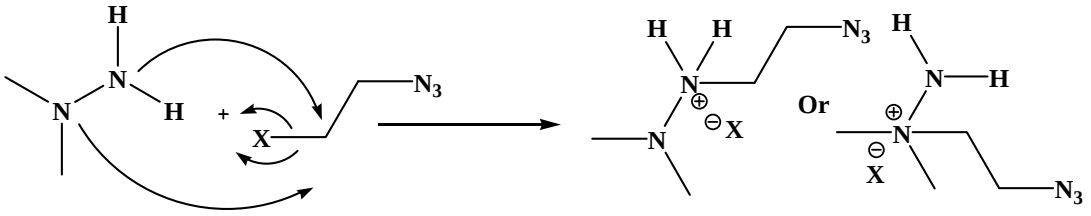

Figure 5.12 Quaternary salts obtained from DMAEH synthesis. X=Cl, OTs

A second synthesis method was developed starting from the molecule 2-mesyl-1-ethyl-N,N-dimethylhydrazine. Ethylene oxide and 1,1-dimethylhydrazine were reacted in glacial acetic acid and water for 18-24 hours at room temperature to form 1,1-dimethyl-2-[2-ethylalcohol]hydrazine (Figure 5.13). This would then be reacted with mesyl chloride to form the desired 2-mesyl-1-ethyl-N,N-dimethylhydrazine. The ethylene oxide reaction was quenched into a bicarbonate solution at room temperature and extracted with ethyl acetate. Along with the desired product, NMR analysis showed that oligomers of ethylene oxide, as well as other unidentified side products were formed, so a full synthesis to DMAEH through this intermediate was not pursued.[14]

A final synthesis beginning with two commercially available starting materials:

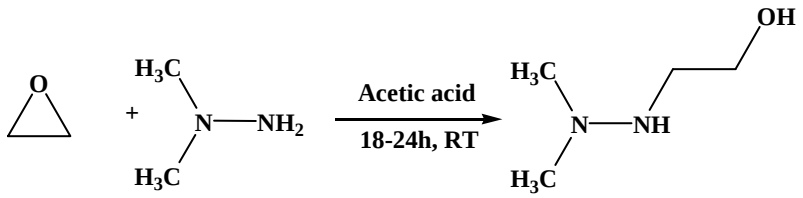

Figure 5.13 Synthesis of 1,1-dimethyl-2-[2-ethylalcohol]hydrazine from ethylene oxide and 1,1-dimethlyhydrazine

1,1-dimethylhydrazine and chloroacetyl chloride was investigated.[14] This was chosen as the reaction of acylchlorides with derivatives of hydrazine has been reported with high yields (up to 87%).[20] A three step reaction sequence was developed (Figure 5.14), beginning with the reaction of 1,1-dimethylhydrazine and chloroacetyl chloride. The first step was carried out in chloroform reacting at room temperature for 2 hours. The desired product, chloroacetic acid-N,N-dimethylhydrazide, was seen in 11% yield by NMR analysis. Regardless of the conditions (temperatures of 0°C, -15°C, and -25°C, reaction times of 2-12 hours, and varying reactant concentrations) yields were consistently low (18% maximum).[14]

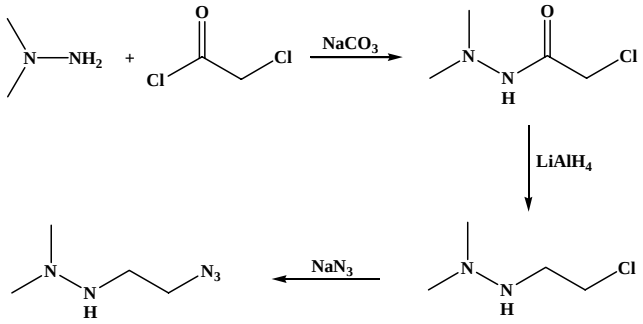

Figure 5.14 Third proposed reaction for DMAEH synthesis

A small amount of work was done on reactions of unsubstituted (symmetrical) hydrazine, as opposed to 1,1-dimethylhydrazine, as it will not have the regioseletivity

issues inherent in 1,1-dimethylhydrazine. Hydrazine was reacted with 2-tosyl-1-ethylazide or 2-chloro1-ethylazide (Figure 5.15). In both cases, reaction appeared to proceed well to desired product, as shown by both NMR and LC-MS testing. Quaternary salt formation did not appear to be a problem, as was seen with the 1,1-dimethylhydrazine reaction. However, the disubstituted hydrazine (1,2-(2-ethylazide)hydrazine) was a major impurity, and it proved difficult to prepare the desired product compound, (2-azidoethyl)hydrazine, on a gram scale with a consistent purity of 95% or better for ignition and combustibility testing.[14]

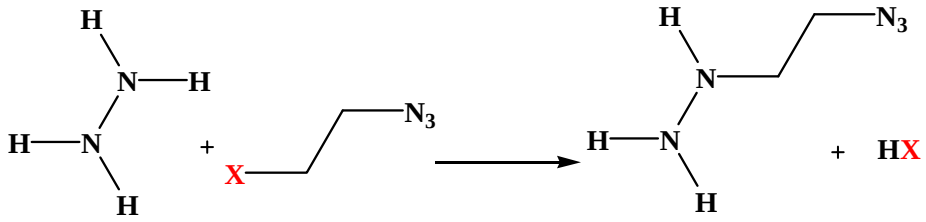

Figure 5.15 Reaction of hydrazine with ethylazide containing various good leaving groups. X=Cl or OTs

5.3. Result and Discussion

5.3.1 New Synthetic Strategy to the DMAEH Molecule

Finding a suitable replacement for hydrazine continues to be an area of much interest both to the private and government aerospace industries. A large commercial market exists for any new, cost competitive liquid rocket fuel that could maintain the same favorable characteristics as hydrazine and MMH but that has fewer hazards to humans and the environment.

A three step reaction sequence was proposed, starting with the reaction of 1,1-dimethylhydrazine with chloroacetaldehyde to form 1,1-dimethyl-2-[2-

chloroethyl]hydrazone (Figure 5.16). This hydrazone would then be reduced, using borane to form 1,1-dimethyl-2-[2-chloroethyl]hydrazine. In the final step, this intermediate would be reacted with sodium azide to displace the chloride and form the desired DMAEH product.

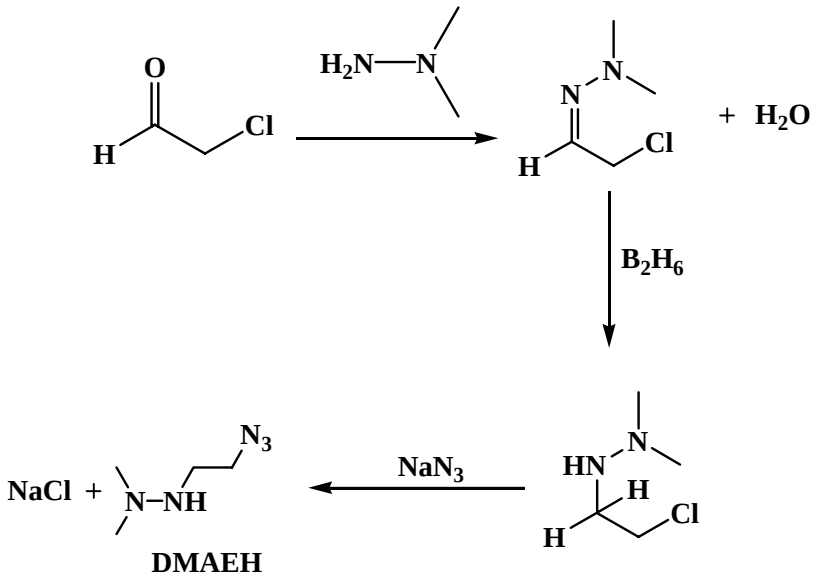

Figure 5.16 New proposed three step synthesis for the formation of 1,1-dimethyl-2-[2-azidoethyl]hydrazine (DMAEH)

Perdicchia and co-workers reported the synthesis of 1,1-dimethyl-2-benzylidene-hydrazone from the reaction of 1,1-dimethylhydrazine with benzaldehyde in toluene.[21] Collection of the water formed drove the reaction to completion and 1,1-dimethyl-2-benzylidene-hydrazone was isolated with a 99% yield. This hydrazone was then reduced to 1,1-dimethyl-2-benzylidene-hydrazine hydrochloride by reaction with $NMe_3 \bullet BH_3$ followed by HCl. This formed the desired hydrazine hydrochloride in 97% yield.[21] In our research, the initial reaction of 1,1-dimethylhydrazine with benzaldehyde was therefore run in toluene at 130°C taking advantage of the toluene/water azeotrope to

collect the water formed and drive the reaction toward completion. For the second step, it was decided to then use $NMe_3 \bullet BH_3$ and HCl followed by neutralization with dimethylaminopyridine (DMAP) in toluene to form DMAEH (Figure 5.17).

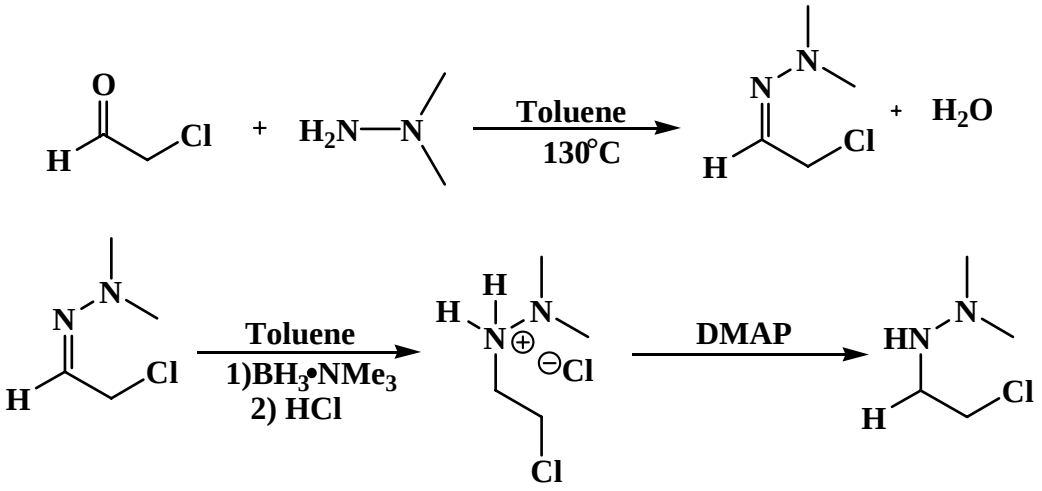

Figure 5.17 Reaction conditions chosen for the new DMAEH synthetic strategy

Chloroacetaldehyde is commercially available as a ~50% solution by weight in water. The chloroacetaldehyde was not isolated prior to beginning this reaction. Instead the chloroacetaldehyde/water solution and 1,1-dimethylhydrazine were mixed together in toluene. A standard Dean-Stark trap and set up were used to remove water from the starting material as well as from the reaction.

After running the reaction for 12 hours at 130°C, a dark brown oil was formed in the reaction flask, which was analyzed by ^{1}H and ^{13}C NMR. Unfortunately, neither peaks indicative of the starting material nor desired product could be seen in the NMR spectra. At this point, issues with the reaction were identified: 1) the chloroacetaldehyde/water

mixture was unstable at the reaction temperature of 130°C and 2) the chloroacetaldehyde should be isolated from the water solution ex situ.

To isolate the chloroacetaldehyde for this reaction, extraction was attempted with chloroform and ether. With each solvent, 3 extractions of 25mL were performed. After extraction, both the organic and the aqueous layers were analyzed by ^{1}H and ^{13}C NMR. Using chloroform as a solvent, after extraction the chloroacetaldehyde was seen in both the organic and the aqueous layers by NMR analysis. However, using ether as the solvent, chloroacetaldehyde was only seen in the organic layer. Within the limits of the NMR, no aldehyde remained in the water, suggesting that chloroacetaldehyde was almost quantitatively extracted in the ether layer. Based on these results, ether was chosen as the favorable solvent for extraction.

In parallel, the isolation of chloroacetaldehyde from water was investigated using an azeotropic distillation. Pentane exhibits an azeotrope with water at 34.6°C. The azeotrope was carried out at reflux conditions using a Dean-Stark set up. Twelve milliliters of ~50% chloroacetaldehyde solution were added to 100mL of pentane. This mixture refluxed for 24 hours. Calculations predicted that 7.85 mL of water should be removed during the drying process. Experimentally 8 mL were removed, a 1.3% difference. The difference was attributed to the commercial mixture that is supplied as approximately 50% by weight, not an exact amount. ^{1}H NMR analysis showed no traces of chloroacetaldehyde. Chloroacetaldehyde remained in the round bottom flask with the pentane, as confirmed by ^{1}H and ^{13}C NMR analysis.

As the reaction of chloroacetaldehyde with 1,1-dimethylhydrazine requires an azeotrope to remove water and drive the reaction to completion, it made the most sense to

use the azeotropic method of chloroacetaldehyde isolation as well. Once the chloroacetaldehyde was isolated, 1,1-dimethylhydrazine was simply added to the same reaction flask. This addition was done with vigorous stirring at 0°C. The reaction mixture was allowed to reflux overnight, still set up with a Dean-Stark trap to collect the water produced in the condensation reaction. After 12 hours, approximately 2 mL of water (a 7% excess from the 1.8mL expected) had been collected and a dark brown oil had been formed.

^{1}H NMR, ^{13}C NMR, and electrospray ionization mass spectrometry (ESI MS) analysis were run on this brown oil. Both ^{1}H and ^{13}C NMR results showed loss of the aldehyde (at 9.5ppm and 198.3ppm respectively) and formation of a new peak (at 6.3ppm and 117ppm respectively) which is in the expected range for a proton attached to the carbon of a dimethylhydrazone.[22-23] They also both showed peaks consistent with the methyl groups from 1,1-dimethylhydrazine at 2.5 in the ^{1}H NMR and 54.5 in the ^{13}C NMR. However, extra peaks that could not be accounted for with the expected structure were also present. The ESI MS results showed the highest peak with a mass of 145 and nothing at 120, the mass of the expected product (Figure 5.18).

From this, it was hypothesized that rather than the desired reaction taking place (Figure 5.17), a double substitution may have occurred to form both hydrazone and a quaternary salt, 1-[2-[2,2-dimethylhydrazono]ethyl]-1,1-dimethylhydrazinium chloride (Figure 5.19). This molecule has the mass of 145, consistent with MS+ analysis. While this result was encouraging because the desired hydrazone was formed, the simultaneous formation of the quaternary ammonium salt via displacement of the Cl was an unexpected result.

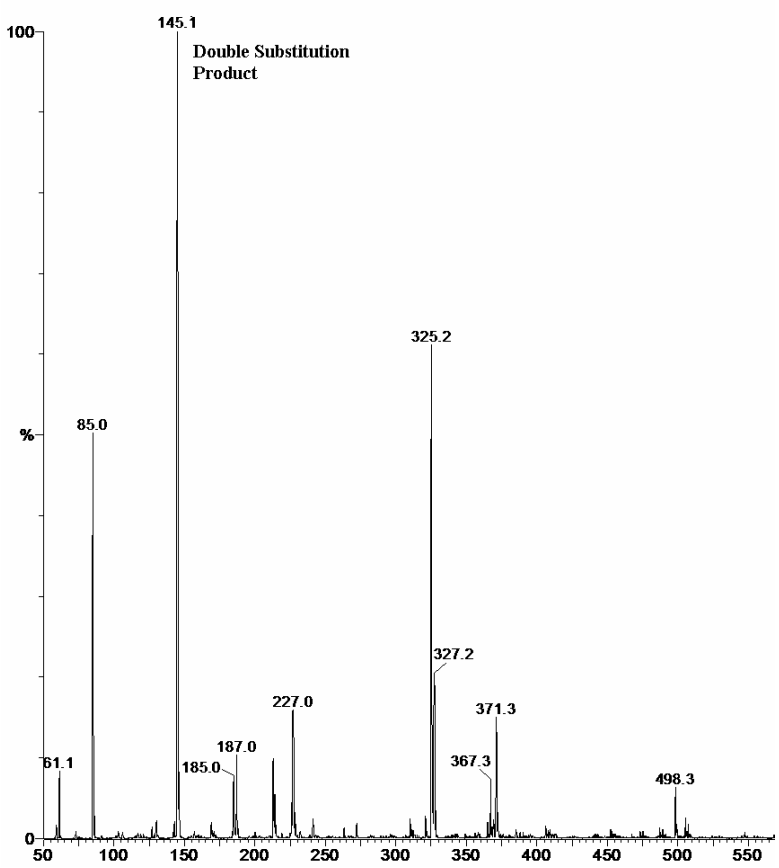

Figure 5.18 ESI MS results showing double substitution product with a mass of 145

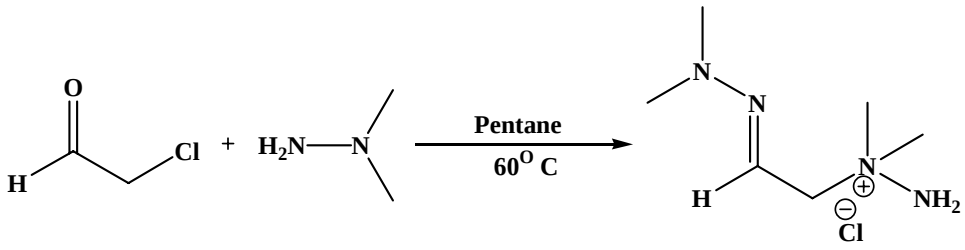

Figure 5.19 Product formed from reaction of chloroacetaldehyde and 1,1-dimethylhydrazine, as determined by NMR and mass spec.

5.3.2 Synthesis of De-DMAEH

The synthesis of 1,1-dimethyl-2-[2-azidoethyl]hydrazone or De-DMAEH (Figure 5.4) was investigated. It was speculated that this molecule should have similar ignition

and combustion characteristics as DMAEH with the added benefit of a simpler synthesis method. Because this molecule contains a C=N double bond, it can actually exist in two different geometric isomers: the syn form in which both substituents are on the same side of the double bond (Figure 5.20 A) and the anti form in which the substituents are on opposite sides of the double bond (Figure 5.20 B). Density functional theory calculations were performed using a density functional wavefunction with a 6-31G* basis set to determine the lowest energy confirmation of each form and whether any intramolecular interactions could take place. In the syn form (Figure 5.20A) the azide group is pointed away from the rest of the molecule, causing both no steric interference and no intramolecular interaction and the energy was found to be -1132829.15kJ/mol. In the anti form (Figure 5.20 B), a similar conformation to DMAEH is observed, with an intramolecular interaction occurring, but not with the terminal amine nitrogen and the energy was found to be -1125825.89kJ/mol.

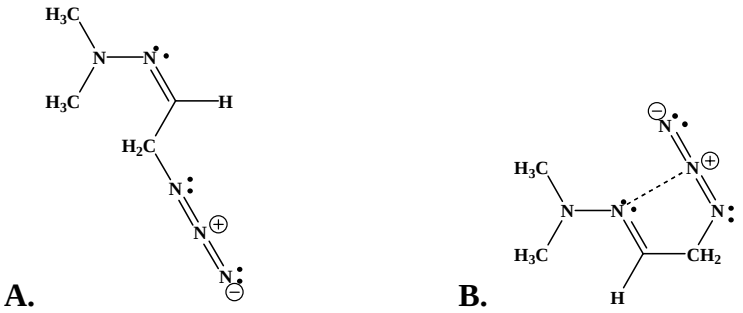

Figure 5.20 1,1-dimethyl-2-[2-azidoethyl]hydrazone in **A**. Syn and **B**. Anti configuration

The proposed reaction was a three step process, beginning with the reaction of chloroacetaldehyde with sodium azide (Figure 5.21). Sodium azide (0.165g, 2.5mmol) was dissolved in 5mL of water. Chloroacetaldehyde solution (0.34mL, 2.3mmol

chloroacetaldehyde) was added, and this mixture was allowed to stir at room temperature for 24 hours. After 24 hours, the reaction mixture was analyzed by ^{1}H NMR and ^{13}C NMR both of which showed no indication of reaction occurring. Only starting material was seen.

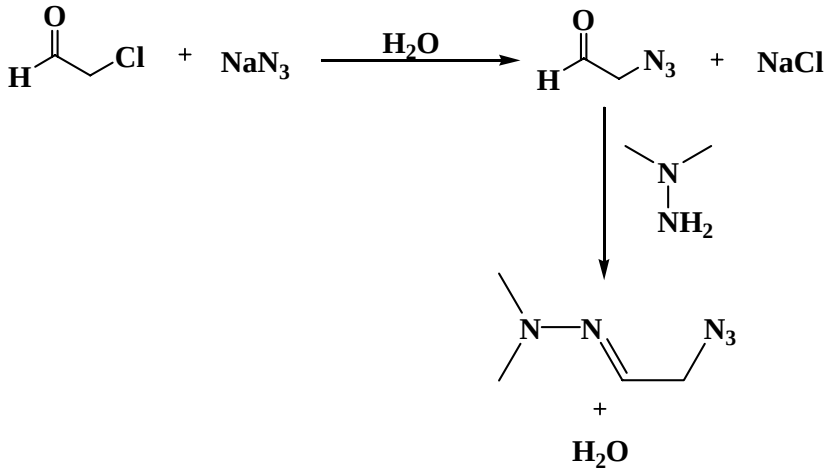

Figure 5.21 New proposed synthesis method for De-DMAEH molecule

The same procedure was repeated with five different sets of conditions, which are summarized in Table 5.1. In these five runs, the reaction time was varied from 4 to 24 hours, and the reaction temperature was varied from 50°C to 90°C. Under these conditions, no product formation was observed by ^{1}H and ^{13}C NMR at the lower temperatures (50°C for 7 hours, and 60°C for 5 hours), while at the higher temperatures and at the longer time complete decomposition was observed. The chloroacetaldehyde appeared to decompose when heated over 60°C for an extended amount of time. It should be pointed out that chloroacetaldehyde can exist as a hydrate and this may be the reason for the low reactivity toward nucleophilic displacement (Figure 5.22).

Table 5.1 Reaction of sodium azide and chloroacetaldehyde in water under various conditions

Run Number	Reaction Time	Reaction Temperature	Yield
1	7 hours	50°C	0
2	4 hours	90°C	Decomposition
3	5 hours	70°C 2hrs, 60°C 3hrs	Decomposition
4	5 hours	60°C	0
5	24 hours	60°C	Decomposition

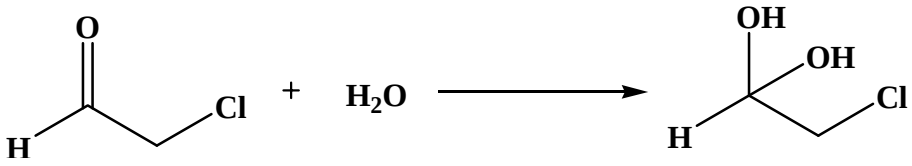

Figure 5.22 Formation of hydrate from chloroacetaldehyde in the presence of water.

In order to address this problem, this reaction was attempted under anhydrous conditions. Three different solvents: ether, toluene and methyl-*tert*-butyl ether were investigated. Chloroacetaldehyde removal by extraction was re-visited at this point and toluene and methyl-*tert*-butyl ether were found upon testing to also be effective extraction solvents. Brine saturation was used when necessary to induce a clear phase split for extraction. After extraction, ^{1}H NMR was used to quantify the concentration of the chloroacetaldehyde in solvent solutions. This was done by comparison of the integrations for known solvent peaks and the aldehyde proton peak at 9.5. These concentrations were found to be 0.93M for ether, 0.43M and 0.72M respectively for two different toluene extractions and 2.4M for methyl-*tert*-butyl ether. Sodium azide was added in a 1:1 molar ratio with the chloroacetaldehyde and each reaction was run using 3.1mmol of both chloroacetaldehyde and NaN_3. Due to the limited solubility of sodium azide in these solvents, in some cases a 5 wt.% amount of the phase transfer catalyst

tetrabutylammonium chloride (TBACl) was added. The reactions were run at either room temperature or 40°C and at time lengths ranging from 2 to 12 hours (Table 5.2). ^{1}H NMR analysis was used to check for product formation as the CH_2 peak for 2-azido-acetaldehyde should shift up field from the peak seen at 4.5 for the corresponding protons of chloroacetaldehyde.[24]

Table 5.2 Reaction of sodium azide and chloroacetaldehyde under a variety of anhydrous conditions

Run Number	Solvent	Phase Transfer Catalyst	Reaction Time (hrs)	Reaction Temp.	Yield
1	Ether	none	2	40°C	0
2	Ether	none	6	40°C	0
3	Ether	none	12	room temperature	decomposition
4	Toluene	TBACl	4	40°C	decomposition
5	Toluene	TBACl	4	40°C	decomposition
6	Methyl *tert*-butyl Ether	none	4	40°C	0
7	Methyl *tert*-butyl Ether	none	2.5	40°C	0

Using ether as the solvent, reaction at 40°C for two hours showed neither reaction nor decomposition when analyzed by ^{1}H NMR and ^{13}C NMR (Table 5.2, Run 1). After reacting for another 4 hours (six hours total) ^{1}H NMR results were inconclusive (Table 5.2, Run 2). The reaction was then run for an additional six hours, bringing the total reaction time to 12 hours to see if a longer time would help drive the reaction to completion. However, under these conditions complete decomposition was seen by NMR analysis (Table 5.2, Run 3).

The next solvent tested was toluene. The same procedure was followed as with ether, however 5% TBACl by weight was also added to the reaction mixture to act as a phase transfer catalyst. After heating for 4 hours at 40°C, the reaction was stopped and

^{1}H NMR analysis was performed. Chloroacetaldehyde was present, but only 77% of the original amount remained. As no product peaks were visible, and several small unidentified peaks appeared in the 3 to 5 ppm range it was determined that amount was lost to decomposition (Table 5.2, Run 4)**.** This experiment was repeated with similar results (Table 5.2, Run 5)

Finally, the solvent methyl-*tert*-butyl ether was investigated. Chloroacetaldehyde and sodium azide were reacted at 40°C for 4 hours and for 2.5 hours. In both cases, starting material was seen by NMR analysis, with no concentration change, indicating neither decomposition nor trace product formation (Table 5.2, Runs 6-7).

The chloroacetaldehyde comes in a ~50% solution with water. Water and chloroacetaldehyde can form a hydrate, (Figure 5.22) as well as other aggregates, such as its trimeric form 2,4,6-tris(chloromethyl)-1,3,5-trioxane (Figure 5.23). This chloroacetaldehyde trimer was identified by ^{1}H NMR in the chloroacetaldehyde starting material by characteristic peaks at 3.55ppm and 5.05ppm which represent the CH_2 and CH protons in this molecule, respectively.[25] Several other small peaks were also present in the 3-5ppm range, that while not identified, indicated the presence of other impurities in the starting material. Though the chloroacetaldehyde was extracted into organic solvents prior to any reaction taking place, ^{1}H NMR analysis indicated that these impurities were being extracted as well (Figure 5.24). At this juncture it was decided to pursue an alternate synthetic route.

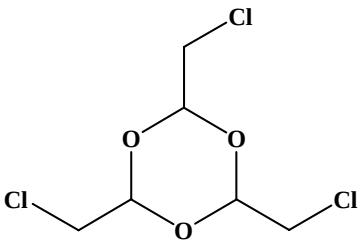

Figure 5.23 2,4,6-tris(chloromethyl)-1,3,5-trioxane

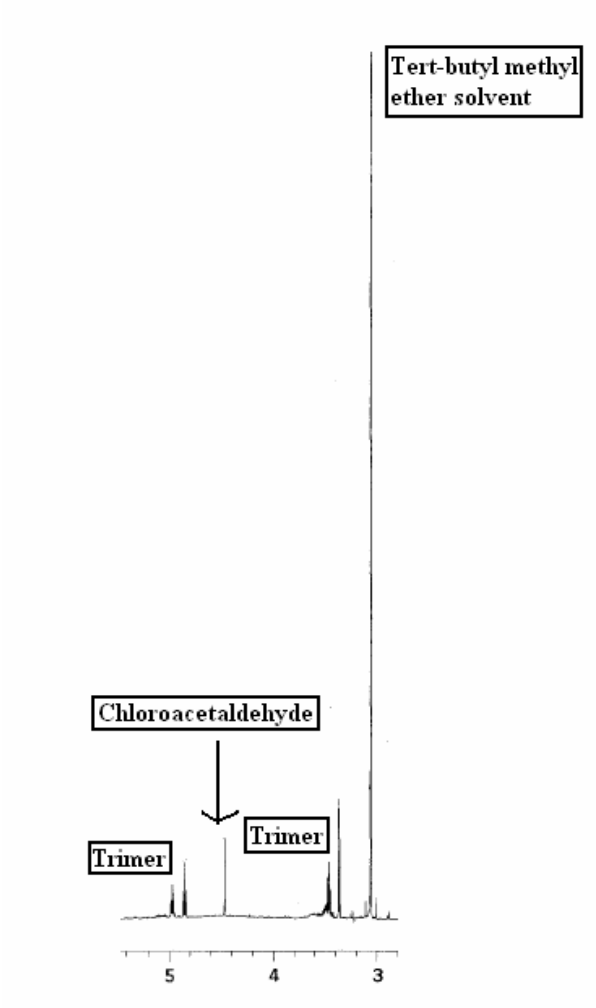

Figure 5.24 ^{1}H NMR, 3-5ppm region, showing impurities extracted with chloroacetaldehyde

5.3.3 De-DMAEH Synthesis from Bromoacetaldehyde Diethyl Acetal

A three step synthetic pathway was developed starting from bromoacetaldehyde diethyl acetal (BADA) (Figure 5.25). This synthesis involves first deprotecting the BADA to form bromoacetaldehyde (BAA) under acidic conditions. BAA is then reacted with sodium azide to form the 2-azido-acetaldehyde, which is subsequently reacted with 1,1-dimethylhydrazine to form the De-DMAEH product. The first two steps of this reaction are known in literature.[26-28] The third step, hydrazone formation, was demonstrated previously in our lab with the chloroacetaldehyde, so it is anticipated that 2-azido-acetaldehyde will react in a similar manner (Figure 5.19).

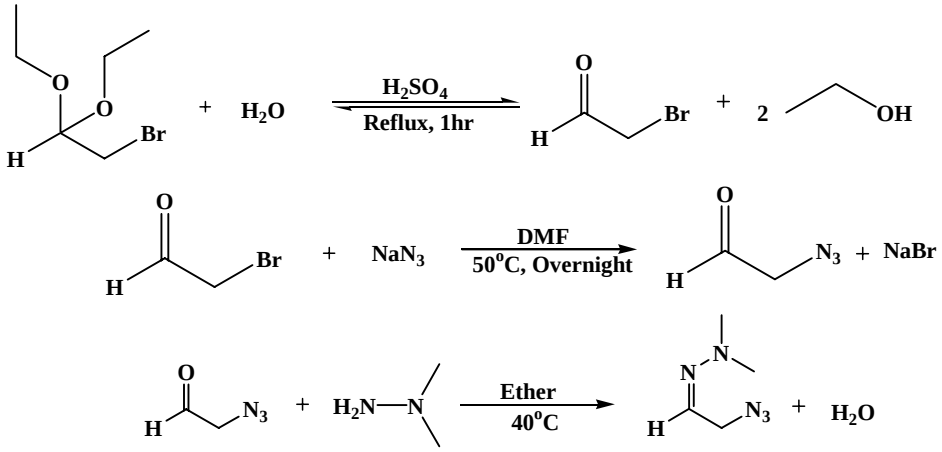

Figure 5.25 Proposed synthesis of DMAEH starting with BADA

To carry out the first step, BADA (5mL) and sulfuric acid (H_2SO_4, 5mL of 0.1N solution) in water were combined and allowed to react for 1 hour at 100°C. The resulting crude product was analyzed by ^{1}H and ^{13}C NMR and both spectra showed the presence of both the desired bromoacetaldehyde (BAA) as well as BADA starting material. NMR was chosen to analyze this reaction as aldehyde formation produces a distinct peak, at

9.5ppm in ^{1}HNMR and in the 190ppm to 195ppm range in ^{13}C NMR, which can be easily identified.[29-30] Using the integration of this peak in the ^{1}H NMR in comparison with BADA peaks also provides a measurement of how much BAA has been formed.

The reaction was repeated with the time increased to 2 hours. In this case, the crude product mixture showed a ratio of 1:3.8 BAA:BADA (21% yield) as determined by integration of ^{1}H NMR. Twenty different sets of conditions were tested to maximize the formation of BAA. Solvent, reaction time, temperature, the amount of water used, and the amount of acid were all examined. The results of these different reactions can be seen in Table 5.3. The use of azeotrope to remove ethanol as it is formed in order to shift the equilibrium towards the formation of BAA was also examined.

When either no solvent or THF solvent were used with no means of removing the ethanol, BADA was always the major component of the product mixture when analyzed by ^{1}H and ^{13}C NMR. With no solvent present, the best ratio achieved was a 1:3 BAA:BADA ratio (25% yield), when heating for 2 hours at 100°C (Table 5.3, Run 4). Using THF as a solvent improved that ratio to 1:1.74 BAA:BADA (36% yield) when heated for 1 hour at 40°C.

One synthesis attempt was made with toluene as the solvent (Table 5.3, Run 14). However, complete decomposition of BADA occurred when heated for 1 hour at 85°C, so it was not pursued further. Ultimately, switching the solvent to acetonitrile and using it in combination with an azeotrope to remove ethanol gave the best results (1 hr., 92°C, 2:1 BAA:BADA, 67% yield, Figure 5.26). In this reaction, water was introduced with the sulfuric acid as it was a 0.1N aqueous solution. Halfway through the reaction, an

Table 5.3 Reaction conditions tested to optimize bromoacetaldehyde synthesis

Run Number	Solvent	Reaction Time	Reaction Temp.	Amt. of Water	Amt. of Acid	Ethanol Removal	Ratio BAA/BADA
1	none	1 hour	100°C	5mL 0.1N H2SO4	5mL 0.1N H2SO4		
2	none	2 hours	100°C	5mL 0.1N H2SO4	5mL 0.1N H2SO4		1/3.8
3	none	overnight	100°C	5mL 0.1N H2SO4	5mL 0.1N H2SO4		Decomposition
4	none	2 hours	100°C	5mL 0.1N H2SO4	5mL 0.1N H2SO4		1/3
5	tetrahydrofuran	1 hour	65°C	5mL 0.1N H2SO4	5mL 0.1N H2SO4		1/2.6
6	tetrahydrofuran	1 hour each temp.	65°C, 70°C	5mL 0.1N H2SO4	5mL 0.1N H2SO4		1/4.2
7	tetrahydrofuran	1 hour 65°C, 2 hours 70°C	65°C, 70°C	5mL 0.1N H2SO4	5mL 0.1N H2SO4		1/5.9
8	tetrahydrofuran	1 hour	40°C	none	0.5mL pure H2SO4		1/1.74
9	tetrahydrofuran	2 hours	40°C	none	0.5mL pure H2SO4		1/1.75
10	tetrahydrofuran	3 hours	40°C	none	0.5mL pure H2SO4		1/2.43
11	tetrahydrofuran	overnight	40°C	none	0.5mL pure H2SO4		1/2.3
12	tetrahydrofuran	overnight	60°C	none	0.5mL pure H2SO4		1/6.76
13	none	overnight	60°C	5mL 0.1N H2SO4	5mL 0.1N H2SO4		1/3.9
14	toluene	1 hour	85°C	none	0.5mL pure H2SO4	azeotrope	Decomposition
15	acetonitrile	1.5 hours	92°C	none	0.5mL pure H2SO4	azeotrope	1/0.84
16	acetonitrile	1.5 hours	96°C	none	0.5mL pure H2SO4	azeotrope	1:2 and Decomposition
17	acetonitrile	1 hour	96°C	none	0.5mL pure H2SO4	azeotrope	Decomposition
18	acetonitrile	1 hour	90°C	none	0.5mL pure H2SO4	azeotrope	1:1 and Decomposition
19	acetonitrile	1 hour	80°C	none	0.5mL pure H2SO4	azeotrope	1:2 and Decomposition
20	acetonitrile	2 hours	92°C	0.5mL	0.5mL pure H2SO4	azeotrope	1/1.0
21	acetonitrile	1 hour	92°C	1.2mL	0.5mL pure H2SO4	azeotrope	1/1.7
22	acetonitrile	1 hour	92°C	5mL 0.1N H2SO4	5mL 0.1N H2SO4	azeotrope	1/0.56

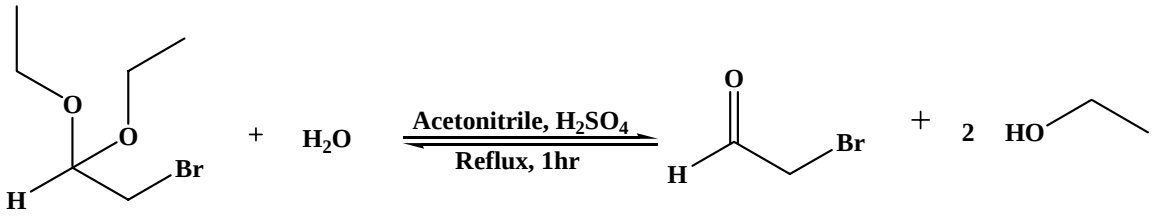

Figure 5.26 Optimized deprotection of BADA to BAA

additional 20mL of acetonitrile were added to the reaction pot to replenish that which was lost in azeotrope collection. The BAA was not purified, instead the entire mixture containing at 2:1 ratio of BAA:BADA in acetonitrile was used in the next step of the synthesis.

Prior to the next step, the H_2SO_4 in the system was neutralized using solid potassium carbonate. An excess amount was added to the reaction mixture, and stirred overnight. It was removed by filtration through a fritted funnel. Sodium azide was added in excess (1.4:1 molar ratio) to 5mL of the BAA solution (0.0025mol BAA). This mixture was reacted overnight at 50°C with stirring (Figure 5.27). This solution turned a very dark brown color after reaction overnight. Prior to NMR analysis, a sample was removed, and concentrated by blowing N_2 gas over the surface to remove solvent. ^{13}C NMR showed disappearance of the aldehyde peak at 191ppm indicating either reaction or

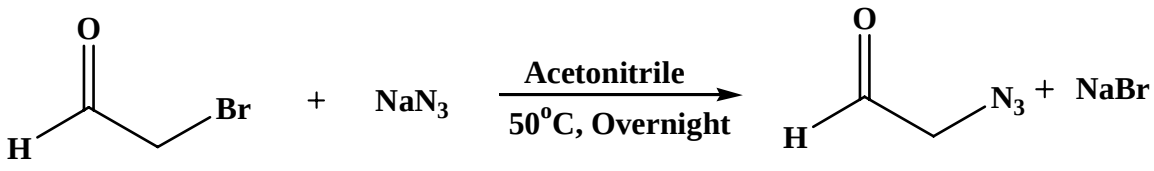

Figure 5.27 Second step in De-DMAEH synthesis.

decomposition of the starting material. A new peak did appear, however, at 178ppm, an upfield shift which is consistent with expected signal for the carbonyl carbon of the desired product. The presence of other peaks indicates that other compounds are present, possibly from the decomposition of the desired product or of the BADA remaining in the system, as both ^{1}H and ^{13}C NMR no longer show the presence of BADA. However, these compounds were not identified. GC-MS analysis of the reaction mixture showed a peak with mass corresponding to the desired intermediate (Figure 5.28). Several other peaks were present as well, all of which appeared to contain one to two bromine atoms. This could correspond to decomposition products from either BADA or unreacted BAA, as was seen by NMR analysis.

This crude reaction mixture was then reacted with dimethyl hydrazine (Figure 5.29). Both ^{1}H NMR and ^{13}C NMR spectra showed the disappearance of the aldehyde peak, and the appearance of a peak upfield at 7.12ppm and 134ppm respectively, which is in the predicted region for the hydrogen attached to the carbon of a dimethylhydrazone.[22-23] The appearance of a peak consistent with methyls attached to a hydrazone group was observed at 2.4ppm in the ^{1}H NMR and 42.4ppm in the ^{13}C NMR. LC-MS and GC-MS were run on the crude product mixture. Both showed two major peaks with masses of 127.9mu and 142.9mu (Figure 5.30). The mass of 127.9mu corresponds to the desired product, while the mass of 142.9mu indicates an undesired side product, which will later be identified. As no internal standard was used, a quantitative amount of the two products could not be determined.

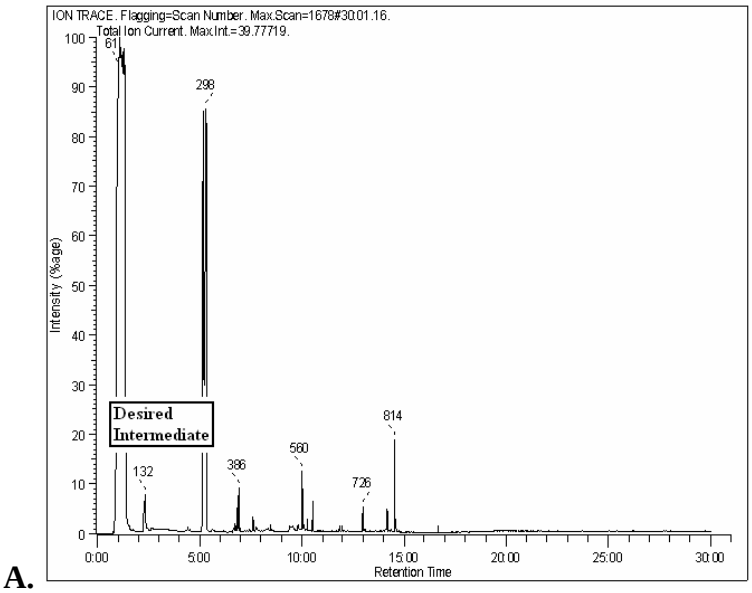

A.

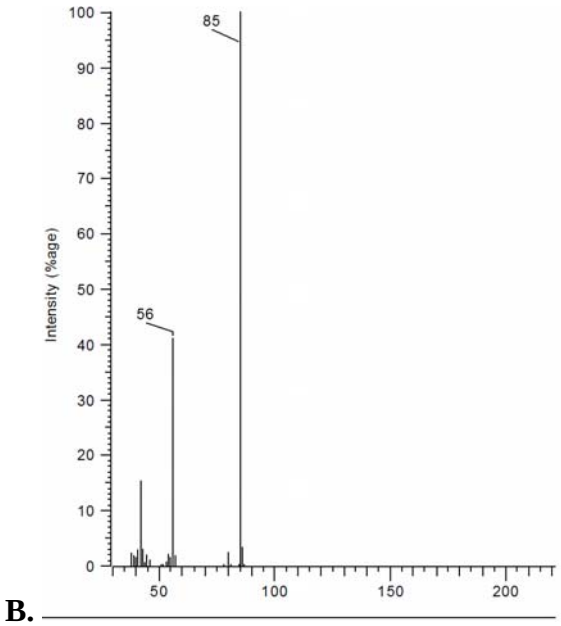

B.

Figure 5.28 A. GC-MS chromatogram of crude product with **B.** Mass spectrum of desired product peak.

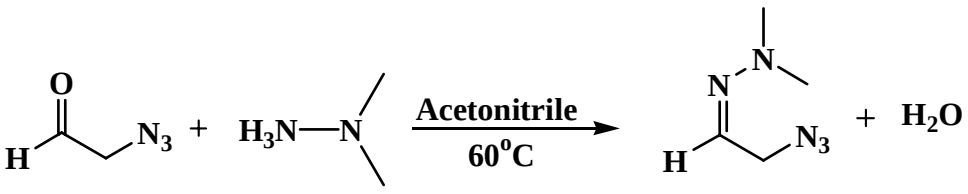

Figure 5.29 Third step of De-DMAEH reaction

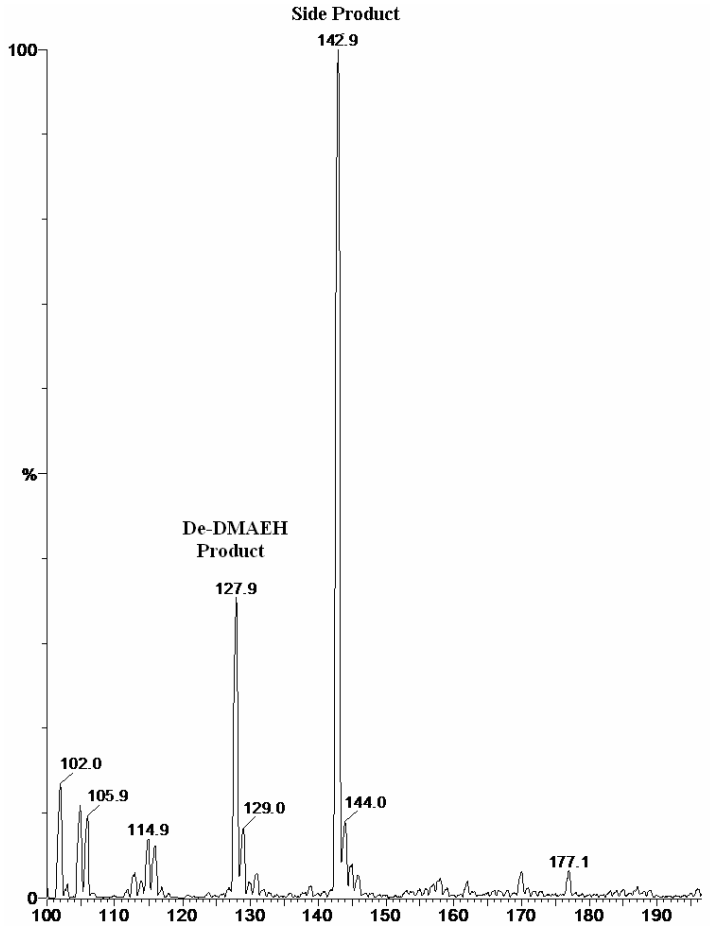

Figure 5.30 Mass spectrum showing the formation of the desired De-DMAEH product, as well as a side product

Though initial results were encouraging, reproducing these results proved difficult. In fifteen repeats of the entire multi-step De-DMAEH synthesis reaction, only four showed signals in the ^{1}H NMR consistent with the formation of the desired product. In order to identify where problems in the reaction method were occurring each step was carried out separately followed by ^{1}H and ^{13}C NMR analysis as well as ESI-MS. These steps included formation of BAA from BADA, neutralization of BAA product solution with potassium carbonate, reaction of BAA solution with NaN_3 to form 2-azido-

acetaldehyde, and reaction of that product solution with 1,1-dimethylhydrazine to form De-DMAEH. From this study it was determined that a problem lay in the neutralization of the BAA product solution. This step was run three separate times, and a comparison of ^{1}H NMR spectra taken before and after the neutralization showed substantial loss of BAA product formed in each instance. Over the three attempts, that loss ranged from 35%-100% of BAA formed.

In order to address this problem, the reaction was modified by using the solid acid resin Dowex^{TM} M-31 instead of liquid H_2SO_4 to form BAA. This resin is sulfonic acid embedded on a styrene matrix and can be removed by filtration, eliminating the need for a neutralization step in the reaction procedure. In the modified reaction sequence, 1 g Dowex resin and 2mL of water were added to the mixture as a substitute for H_2SO_4 solution in water and the reaction was run under the same conditions as before. After the reaction was completed the ^{1}H NMR of this initial reaction showed a ratio of 1.6:1 BAA:BADA (62% yield), slightly lower than the 2:1 seen with H_2SO_4. However, when the reaction time was increased to 90 minutes from the initial 60 minutes, this ratio improved to 2.8:1 BAA:BADA (74% yield). As the Dowex resin showed the same or better catalytic ability as H_2SO_4 with the benefit of no neutralization step needed, its use was incorporated into the reaction procedure, and consistent product formation was now observed.

5.3.4 Identification of De-DMAEH Side Product

Before attempts were made to purify the De-DMAEH the identity of the side product was determined. A mass of 143 is in agreement with the structure shown in Figure 5.31.

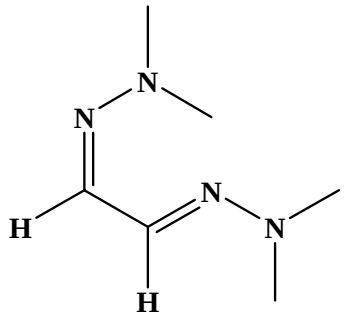

Figure 5.31 Side product formed in De-DMAEH synthesis reaction, glyoxal, bis(dimethylhydrazone)

This compound is the known molecule glyoxal bis(dimethylhydrazone), which can be isolated as a clear yellow oil. It was speculated that along with the desired reaction outlined above, a parallel competing reaction path was also occurring (Figure 5.32). In this mechanism, after the hydrazone (compound 3, Figure 5.32) is formed by reaction with 1,1-dimethylhydrazine, a beta hydrogen abstraction can occur. This intermediate molecule (compound 4, Figure 5.32) can then lose nitrogen to form compound 5 (Figure 5.32). This compound is attacked by a second molecule of 1,1-dimethylhydrazine leading to the loss of ammonia and formation of this side product. This was an important discovery as now that the side product has been identified as glyoxal, bis(dimethylhydrazone) and its mechanism proposed, attempts could be made to prevent its formation.[31]

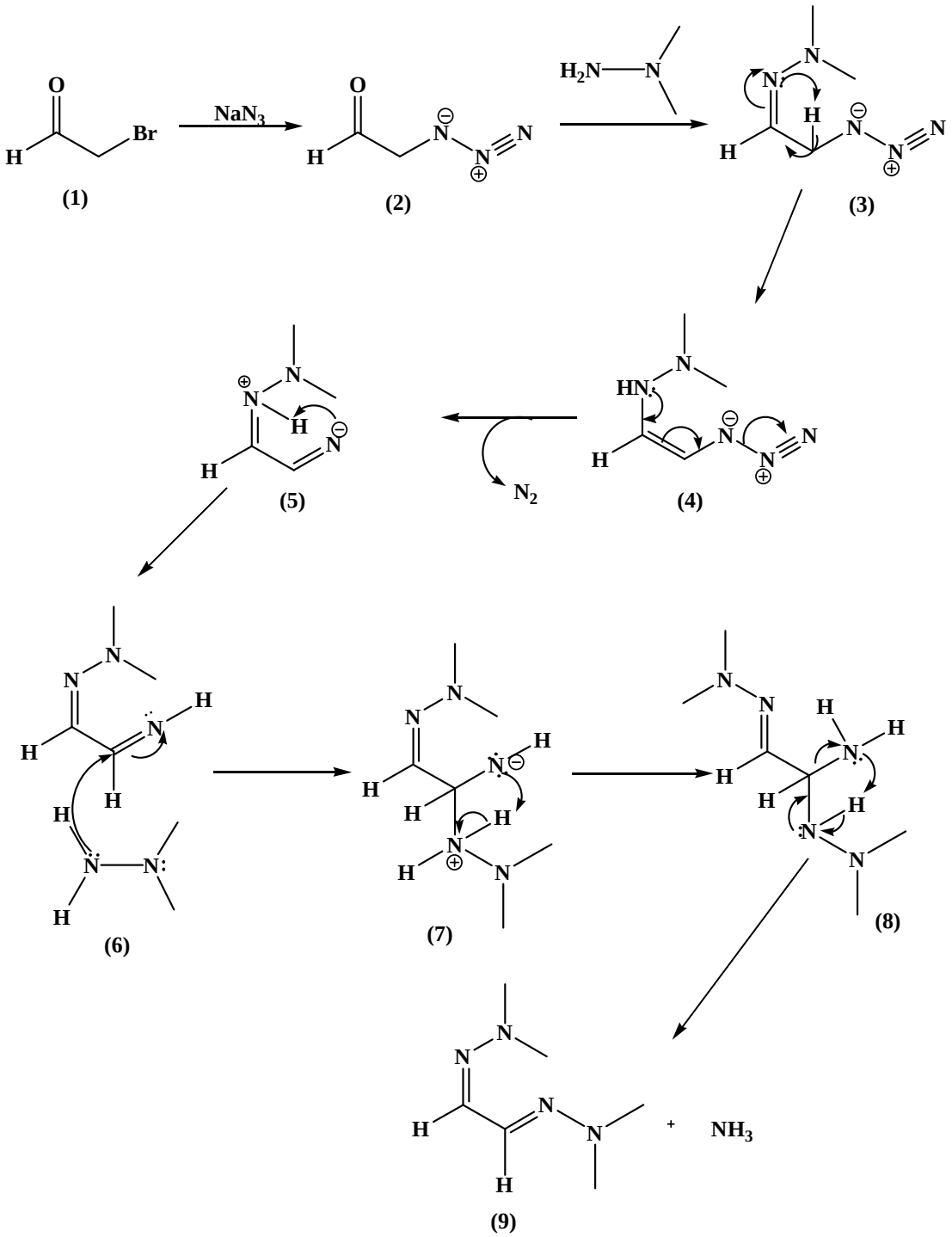

Figure 5.32 Mechanism for side product formation in De-DMAEH reaction

5.3.5 Purification of De-DMAEH Product

In order to determine if separation by of De-DMAEH from the glyoxal, bis(dimethylhydrazone) side product by column chromatography would be possible thin layer chromatography was run on the reaction product mixture. Ethyl acetate, hexane, and combinations of the two were tested as separation solvents. Pure ethyl acetate was found to be the most effective. Using this eluent, two spots could be visualized after treatment of the plate with tungstophosphoric acid, one with a retention value close to 1 and one with a value of 0. It was anticipated that these two spots corresponded to the two products seen by LC-MS and GC-MS.

A silica column was prepared and run using ethyl acetate. As the materials have a bright yellow color it was very easy to see when all of the first product had moved through the column. This was also confirmed by TLC. After the first component had eluted, methanol was used to elute the other compound. Again, being highly colored it was easy to see as it moved through the column. Both samples were concentrated and examined by ^{1}H NMR, ^{13}C NMR, and ESI-MS.

The compound eluted by ethyl acetate was pure glyoxal bis(dimethylhydrazone) (Figure 5.31), which was confirmed by both mass spectroscopy (Figure 5.33) and comparison with ^{1}H NMR and ^{13}C NMR found in literature.[32] The methanol fraction was also analyzed by ^{1}H NMR, ^{13}C NMR and ESI-MS. By NMR, no desired product was seen, though the ^{1}H NMR showed small unidentified peaks at 1.1ppm and 1.9ppm. The mass spec showed a mixture of peaks and fragments, one of which did have the desired mass, however, the mass spec was not clean and no conclusion can be drawn from this. This same procedure was repeated with a second reaction, and the same results

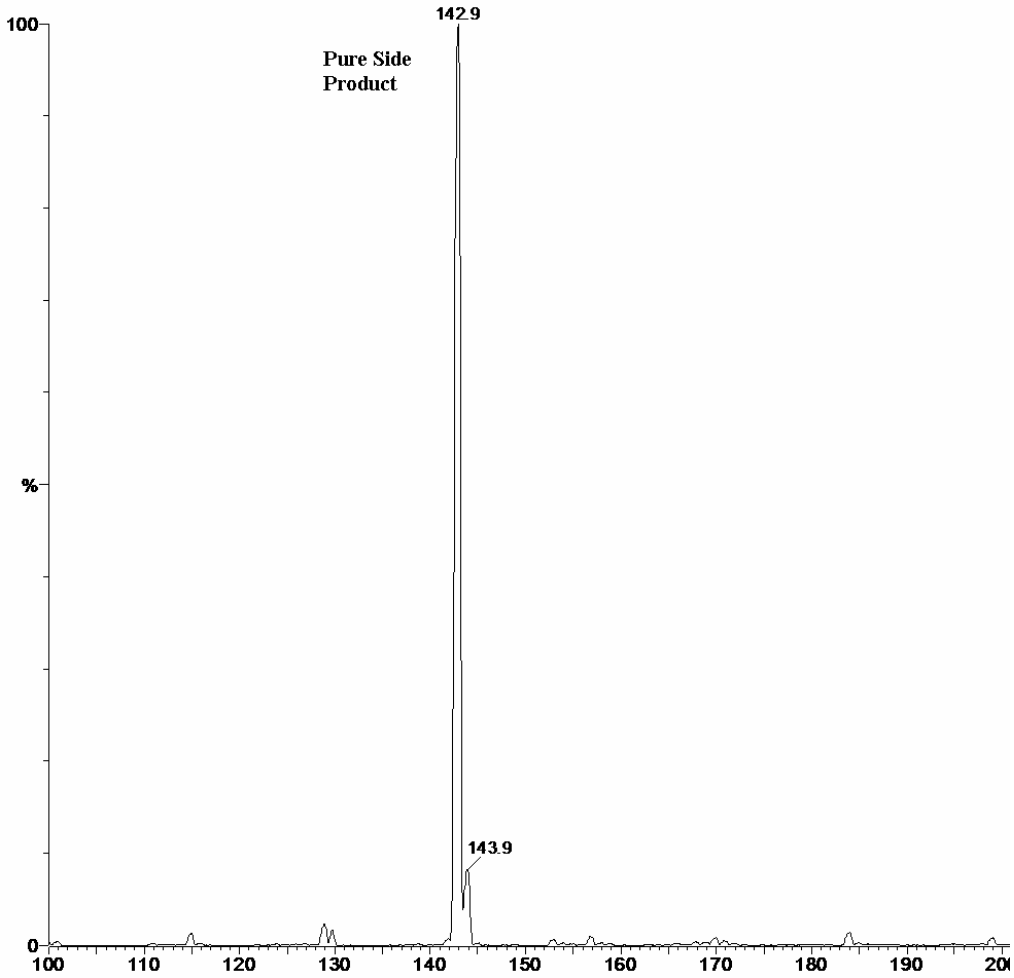

Figure 5.33 Pure glyoxal, bis(dimethylhydrazone) side product after column separation

were obtained. From these results, it was theorized that De-DMAEH breaks down on the column due to the acidic nature of the silica, as an acidic proton could be abstracted by and react with any of the nitrogen atoms present in the molecule.

The silica and TLC plates were pretreated with a 5% triethylamine solution in ethyl acetate, to neutralize acidic sites. As with the original tests, two spots were seen, one that moved with the ethyl acetate solvent front, and one that remained at the baseline. The pre-treated silica was then loaded into a column and the separation was run as previously, using pure ethyl acetate followed by pure methanol as the mobile phase. As

before, one bright yellow product compound eluted off the column using ethyl acetate as the mobile phase and a second was removed when methanol was used. Both were concentrated by evaporation of the solvent, and analyzed by ^{1}H and ^{13}C NMR and ESI MS. The sample collected in ethyl acetate was glyoxal bis(dimethylhydrazone). The product collected in methanol was a single compound, which ESI MS showed to have a mass of 101.9. Identification of this compound has not been determined at this time. This separation was repeated with identical results.

5.3.6 De-DMAEH Synthesis Modification

After the separation difficulties that were encountered, a few modifications were made to the reaction in an effort to both increase the yields of De-DMAEH being formed and simultaneously suppress formation of the glyoxal, bis(dimethylhydrazone) side product. In the first reaction step, formation of BAA from BADA, an azeotrope was used to collect ethanol formed in the reaction, however, the water present in the reaction can also be lost as it too forms an azeotrope with the acetonitrile solvent. Without water present the deprotection reaction to form BAA cannot occur (Figure 5.26). To compensate for this, an additional 2mL of water were added to the reaction, halfway through. Water addition appeared to have the desired affect as the crude product mixture now showed a 3.6:1 BAA:BADA (78% yield) ratio compared to the 2:1 ratio previously observed, however this has not been repeated at this time.

The other modification made was in the third step, addition of 1,1-dimethyl hydrazine to 2-azido-acetaldehyde (Figure 5.34).

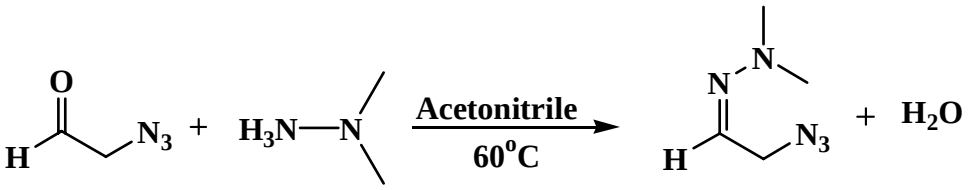

Figure 5.34 Addition of 1,1-dimethyl hydrazine to 2-azido-acetaldehyde

As discussed previously, it is believed that for glyoxal, bis(dimethylhydrazone), the De-DMAEH must react with a second 1,1-dimethyl hydrazine molecule after it has already formed. In an effort to prevent that from happening, the 1,1-dimethylhydrazine was diluted in 1mL of acetonitrile prior to addition. It was hoped this would decrease the amount of De-DMAEH that reacted further to form glyoxal bis(dimethylhydrazone). However, when ESI MS was run on the product mixture, the side product still appeared as the major peak (Figure 5.35).

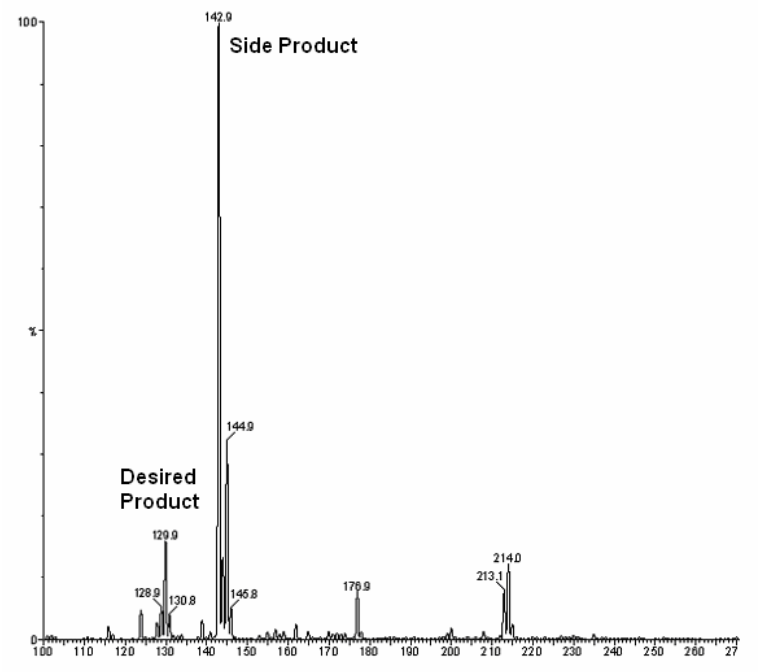

Figure 5.35 ESI spectrum of final product mixture after modifications.

5.4. Conclusions

DMAEH and its hydrazone derivative De-DMAEH were proposed as potential propellants and their syntheses were investigated. If successful, these can be alternatives to hydrazine, alleviating some of hydrazine's limitations (high vapor pressure and toxicity). A new three step reaction method was proposed starting from bromoacetaldehyde diethyl acetal. Following this method, it is believed that De-DMAEH was successfully formed, as analysis of the crude product mixture showed a compound with the desired mass, and ^{1}H and ^{13}NMR analyses showed peaks consistent with its formation. However, De-DMAEH was formed with the side product glyoxal bis(dimethylhydrazone). Attempts were made to separate the product by column chromatography, however they were unsuccessful. Once isolated, a one step reduction with borane could, in principle, be used to transform this molecule into DMAEH.

5.5. Experimental

All chemicals were ordered from Aldrich and used as received, unless noted. NMR spectra were obtained from a Bruker DRX 500 and Varian-Mercury VX400 MHz spectrometer. All mass spec analysis was performed by the The Georgia Institute of Technology Bioanalytical Mass Spectrometry Facility. The electrospray ionization mass spectrometry was performed using an Applied Biosystems 4000 QTrap hybrid quadrupole / linear ion trap tandem mass spectrometer. A VG Instruments 70SE was used for the GC mas spectrometry, and the LC mass spectrometry was done by a Micromass Quattro LC interfaced with an Agilent 1100 binary HPLC system. Lowest energy configuration calculations were performed using the Spartan software.

Synthesis of DMAEH from chloroacetaldehyde solution

Initial Reaction Conditions: Under an argon atmosphere, 1,1-dimethylhydrazine (3.2 mL, 42 mmol) was placed in a 150mL round bottom flask. A 50% solution of chloroacetaldehyde in water (6 mL, 42 mmol chloroacetaldehyde) was added drop wise with vigorous stirring at 0°C. The mixture turned a dark red color. Toluene (50 mL) was added to the mixture. The solution was warmed to 115°C and refluxed for 12 hours. No work up procedure was performed. Crude product was analyzed by ^{1}H and ^{13}C NMR; no traces of desired product seen.

Chloroacetaldehyde Extraction

Chloroacetaldehyde is available from SigmaAldrich as an approximately 50 weight % solution in water. The chloroacetaldehyde was extracted into ether (3 extractions of 25 mL each). After extraction, ^{1}H NMR analysis was performed on both the organic and aqueous layers. As no traces of chloroacetaldehyde were seen in the aqueous layer, the assumption was made that all had been successfully transferred into the organic layer. *Chloroacetaldehyde:* ^{1}H NMR ($CDCl_3$): 9.6 (s, 1H), 4.0 (s, 2H).

Chloroacetaldehyde Purification by Pentane Azeotrope

The pentane/water azeotrope occurs at 34.6°C with a composition of 1.4% water, and 98.6% pentane. Under an argon atmosphere, a 50% solution of chloroacetaldehyde in water (12 mL, 84 mmol) and pentane (100 mL) were mixed in 250 mL round bottom flask. The mixture was heated to 60°C with vigorous stirring and refluxed overnight. A Dean-Stark trap was used to collect the azeotrope. Theoretical water collected: 7.85mL.

Actual water collected: 8mL (1.3% difference). The chloroacetaldehyde remained as a clear yellowish oil layer underneath the pentane layer in the round bottom flask. ^{1}H NMR analysis showed both the water layer to be free of chloroacetaldehyde, and the chloroacetaldehyde layer to be pure compound. *Chloroacetaldehyde:* ^{1}H NMR ($CDCl_3$): 9.6 (s, 1H), 4.0 (s, 2H).

Synthesis of DMAEH from pure chloroacetaldehyde

Chloroacetaldehyde (84mmol) in pentane was cooled to 0°C under an argon atmosphere. To this, 1,1-dimethylhydrazine (6.5 mL, 85 mmol) was added dropwise with stirring. The solution was warmed to 60°C and stirred overnight. A Dean Stark trap was used to collect water (~2mL) formed during the reaction. After 12 hours, a dark brown oil formed. The crude product was analyzed by ^{1}H NMR, ^{13}C NMR and ESI MS, which confirmed formation of the double substitution product, 1-[2-[2,2-dimethylhydrazono]ethyl]-1,1-dimethylhydrazinium chloride. ^{1}H NMR ($CDCl_3$): 6.3, 4.2, 2.59, 2.56, 1.8. ^{13}C NMR ($CDCl_3$): 117.4, 69,9, 54.5, 48.9m 42.4 ESI-MS *m/z* (relative intensity): 145 ES+

ESI spectra shown in body of chapter, Figure 4.20.

Synthesis of De-DMAEH from chloroacetaldehyde solution

NaN_3 (0.165 g, 2.5 mmol) was dissolved in water (5mL) in a 50 mL round bottom flask. A 50% solution of chloroacetaldehyde in water (0.335 mL, 2.3 mmol) was added with stirring. The solution was heated to 50°C for seven hours with vigorous stirring. After cooling to room temperature, the crude product was examined by ^{1}H and ^{13}C NMR in

D_2O solvent. This was reacted under a variety of different reaction conditions as detailed in Table 4.1. In all cases either no change in the starting material or complete decomposition to small molecules was observed.

Synthesis of De-DMAEH from pure chloroacetaldehyde

Chloroacetaldehyde solution (0.335 mL, 2.3mmol chloroacetaldehyde) was extracted into tert-butyl methyl ether. NaN_3 (0.165 g, 2.5 mmol) was added to this solution. Only partial solubility was observed, so in all cases this was a heterogeneous reaction. Under an argon atmosphere, the mixture was warmed to 40°C with vigorous stirring. After four hours, heating was stopped, and all solid was removed by filtration. All reaction products were analyzed by ^{1}H and ^{13}C NMR. The same procedure was followed using anhydrous ether, tetrahydrofuran and toluene. Reaction condition modifications are described in Table 4.2

Optimized Synthesis of BAA using sulfuric acid

Under an argon atmosphere, bromoacetaldehyde diethyl acetal (5 mL, 33 mmol) and 0.1N aqueous H_2SO_4 solution (5 mL, 1 mmol) were dissolved in acetonitrile (45mL) in a 50 mL round bottom flask. This solution stirred for 1 hour at 90°C. Ethanol and acetonitrile form an azeotrope (72.9°C, 43% acetonitrile, 57% ethanol) which was collected to drive BAA product formation. After 30 minutes, additional acetonitrile (20mL) was added to the mixture to replace what was collected. After cooling to room temperature an excess of potassium carbonate (0.25g, 1.8mmol) was added. The mixture was stirred at room temperature for 12 hours. All solid was removed by filtration. The

crude product in acetonitrile was analyzed by ^{1}H and ^{13}C NMR. By these methods, a mixture was seen of BAA and the BADA starting material. *Bromoacetaldehyde diethylacetal:* ^{1}H NMR ($CDCl_3$): 4.534 (t, 1H), 3.585 (m, 2H), 3.483 (m, 2H), 1.107 (t, 6H); ^{13}C NMR ($CDCl_3$): 100.668, 61.858, 31.325, 14.416: *Bromoacetaldehyde:* ^{1}H NMR ($CDCl_3$): 9.309 (t, 1H); ^{13}C NMR ($CDCl_3$): 192.296, 35.448

Synthesis of BAA using Dowex Resin

Bromoacetaldehyde diethyl acetal (5 mL, 33 mmol), deionized water (2 mL, 111 mmol), acetonitrile (45 mL) and Dowex^{TM} M-31 resin (1 g) were mixed in a round bottom flask. This mixture was heated for 90 minutes at 90°C. Ethanol and acetonitrile form an azeotrope (72.9°C, 43% acetonitrile, 57% ethanol) which was collected to drive BAA product formation. After 30 minutes and again after 60 minutes, 20 mL of additional acetonitrile were added to replace what was lost in the azeotrope collection. After cooling to room temperature, the solution was filtered to remove Dowex resin. ^{1}H and ^{13}C NMR analysis were run on the crude product mixture in acetonitrile. *Bromoacetaldehyde diethylacetal:* ^{1}H NMR ($CDCl_3$): 4.534 (t, 1H), 3.585 (m, 2H), 3.483 (m, 2H), 1.107 (t, 6H); ^{13}C NMR ($CDCl_3$): 100.668, 61.858, 31.325, 14.416: *Bromoacetaldehyde:* ^{1}H NMR ($CDCl_3$): 9.309 (t, 1H); ^{13}C NMR ($CDCl_3$): 192.296, 35.448

BAA reaction with NaN_3 to form azidoacetaldehyde

An amount of solution mixture equivalent to 2.5mmol BAA in acetonitrile was placed in a flask with 230mg of NaN_3 (230mg, 3.5mmol) and acetonitrile (2 mL) for dilution. The

solution was heated at 50°C for 12 hours. Argon was flowed through flask for 5 minutes. After 5 minutes, flow was stopped and the system was left under static argon pressure. The solution was cooled to room temperature and filtration was used to remove all solid (unreacted NaN_3 and NaBr formed during reaction) from the solution. The crude product was analyzed by ^{1}H and ^{13}C NMR as well as GC MS, showing both product peaks and unidentified peaks. ^{1}H NMR ($CDCl_3$): 9.64, 7.0, 5.4, 4.7, 4.6, 4.1, 3.7, 3.6, 3.5, 3.4, 2.1, 1.2. ^{13}C NMR ($CDCl_3$): 178.2, 116.4, 101.2, 95.3, 63.2, 62.4, 60.3, 58.2, 54.9, 53.6, 31.7, 18.0, 15.0, 1.7. GC MS *m/z* (relative intensity): 85 M+ (Figure 4.31)

Reaction of 2-azido-acetaldehyde with 1,1-dimethylhydrazine

Without purification, the 2-azido-acetaldehyde solution in acetonitrile was placed in a small round bottom flask. To this, 1,1-dimethylhydrazine (0.19mL, 2.5mmol) was added slowly with vigorous stirring. The solution was heated at 60°C for 12 hours under static argon. The solution was cooled to room temperature. A sample of crude product was analyzed by ^{1}H and ^{13}C NMR as well as LC and GC MS. Analysis showed a mixture of De-DMAEH and glyoxal, bis(dimethylhydrazone). ^{1}H NMR ($CDCl_3$): 6.9, 3.7, 3.5, 3.2, 2.8, 2.6, 2.4, 2.1, 1.9, 1.8, 1.0 ^{13}C NMR ($CDCl_3$): 134.3, 116.3, 62.1, 57.7, 42.4, 15.0, 1.6 LC MS *m/z* (relative intensity): 128, 143 ES+ (Figure 4.33)

Separation by silica column

A solution was made of 5% triethylamine in ethyl acetate. Several hundred grams of silica were stirred in this solution for 3 days. This silica was loaded onto a column. Pure ethyl acetate (300mL) was flushed through the column to remove any excess

triethylamine. Product mixture was loaded onto silica as is, in acetonitrile. Ethyl acetate was used to run the column until it was clear by both visual color change and TLC testing that the first product was removed from the column. The solvent was switched to methanol. This was run through the column until it was clear both visually and by TLC plate testing that the second product was completely removed from the system. Both the ethyl acetate and the methanol fractions were concentrated to ~20 mL by reduced pressure.

5.6 References

1. Richman, D. W.; Griffith, K. N.; Liotta, C. L.; Pollet, P.; *Investigation of Ignition Delay: Novel Beta-Substituted Ethylazide Derivatives as Potential New Liquid Propellant Fuels* Report, SBIR FA9300-05-M-3013, 2006.

2. Thompson, D. M.; *Tertiary Amine Azides in Hypergolic Liquid or Gel Fuels Propellant Systems,* U. S. Patent 6,013,143, 2000.

3. Sengupta, D.; Raman, S.; *Theoretical Investigation of Some High-Performance Novel Amine Azide Propellants,* Prop. Exp. Pyro., 2007, **32(4),** p: 338-347.

4. McQuaid, M. J.; *Small-ring Cyclic Amine Azides as Components of Hypergolic Rocket Propellants,* U. S. Patent 6962633, 2005

5. Mellor, B.; *A Preliminary Technical Review of DMAZ: A Low-Toxicity Hypergolic Fuel,* European Space Agency Special Publication, 2004, **SP-557,** p: 130-135.

6. Hallit, R. E.; Bauerle, G.; *Hypergolic Liquid Propellants Containing a Tertiary Alkyl Amine Azide and Hydrogen Peroxide Oxidant,* U. S. Patent Appl. 2004221933, 2004

7. Miksa, D.; Brill, T. B.; *Spectroscopy of Hydrothermal Reactions. 24. Kinetics of Alkyl Azide Decomposition Channels and N3-Behavior in Water above 200°C at 275 bar,* J. Phys. Chem. A., 2003, **107(19),** p: 3764-3768.

8. Wagaman, K. L.; *Aqueous Hydrogen Peroxide-Hydroxylammonium Nitrate Gas Generating Compositions,* U. S. Patent 6328831, 2001

9. Thompson, D. M.; *Amine Azides used as Monopropellants,* U. S. Patent 6299654, 2001

10. Thompson, D. M.; *Azidoalkyl-Substituted Tertiary Amines as Fuel Components for Liquid or Gel-based Rocket Propellants,* U. S. Patent 6210504, 2001

11. Stevenson, W. H.; Felton, L. D.; Slocum-Wang, Z.; *Hypergolic Liquid or Gel Fuel Mixtures,* U. S. Patent Appl. 11/564990, 2008.

12. McQuaid, M. J.; McNeesby, K. L.; Rice, B. M.; Chabalowski, C. F.; *Density Functional Theory Characterization of the Structure and Gas-phase, Mid-infrared Absorption Spectrum of 2-Azido-N,NN-dimethylethanamine (DMAZ),* Theochem., 2002. **587,** p: 199-218.

13. Pollet, P.; Aronson, J.; Samanta, S.; Liotta, C. L.; Richman, K.; Griffith, K.; *American Pacific Corporation and Georgia Institute of Technology Collaborative Research,* Comprehensive Technical Report Fiscal Year 2005.

14. Pollet, P.; Samanta, S.; John, E.; Charney, R.; Liotta, C. L.; Richman, K.; Griffith, K.; *American Pacific Corporation and Georgia Institute of Technology Collaborative Research,* Comprehensive Technical Report Fiscal Year 2006.

15. Smith, C. P.; O'Connor, J. M.; *Spandex Fibers Made using Low Unsaturation Polyols,* U. S. Patent 5340902, 1994

16. Choudhary, G.; Ilansen, H.; Donkin, S.; Kirman, C.; *Toxicological Profile for Hydrazines,* U. S. Department of Health and Human Services, Public Health Service, Agency for Toxic Substances and Disease Registry, 2007.

17. Vieira, R.; Pham-Huu, C.; Keller, N.; Ledoux, M. J.; *New Carbon nanofiber/graphite Felt Composite for Use as a Catalyst Support for Hydrazine Catalytic Decomposition,* Chem. Commun., 2002, **9,** p: 954-955.

18. Chen, X.; Zhang, T.; Xia, L.; Li, T.; Zheng, M.; Wu, Z.; Wang, X.; Wei, Z.; Xin, Q.; Li, C.; *Catalytic Decomposition of Hydrazine over Supported Molybdenum Nitride Catalysts in a Monopropellant Thruster,* Catal. Lett., 2002, **1-4,** p: 21-25.

19. Zakirow, V.; Sweeting, M.; Lawrence, T.; Sellers, J.; *Nitrous Oxide as a Rocket Propellant,* Acta. Astronautica, 2001, **48,** p: 353-362.

20. Hope, P.; Wiles, L. A.; *Action of Sulfur Monochloride on 2-Acyl-1,1-dimethylhydrazines. Formation of Tetrazans and Oxadiazolines*, J. Chem. Soc. (C), 1987, 2636-2637**.**

21. Perdicchia, C.; Licandro, E.; Maiorana, S.; Baldoli, C.; Giannini, C.; *A New 'One-Pot' Synthesis of Hydrazides by Reduction of Hydrazones,* Tetrahedron, 2003, **59,** p: 7733-7742.

22. Acetonitrile, 2-(2,2-dimethylhydrazinylidene)- Predicted NMR data calculated using Advanced Chemistry Development, Inc. (ACD/Labs) Software V9.07 (1994-2010 ACD/Labs)

23. 2-Propenal, 2-chloro-, 2,2-dimethylhydrazone –Predicted NMR data calculated using Advanced Chemistry Development, Inc. (ACD/Labs) Software V9.07 (1994-2010 ACD/Labs)

24. Hung, R. R.; Straub, J. A.; Whitesides, G. M.; *α-Amino Aldehyde Equivalents as Substrates for Rabbit Muscle Aldolase: Synthesis of 1,4-Dideoxy*-D-*arabinitol and 2(R),5(R)-Bis(hydroxymethyl)-3(R),4(R)-dihydroxypyrrolidine,* J. Org. Chem., 1991, **56,** p: 3849-3855.

25. AIST: Integrated Spectral Database System of Organic Compounds. (Data were obtained from the National Institute of Advanced Industrial Science and Technology (Japan))

26. McLean, M. J.; Larson, J. E.; Wohlrab, F.; Wells, R. D.; *Reaction Conditions Affect the Specificity of Bromoacetaldehyde as a Probe for DNA Cruciforms and B-Z Junctions,* Nucl. Acids Res., 1987, **15,** p: 6917-6935.

27. Folkman, W.; Kusmierek, J. T.; Singer, B.; *A New One-step Method for the Preparation of 3',5'-bisphosphates of Acid-labile Deoxynucleosides,* Chem. Res. Toxic., 1990, **3,** p: 536-539.

28. Ma, Y.; *A Tandem Reaction of 4-Bromoalkyl Aldehydes with Sodium Azide: Synthesis of 5,6,7,7a-Tetrahydro-pyrrolo[1,2-d]-[1.2.3.4]oxatriazole,* Hetero. Chem., 2002, **4,** p: 307-309.

29. Kraus, G. A.; Gootachalk, P.; *Direct Preparation of Bromoacetaldehyde,* J. Org. Chem., 1983, **48,** p: 2111-2112.

30. Predicted NMR data calculated using Advanced Chemistry Development, Inc. (ACD/Labs) Software V9.07 (1994-2010 ACD/Labs)

31. Mangelinckx, S.; Van Vooren, P.; De Clerck, D.; Fülöp, F.; De Kimpe, N.; *An Efficient Synthesis of γ-imino- and γ-amino-β-enamino Esters,* ARKIVOC, 2006, **3**, p: 202-209.

32. Mino, T.; Shirae, Y.; Sasi, Y.; Sakamoto, M.; Fujita, T.; *Phosphine-Free Palladium Catalyzed Mizoroki-Heck Reaction Using Hydrazone as a Ligand,* J. Org. Chem., 2006, **71,** p: 6834-6839.

CHAPTER SIX
CONCLUSIONS AND RECOMMENDATIONS

6.1 2: Development of New Chemistry for a Dual Use Hydrazine Thruster

The goal of this project was to develop a catalyst that could decompose hydrazine at low temperatures (25°C-75°C) in a controlled manner to selectively produce the highest amount of ammonia possible so that this product stream could then be ionized for electric propulsion. Toward this goal, a synthesis method was developed for making supported metal nanoparticle catalysts of nickel, copper, cobalt, iridium, ruthenium, and rhodium. Supported metal catalysts were analyzed by UV-vis, chlorine and metals analysis, electron microscopy imaging and XRD. The method for making commercial catalyst Shell 405[1] was also modified to make supported catalysts of nickel, copper and cobalt. A reactor, including a first and second generation, was designed and built in our lab with which these catalysts were safely tested for the decomposition of hydrazine to its product gases of nitrogen, hydrogen and ammonia. The analysis of the product stream was obtained with a GC-TCD.

Supported nanoparticle catalysts of nickel, copper, cobalt, ruthenium, rhodium, and iridium were tested for their activity towards the decomposition of hydrazine, and selectivity for the formation of ammonia. For these tests, the hydrazine was kept at room temperature with a flow rate of 29.4mL/min, and the catalyst bed was heated to 75°C. Under these conditions, nickel was found to be the most successful as it showed 100% conversion of hydrazine and produced ammonia in 94% ± 3% yields. Rhodium, ruthenium and iridium also showed 100% conversion, however, ammonia yields were lower. Ruthenium and iridium produced ammonia in 67% ± 6% and 62% ± 6% yields

respectively and rhodium only produced a yield of 57% ± 4%. Cobalt and copper both showed no product under these conditions.

As a 3% supported nickel sample has been found to produce the highest amount of ammonia with complete conversion of hydrazine it should be studied further and ultimately optimized for commercial use. In a working thruster system, the chosen catalyst will have to maintain its activity for months or years, so it is also crucial to study how this catalyst will behave over long periods of time. A lifetime study will be necessary to see if this catalyst can continue to run with high selectivity and conversion for many days. Whether the catalyst can physically withstand the conditions it would be subjected to inside a rocket engine is also a question that needs to be answered. To investigate this, the chosen and optimized catalyst will need to undergo vibration testing and crush testing to ensure robustness and stability.

Also in a working thruster system, the hydrazine will be passed over the catalyst bed in a liquid form, not as a gas stream, so once an ideal catalyst is developed, it will have to be tested for its decomposition behavior with a liquid hydrazine stream. However, these tests will be performed at the facilities of our industrial partner American Pacific (AMPAC), as they have the equipment and safety precautions in place necessary for dealing with the decomposition of liquid hydrazine.

By SEM imaging, the supported nanoparticle and Shell catalysts have been shown to have different surface characteristics. In the case of cobalt the metal has a different crystal structure, meaning the hydrazine will interact with a different metallic face during reaction. Due to these differences, one type of catalyst may prove more beneficial for the production of ammonia than the other. The Shell method should be used to make

catalysts of the same six metals as supported nanoparticle catalysts, and these catalysts should then be tested in the reactor under the same conditions to determine their activity and selectivity.

Along with optimizing catalyst metal and synthesis method, pretreatment of the catalysts should be studied. While drying the catalyst overnight at 90°C with flowing argon appears to remove most of the activation period previously seen, there is still a significant time period required for the system to reach equilibrium, ranging from 0.8 hours for iridium catalyst to 5 hours for ruthenium catalyst. It is possible that a pretreatment with hydrogen gas, or hydrazine itself could reduce this time period.

Finally a complete engine must be assembled in which our hydrazine production system is coupled with the electric propulsion thruster currently being developed. Having a way to feed the ammonia gas stream into the thruster with high enough amounts and rates for successful electric propulsion will be crucial for the overall success of this entire project. This must be done as a joint project between our group, and the research group of Dr. Mitchell Walker, a professor of aerospace engineering at the Georgia Institute of Technology, who is currently working on the design and manufacture of the electric propulsion thruster.

6.2 3: Switchable Room Temperature Ionic Liquids

A new class of reversible room temperature ionic liquids has been designed, synthesized and tested for use as a recyclable reaction solvent and for the separation of impurities from bitumen and crude oil. Both a two component system based on a mixture of 2-butyl-1,1,3,3-tetramethylguanidine (TMBG) and an alcohol (methanol, butanol,

hexanol, octanol, and dodecanol have been studied) and a one component system based on commercially available (3-aminopropyl)-trialkoxysilane precursors have been developed (Figure 6.1).[2-3] While all initial work was performed on the two component system, focus shifted to the one component system as it will be more practical in large scale industrial applications since it does not require two components to be kept in an exact 1:1 ratio. For both systems, ionic liquid formation occurs with the addition of CO_2 to the system, and is reversed with the removal of CO_2 via heating or sparging with an inert gas.

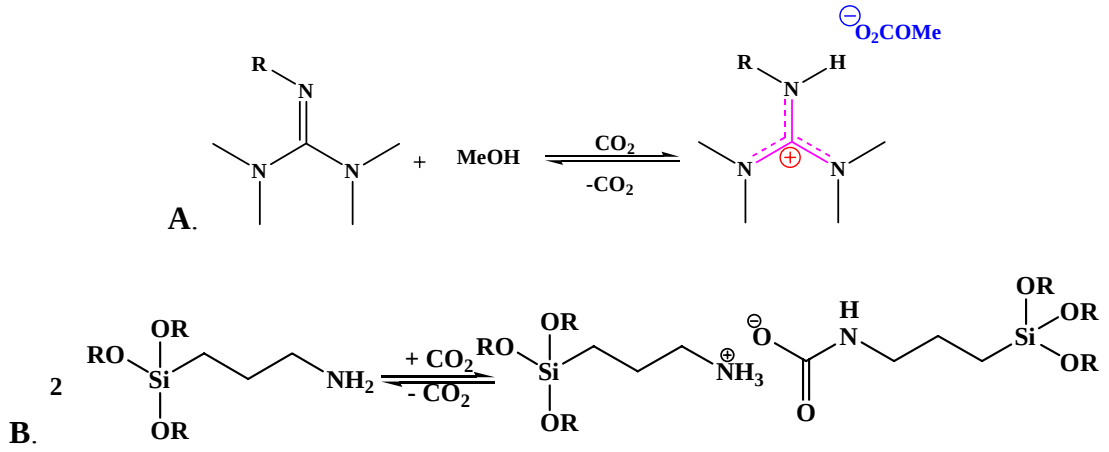

Figure 6.1 A. Formation of switchable ionic liquid 2-butyl-1,1,3,3-tetramethylguanidium methylcarbonate (TMBG MC IL) from 2-butyl-1,1,3,3-tetramethylguanidine (TMBG) and methanol **B**. Formation of switchable 3-(trialkoxysilyl)-propylammonium 3-(trialkoxysilyl)-propyl carbamate from (3-aminopropyl)trialkoxysilane

This switch was found to drastically change the polarity of the solvent system. For the two component system with methanol as the alcohol, switching from the ionic to the neutral liquid form was like switching from acetic acid to chloroform.[2] The one component system was also found to have a large polarity shift consistent to switching from chloroform to benzene between ionic and neutral forms.[3] Along with being reversible, these systems were also found to be highly tunable. By changing either the

alkyl substitution in the 2-position of the guanidine, or simply using a different length alcohol chain, the properties of the two component system could be modified. For the one component system, substituting the alkoxy groups also caused modifications to the solvent properties of the system. For example, switching from the methoxy substituents to the ethoxy substituents decreased the viscosity of the corresponding ionic liquids from 2,160 cP to 930 cP.[3]

The polarity change between ionic and neutral forms in the TMBG IL system has been taken advantage to develop a recyclable solvent system to carry out reaction and separation in a single pot. The Claisen-Schmidt condensation of butanone and benzaldehyde carried out in TMBG was achieved successfully three times with consistent yields (32%-34%) upon complete ionic liquid reversal and recycle.[4] Unfortunately, the reaction attempted in the TMBG MC IL (as opposed to in TMBG) oxidation of benzyl alcohol was not successful. As another possible proof of concept reaction I recommend the carbon bond forming Henry reaction between nitroalkanes and carbonyl compounds (Figure 6.2). Recent work has shown that this reaction can be successfully carried out in traditional non-reversible guanidinum ionic liquids in 6 to 20 hours at 20°C with low to good yields (14%-73%) depending on the choice of reactants.[5] As literature has shown no evidence of side product formation, and products could be isolated by ionic liquid

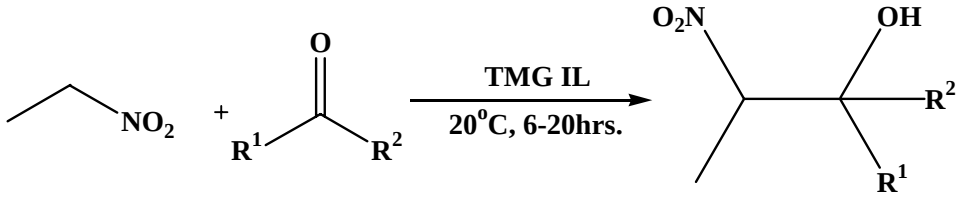

Figure 6.2 Henry reaction between nitromethane and a carbonyl compound using a standard TMG IL as solvent and catalyst. R^1 and R^2 are H or an alkyl chain

reversal to molecular liquid followed by vacuum distillation, I believe this would be a good reaction to test in our system.

The polarity change also causes these ionic liquids to be immiscible with hydrocarbons in the ionic form, but miscible in the neutral form. This property was taken advantage of to develop a reversible system for the treatment of crude oil and bitumen for the isolation of pure alkanes. The TMBG MC IL two component system successfully separated from crude oil with only trace TMBG contamination in the alkane phase, and the 3-(trialkoxysilyl)-propylammonium 3-(trialkoxysilyl)-propyl carbamate (TESAC) one component IL showed 4% or less contamination of the alkane phase.[6] Based on these results, both ionic liquids were tested for their ability to extract pure alkanes from bitumen for potential application in the oil industry. With both ionic liquids, after the phase split, a hydrocarbon layer was successfully separated and isolated.

For these ionic liquids, specifically the one component ionic liquids to be successful in oil extraction on a commercial scale, however, two issues must be addressed. The first is the water reactivity of the precursor molecules. This issue can be overcome by substituting the alkoxy groups with alkyl chains (Figure 6.3), research that is currently being pursued in our group. However, this does not help with, and in fact may be detrimental to the second issue, which is the cross contamination between the oil layer and the ionic liquid layer.

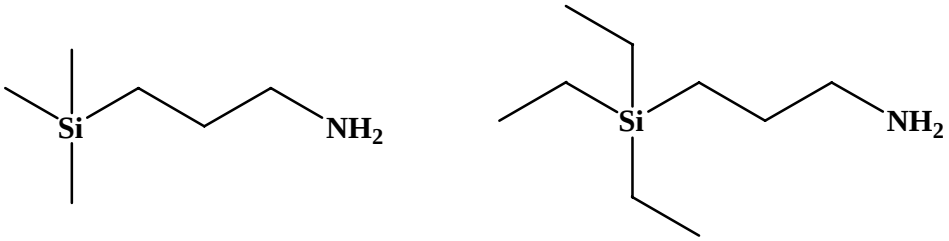

Figure 6.3 Alkylsilylpropylamines to test for the formation of reversible one component ionic liquids

In order to decrease the miscibility of the ionic liquid with the alkane layer, a system must be developed that has a greater polarity switch between the ionic and neutral forms. The ionic liquid formed must be more polar. To achieve this, I recommend the use of silylmethylamine precursors (Figure 6.4, A). While these molecules are not commercially available, they can be readily synthesized from the corresponding chlorosilane compounds.[7]

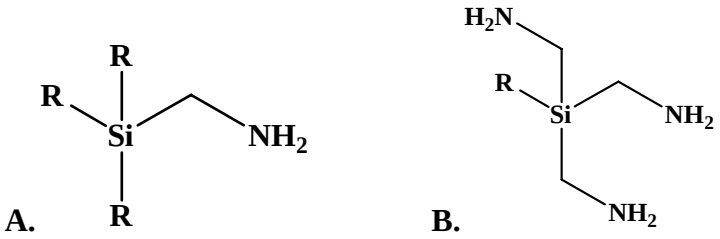

Figure 6.4 Potential silylmethylamine precursor molecules. R=alkyl group, aromatic, ether

By decreasing the length of the carbon chain, the total volume of the system is decreased, which will increase the ionic character of the ionic liquid and should therefore increase the polarity. Modification of the other three substituents on the silicon atom can be done to tune the system properties and ensure that the molecular liquid remains miscible with the crude oil and that the ionic species formed after CO_2 bubbling is a liquid and not a solid. I also recommend studying precursor molecules in which multiple substituents contain a terminal amine group (Figure 6.4 B). This will allow multiple ion pairs on each molecule which will further increase the ionic character of the ionic liquid.

To gain a better understanding of the structure property relationships in these ionic liquid systems, I believe it will also be beneficial to study precursors containing groups other than just linear alkanes for the one component ionic liquid system. Some

examples of these are the dimethylethyl derivative to examine a branched chain substitutent, as well as an asymmetric aromatic fluorinated derivative to study how the electron withdrawing properties of the aromatic group as well as the altered packing due to asymmetry affect the ionic liquid's properties (Figure 6.5).

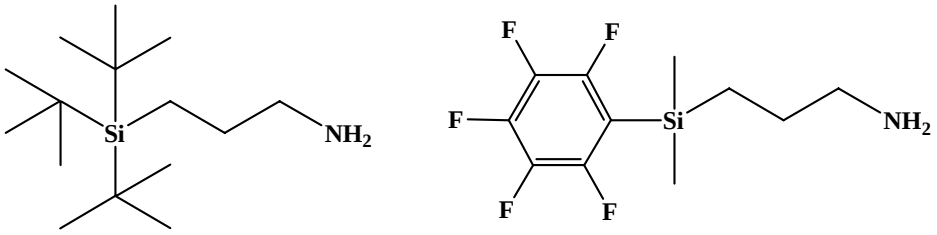

Figure 6.5 Potential one component ionic liquid precursors

6.3 4: A Study of Silane Grafting to Model Polyethylene Compounds

The grafting of vinyltrimethoxysilane onto the polyethylene model compounds dodecane and heptane has been carried out as confirmed by NMR, GPC and mass spec analysis. Substitution of the methoxy groups with phenyl using phenyllithium (PhLi) has been performed to prevent chain crosslinking.[8] This allows study of the grafting reaction itself in order to answer questions such as how many grafts per chain are there and where are they located in relation to each other. From this work it was found that PhLi quenching of 24 hours is not sufficient to fully substitute all methoxy groups, instead between three and four days is required. Also, it is questionable that the grafting proceeds solely by a 1,5- hydrogen shift mechanism, more realistically, there is a competition between the 1,4- and 1,5- hydrogen shift mechanisms and possibly some contribution from the 1,3-hydrogen shift mechanism (Figure 6.6).

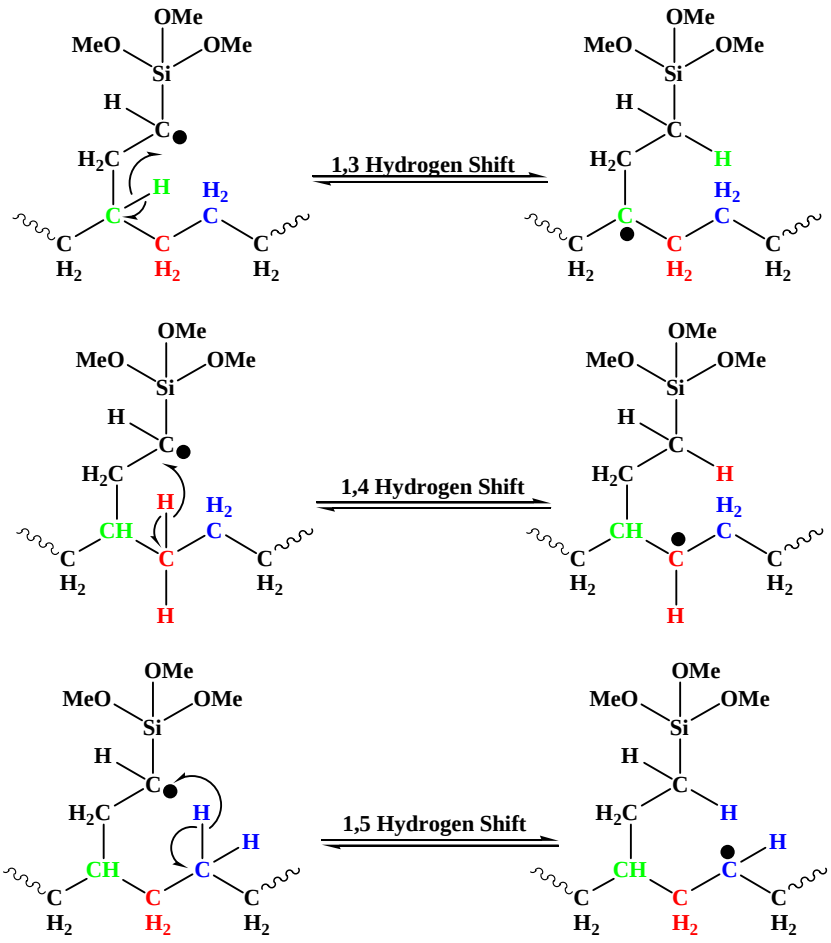

Figure 6.6 Possible hydrogen shift mechanisms for graft propagation along a hydrocarbon backbone

By the 1,5 mechanism that is assumed in literature at most three grafts could be placed on a heptane chain and six on a dodecane chain, assuming only one graft per carbon, yet we have evidence of up to five and eight grafts per chain respectively.[8-10] Separation using Chromatotron chromatography has allowed us to separate fractions from the grafted heptane product mixture, and from this isolate what appears to be a pure di-grafted fraction as confirmed by ^{1}H NMR and MALDI-MS. In future work, HPLC analysis should be used to confirm the presence of only one compound in this fraction, and if necessary preparative HPLC be used to purify and isolate the di-grafted fraction.

Once purity is affirmed, full analysis of this material by DEPT NMR in combination with 2-dimensional NMR and EI and CI MS will determine the regiochemistry of the isomers and from this exactly which hydrogen shift mechanism or mechanisms are being followed. If even some of the grafts are found to be on adjacent carbons, the literature held belief of only a 1,5 hydrogen shift mechanism will be disproved.

Currently, this work is fundamental research. Ultimately, having a more accurate understanding of the reaction mechanism will allow a more efficient industrial process to be developed leading to less waste and lower cost. However, until a clearer picture of the reaction mechanism or mechanisms is obtained, specific process modifications cannot be proposed.

As further means of studying this reaction mechanism, however, both different grafting molecules, aside from VTMS and different model compounds can be used. One such example is the molecule 1-(trimethoxysilyl)ethenyl-benzene (Figure 6.7).

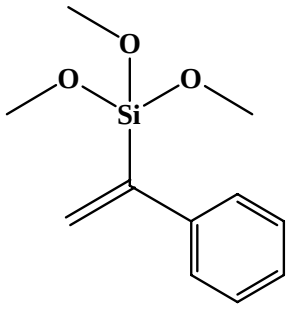

Figure 6.7 1-(trimethoxysilyl)ethenyl-benzene

With this molecule, the phenyl in the vinylic position should prevent any hydrogen shift from occurring, allowing formation of only the singly grafted product if all radical propagation occurs solely by intramolecular abstraction. Current research appears to

support this method, however, if multiple grafts arise with this grafting molecule then it will show that intermolecular chain transfer also plays a contributing role in this reaction mechanism.

Branched hydrocarbons should also be studied as model compounds as they will allow us to look at the selectivity between a 1,4 and 1,5 hydrogen shift mechanism. Specifically, with the model compound 3,3,4,4-tetramethyl hexane, only a 1,4-hydrogen shift can occur while the model 2,2,4,4,6,6-hexamethyl heptane would allow only a 1,5-hydrogen shift. Finally, the symmetrical model, 4,4-dimethyl heptane will allow us to look at the competition between 1,4, and 1,5 propagation in a situation where only a limited and controlled number of grafts can occur. Separating the individual grafted products formed on each of these models and determining the isomers formed through the methods we have developed will give insight into both the selectivity and mechanism of this reaction.

Towards the goal of understanding the grafting reaction, work was also done on the use of CO_2 pressure and its affect on the grafting mechanism. From this work it was found that the addition of only moderate pressures of CO_2 (100 – 150 bars) leads to fewer grafts per individual hydrocarbon chain (5 grafts at 150 bar and 4 grafts at 100 bar versus 6 grafts with no CO_2). UV-vis studies have shown that this change is not due to a change in solvent polarity from CO_2 dissolution. However, beyond this, the exact cause has not yet been determined. It is my recommendation that the path forward for this needs to focus on determining exactly what affect the CO_2 is having on the reaction.

CO_2 can have a physical affect, a chemical affect, or a combination of both on the reaction. So, the next step should be to carry out these studies using a small gas molecule

with no chemical interactions, for example N_2. If other small molecules cause the same reaction changes as CO_2, then this indicates a physical effect such as a dilution effect of the gas expanding the hydrocarbon phase and causing the concentration of the VTMS and peroxide in the liquid phase to decrease, a decrease in solvent viscosity that is affecting the mass transfer, or simply the affect of that high a hydrostatic pressure pushing down on the liquid phase.

6.4 5: Synthesis of the Novel Hydrazine Replacement Fuel Molecules 1,1-Dimethyl-2-[2-azidoethyl] Hydrazine and 1,1-Dimethyl-2-[2-azidoethyl]Hydrazone

The molecule 1,1-dimethyl-2-[2-azidoethyl] Hydrazine (DMAEH) and its hydrazone analog 1,1-dimethyl-2-[2-azidoethyl]hydrazone (De-DMAEH) were proposed as potential liquid propellant molecules (Figure 6.8).

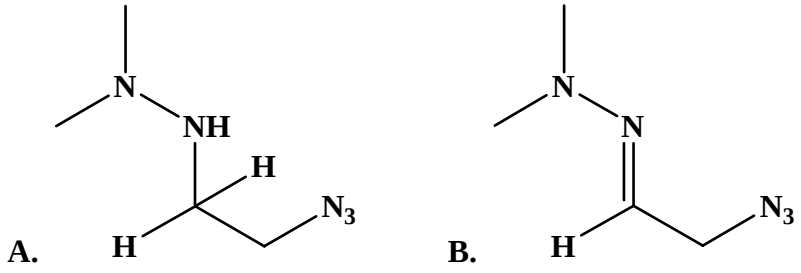

Figure 6.8 A. 1,1-Dimethyl-2-[2-azidoethyl] hydrazine (DMAEH) and **B.** 1,1-dimethyl-2-[2-azidoethyl]hydrazone (De-DMAEH)

While initial work focused on the formation of DMAEH, work shifted to the synthesis of De-DMAEH from the starting molecule bromoacetaldehyde diethyl acetal (BADA). A three step synthesis was developed involving deprotection of the BADA, reaction of the resulting acetal with sodium aizde to form 2-azido-acetaldehyde and finally reaction with 1,1-dimethylhydrazine to form De-DMAEH. Based on ^{1}H and ^{13}C NMR, as well as MS

analysis, it appeared that with this reaction, De-DMAEH was successfully formed in conjunction with the by-product glyoxal, bis(dimethylhydrazone) (Figure 6.9). Attempts at separation were made using silica column chromatography with both acidic and neutralized silica. However, in both cases, while pure side product was collected using ethyl acetate as eluent, the pure De-DMAEH was not successfully isolated.

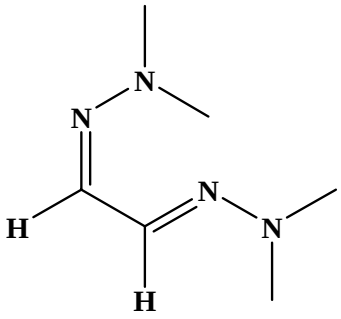

Figure 6.9 Reaction side product glyoxal bis(dimethylhydrazone)

Based on these results, it is my recommendation that another separation method be attempted for the purification of De-DMAEH. The side product glyoxal, bis(dimethylhydrazone) has a boiling point of 188.1°C.[11] As De-DMAEH is a new molecule, its boiling point is not known, however, by comparison with molecules of similar structure such as 2-dimethylaminoethylazide (DMAZ, Figure 6.10A) and 2-(2,2-dimethylhydrazinylidene)-acetonitrile (Figure 6.10B), which have boiling points of 135°C and 113°C respectively[12-13], its boiling point is expected to be lower. Based on this, it is my recommendation that distillation be attempted for separation of pure De-DMAEH. NMR analysis, mass spec, and elemental analysis can be used to provide positive identification of the molecule obtained.

Figure 6.10 A. 2-dimethylaminoethylazide (DMAZ) and **B.** 2-(2,2-dimethylhydrazinylidene)-acetonitrile

Once De-DMAEH is obtained as a pure molecule, a one step reduction with borane could be used to form the initial molecule of interest, DMAEH (Figure 6.11).

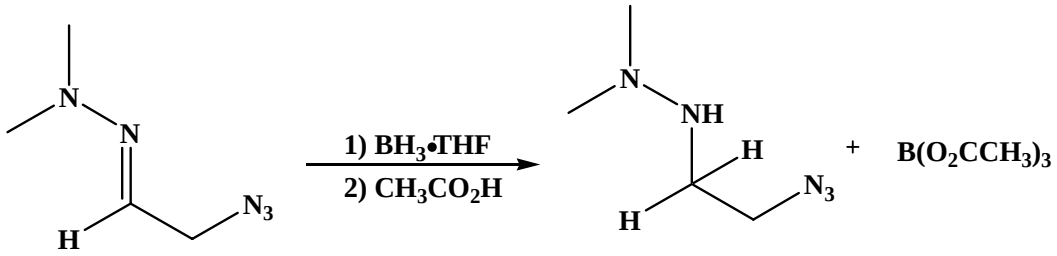

Figure 6.11 Reduction of De-DMAEH to form DMAEH

With this molecule as well, NMR analysis, mass spec, and elemental analysis can be used for positive identification. Once both molecules are formed I recommend that the next goal be to scale up the synthesis. On the current scale, at best a few milligrams can be produced. However, with a few grams of material, testing can then be done on these molecules to study their potential as fuel molecules, including ignition ability and combustion characteristics including thrust and specific impulse.

6.5 References

1. Armstrong, W. E.; Ryland, L. B.; Voge, H. H.; *Catalyst Comprising Ir or Ir and Ru for Hydrazine Decomposition,* US Patent 4124538, **2004.**

2. Phan, L.; Chiu, D.; Heldebrant, D. J.; Huttenhower, H.; John, E.; Li, X.; Pollet, P.; Wang, R.; Eckert, C. A.; Liotta, C. L.; Jessop, P. G., *Switchable Solvents Consisting of Amidine/Alcohol or Guanidine/Alcohol Mixtures.* Ind. Eng. Chem. Res. 2008, **47** (3) p. 539-545.

3. Blasucci, V.; Dilek, C.; Huttenhower, H.; John, E.; Llopis-Mestre, V.; Pollet, P.; Eckert, C.; Liotta, C.; *One Component, Switchable Ionic Liquids Derived from Siloxylated Amines*. Chem. Commun. 2009, **1**: p. 116-118.

4. Hart, R.; Pollet, P.; Hahne, D.; John, E.; Llopis-Mestre, V.; Blasucci, V.; Huttenhower, H.; Leitner, W.; Eckert, C.; Liotta, C.; *Benign Coupling of Reactions and Separations with Reversible Ionic Liquids*. Tetrahedron. 2010, **66**(5): p. 1082-1090.

5. Jiang, T.; Gao, H.; Han, B.; Zhao, G.; Chang, Y.; Wu, W.; Gao, L.; Yang, G.; *Ionic liquid catalyzed Henry reactions.* Tet. Lett, 2004. **45**: p. 2699-2701.

6. Blasucci, V.; Hart, R.; Llopis-Mestre, V.; Hahne, D.; Burlager, B.; Huttenhower, H.; Thio, B. J. R.; Pollet, P.; Liotta, C.; Eckert, C.; *Single Component Reversible Ionic Liquids for Energy Applications*. Fuel. 2010, **89:** p. 1315-1319.

7. Vlasova, N. N.; Pestunovich, A. E.; Voronkov, M. G.; *Reaction of Triethylsilylmethylamine and some Secondary Organosilicon Amines with Formaldehyde and Sulfur.* Izvestiya Akademii Nauk SSR, Seriya Khimicheskaya, 1982, **10**: p. 2380-2383,

8. Spencer, M.; Parent, J. S.; Whitney, R. A.; *Composition distribution in poly(ethylene-graft-vinyltrimethoxysilane)*. Polymer 2003. **44**: p. 2015-2023.

9. Forsyth, J. C.; Baker, W. E.; Russell, K. E.; Whitney, R. A.; *Peroxide-Initiated Vinylsilane Grafting: Structural Studies on a Hydrocarbon Substrate*. J. Polym. Sci., 1997. **35**: p. 3517-3525.

10. Freidlina, R. Kh.; Terent'ev, A. B.; *Free-radical Rearrangements in Telomerization.* Acc. Chem. Res., 1977. **10**(1): p. 9-15.

11. Calculated using Advanced Chemistry Development (ACD/Labs) Software V8.14 for Solaris (© 1994-2010 ACD/Labs)

12. Mellor, B.; *A Preliminary Technical Review of DMAZ: A Low-Toxicity Hypergolic Fuel,* European Space Agency Special Publication, 2004, **SP-557,** p: 130-135.

13. Brederck, H.; Foehlich, B.; Walz, K.; *N-Isocyanodialkylamines,* Justus Liebigs Annalen der Chemie, 1965. **686**: p. 92-101.

VITA

Hillary Anne Huttenhower was born in Pittsburgh, PA on April 25, 1984 to Edward and Donna Huttenhower. She attended Central Cambria High School in Ebensburg, PA. Upon graduation she then attended the College of William and Mary in Williamsburg, VA where she graduated magna cum laude with a Bachelor of Science in chemistry, as well as minors in biology and religion, in May of 2005. She proceeded straight into graduate school for which she attended the Georgia Institute of Technology beginning in August of 2005. As a graduate researcher, she was co-advised by Dr. Charles Liotta and Dr. Charles Eckert. She will receive her PhD in chemistry in August of 2010. After graduation, her plans include moving to Hartford, CT where she will be working for Pratt and Whitney in their composite materials division.